

School of Chemistry Cardiff University



Applications of *N*-heterocyclic carbenes

A thesis submitted to Cardiff University in accordance with the requirements for the degree of Doctor of Philosophy

Ibrahim Olakunle Shoetan

SUPERVISORS:

Dr. Ian Fallis

Dr. Athanasia Dervisi

Prof. David Williams

July, 2021

Acknowledgement

Life is a journey no one goes through alone. This PhD study has been a life-changing moment and it has afforded me the opportunity to work with people with immense knowledge, profound experience, and professional expertise.

My profound gratitude goes to my supervisors: Dr Ian Fallis, for giving me the opportunity to undertake my PhD under his supervision, his continuous support throughout the program, his mentorship and guidance, Dr Nancy Dervisi, for her support before and during this program, her thoughtfulness and invaluable contribution and Prof. David Williams for his contribution and mentorship.

This PhD study would not have been possible without the funding and strategic support I received from Commonwealth Scholarship Commission. Thank you very much and I will forever cherish this moment. In addition, I also want to thank Cardiff University for accepting me into this program.

I would like to thank members of my review panel, Prof. Davide Bonifazi, Dr Tim Easun and Prof. Simon Pope for their support and encouragement during this program.

I am extremely grateful to all the technical staff for their support.

I am very much thankful to my colleagues in Lab 1.124 East and West and all the postdoctoral research fellows that I worked with during this program for all the fun and good times we shared.

Lastly, this research work is dedicated to Ayoola Shoetan (my wife), Olakunmi Shoetan (my daughter), Aremu Shoetan (my dad) and to the memory of Abewun Shoetan (my late mother).

Abbreviations

| | |
|-------------------------------------|---|
| % V _{bur} | Percent Buried Volume |
| Å | Angstrom |
| ATCC | American Type Culture Collection |
| ATP | Adenosine triphosphate |
| CHCl ₃ | Chloroform |
| CBr ₄ | Carbon tetrabromide |
| ClMe ₂ SiH | Chlorodimethylsilane |
| DBU | 1,8-Diazabicyclo[5.4.0]undec-7-ene |
| DBN | 1,5-Diazabicyclo[4.3.0]non-5-ene |
| DFT | Density Functional Theory |
| DMAD | Dimethyl- acetylenedicarboxylate |
| DMSO | Dimethylsulfoxide |
| EPS | Extracellular polymer matrices |
| ESKAPE | Enterococcus faecium, Staphylococcus aureus, Klebsiella pneumoniae, Acinetobacter baumannii, Pseudomonas aeruginosa, and Enterobacter species |
| ES-MS | Electrospray Mass Spectrometry |
| ESI-TOF | Electrospray Ionization Time-of-Flight |
| Et ₃ SiH | Triethylsilane |
| Et | Ethyl |
| HOMO | Highest Occupied Molecular Orbital |
| HRMS | High Resolution Mass Spectrometry |
| IDSA | The Infectious Diseases Society of America |
| <i>i</i> Pr | Isopropyl |
| KN(SiMe ₃) ₂ | Potassium bis(trimethylsilyl)amide |
| LUMO | Lowest Unoccupied Molecular Orbital |
| MBC | Minimal Bactericidal Concentration |

| | |
|-----------------------|---|
| MBEC | Minimal Biofilm Eradication Concentration |
| Me | Methyl |
| MIC | Minimal Inhibitory Concentration |
| MMA | Methyl methacrylate |
| NCIMB | National Collection of Industrial, Food and Marine Bacteria |
| NCTC | National Collection of Type Cultures |
| NHC | <i>N</i> -heterocyclic carbene |
| NMR | Nuclear Magnetic Resonance |
| PhMe ₂ SiH | Phenyldimethylsilane |
| <i>t</i> Bu | Tertiary Butyl |
| TEP | Tolman's Electronic Parameter |
| THF | Tetrahydrofuran |
| ROMP | Ring-Opening Metathesis Polymerization |
| W.H.O. | World Health Organisation |

Abstract

This study is on the synthesis and metal coordination of *N*-heterocyclic carbenes and their application as antimicrobial agents and as catalysts in hydrosilylation reaction.

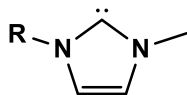
Chapter 2 discusses the synthesis and characterisation of surface-active proligands (imidazolium salts). Three sets of monocationic amphiphilic salts bearing methyl-imidazole, mesityl-imidazole and imidazolyl-propane-1-sulfonate head group and three sets of Gemini dicationic amphiphilic salts with head group comprising of methyl-imidazole-tethered-to-imidazole, mesityl-imidazole-tethered-to-imidazole and trimethylamine-tethered-to-imidazole with a propyl linker respectively. The hydrophobic/lipophilic part of all the amphiphilic salts are made up of alkyl chains with lengths ranging from 8 – 16 and with bromide ion as a counter anion. The critical micelle concentrations (CMC) of these amphiphilic proligands were determined by conductometric method.

The synthesis of five series of Ag(I)-NHC complexes of general composition **[NHC-Ag-Br]** and **Na⁺[NHC-Ag-Cl]⁻** derived from the amphiphilic proligands and their characterisation by ¹H and ¹³C NMR spectroscopy and High-Resolution Mass Spectrometry (HRMS) are described in chapter 3 while their *in vitro* antimicrobial activity against *Escherichia coli* NCTC 12923, *Staphylococcus aureus* NCTC 6571, *Staphylococcus aureus* NCIMB 9518, *Pseudomonas aeruginosa* ATCC 15692, *Staphylococcus epidermidis* ATCC 14990, *Staphylococcus epidermidis* ATCC RP62A and *Candida albicans* ATCC 90028 are reported in chapter 4.

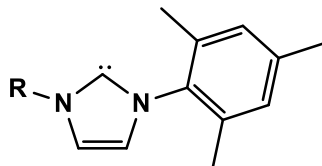
Chapter 5 describes the synthesis of novel metallosurfactant bearing NHC ligand systems with Pt(II) metal centre as the head group and hydrophobic tail comprising of hydrocarbon chain. These complexes were characterised by ¹H and ¹³C NMR spectroscopy, HRMS and their application as catalysts for the hydrosilylation of terminal alkenes and an alkyne with three different hydrosilanes in water are discussed. These metallosurfactants provide extended functionality beyond their amphiphilic nature. They achieved excellent conversions and regioselectivity for the synthesis of organosilanes in a sustainable way.

N-heterocyclic carbenes

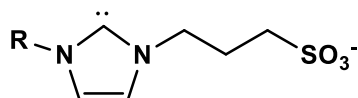
L_{8-16}



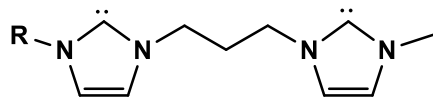
L_{8-16}^{mes}



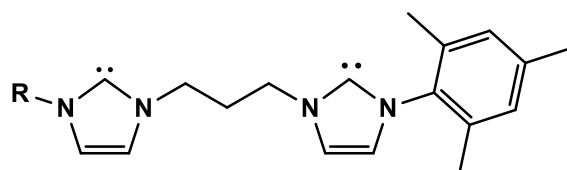
L_{8-16}^{bet}



G_{8-16}



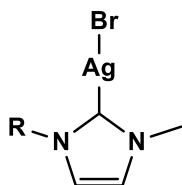
G_{8-16}^{mes}



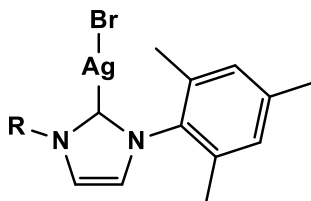
$R = C_8H_{17}, C_{10}H_{21}, C_{12}H_{25},$
 $C_{14}H_{29}, C_{16}H_{33}$

Ag(I)NHCs

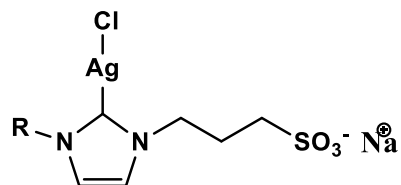
L₈₋₁₆-Ag-Br



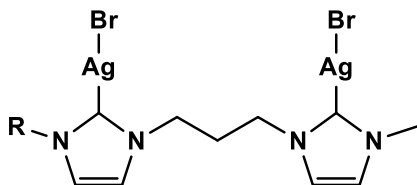
L^{mes}₈₋₁₆-Ag-Br



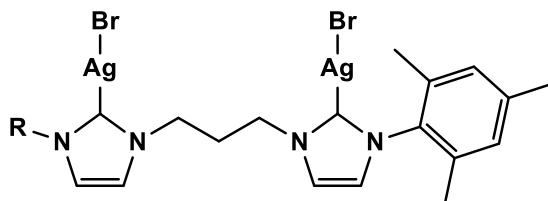
Na [L^{bet}₈₋₁₆-Ag-Cl]



G₈₋₁₆-Ag-Br



G^{mes}₈₋₁₆-Ag-Br



**R = C₈H₁₇, C₁₀H₂₁, C₁₂H₂₅,
C₁₄H₂₉, C₁₆H₃₃**

Pt(II)NHCs

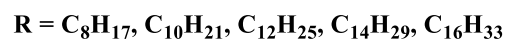
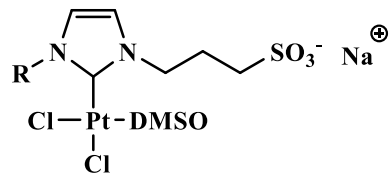
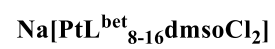


Table of contents

| | |
|---|-----------|
| 1.0. Introduction | |
| 1.1.N-heterocyclic carbenes..... | 2 |
| 1.2. Structural features of NHCs and their effects on stability..... | 3 |
| 1.3. How carbenes evolve from mere intermediate to an important auxiliary ligand in organometallics..... | 6 |
| 1.4. Reactivity of N-heterocyclic carbenes..... | 11 |
| 1.4.1. Basicity..... | 11 |
| 1.4.2. Towards C=C multiple bonds..... | 13 |
| 1.4.3. Towards chlorinated compounds..... | 15 |
| 1.4.4. Towards aldehyde..... | 16 |
| 1.4.5. Towards CO ₂ and CO..... | 17 |
| 1.4.6. Towards transition metals..... | 18 |
| 1.5. The nature of the metal-NHC bond..... | 21 |
| 1.6. Preparation of NHCs..... | 22 |
| 1.7. Preparation of NHC-metal complexes..... | 23 |
| 1.7.1. By free carbene route..... | 25 |
| 1.7.2. By reacting NHC precursor with basic metal salts..... | 25 |
| 1.7.3. By carbene transfer technique..... | 26 |
| 1.8. Applications of NHC-metal complexes..... | 27 |
| 1.9. Surfactants and Metallosurfactants..... | 30 |
| 1.10. Aims and objectives of this work..... | 32 |
| 1.11. References..... | 33 |
| 2.0. Synthesis of Surface-Active Imidazolium salts and the Evaluation of their Critical Micelle Concentration..... | 40 |
| 2.1. Introduction..... | 41 |
| 2.2. Strategy for Designing New Amphiphilic Imidazolium salts..... | 45 |
| 2.3. Aims..... | 46 |
| 2.4. Results and Discussion..... | 47 |
| 2.4.1. Synthesis of 1-methyl-3-alkyl-imidazolium bromide (HL ₈₋₁₆)..... | 47 |

| | |
|---|------------|
| 2.4.2. Synthesis of 1-(2,4,6-Trimethylphenyl)-1 <i>H</i> -Imidazole..... | 50 |
| 2.4.3. Synthesis of 1-mesityl-3-alkyl-imidazolium bromide (HL ^{mes} ₈₋₁₆)..... | 50 |
| 2.4.4. Synthesis of 3-(3-alkyl-imidazolium-1-yl)propanesulfonate (HL ^{bet} ₈₋₁₆)..... | 51 |
| 2.4.5. Synthesis of Gemini Amphiphilic Imidazolium Salts..... | 52 |
| 2.4.6. Determination of Critical Micelle Concentration (CMC)..... | 56 |
| 2.4.7. Structural effects of monocationic and dicationic ionic Surfactants on critical micelle concentration..... | 57 |
| 2.4.8. Comparison of Critical Micelle Concentration Values of Monocationic and Dicationic Surfactants..... | 58 |
| 2.5. Experimental..... | 59 |
| 2.6. References..... | 78 |
| 3.0. Synthesis and Characterisation of silver (I) <i>N</i>-heterocyclic carbenes..... | 81 |
| 3.1. Introduction..... | 82 |
| 3.2. Aims..... | 84 |
| 3.3. Results and Discussion..... | 88 |
| 3.3.1. Synthesis of silver(I) <i>N</i> -heterocyclic carbene complexes..... | 88 |
| 3.3.2. ¹ H and ¹³ C NMR study of silver(I) complexes..... | 91 |
| 3.3.3. HRMS study of silver(I) complexes..... | 98 |
| 3.4. Experimental..... | 105 |
| 3.5. References..... | 115 |
| 4.0. <i>In vitro</i> Antimicrobial screening of Ag(I)-NHCs against planktonic and biofilm cells..... | 118 |
| 4.1. Introduction..... | 119 |
| 4.2. Aims..... | 121 |
| 4.3. Results and Discussion..... | 123 |
| 4.3.1. Preliminary antimicrobial screening..... | 123 |
| 4.3.2. Determination of MIC, MBC and MBEC..... | 123 |
| 4.3.2.1. HL ₈₋₁₆ and L ₈₋₁₆ -Ag-Br..... | 123 |
| 4.3.2.2. HL ^{mes} ₁₀₋₁₆ and L ^{mes} ₁₀₋₁₆ -Ag-Br..... | 128 |
| 4.3.2.3. H ₂ G ₈₋₁₆ and G ₈₋₁₆ -Ag ₂ -Br ₂ | 132 |
| 4.3.2.4. H ₂ G ^{mes} ₈₋₁₆ and G ^{mes} ₈₋₁₆ -Ag ₂ -Br ₂ | 136 |

| | |
|---|------------|
| 4.4. Conclusions..... | 139 |
| 4.5. Experimental..... | 142 |
| 4.5.1. Biological Activity..... | 142 |
| 4.5.1.1. MIC and MBC Determinations..... | 142 |
| 4.5.1.2. Biofilm Cells Susceptibility Test..... | 142 |
| 4.6. References..... | 143 |
| 5.0. Synthesis and characterisation of surface-active platinum(II) | |
| <i>N</i>-heterocyclic carbenes..... | 146 |
| 5.1. Introduction..... | 147 |
| 5.2. Aims..... | 153 |
| 5.3. Results and Discussion..... | 154 |
| 5.3.1. Synthesis of surface-active platinum(II) <i>N</i> -heterocyclic carbene complexes..... | 154 |
| 5.3.2. Catalytic application of Na[PtL ^{bet} ₈₋₁₆ dmsOCl ₂] in Hydrosilylation of terminal alkenes and alkyne in water..... | 157 |
| 5.3.2.1. Hydrosilylation of 1-octene with PhMe ₂ SiH, Et ₃ SiH and ClMe ₂ SiH in water..... | 157 |
| 5.3.2.2. Hydrosilylation of styrene with PhMe ₂ SiH and ClMe ₂ SiH in water..... | 161 |
| 5.3.2.3. Hydrosilylation of 1-octyne with PhMe ₂ SiH, Et ₃ SiH and ClMe ₂ SiH in water..... | 166 |
| 5.3.2.4. Structure-activity relationship..... | 169 |
| 5.4. Experimental..... | 171 |
| 5.5. References..... | 175 |
| 6.1. Conclusions and Future Work..... | 178 |

Chapter

1

Introduction

1.0. Introduction

| | |
|--|----|
| 1.1.N-heterocyclic carbenes..... | 2 |
| 1.2. Structural features of NHCs and their effects on stability..... | 3 |
| 1.3. How carbenes evolve from mere intermediate to an important auxiliary ligand in organometallics..... | 6 |
| 1.4. Reactivity of N-heterocyclic carbenes..... | 11 |
| 1.4.1. Basicity..... | 11 |
| 1.4.2. Towards C=C multiple bonds..... | 13 |
| 1.4.3. Towards chlorinated compounds..... | 15 |
| 1.4.4. Towards aldehydeS..... | 16 |
| 1.4.5. Towards CO ₂ and CO..... | 17 |
| 1.4.6. Towards transition metals..... | 18 |
| 1.5. The nature of the metal-NHC bond..... | 21 |
| 1.6. Preparation of NHCs..... | 22 |
| 1.7. Preparation of NHC-metal complexes..... | 23 |
| 1.7.1. By free carbene route..... | 25 |
| 1.7.2. By reacting NHC precursor with basic metal salts..... | 25 |
| 1.7.3. By carbene transfer technique..... | 26 |
| 1.8. Applications of NHC-metal complexes..... | 27 |
| 1.9. Surfactants and Metallosurfactants..... | 30 |
| 1.10. Aims and objectives of this work..... | 32 |
| 1.11. References..... | 33 |

Chapter one

Introduction

1.1. N-Heterocyclic Carbenes

N-heterocyclic carbenes (NHCs) are singlet carbenes with a heterocyclic core, in which the divalent carbene carbon is connected directly to at least one nitrogen atom within the heterocycle.^{1, 2} They are a specific form of carbene demonstrating a particular stability, where the carbene is located in an N-heterocyclic scaffold (Figure 1.1). However, they were considered unstable and highly reactive because they contain six valence electrons and are coordinatively unsaturated. Contrary to other carbenes, which are generally found to be electrophilic, N-heterocyclic carbenes are electron-rich nucleophilic species in which the carbene centre benefits from the stabilization associated with both the σ -electron-withdrawing and π -electron-donating character of the nitrogen centers. The first attempt to isolate an NHC by Wanzlick in 1960 was unsuccessful³ but a very important milestone was achieved in carbene chemistry when Arduengo proved that a carbene in principle can be tailored to be kinetically stable and opened the access to free, isolable NHCs in 1991.⁴

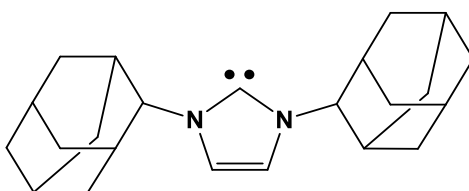


Figure 1.1: The first example of a free and stable N-heterocyclic carbene

Remarkably, in the absence of oxygen and moisture, this 1,3-diadamantyl substituted imidazol-2-ylidene (Figure 1.1) was found to be stable at room temperature and melts at 240°C without decomposition.

1.2. Structural Features of NHCs and their Effects on its Stability

The unusual stability of NHCs is in part a result of shielding by sterically demanding substituents on the ring which help to kinetically stabilize the species by sterically inhibiting dimerization. The electronic stabilization provided by the nitrogen atoms, however, is a much more important factor.⁵ The adjacent σ -electron-withdrawing and π -electron-donating nitrogen atoms stabilize this structure both inductively by lowering the energy of the occupied sp^2 -orbital and mesomerically by donating electron density into the empty p-orbital (Figure 1.2).

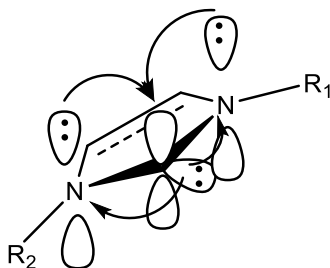


Figure 1.2: Ground-state electronic structure of imidazol-2-ylidenes and the σ -withdrawing and π -donating effects of the nitrogen heteroatoms

NHCs exhibit a singlet ground-state electronic configuration with the highest occupied molecular orbital (HOMO) and the lowest unoccupied molecular orbital (LUMO) best described as a formally sp^2 -hybridized lone pair and an unoccupied p-orbital at the C_2 carbon, respectively (Figure 1.2). The cyclic nature of NHCs also stabilises the singlet state by forcing the carbene carbon into a bent, more sp^2 -like arrangement. This ground-state structure is reflected in the C2-N bond lengths of 1.37 Å observed for 1,3-diamantyl imidazol-2-ylidene which falls in between those of its corresponding imidazolium salt (1.33 Å) and its C2-saturated analogue (1.49 Å),⁶ signifying that the C2-N bonds possess partial double bond character (Figure 1.3).⁷ These findings indicate an increased σ -bond character in NHCs and the NCN bond angle, ring size and substitution pattern of the nitrogen heterocycle can have a pronounced effect on the properties of the NHCs.

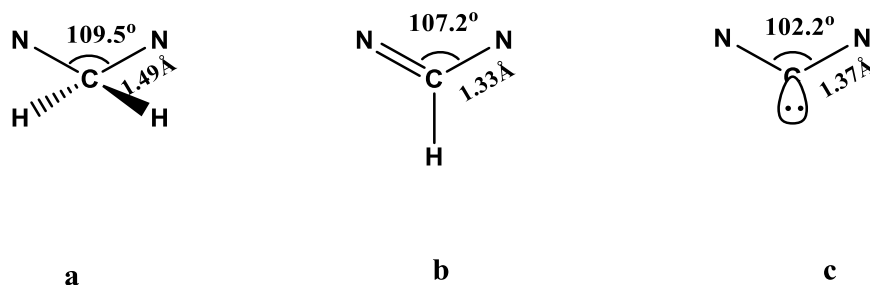


Figure 1.3: How ring constrain affects the geometry, steric and electronic arrangement of N_2CH_2 , N_2CH and $\text{N}_2\text{C:}$ units.

The inherent features of the NHC heterocycle, particularly the position and choice of the heteroatoms have a major influence on the electronic properties of NHCs and some of the ways by which their electron-donor properties can be quantified are by ^{13}C NMR,⁸ electrochemical E^0 value also known as Lever electronic parameters (LEP)⁹ and by Tolman's electronic parameter (TEP).¹⁰⁻¹² In addition, the shape and the steric demand of the N-substituents are important factors for the stability of NHCs. The steric properties of NHCs can be assessed using the 'buried volume' parameter ($\%V_{\text{bur}}$) concept developed by Nolan, Cavallo and co-workers.¹³ The $\%V_{\text{bur}}$ represents the part of a sphere with a radius r of 3.5 \AA around the metal and a distance of 2 \AA between the metal and the coordinating carbene carbon that is buried by the atoms of the ligand under investigation (Figure 1.4).

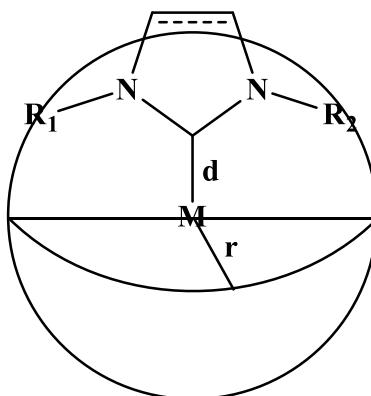


Figure 1.4: Depiction of the $\%$ buried volume concept

Another factor that is quite important to understanding NHCs is a knowledge of their acid–base properties. Higgins and coworkers (2011) determined the pK_a s for the conjugate acids of a large series of NHCs in water and found their pK_a s to range from 19.8–28.2. The largest effect on pK_a was observed by varying the N-substituent or ring size, while the effect of C_4 – C_5 saturation is small.¹⁴ Besides 5-membered ring NHCs, examples containing 4-membered and larger ring sizes of 6-, 7- and bicyclic 6- and 7-membered ring NHCs have also been reported.^{15–17} A detailed study by Alder et al. examined a series of cyclic NHCs of variable size (5-, 6- and 7-membered rings) with different alkyl substituents on the N atoms. They found that increasing the bulkiness of the alkyl group (Me, Et, *i*Pr and *t*Bu) increases the stability of the monomeric NHC. Furthermore, the NCN bond angle increases as the size of the ring increases and consequently, the N-substituents are pushed closer to the carbene centre, although, this effect is less pronounced for the 5-membered NHC.¹⁸ The successful isolation by Arduengo and coworkers in 1991 and the unusual stability of NHCs have spurred scientists on and this has led to many different classes of NHCs with various substitution patterns, ring sizes and degrees of heteroatom stabilization and below in Figures 1.5 and 1.6 are classification of the constituting units of NHCs and some representation of the general structures of NHCs respectively.^{4, 15–17, 19–25}

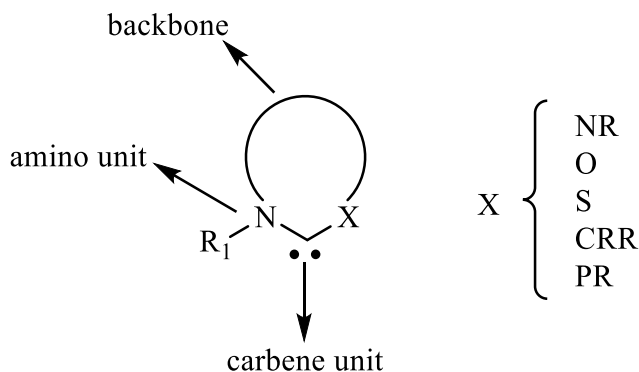


Figure 1.5: General classification of the constituting units of NHCs

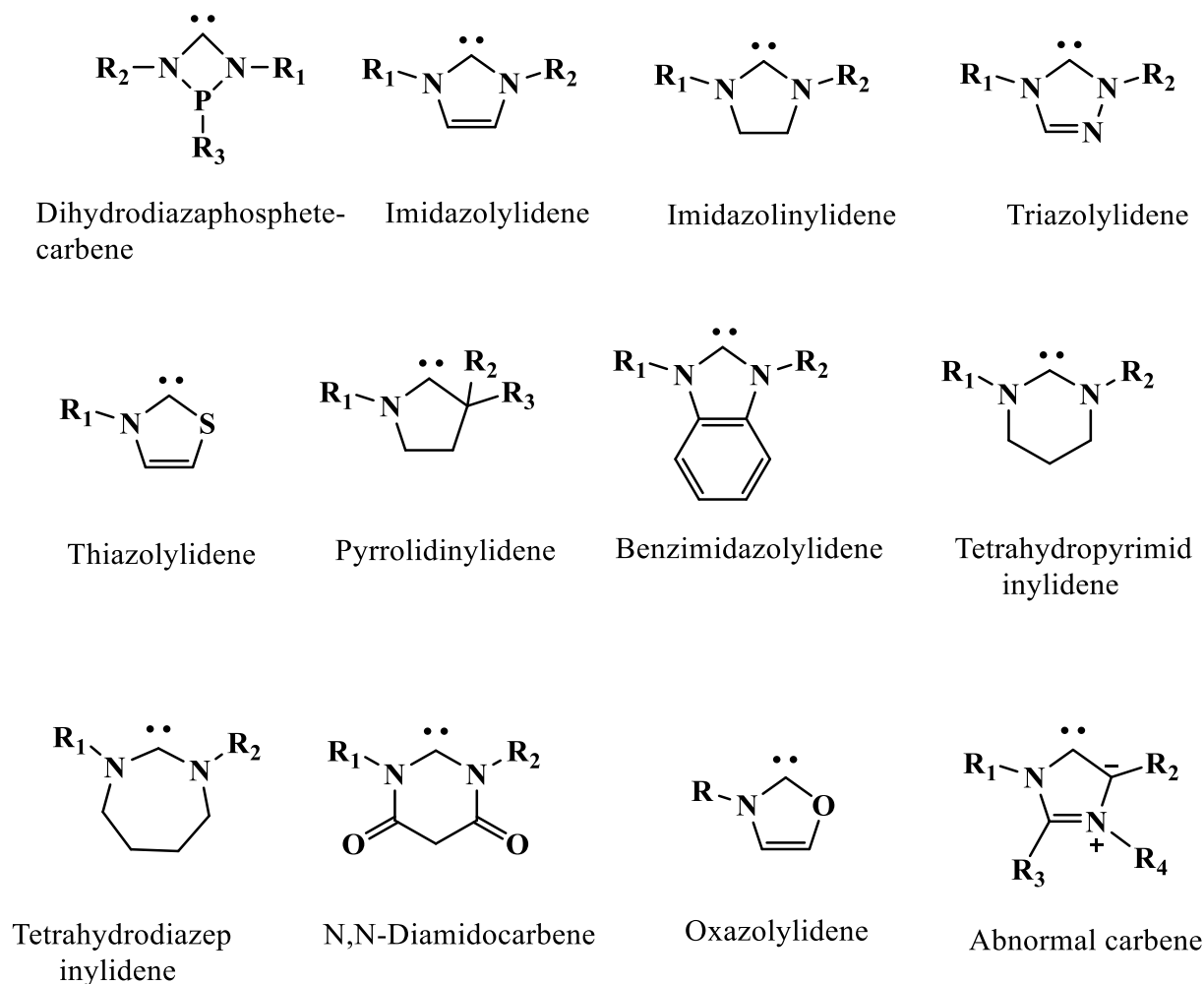
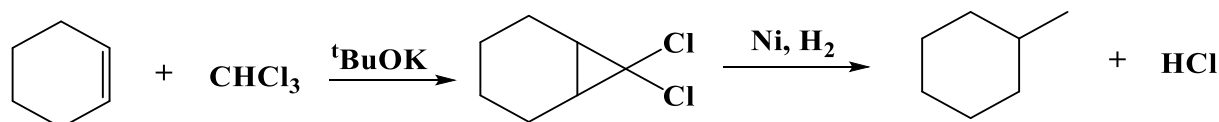


Figure 1.6: General structure of different classes of NHCs

1.3. How Carbenes Evolve from Mere Intermediate to an Important Auxiliary Ligand in Organometallics

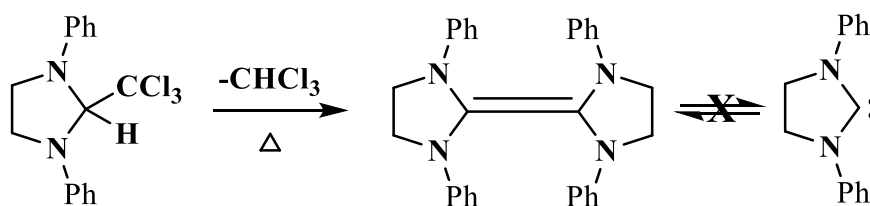
The first assumption of a carbene species was made in 1862 by A. Geuther when he suggested that the alkaline hydrolysis of chloroform proceeds via the formation of an intermediate with a divalent carbon called dichlorocarbene.²⁶ Later on, Eduard Buchner in 1903 theorised that cyclopropanation studies of ethyl diazoacetate with toluene proceeded through a carbene intermediate²⁷ and Hermann Staudinger in 1912 also arrived at the same conclusion when he converted alkenes to cyclopropanes with diazomethane.²⁸ These works did not change much about

the outlook of carbenes and up until the early 1950s, carbene moieties were regarded as diradicals and the methylene carbene was seen as a linear species, with two degenerate p-orbitals inevitably leading to a triplet state.²⁹ However, Doering and Hoffman changed this notion in 1954 when they substantiated the suggestion by Geuther, Buchner, Staudinger and others by proving beyond doubt the existence of a dichlorocarbene intermediate, in the first well defined cyclopropanation studies via the addition of chloroform to an alkene³⁰ (Scheme 1.1).



Scheme 1.1: Alkene methylation via a $:\text{CCl}_2$ intermediate

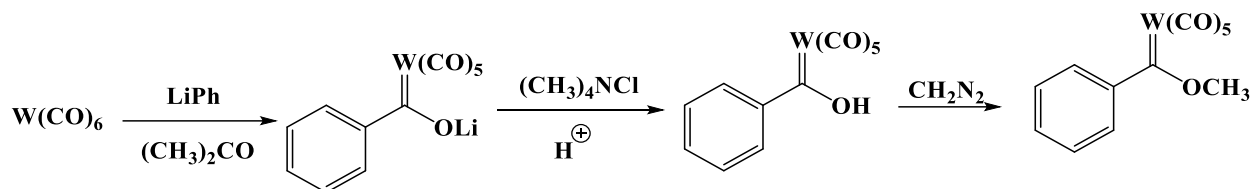
This prompted chemists to do more organic synthesis involving the use of methylene and had a closer look at this carbene intermediate.³¹⁻³³ Discussions about stable carbenes were initiated in 1960 by Wanzlick's report about the α -elimination of chloroform from 2-(trichloromethyl)-1,3-diphenylimidazolidine (Scheme 1.2). However, he was unable to isolate the postulated imidazolidin-2-ylidene (1,3-diphenylimidazolidine), instead, he isolated its dimer, the enetetraamine.³



Scheme 1.2: Failed attempt by Wanzlick to isolate a stable carbene

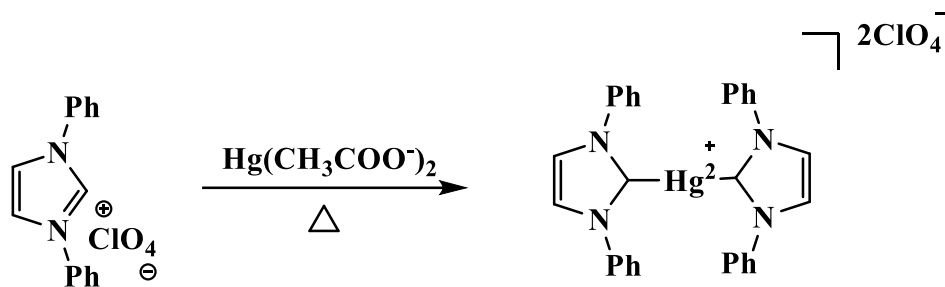
Fischer and his students in 1964 introduced carbenes into inorganic and organometallic chemistry and reported the first metal-carbene complex of tungsten(0) coordinated to methoxyphenyl methylene and five carbonyl group (Scheme 1.3).³⁴ The successful isolation and characterization

of a protected monomeric carbene by Fischer gave birth to a type of carbene known as “Fischer carbene”.



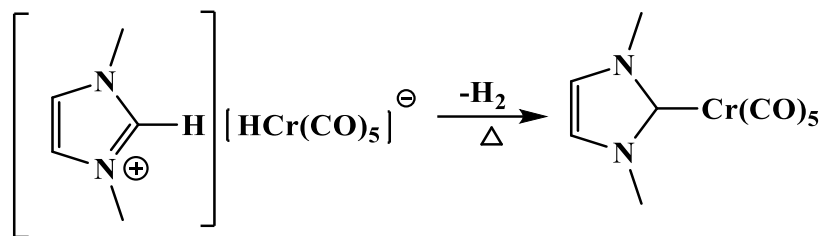
Scheme 1.3: Synthesis of the first metal–carbene complex

Motivated by the failed attempt to isolate a carbene, Wanzlick, in 1968 was able to stabilize unsaturated imidazol-2-ylidenes by deprotonation of 1,3-diphenylimidazolium perchlorate salt in the presence of a suitable coordinatively unsaturated metal complex. He treated the imidazolium salt with mercury(II) acetate to form the complex shown below (Scheme 1.4).³⁵



Scheme 1.4: 1,3-diphenylimidazolin-2-ylidene stabilized by mercury

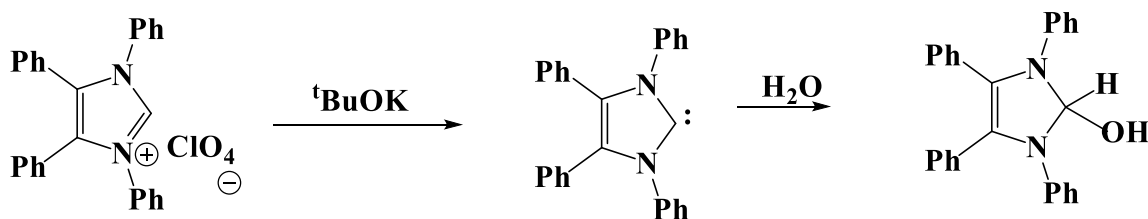
In the same year, Öfele also reported the stabilization of 1,3-dimethylimidazol-2-ylidene by heating dimethylimidazolium hydridopentacarbonylchromate(-II)³⁶ (Scheme 1.5).



Scheme 1.5: 1,3-dimethylimidazol-2-ylidene stabilized by chromium

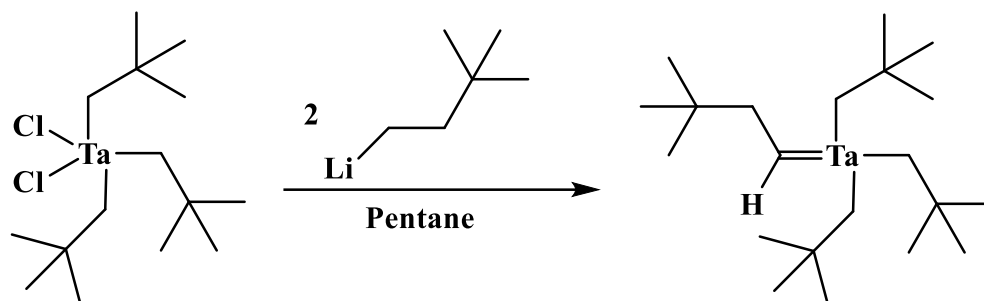
The outstanding feature in these two independent studies is that a ligand of the metal salt used acted as a base for the deprotonation of the imidazolium salt to the imidazol-2-ylidene after which coordination to the metal center stabilized it.³

In 1970, Wanzlick and co-workers, again, made another attempt at obtaining an isolable carbene by demonstrating that 1,3,4,5-tetraphenylimidazolium perchlorate could be deprotonated by potassium *tert*-butoxide to afford the corresponding imidazol-2-ylidene. Unfortunately, they were only able to trap it (Scheme 1.6).³⁷



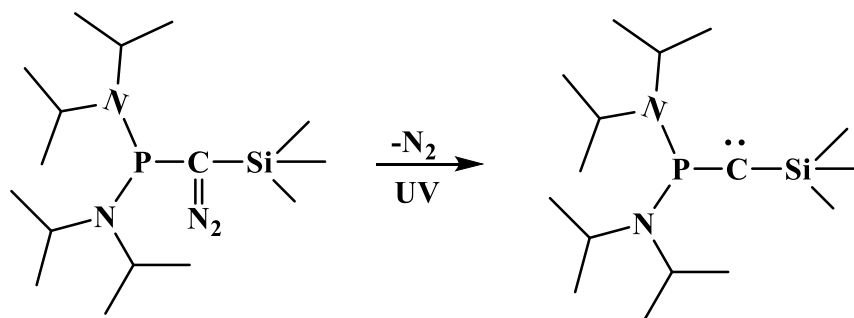
Scheme 1.6: Attempt by Wanzlick *et al.* to isolate a carbene

Schrock described the first synthesis of acyclic carbene stabilized by a high oxidation state (d^0) tantalum in 1974 by an α -hydrogen abstraction on the tris(2,2-dimethylpropyl)methyl tantalum(V) dichloride precursor (Scheme 1.7).³⁸ This success led to the so called “Schrock Carbene”.



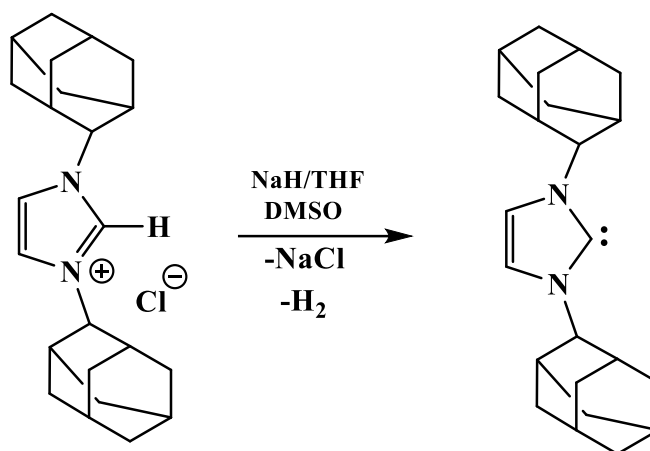
Scheme 1.7: Synthesis of the first acyclic carbene stabilized by tantalum

Fifteen years after the third attempt by Wanzlick to isolate a carbene, Bertrand and co-workers succeeded in isolating the first stable acyclic carbene in 1985 by photolysis of (trimethylsilyl)[bis(diisopropylamino)phosphino]diazomethane under vacuum to yield phosphorus vinyllylide-phosphaacetylene (Scheme 1.8). Unfortunately, the reported phosphine silyl carbene did not show any ability as a ligand for transition metals.^{39, 40}



Scheme 1.8: Synthesis of the first stable acyclic carbene by Bertrand *et al.*

Ultimately, Arduengo changed the course of history by opening access to free, isolable N-heterocyclic carbenes (NHCs) in 1991 following the principles laid down by Wanzlick. Arduengo and coworkers carried out the deprotonation reaction of sterically demanding substituted N,N'-diadamantyl imidazolium salt with sodium hydride and a catalytic amount of dimethyl sulfoxide (Scheme 1.9).⁴



Scheme 1.9: Synthesis of the first stable N-heterocyclic carbene by Arduengo *et al.*

As a result of the giant stride achieved by Arduengo, NHCs have been elevated from unisolable intermediates to compounds of enormous practical significance. The chemistry of stable carbenes has been enriched and more research is still being undertaken to unravel more information about their chemistry, physics, classification and applications.

1.4. Reactivity of N-Heterocyclic Carbenes

1.4.1. Basicity

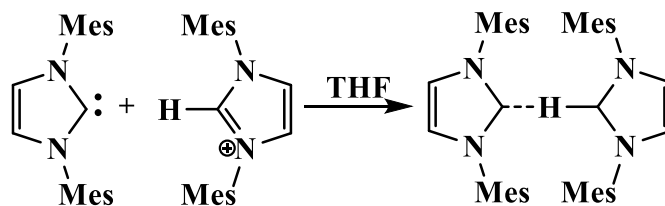
The pronounced basicity of N-heterocyclic carbene were confirmed by Alder *et al.*, and Kim and Streitweiser when they reported the pK_{a} s of 1,3-diisopropyl-4,5-dimethyl-imidazol-2-ylidene in DMSO and 1,3-di(*tert*butyl)imidazol-2-ylidene in THF as 24⁴¹ and 20⁴² respectively (Figure 1.7). These NHCs were found to be a much stronger base than 1,5-diazabicyclo[3.4.0]-non-5-ene (DBN), 1,8 diazabicyclo[5.4.0]undec-7-ene (DBU), and proton sponge (1,8-bis (dimethylamino) naphthalene).

1,3-diisopropyl-4,5-dimethyl
-imidazol-2-ylidene

1,3-di(tertbutyl)imidazol-2-ylidene

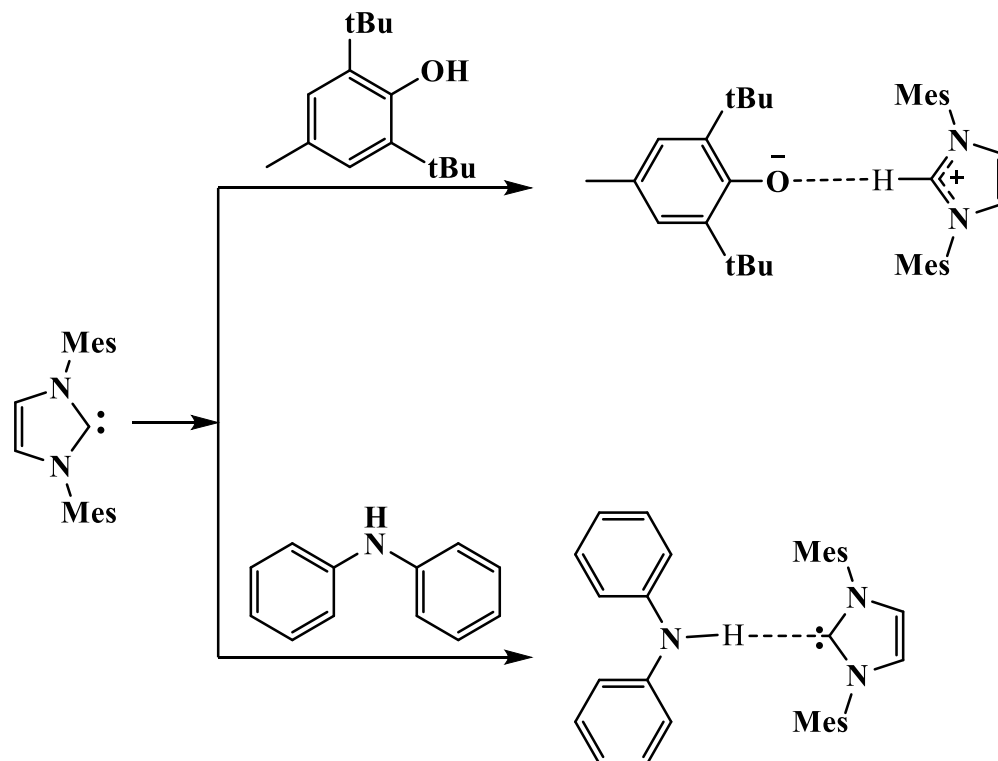
Figure 1.7: Structure of 1,3-diisopropyl-4,5-dimethyl-imidazol-2-ylidene and 1,3-di(tertbutyl)-imidazol-2-ylidene

The basicity of NHCs was evident when Arduengo *et al.* reacted 1,3-di(mesityl)imidazol-2-ylidene with 1,3-dimesitylimidazolium salt to form the bis(carbene)-proton complex with a rare 3-centre 4-electron C—H····C interaction (Scheme 1.10).⁴³ This unique C—H····C interaction suggests the potential of using carbenes to promote unusual interactions in the solid state.



Scheme 1.10: Synthesis of bis(carbene)—proton complex with 3-centre 4-electron C—H····C interaction by Arduengo *et al.*

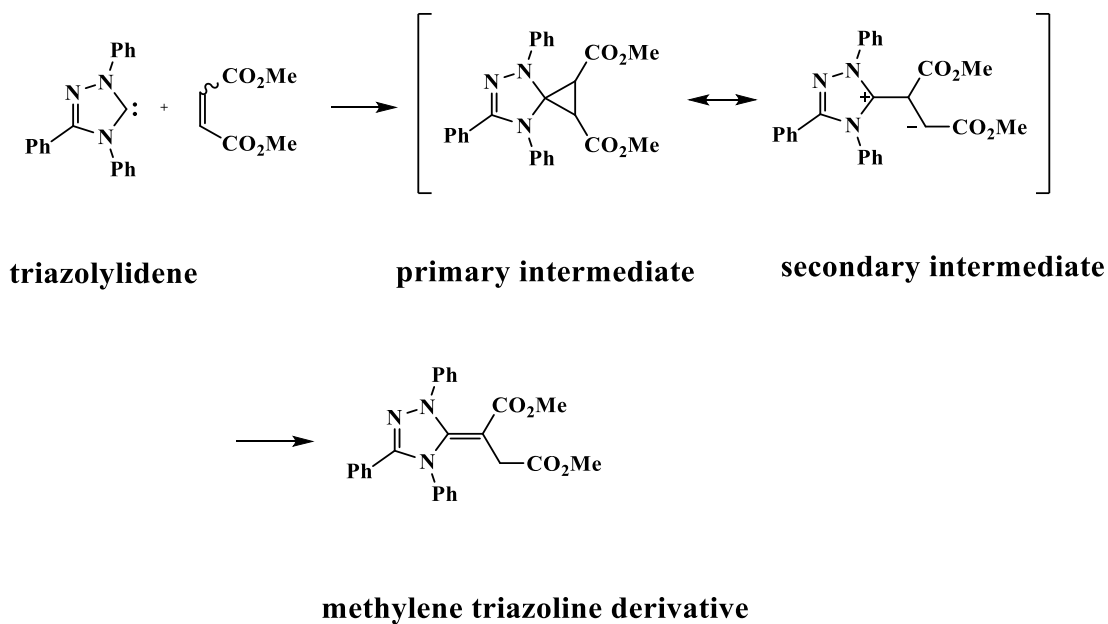
Fascinated by this development, Clyburne and coworkers in 2002 studied the interactions between organic substrates and carbenes with a view to synthesising and characterising NHC-organic substrate adducts with hydrogen bonded center with C—H····O and C····H—N interactions. They observed that 2,6-di-tert-butyl-4-methylphenol protonated 1,3-dimesitylimidazol-2-ylidene to form an imidazolium-aryloxide adduct with a hydrogen bonded center which contains unusually short C—H····O interactions in the solid state (Scheme 1.11).⁴⁴ A neutral adduct with C····H—N interactions was observed between diphenylamine and 1,3-dimesitylimidazol-2-ylidene (Scheme 1.11).



Scheme 1.11: Synthesis of bis(carbene)—proton complexes with C—H••••O and C••••H—N interactions by Clyburne *et al.*

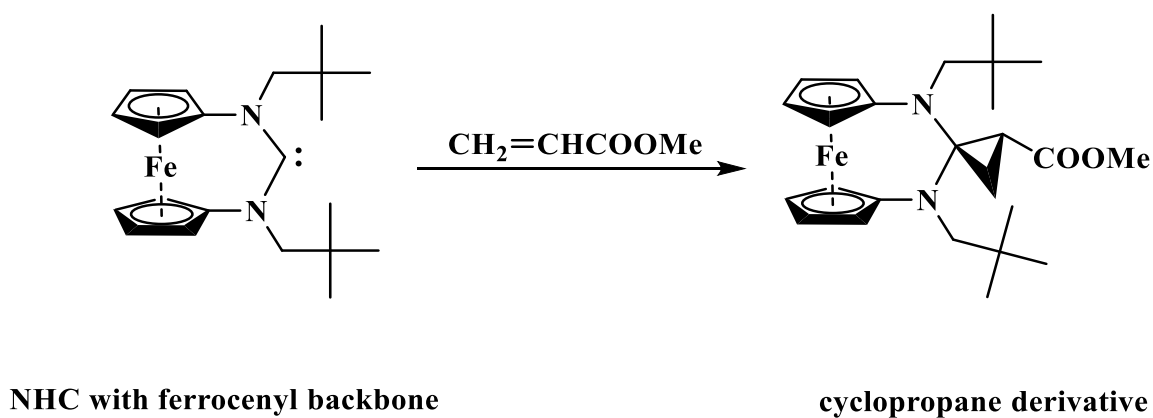
1.4.2. Towards C=C Multiple Bonds

The ability of NHCs to participate as reactants towards a variety of electrophilic species, leading to novel molecular frameworks offers promise for their use in organic synthesis. The reactivity of stable NHCs towards electron deficient C=C multiple bonds has been studied by Enders and co-workers. They found that triazolylidenes reacted with dimethyl fumarate to give methylene triazoline derivatives. According to them, the initial event involves the formation of a primary intermediate by [2+1] cycloaddition of the carbene with the alkene to form the cyclopropane derivative, which undergoes rapid ring opening to afford the zwitterionic secondary intermediate. Subsequent [1,2]-hydrogen shift affords the methylene triazoline derivative (Scheme 1.12).⁵



Scheme 1.12: Reactivity of stable NHCs towards C=C multiple bonds

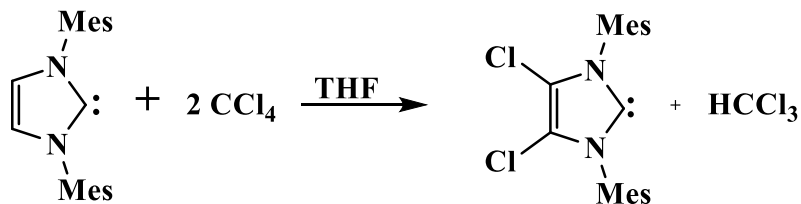
Frenking and coworkers also reacted an NHC with a ferrocenyl backbone with methyl acrylate and this time, the cyclopropane derivative seems to be very stable and it was the only product isolated (Scheme 1.13).⁴⁵



Scheme 1.13: Reactivity of a stable NHC with a ferrocenyl backbone towards C=C multiple bonds

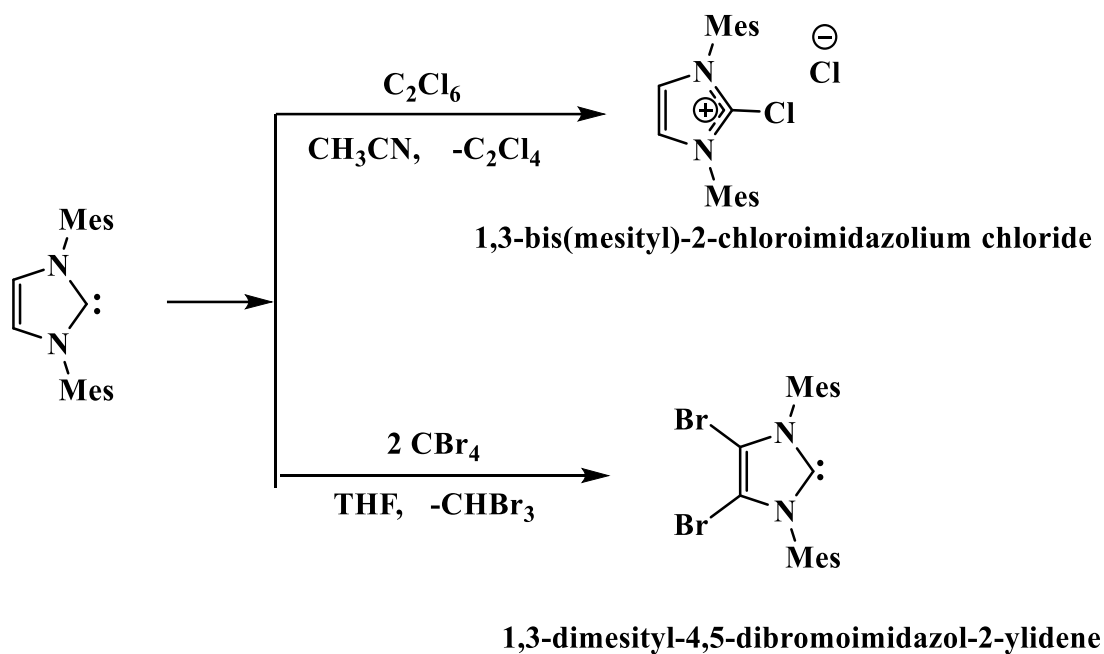
1.4.3. Towards Chlorinated Compounds

Arduengo et al. in 1997 reported the reactivity of NHCs towards chlorinated compounds. They observed that the reaction of 1,3-dimesitylimidazol-2-ylidene with carbon tetrachloride in tetrahydrofuran at room temperature gave another air-stable crystalline carbene, 1,3-dimesityl-4,5-dichloroimidazol-2-ylidene (Scheme 1.14).⁴⁶



Scheme 1.14: Reactivity of stable NHC towards chlorinated compounds reported by Arduengo et al.

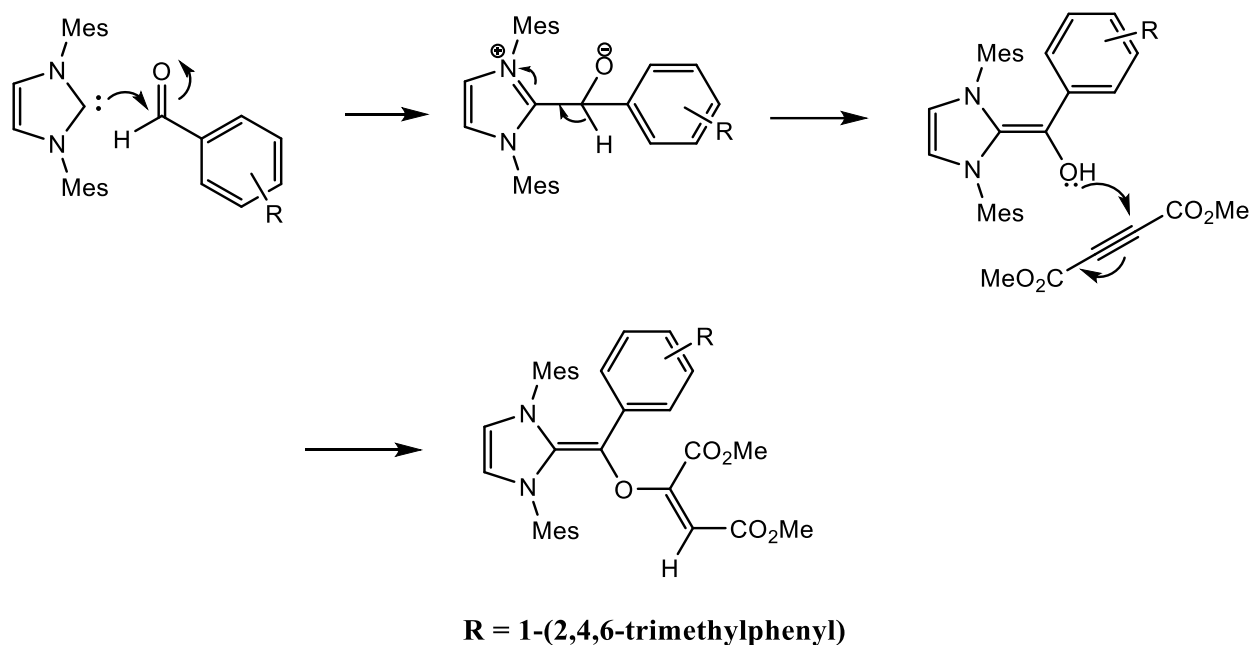
However, studies conducted by Junk and coworkers on the reactivity of NHCs towards chlorinated compounds raised doubts as to the specificity of the preparation of 1,3-dimesityl-4,5-dichloroimidazol-2-ylidene detailed by Arduengo et al.⁴⁶ using the route in Scheme 1.14. In their article published in 2002, the reaction shown in Scheme 1.14 proved difficult to control stoichiometrically, leading to the random formation of unidentified imidazolium by-products. In an attempt to further define the reactivity of NHCs towards halogen/halide containing reagents, Junk and coworkers reported the formation of the 1,3-bis(mesityl)-2-chloroimidazolium chloride, after reacting 1,3-dimesityl-imidazol-2-ylidene with hexachloroethane. Also, treatment of 1,3-dimesityl-imidazol-2-ylidene with 2 equivalent of CBr₄ in tetrahydrofuran or benzene gave a new air-stable 1,3-dimesityl-4,5-dibromoimidazol-2-ylidene (Scheme 1.15).⁴⁷



Scheme 1.15: Reactivity of an NHC towards chlorinated compounds reported by Junk et al.

1.4.4. Towards Aldehydes

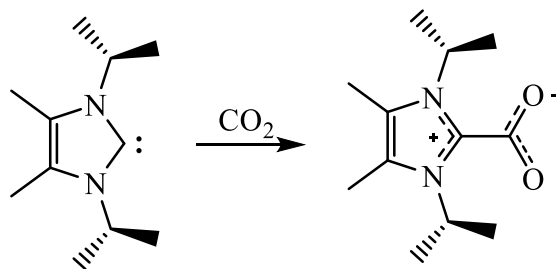
The reactivity of NHCs towards aldehydes was reported by Nair and coworkers when they investigated the participation of NHCs in multicomponent reactions. 1,3-dimesityl imidazol-2-ylidene was generated in situ by the reaction of 1,3-dimesityl-imidazolium chloride with NaH in THF under an argon atmosphere after which it was exposed to 3-nitrobenzaldehyde and dimethyl-acetylenedicarboxylate (DMAD). This reaction led to the exclusive formation of 2-oxy maleate derivative (Scheme 1.16).⁴⁸



Scheme 1.16: Reactivity of stable NHC towards aldehydes reported by Nair et al.

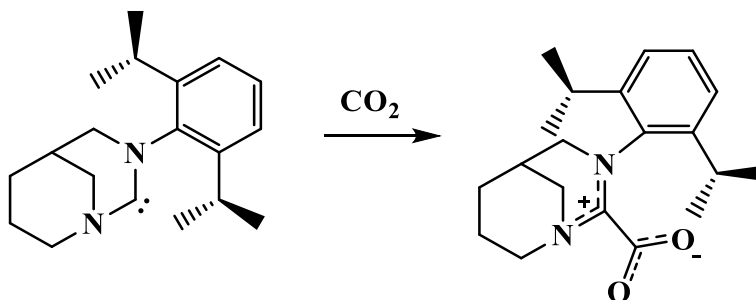
1.4.5. Towards CO₂ and CO

The direct reaction between NHCs and CO₂ otherwise known as CO₂ capture was first reported by Kuhn and coworkers in 1999. The direct carboxylation of 1,3-diisopropyl-4,5-dimethylimidazol-2-ylidene to yield imidazolium carboxylate, a betaine, was achieved for the first time (Scheme 1.17).⁴⁹



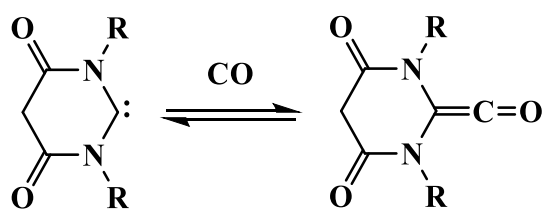
Scheme 1.17: Reactivity of a stable NHC towards CO₂ reported by Kuhn et al.

A similar reaction in which a free N-pyramidalised NHC was also used to capture CO₂ directly and was reported by Bertrand et al. in 2012 (Scheme 1.18).⁵⁰



Scheme 1.18: Reactivity of a stable NHC towards CO₂ reported by Bertrand et al.

NHCs have been adjudged to be insufficiently electrophilic enough to react with CO. However, their electronic structure can be tuned and this can be achieved by directing the nitrogen lone pair donation away from the empty p-orbital at the carbene carbon.⁴⁵ A good example of this electron tuning is found in diamidocarbenes in which the carbon next to the N-C-N frontier orbital is replaced by a carbonyl group. Belawski and coworkers achieved this feat by altering the electronic nature of NHC in their report on the synthesis of diamidocarbenes and their chemical reaction in which they observed that they can bind reversibly to CO to form ketene derivative.⁵¹

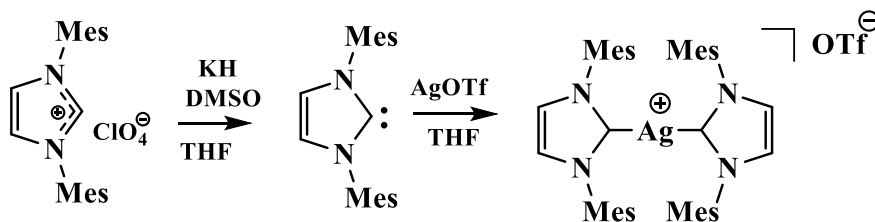


R = 2,6-diisopropylphenyl

Scheme 1.19: Reactivity of stable diamido-NHC towards CO reported by Belawski et al.

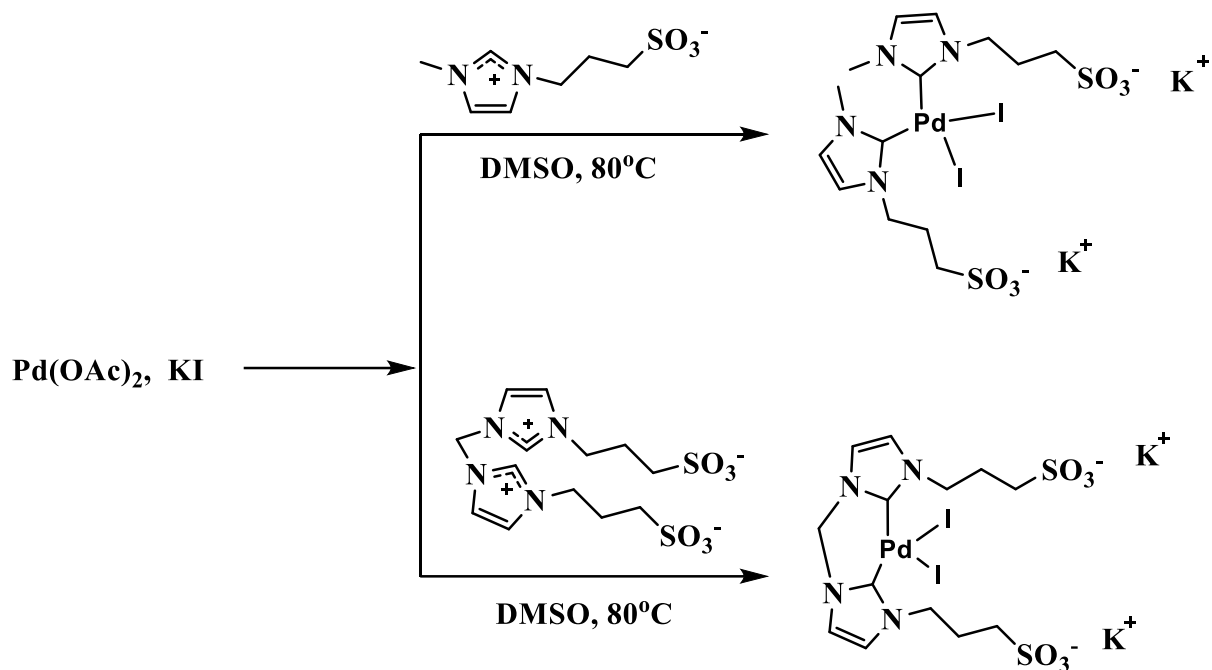
1.4.6. Towards Transition Metals

The strong σ -donor and comparatively weak π -acceptor properties of NHCs make them suitable as ligands for transition metals.² NHCs have become universal ligands in organometallic and inorganic coordination chemistry. They not only bind to any transition metal, be it in low or high oxidation states, but also to main group elements such as beryllium, sulfur, and iodine. Because of their specific coordination chemistry, NHCs can stabilize and activate metal centres. NHCs form intriguingly stable bonds with the majority of metals and similar bond dissociation energies have been observed for saturated and unsaturated N-heterocyclic carbenes of comparable steric demand.⁵²⁻⁵⁴ Arduengo *et. al.*, in 1993, synthesized the first Ag(I)-NHC from a free carbene route by deprotonating 1,3-dimesityl imidazolium salt with KH and subsequent reaction of the free carbene with AgO_3SCF_3 (Scheme 1.20).⁵⁵



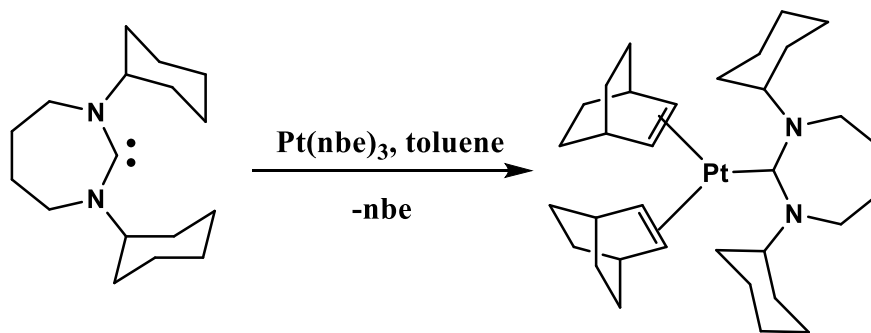
Scheme 1.20: Synthesis of the first Ag-NHC

Peris and coworkers in 2010 synthesised water soluble Pd-NHC complexes with sulfonate functionalized NHC ligands in which the ligands adopted a monodentate and bis-chelating coordination form. $\text{Pd}(\text{OAc})_2$ was used as the starting material and it is basic enough to deprotonate the proligands in situ and bind to the NHC generated afterwards (Scheme 1.21).⁵⁶



Scheme 1.21: Syntheses of $[\text{Pd}(\text{NHC})_2\text{I}_2]$ and $[\text{Pd}(\text{bisNHC})\text{I}_2]$ complexes

The first example of platinum(0)-diazepanilidene was reported by Fallis and coworkers in 2007. The 7-membered ring NHC was generated in situ by adding 1 equivalent of $\text{KN}(\text{SiMe}_3)_2$ to the precursor in toluene and subsequently adding platinum(0) trisnorbornene to form the corresponding air-sensitive monocarbene complex in Scheme 1.22.⁵⁷



Scheme 1.22: Synthesis of $[\text{Pt}(\text{NHC})(\text{nbe})_2]$

1.5. The Nature of the Metal-NHC Bond

The first examples of metal-NHC complexes were reported over 50 years ago, by Wanzlick³⁵ and Ofele³⁶ independently synthesizing imidazol-2-ylidene bearing mercury(II) and chromium(0). The preponderance of applications of NHCs is as ligands for transition metal centres. Therefore, understanding the dynamics of NHC bonding to metals and how it influences the properties of metal centres is of great importance. NHC ligands can bind to metal centres via dative coordination using the non-bonding pair of electrons.⁵⁸ The suitability of NHCs as ligands for transition metals can be rationalized by their inherent σ -donor ability with a formal sp^2 -hybridized lone pair available for donation into a σ -accepting orbital of the transition metal (Figure 1.8) and both π -back-bonding into the carbene p-orbital (Figure 1.9) and π -donation from the carbene p-orbital (Figure 1.10).^{7, 59}

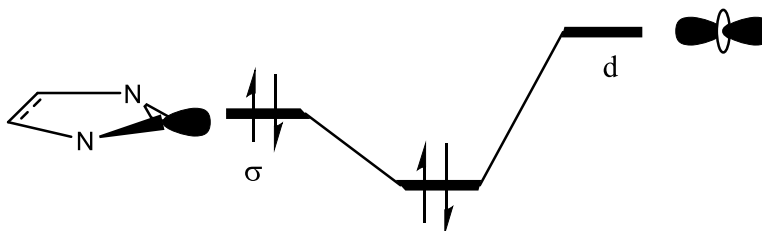


Figure 1.8: NHC \rightarrow M σ -donation

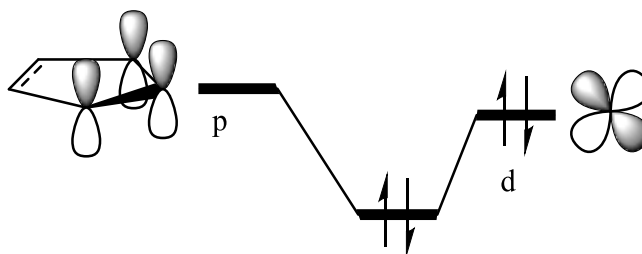


Figure 1.9: M \rightarrow NHC π^* -backdonation

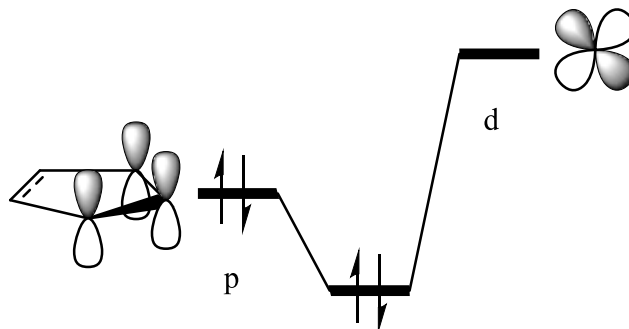


Figure 1.10: NHC \rightarrow M π -donation

The steric and electronic properties of NHCs have been found to have a great influence on the nature of adducts formed with transition metals. These two factors are at play in the excellent efficiency of Grubbs' second-generation olefin metathesis catalyst NHC–Ru(II) complex (Figure 1.11b) which was found to exhibit substantially greater thermal stability and remain catalytically active for cross- and ring-closing metathesis, and ring-opening metathesis polymerization (ROMP) reactions at much lower catalyst loadings compared to the first-generation Grubbs' catalyst (Figure 1.11a).^{60, 61}

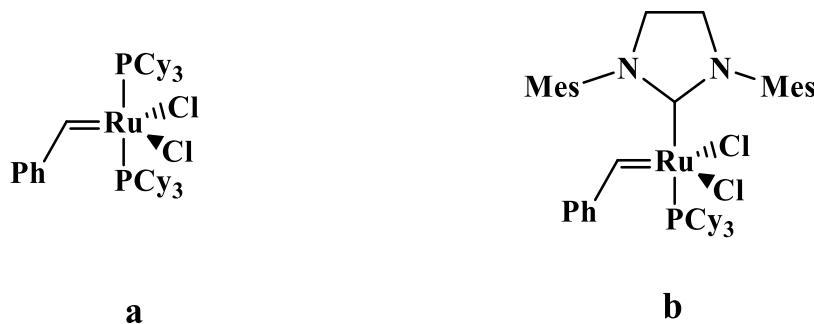


Figure 1.11: Grubbs' first- (a) and second-generation (b) olefin metathesis catalysts

Frenking and co-workers in 2004 investigated NHC–M–Cl systems of group 11 metals and observed an increase in the interaction energy in the order Ag < Cu < Au. About 75% of the attractive energy is attributed to the electrostatic contribution while π contribution to the total

orbital energy falls in the range 27–38%.⁶² In 2009, Nechaev et al. studied at the DFT level the electronic structure, thermodynamic stability and ligand properties of a series of NHC-Rh(CO)₂Cl complexes. They observed that the main structural feature influencing the properties of the NHCs is the number of nitrogen atoms bound to the carbene carbon and that a decrease in the number of nitrogen atoms leads to an increase in donor ability and ligand-to-metal bond strength but lowers the stability of the NHCs in the order shown in Figure 1.12.⁶³

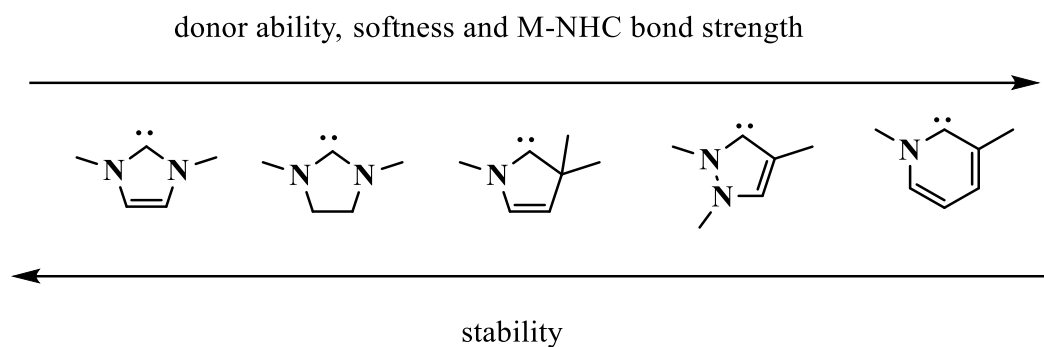
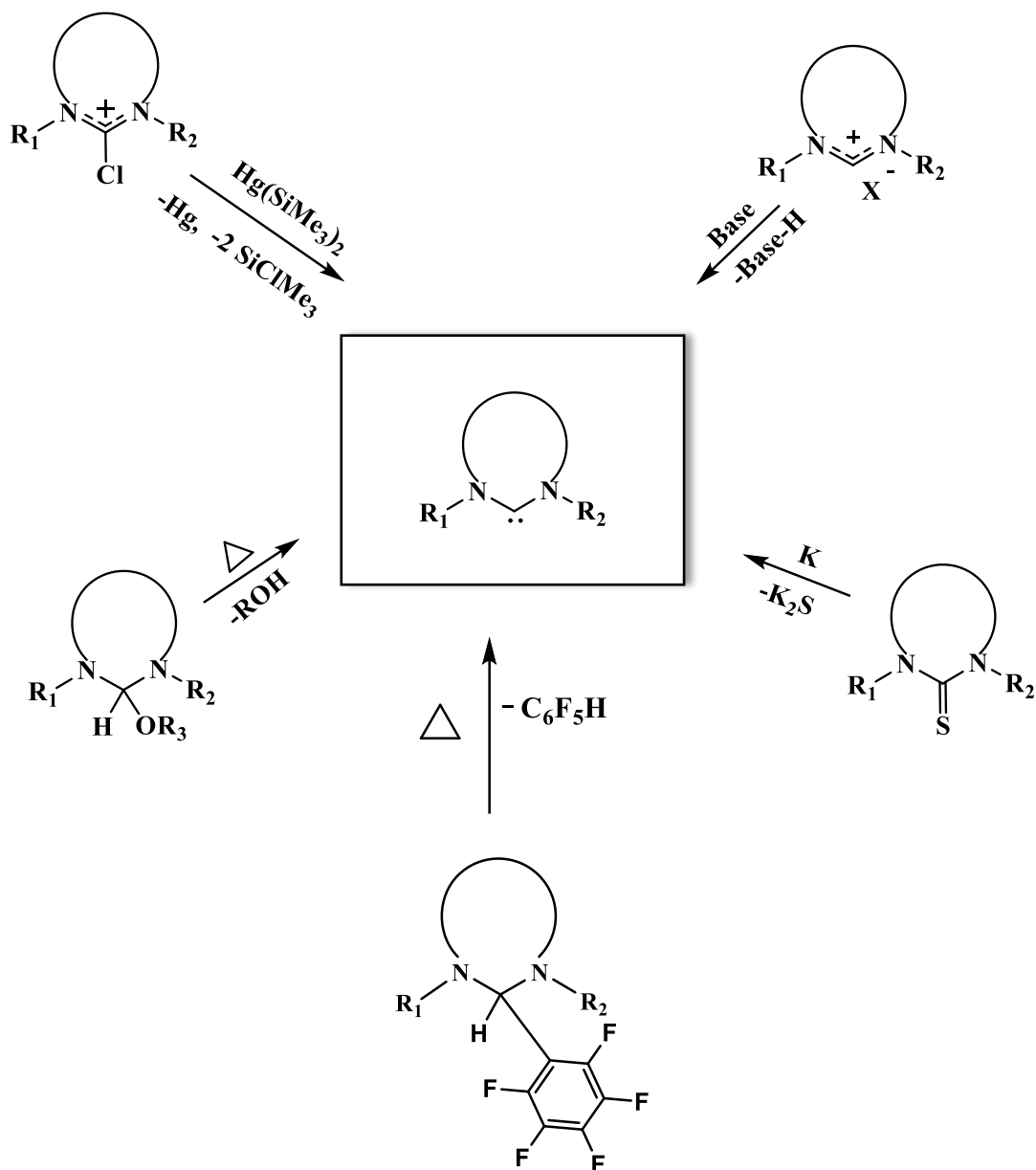


Figure 1.12: Arrangement of NHCs in order of their donor ability, softness, M-NHC bond strength and stability

1.6. Preparation of NHCs

In the majority of cases, NHCs are generated upon deprotonation of the corresponding heterocyclic azolium salts (Scheme 1.23) and as a result, synthetic routes to NHCs benefit from centuries of research on the preparation of heterocyclic compounds.⁶⁴ Other ways by which NHCs can be generated include: reduction of thiourea with molten potassium in boiling THF⁶⁵; vacuum pyrolysis of an NHC-volatile compound adduct (like MeOH, CHCl₃, CHF₃, C₆F₅H)⁶⁶; in situ release of NHC from NHC-CO₂ or NHC-metal (SnII, MgII, ZnII) adducts⁶⁷ and; reduction of a chloroformamidinium salt with Hg(TMS)₂⁶⁸ or with Pd(0) and Ni(0) complexes.⁶⁹



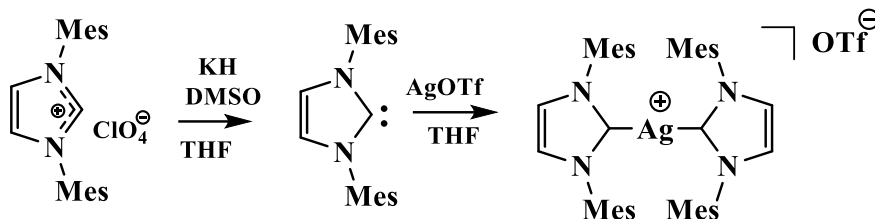
Scheme 1.23: Generation of NHCs from heterocyclic azolium precursors

1.7. Preparation of NHC-Metal Complexes

Transition metal complexes of NHCs can be prepared primarily in three ways: by the free carbene route; by reacting an NHC precursor with basic metal salts and; by carbene transfer.

1.7.1. By the Free Carbene Route

This method was first reported by Arduengo in 1993 after generating a free N,N-dimesityl imidazolium salt with potassium hydride and the subsequent reaction of the generated free NHC with silver triflate (Scheme 1.24) in THF afforded the Ag-NHC complex.⁵⁵

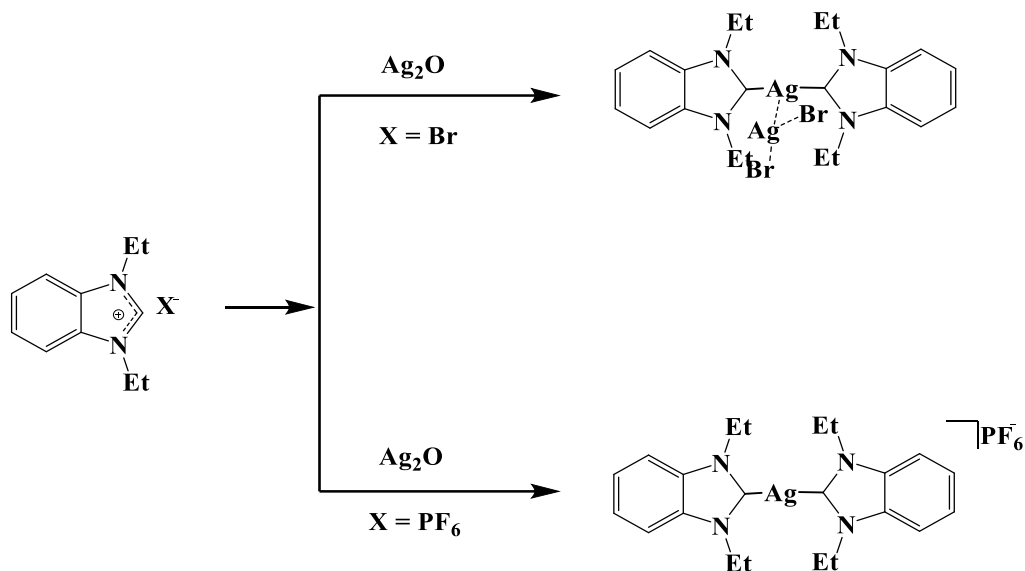


Scheme 1.24: Preparation of metal-NHC by the free carbene route

The laborious precautions required to synthesize free carbenes is a major setback for this method and most of the free carbenes generated are air-, moisture-, and temperature-sensitive.

1.7.2. By Reacting an NHC Precursor with Basic Metal Salts

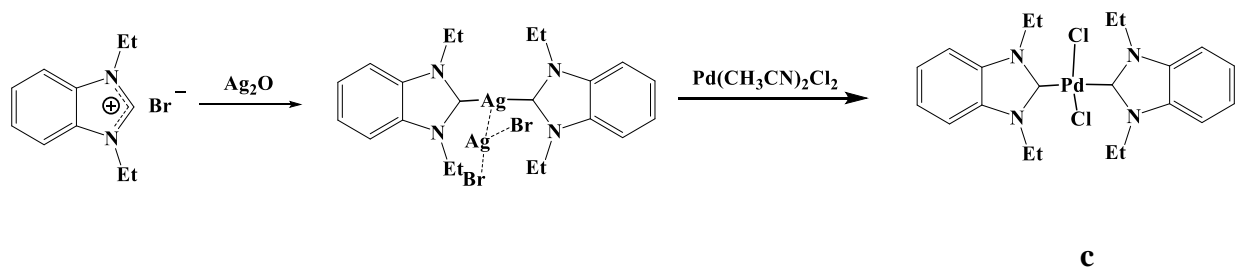
Wang and Lin in 1998, described a very convenient method of synthesising metal-NHC complexes simply by mixing an imidazolium salt with basic Ag_2O (Scheme 1.25). This method circumvents the difficulties arising from the employment of free and stable NHCs.⁷⁰ It featured several advantages and has been the most widely used method in the syntheses of N-heterocyclic carbene complexes of silver. Apart from Ag_2O , this procedure can be accomplished by AgOAc and Ag_2CO_3 as reported by Bertrand *et al.* (1997)⁷¹ and Danopoulos and co-workers (2000)⁷² respectively. In a related development, Danopoulos *et al.* reported for the first time the in-situ reaction of Cu_2O and N-heterocyclic carbenes in a manner similar to Ag_2O ⁷³ while Peris and coworkers prepared some water soluble Pd-NHC complexes using basic $\text{Pd}(\text{OAc})_2$ ⁵⁶ in 2001 and 2011 respectively.



Scheme 1.25: Preparation of metal-NHC by *in-situ* deprotonation

1.7.3. By Carbene Transfer Technique

In this technique, basic metals are used to deprotonate the azolium salts to produce a metal-NHC complex, after which transmetalation can be employed to transfer the ligand onto another metal centre to produce an analogous NHC complex of the desired metal. The first example of carbene transfer technique is shown in Scheme 1.126. Imidazolium salt is treated with silver(I) oxide, affording Ag(I)-NHC complex (with dibromoargentate(I) as counterion) after which the Ag(I)-NHC is mixed with bis(acetonitrile)palladium(II) chloride.^{70, 74} NHC transfer occurs within 30 min, affording NHC-Pd complex (c). In recent developments, Marc and Cazin (2010),⁷⁵ and Liu *et al* (2011)⁷⁶ reported the synthesis of metal NHC complexes via carbene transfer technique from copper-NHC and nickel-NHC adducts respectively.



Scheme 1.126: Preparation of Pd(II)-NHC (c) by carbene transfer technique

1.8. Applications of NHC-Metal Complexes

The flexible nature of the steric and electronic properties of NHCs and the thermal stability of metal–NHC complexes are attractive features that have led to the use of metal-NHCs as ancillary ligands in homogeneous transition-metal catalysis.² The use of transition metal complexes of NHCs for applications other than catalysis has been gaining attention in recent years.⁷⁷ Much of this interest stems from recent studies demonstrating the photophysics, chemotherapeutic and exceptional antimicrobial efficacy of these complexes against a broad spectrum of both gram-positive and gram-negative bacteria and fungi.⁷⁸⁻⁸² Among metal-NHC complexes, there is a growing interest in Ag(I)-NHC complexes, due to the rich history of silver for its antimicrobial properties and their application as carbene transfer agents in the synthesis of both transition and inner transition metal-NHC complexes.⁸³ Several authors have published many articles on the synthesis, characterisation and medicinal applications of coordination complexes derived from NHCs with emphasis on silver(I)- and gold(I)-NHC complexes. Dervisi *et al.* investigated the activity of cyanuric chloride-derived NHC-Ag(I) complex (d) (Figure 1.13) against methicillin-resistant *Staphylococcus aureus* (MRSA) NCTC 13277, *S. aureus* NCTC 6571, *Pseudomonas aeruginosa* NCTC 10662, and *Proteus mirabilis* NCTC 11938 and the fungal organism, *Candida albicans* ATCC 90028. Their result showed high activity against MRSA and moderate activity against all other tested microbes.⁷⁹

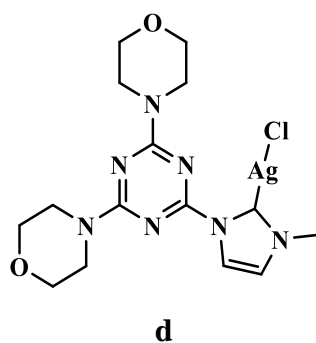


Figure 1.13: Cyanuric chloride-derived NHC-Ag(I) complex (d) by Dervisi *et al.*

The potential of NHC-Au(I) complexes to act as antiproliferative agent has been confirmed by many publications in peer review journals and recent developments in cancer chemotherapy has identified mitochondria as an important target in order to facilitate programmed cell death.^{2, 84, 85}

Due to the ease with which NHC ligands can be fine-tuned, the lipophilicity of the NHC-Au(I) can be modified by carefully selecting the substituents on the N in the heterocycle. This is crucial because anticancer activity is highly dependent on the ability to penetrate the mitochondrial membrane. Filipovska et al. in 2008 designed the NHC-Au(I) complexes in Figure 1.14 with the ability to target mitochondria and inhibit thioredoxin reductase selectively and hence, primarily induce apoptosis in cancer cells, but not normal cells.⁸⁶

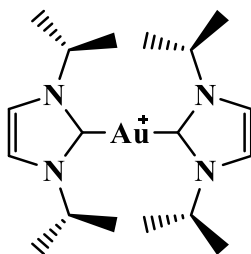


Figure 1.14: NHC-Au(I) chemotherapeutic agent designed by Filipovska et al.

One of the most useful techniques of preparing organosilicon compounds both in the laboratory and in the industry is the hydrosilylation reaction often catalysed by platinum(0) complexes. The hydrosilylation reaction is the addition of a Si-H bond in a hydrosilane to a C=C double bond of an alkene, C≡C triple bond of an alkyne or the C=O bond of an aldehyde or a ketone, C=N bond of an imine, or C≡N bond of a nitrile compound.⁸⁷ The two leading catalysts for this process are Speier's and Karstedt's catalysts. However, in spite of the high activities demonstrated by these catalysts, they have been found to be unstable and form colloidal platinum particles with undesired side reactions.⁸⁸ Cavell and coworkers reported a series of 6 and 7 membered Pt(II)-NHC complexes with enhanced stability and activity towards the hydrosilylation reaction. For example, the Pt(0)-NHC complex below was found to catalyse the hydrosilylation reaction between 1-octene and bis(trimethylsiloxy)methylsilane with yield and selectivity higher than that exhibited by Speier's and Karstedt catalysts.⁸⁹

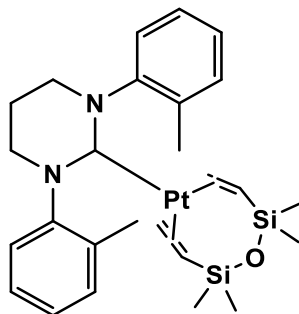


Figure 1.15: Chemical structure of Pt(0)-NHC by Cavell *et al.*

de Jesus and coworkers in 2012 prepared a water-soluble platinum(0) complex bearing an NHC with sulfonate functionality and divinyltetramethylsiloxane (dvtms) ligands (Figure 1.16) and it was found to be an active (94% isolated yield) and recyclable catalyst for the hydrosilylation of 1-octyne with triethylsilane at room temperature in water.⁹⁰

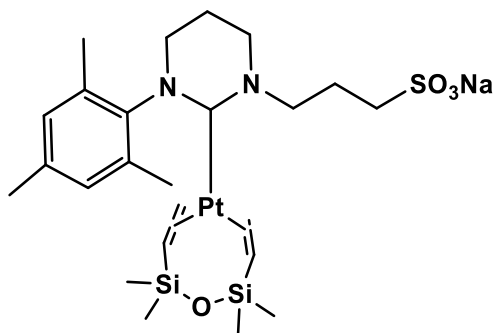


Figure 1.16: Chemical structure of Pt(0)-NHC by de Jesus *et al.*

The real challenge in the design of a given N-heterocyclic carbene rests on the construction of its precursor, whose architecture permits introduction of varying aryl/alkyl groups to achieve a specific design.

1.9. Surfactants and Metallosurfactants

Surface active agents comprise a fascinating class of molecules with exceptional structural features and their properties are determined by the forces acting on surfaces.⁹¹ Surfactants are amphiphilic in nature with dual characteristics of hydrophilicity and hydrophobicity.⁹² The polar portion that is hydrophilic exhibits a strong affinity or attraction towards polar solvents while the non-polar part termed hydrophobic gets attracted towards oil/non-polar solvents.⁹³ Surfactants can be classified into four broad categories: anionic surfactants, which give rise to a negatively charged surfactant ion upon dissolution in water and are widely used for laundering; cationic surfactants with positively charged head group are often used as emulsifying and bactericidal agents, amphoteric/zwitterionic surfactants contain two charged groups of different signs on the same molecule and are relatively mild and with good dermatological properties and lastly nonionic surfactants which contain hydrophilic groups that do not dissociate in water and are often used as drug delivery agents.⁹⁴ Apart from the regular surfactants with one hydrophilic head group and one hydrophobic tail, gemini surfactants with two hydrophilic head groups and two hydrophobic tails separated by covalent linkers per one molecule have equally been well studied for their unique features. Essentially, surfactants have been found to concentrate at interfaces and spontaneously form aggregates in solution of which the simplest form is called micelles. In micelles, polar head groups form an outer shell in contact with water, while nonpolar tails are secluded in the interior (Figure 1.17), hence, at the core of a micelle, is the assembly of long non-polar tails.⁹⁵ It is an important phenomenon since surfactant molecules behave very differently depending on whether they are present in micelles or as free monomers. The size of the micelle is measured by the aggregation number which is the number of surfactant molecules associated with a micelle and only surfactant monomers contribute to surface and interfacial tension lowering.⁹⁶ Furthermore, a new class of surfactants that has been found to exhibit features similar to conventional surfactants is metallosurfactant.⁹¹ Metallosurfactants are a type of surfactants in which *d*- or *f*-block metal is integrated into the polar head group of the surface-active molecule. The integration of *d*- or *f*-block metal into a surface-active molecule leads to new functionality, such as catalytic activity, to be concentrated at interfaces⁹⁷ and metallosurfactants are beginning to find application in, magnetic resonance imaging, templating of mesoporous materials, thin-film optoelectronics, interfacial photophysics, and homogeneous catalysis.^{98,99}

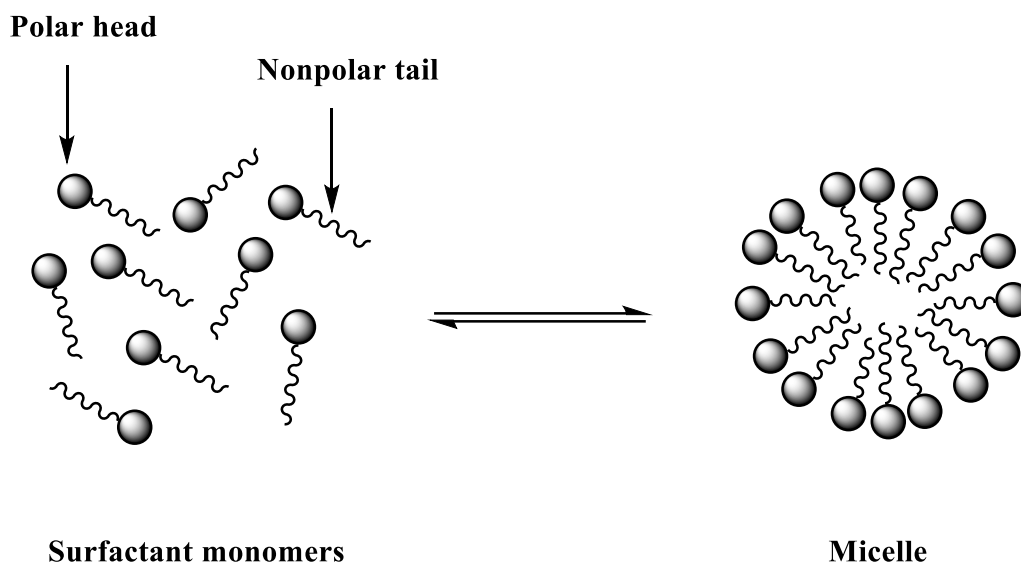


Figure 1.17: Structure of surfactant monomers and micelle

The design strategies of metal complexes and the ligands bonded to them have become important and the use of multifunctional ligands that adequately bind metal ions with specific features that could enhance the efficacy of metal complexes towards specific applications beyond features like oxidation state stability, modification of reactivity and substitution inertness offer many exciting possibilities.

1.10. Aims and Objectives of this Work

The aim of this project was to synthesise monocationic, dicationic and zwitterionic amphiphilic imidazolium salts bearing different water loving head groups and hydrophobic hydrocarbon chains ranging from 8 – 16 carbon atoms and the tethering of the monocationic and dicationic salts to Ag(I) and the zwitterionic salt to Pt(II) centres respectively by deprotonation of the acidic hydrogen. The imidazolium salts used in this work have been designed specifically to be amphiphilic with a hydrophilic head group made up of methyl-imidazole, mesityl-imidazole, propylsulfonate-imidazole, methyl-imidazole-tethered-to-imidazole, mesityl-imidazole-tethered-to-imidazole head groups and alkyl group with varying chain length as the hydrophobic tail and these salts served as precursors to the ligand system used in this study, N-heterocyclic carbenes.

The first part of this work is on the synthesis of novel Ag(I)-NHC complexes derived from amphiphilic precursors and their application as antimicrobial agents *in vitro* against planktonic and biofilm cells. One of the advantages of using these Ag(I)-NHCs as antimicrobials is that the NHC precursors (surface active quaternary ammonium ions) and silver(I) ion tethered to each of them are both active biologically. We hope that this multi-component system would offer the advantage to rapidly ‘dial’ new antibiotics, with the clinical advantage of a drug technology to which the acquisition of resistance by target pathogens would be inherently difficult. The design, synthesis, characterization and catalytic activity (hydrosilylation) in water of novel Pt(II)-NHC metallosurfactants form the second part of this project.

1.11. References

1. W. A. Herrmann and C. Koecher, *Angew. Chem. Int. Ed.*, 1997, **36**, 2162-2187.
2. M. N. Hopkinson, C. Richter, M. Schedler and F. Glorius, *Nature*, 2014, **510**, 485-496.
3. F. E. Hahn and M. C. Jahnke, *Angew. Chem. Int. Ed.*, 2008, **47**, 3122-3172.
4. A. J. Arduengo, R. L. Harlow and M. Kline, *J. Am. Chem. Soc.*, 1991, **113**, 361-363.
5. D. Enders, K. Breuer, G. Raabe, J. Runsink, J. H. Teles, J.-P. Melder, K. Ebel and S. Brode, *Angew. Chem. Int. Ed.*, 1995, **34**, 1021-1023.
6. J. W. Runyon, O. Steinhof, H. V. R. Dias, J. C. Calabrese, W. J. Marshall and A. J. Arduengo, *Aust. J. Chem.*, 2011, **64**, 1165.
7. A. J. Arduengo iii, H. V. R. Dias, R. L. Harlow and M. Kline, *J. Am. Chem. Soc.*, 1992, **114**, 5530-5534.
8. H. V. Huynh, Y. Han, R. Jothibasur and J. A. Yang, *Organometallics*, 2009, **28**, 5395-5404.
9. V. Sashuk, L. H. Peeck and H. Plenio, *Chem. - A Eur. J.*, 2010, **16**, 3983-3993.
10. C. A. Tolman, *Chem. Rev.*, 1977, **77**, 313-348.
11. A. R. Chianese, X. Li, M. C. Janzen, J. W. Faller and R. H. Crabtree, *Organometallics*, 2003, **22**, 1663-1667.
12. R. A. Kelly iii, H. Clavier, S. Giudice, N. M. Scott, E. D. Stevens, J. Bordner, I. Samardjiev, C. D. Hoff, L. Cavallo and S. P. Nolan, *Organometallics*, 2008, **27**, 202-210.
13. A. C. Hillier, W. J. Sommer, B. S. Yong, J. L. Petersen, L. Cavallo and S. P. Nolan, *Organometallics*, 2003, **22**, 4322-4326.
14. E. M. Higgins, J. A. Sherwood, A. G. Lindsay, J. Armstrong, R. S. Massey, R. W. Alder and A. C. O'Donoghue, *Chem. Commun.*, 2011, **47**, 1559-1561.

15. K. R. Sampford, J. L. Carden, E. B. Kidner, A. Berry, K. J. Cavell, D. M. Murphy, B. M. Kariuki and P. D. Newman, *Dalton Trans.*, 2019, **48**, 1850-1858.
16. E. Despagnet-Ayoub and R. H. Grubbs, *J. Am. Chem. Soc.*, 2004, **126**, 10198-10199.
17. M. Iglesias, D. J. Beetstra, J. C. Knight, L.-L. Ooi, A. Stasch, S. Coles, L. Male, M. B. Hursthouse, K. J. Cavell, A. Dervisi and I. A. Fallis, *Organometallics*, 2008, **27**, 3279-3289.
18. R. W. Alder, M. E. Blake, L. Chaker, J. N. Harvey, F. Paolini and J. Schütz, *Angew. Chem. Int. Ed.*, 2004, **43**, 5896-5911.
19. J. P. Moerdyk and C. W. Bielawski, *Organometallics*, 2011, **30**, 2278-2284.
20. K. F. Donnelly, A. Petronilho and M. Albrecht, *Chem. Commun.*, 2013, **49**, 1145-1159.
21. D. Enders and H. Gielen, *J. Organomet. Chem.*, 2001, **617-618**, 70-80.
22. A. L. Schöffler, A. Makarem, F. Rominger and B. F. Straub, *Beilstein J. Org. Chem.*, 2016, **12**, 1566-1572.
23. V. Lavallo, Y. Canac, C. Präsang, B. Donnadieu and G. Bertrand, *Angew. Chem. Int. Ed.*, 2005, **44**, 5705-5709.
24. X. Zhang, S. Gu, Q. Xia and W. Chen, *J. Organomet. Chem.*, 2009, **694**, 2359-2367.
25. A. Krüger, L. J. L. Häller, H. Müller-Bunz, O. Serada, A. Neels, S. A. Macgregor and M. Albrecht, *Dalton Trans.*, 2011, **40**, 9911-9920.
26. P. de Frémont, N. M. Scott, E. D. Stevens, T. Ramnial, O. C. Lightbody, C. L. B. Macdonald, J. A. C. Clyburne, C. D. Abernethy and S. P. Nolan, *Organometallics*, 2005, **24**, 6301-6309.
27. E. Buchner and L. Feldmann, *Berichte Der Deut. Chem. Gesell.*, 1903, **36**, 3509-3517.
28. H. Staudinger and O. Kupfer, *Berichte Der Deut. Chem. Gesell.*, 1912, **45**, 501-509.

29. P. de Frémont, N. Marion and S. P. Nolan, *Coord. Chem. Rev.*, 2009, **253**, 862-892.
30. W. von E. Doering and A. K. Hoffmann, *J. Am. Chem. Soc.*, 1954, **76**, 6162-6165.
31. W. E. Parham and H. E. Reiff, *J. Am. Chem. Soc.*, 1955, **77**, 1177-1178.
32. W. E. Parham and R. R. Twelves, *J. Org. Chem.*, 1957, **22**, 730-734.
33. P. S. Skell and S. R. Sandler, *J. Am. Chem. Soc.*, 1958, **80**, 2024-2025.
34. E. O. Fischer and A. Maasbol, *Angew. Chem. Int. Edit.*, 1964, **3**, 580-&.
35. H. W. Wanzlick and Schonher.Hj, *Angew. Chem. Int. Edit.*, 1968, **7**, 141-&.
36. K. Ofele, *J. Organomet. Chem.*, 1968, **12**, P42-P48.
37. H. J. Schonherr and H. W. Wanzlick, *Liebigs Ann. Chem.*, 1970, **731**, 176-+.
38. R. R. Schrock, *J. Am. Chem. Soc.*, 1974, **96**, 6796-6797.
39. W. A. Herrmann, T. Weskamp and V. P. W. Böhm, Elsevier, 2001, pp. 1-69.
40. A. Igau, H. Grutzmacher, A. Baceiredo and G. Bertrand, *J. Am. Chem. Soc.*, 1988, **110**, 6463-6466.
41. R. W. Alder, P. R. Allen and S. J. Williams, *J. Am. Chem. Soc. Chem. Comm.*, 1995, 1267-1268.
42. Y.-J. Kim and A. Streitwieser, *J. Am. Chem. Soc.*, 2002, **124**, 5757-5761.
43. A. J. Arduengo, III, S. F. Gamper, M. Tamm, J. C. Calabrese, F. Davidson and H. A. Craig, *J. Am. Chem. Soc.*, 1995, **117**, 572-573.
44. J. A. Cowan, J. A. C. Clyburne, M. G. Davidson, R. L. W. Harris, J. A. K. Howard, P. Küpper, M. A. Leech and S. P. Richards, *Angew Chem. Int. Ed.*, 2002, **41**, 1432-1434.
45. U. Siemeling, C. Färber, C. Bruhn, M. Leibold, D. Selent, W. Baumann, M. von Hopffgarten, C. Goedecke and G. Frenking, *Chem. Sci.*, 2010, **1**, 697-704.

46. A. J. Arduengo, F. Davidson, H. V. R. Dias, J. R. Goerlich, D. Khasnis, W. J. Marshall and T. K. Prakasha, *J. Am. Chem. Soc.*, 1997, **119**, 12742-12749.
47. M. L. Cole, C. Jones and P. C. Junk, *New J. Chem.*, 2002, **26**, 1296-1303.
48. V. Nair, S. Bindu, V. Sreekumar and N. P. Rath, *Org. Lett.*, 2003, **5**, 665-667.
49. N. Kuhn, M. Steimann and G. Weyers, *Z. Naturforsch. B.*, 1999, **54**, 427-433.
50. D. Martin, N. Lassauque, B. Donnadiou and G. Bertrand, *Angew. Chem.*, 2012, **124**, 6276-6279.
51. T. W. Hudnall and C. W. Bielawski, *J. Am. Chem. Soc.*, 2009, **131**, 16039-16041.
52. S. H. Hong, M. W. Day and R. H. Grubbs, *J. Am. Chem. Soc.*, 2004, **126**, 7414-7415.
53. A. K. Chatterjee, J. P. Morgan, M. Scholl and R. H. Grubbs, *J. Am. Chem. Soc.*, 2000, **122**, 3783-3784.
54. F. Glorius, in *N-Heterocyclic Carbenes in Transition Metal Catalysis*, ed. F. Glorius, Springer Berlin Heidelberg, 2007, vol. 21, pp. 1-20.
55. A. J. Arduengo, H. V. R. Dias, J. C. Calabrese and F. Davidson, *Organometallics*, 1993, **12**, 3405-3409.
56. F. Godoy, C. Segarra, M. Poyatos and E. Peris, *Organometallics*, 2011, **30**, 684-688.
57. M. Iglesias, D. J. Beetstra, A. Stasch, P. N. Horton, M. B. Hursthouse, S. J. Coles, K. J. Cavell, A. Dervisi and I. A. Fallis, *Organometallics*, 2007, **26**, 4800-4809.
58. J. C. Garrison and W. J. Youngs, *Chem. Rev.*, 2005, **105**, 3978-4008.
59. H. Jacobsen, A. Correa, A. Poater, C. Costabile and L. Cavallo, *Coord. Chem. Rev.*, 2009, **253**, 687-703.
60. G. C. Vougioukalakis and R. H. Grubbs, *Chem. Rev.*, 2010, **110**, 1746-1787.

61. C. Samojłowicz, M. Bieniek and K. Grela, *Chem. Rev.*, 2009, **109**, 3708-3742.
62. D. Nemcsok, K. Wichmann and G. Frenking, *Organometallics*, 2004, **23**, 3640-3646.
63. A. A. Tukov, A. T. Normand and M. S. Nechaev, *Dalton Trans.*, 2009, 7015.
64. L. Benhamou, E. Chardon, G. Lavigne, S. Bellemin-Laponnaz and V. César, *Chem. Rev.*, 2011, **111**, 2705-2733.
65. M. K. Denk, A. Hezarkhani and F.-L. Zheng, *Eur. J. Inorg. Chem.*, 2007, **2007**, 3527-3534.
66. G. W. Nyce, S. Csihony, R. M. Waymouth and J. L. Hedrick, *Chem. - A Eur. J.*, 2004, **10**, 4073-4079.
67. B. Bantu, G. M. Pawar, U. Decker, K. Wurst, A. M. Schmidt and M. R. Buchmeiser, *Chem. - A Eur. J.*, 2009, **15**, 3103-3109.
68. M. Otto, S. Conejero, Y. Canac, V. D. Romanenko, V. Rudzevitch and G. Bertrand, *J. Am. Chem. Soc.*, 2004, **126**, 1016-1017.
69. D. Kremzow, G. Seidel, C. W. Lehmann and A. Fürstner, *Chem. - A Eur. J.*, 2005, **11**, 1833-1853.
70. H. M. J. Wang and I. J. B. Lin, *Organometallics*, 1998, **17**, 972-975.
71. O. Guerret, S. Solé, H. Gornitzka, M. Teichert, G. Trinquier and G. Bertrand, *J. Am. Chem. Soc.*, 1997, **119**, 6668-6669.
72. A. A. D. Tulloch, A. A. Danopoulos, S. Winston, S. Kleinhenz and G. Eastham, *Journal of the Chemical Society, Dalton Trans.*, 2000, 4499-4506.
73. A. A. D. Tulloch, A. A. Danopoulos, S. Kleinhenz, M. E. Light, M. B. Hursthouse and G. Eastham, *Organometallics*, 2001, **20**, 2027-2031.
74. R.-Z. Ku, J.-C. Huang, J.-Y. Cho, F.-M. Kiang, K. R. Reddy, Y.-C. Chen, K.-J. Lee, J.-H. Lee, G.-H. Lee, S.-M. Peng and S.-T. Liu, *Organometallics*, 1999, **18**, 2145-2154.

75. M. R. L. Furst and C. S. J. Cazin, *Chem. Comm.*, 2010, **46**, 6924-6925.
76. B. Liu, X. Liu, C. Chen, C. Chen and W. Chen, *Organometallics*, 2012, **31**, 282-288.
77. K. M. Hindi, M. J. Panzner, C. A. Tessier, C. L. Cannon and W. J. Youngs, *Chem. Rev.*, 2009, **109**, 3859-3884.
78. M. J. Panzner, K. M. Hindi, B. D. Wright, J. B. Taylor, D. S. Han, W. J. Youngs and C. L. Cannon, *Dalton Trans.*, 2009, 7308-7313.
79. F. Almalioti, J. MacDougall, S. Hughes, M. M. Hasson, R. L. Jenkins, B. D. Ward, G. J. Tizzard, S. J. Coles, D. W. Williams, S. Bamford, I. A. Fallis and A. Dervisi, *Dalton Trans.*, 2013, **42**, 12370-12380.
80. Y. Li, G.-F. Liu, C.-P. Tan, L.-N. Ji and Z.-W. Mao, *Metallomics*, 2014, **6**, 1460-1468.
81. A. Poethig and T. Strassner, *Organometallics*, 2011, **30**, 6674-6684.
82. Q.-X. Liu, F.-B. Xu, Q.-S. Li, X.-S. Zeng, X.-B. Leng, Y. L. Chou and Z.-Z. Zhang, *Organometallics*, 2003, **22**, 309-314.
83. B. D. Wright, P. N. Shah, L. J. McDonald, M. L. Shaeffer, P. O. Wagers, M. J. Panzner, J. Smolen, J. Tagaev, C. A. Tessier, C. L. Cannon and W. J. Youngs, *Dalton Trans.*, 2012, **41**, 6500-6506.
84. D. R. Green, *Science*, 2004, **305**, 626-629.
85. M. Porchia, M. Pellei, M. Marinelli, F. Tisato, F. Del Bello and C. Santini, *European J. Med. Chem.*, 2018, **146**, 709-746.
86. J. L. Hickey, R. A. Ruhayel, P. J. Barnard, M. V. Baker, S. J. Berners-Price and A. Filipovska, *J. Am. Chem. Soc.*, 2008, **130**, 12570-12571.
87. B. Marciniec, *Silicon Chem.*, 2002, **1**, 155-174.
88. I. E. Markó, S. Stérin, O. Buisine, G. Mignani, P. Branlard, B. Tinant and J.-P. Declercq, *Science*, 2002, **298**, 204-206.

89. J. J. Dunsford, K. J. Cavell and B. Kariuki, *J. Organomet. Chem.*, 2011, **696**, 188-194.
90. G. F. Silbestri, J. C. Flores and E. de Jesús, *Organometallics*, 2012, **31**, 3355-3360.
91. P. C. Griffiths, I. A. Fallis, C. James, I. R. Morgan, G. Brett, R. K. Heenan, R. Schweins, I. Grillo and A. Paul, *Soft Matt.*, 2010, **6**, 1981-1989.
92. T. R. Neu, *Microbiol. Rev.*, 1996, **60**, 151-166.
93. V. P. Torchilin, *J. Controll. Rel.*, 2001, **73**, 137-172.
94. T. Tadros, in *Encyclopedia of Colloid and Interface Science*, ed. T. Tadros, Springer Berlin Heidelberg, Berlin, Heidelberg, 2013, pp. 1242-1290.
95. *Surfactants and polymers in aqueous solution*, John Wiley & Sons, Chichester, West Sussex, England ; Hoboken, NJ, 2nd edn., 2003, 1-61.
96. Z. J. Yu and G. Xu, *J. Phy. Chem.*, 1989, **93**, 7441-7445.
97. P. C. Griffiths, I. A. Fallis, T. Tatchell, L. Bushby and A. Beeby, *Adv. Coll. Interf. Sci.*, 2008, **144**, 13-23.
98. I. A. Fallis, P. C. Griffiths, T. Cosgrove, C. A. Dreiss, N. Govan, R. K. Heenan, I. Holden, R. L. Jenkins, S. J. Mitchell, S. Notman, J. A. Platts, J. Riches and T. Tatchell, *J. Am. Chem. Soc.*, 2009, **131**, 9746-9755.
99. R. W. Hay, N. Govan and K. E. Parchment, *Inorg. Chem. Comm.*, 1998, **1**, 228-231.

Chapter

2

Synthesis of Surface-Active Imidazolium salts and the Evaluation of their Critical Micelle Concentrations

| | |
|---|-----------|
| 2.0. Synthesis of Surface-Active Imidazolium salts and the Evaluation of their Critical Micelle Concentration..... | 40 |
| 2.1. Introduction..... | 41 |
| 2.2. Strategy for Designing New Amphiphilic Imidazolium salts..... | 45 |
| 2.3. Aims..... | 46 |
| 2.4. Results and Discussion..... | 47 |
| 2.4.1. Synthesis of 1-methyl-3-alkyl-imidazolium bromide (HL ₈₋₁₆)..... | 47 |
| 2.4.2. Synthesis of 1-(2,4,6-Trimethylphenyl)-1 <i>H</i> -Imidazole..... | 50 |
| 2.4.3. Synthesis of 1-mesityl-3-alkyl-imidazolium bromide (HL ^{mes} ₈₋₁₆)..... | 50 |
| 2.4.4. Synthesis of 3-(3-alkyl-imidazolium-1-yl)propanesulfonate (HL ^{bet} ₈₋₁₆)..... | 51 |
| 2.4.5. Synthesis of Gemini Amphiphilic Imidazolium Salts..... | 52 |
| 2.4.6. Determination of Critical Micelle Concentration (CMC)..... | 56 |
| 2.4.7. Structural effects of monocationic and dicationic ionic Surfactants on critical micelle concentration..... | 57 |
| 2.4.8. Comparison of Critical Micelle Concentration Values of Monocationic and Dicationic Surfactants..... | 58 |
| 2.5. Experimental..... | 59 |
| 2.6. References..... | 78 |

Chapter 2

Synthesis of Surface-Active Imidazolium Salts and the Evaluation of their Critical Micelle Concentrations

2.1. Introduction

One of the many ways by which imidazolium salts are prepared is by alkylation of the two nitrogen atoms in the heterocycle changing it into a discrete cation and anion pair. They have been given considerable interests in recent times for their versatile properties and wide and varying applications in chemistry as well as pharmacology.^{1,2} One of the most important and attractive properties of imidazolium salts is the flexibility in the design of the physical, chemical and biological properties by the independent modification of the features of the cation and anion moiety.³ Imidazolium-based cationic with five-membered ring can be selectively tailored/substituted at each of the N and C (backbone carbon) positions.⁴ Besides the regular imidazolium salts with one distinct imidazole and two substituents on the two nitrogen atoms, the imidazolium platform is amenable to the synthesis of Gemini salts with two tethered imidazolium cationic head groups.⁵ The general structures of the imidazolium salts synthesized for this work are shown below (Figures 2.1 and 2.2).

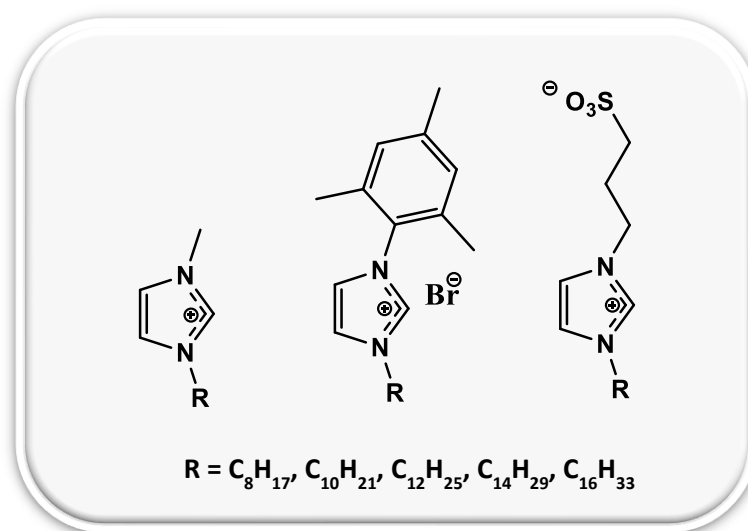


Figure 2.1: General structure of synthesized imidazolium salts

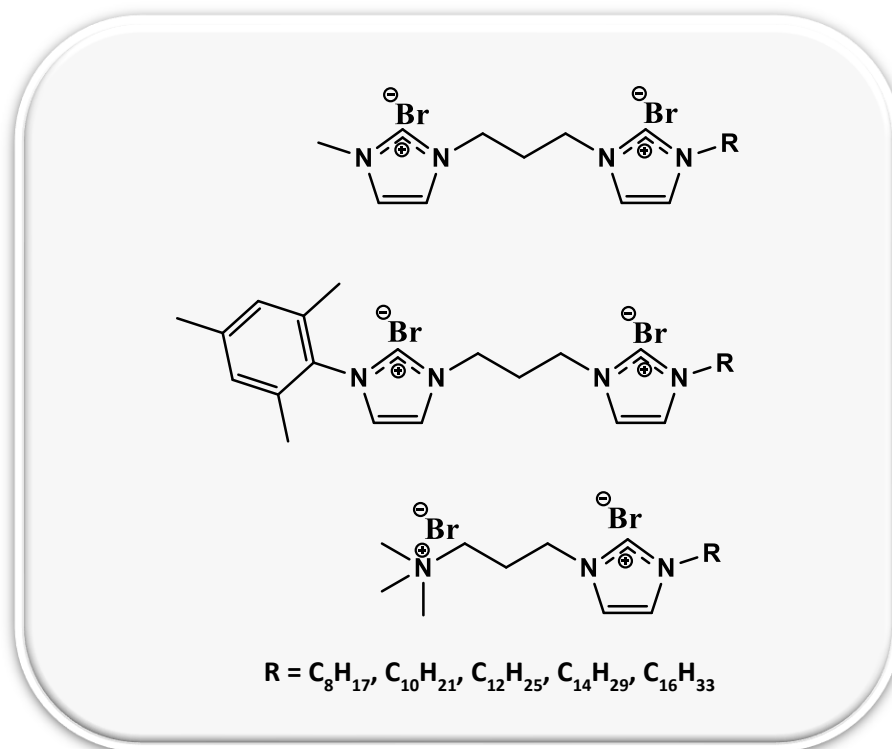


Figure 2.2: General structure of synthesised Gemini imidazolium salts

These imidazolium salts have been designed to be amphiphilic with a hydrophilic head group made up of the imidazole ring, and an alkyl group with varying chain length from 8 – 16 carbon atoms as the hydrophobic tail. Typically, an amphiphilic molecule consists of a polar hydrophilic group, usually called the head, joined to a nonpolar hydrophobic moiety called the tail. However, the number of the polar head(s) and of the hydrophobic tail(s) and the kind of tethering among them can vary, which leads to different classes of amphiphiles.

Generally, the specific design of the amphiphilic structure of imidazolium salts can be achieved with certain substitutions on the imidazole ring, consequently leading to a hydrophilic cation head and a hydrophobic tail, and this can result in neutral, cationic, anionic or amphoteric amphiphiles (Figure 2.3).⁶ Cationic surfactants offer a few additional advantages over other classes of surfactants and besides the fact that they are surface-active, they equally show antibacterial properties and are used as cationic softeners, lubricants, antistatic agents, etc.⁷

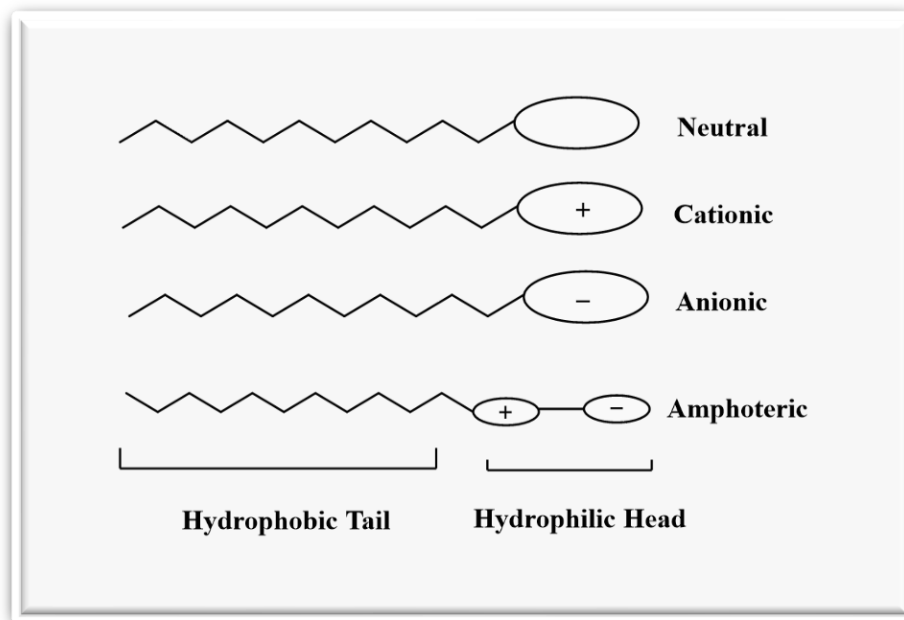


Figure 2.3: Depiction of neutral, anionic, cationic and amphoteric amphiphiles

Common amphiphiles are surfactants, such as detergents, soaps and fatty acids, or diglycerides, such as phospholipids, the latter being the main components of bio membranes. Surfactants (short for surface-active agents) are amphiphilic molecules that exhibit interfacial activity usually consisting in their ability to lower the surface tension of a liquid or the interfacial tension between two liquids of different polarity due to their property of accumulating at the interface.⁸ As a consequence of their double affinity, amphiphilic molecules self-organize in water to form assemblies in which the hydrophobic moieties are buried into the aggregate, shielded from the contact with water, while the hydrophilic groups remain exposed at the surface ensuring solubility (Figure 2.4a and 2.4b).

Two opposing forces are responsible for the formation of such assemblies. The hydrophobic effect drives the segregation of the hydrocarbon chains in water, thus providing the impetus for self-organization. On the other hand, repulsive forces and steric effects between the polar heads prevent the formation of large three-dimensional crystals and hence phase separation.⁹⁻¹¹

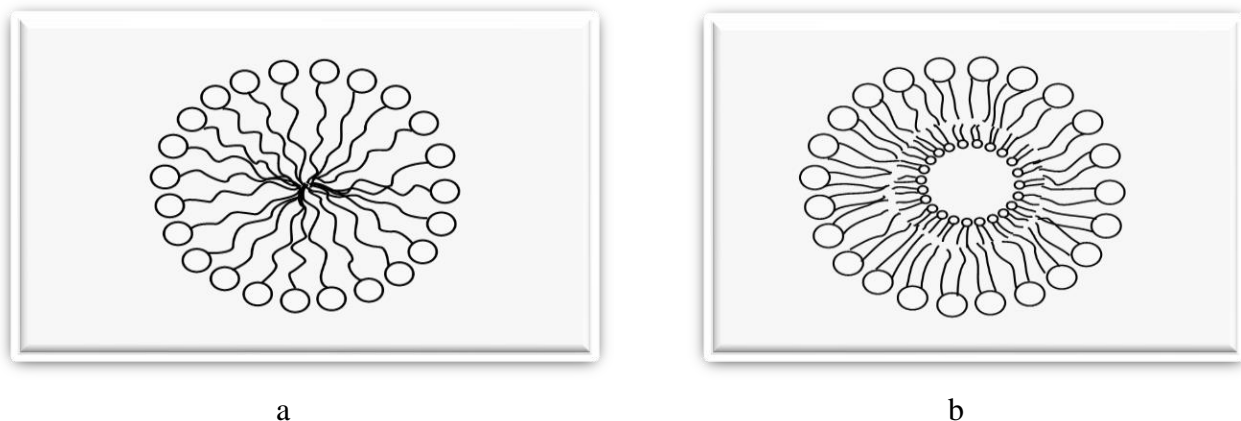
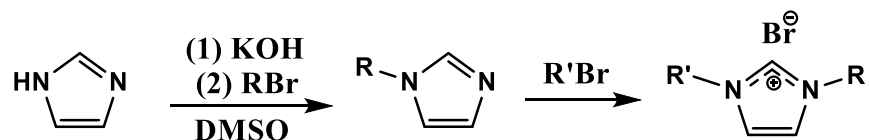


Figure 2.4: Amphiphile assemblies; a – Micelle, b – Vesicle

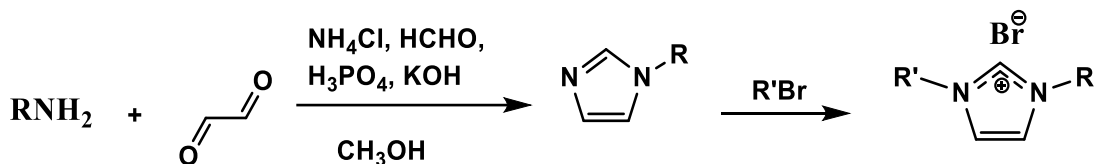
The self-assembly of amphiphilic molecules gives a rich variety of aggregates, and the aggregates formed depend on the molecular structure of the amphiphile and experimental conditions, such as concentration, temperature, pH and ionic strength.^{11, 12}

As enumerated in Chapter 1, imidazolium salts can be synthesized by the alkylation of imidazole to form a discrete cation and anion pair. Unsymmetrical imidazolium salts can be accessed by the deprotonation of imidazole with a strong base and the subsequent reaction with a suitable alkyl, acyl or benzyl halide, forming a 1-substituted imidazole. A second alkylation with a suitable alkyl, acyl or benzyl halide under reflux conditions yields the desired salts (Scheme 2.1) that can be easily purified by recrystallization.^{13, 14}



Scheme 2.1: Synthetic pathway to imidazolium salts

Furthermore, aryl/alkyl substituted imidazolium salts can also be made by the condensation of the appropriate primary amine with glyoxal followed by reaction with ammonium chloride (for unsymmetrical imidazolium salts) and paraformaldehyde to produce N-substituted imidazoles, after which nucleophilic addition with alkyl halide produces the desired imidazolium salts (Scheme 2.2).¹⁵



Scheme 2.2: Synthetic pathway to imidazolium salts

2.2. Strategy for Designing New Amphiphilic Imidazolium salts

Imidazolium salts have been studied extensively for their inherent properties and wide area of applications.^{1,2} In particular, amphiphilic imidazolium salts have been studied especially for their antimicrobial activity because they are water-soluble and can cross cell walls surrounding the outer sphere of bacteria and fungi. Their biological activities have been attributed partly to their lipophilicity, which correlates to the alkyl chain length and functionality of the cationic moiety.¹⁶⁻¹⁹ These attributes prompted us to develop new sets of cationic amphiphilic imidazolium salts that would act as proligands and as scaffolds about which new silver(I) N-heterocyclic carbene complexes have been assembled and the advantage of this system is that the amphiphilic imidazolium salts (proligands) and the silver ion are both active biologically.

The hydrophobic/lipophilic part of all the amphiphilic salts are made up of alkyl chains with carbon length ranging from 8 – 16 and with bromide ion as a counter anion (Figure 2.1 and 2.2). The structure and charges on the head group and the chain length of the tail were varied to study their effects on aggregate formation and their biological activity.

2.3. Aims

The aim of this chapter was to prepare amphiphilic imidazolium salts which will act as proligands towards the assembly of new metal-NHC complexes. The amphiphilic nature of the ligand systems will ensure their participation beyond acting as mere spectator ligand in order to create new multi-component metal complexes that can act as therapeutic agents against microbes and as catalysts in hydrosilylation reaction.

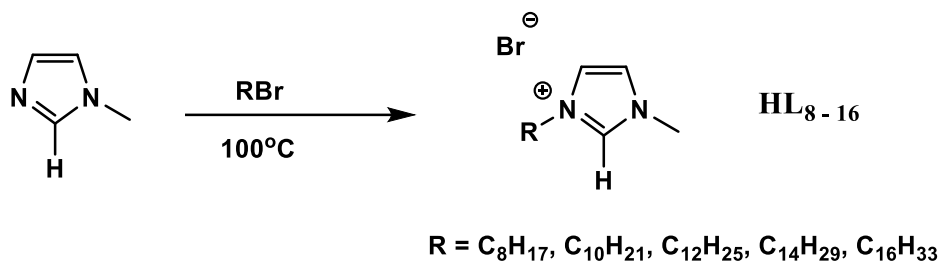
^1H and ^{13}C NMR spectroscopy and HRMS were used to provide structural characterisation. The ability to self-aggregate in aqueous solution was investigated and the concentrations at which these amphiphiles aggregate into organized molecular assemblies were determined by conductometric methods.

Lastly, in this chapter, the effect of the structure and charges on the head groups and the lipophilicity of the alkyl chains that make up the tails on aggregate formation were studied. The CMC Values of the monocationic and the dicationic amphiphiles were compared.

2.4. Results and Discussion

2.4.1. Synthesis of HL₈₋₁₆

The series of 1-methyl-3-alkyl-imidazolium bromide (**HL₈₋₁₆**) was synthesized in good yields as previously reported²⁰⁻²⁴ by reacting a long-chain alkyl bromide ($n = 8, 10, 12, 14,$ and 16) with methyl imidazole as outlined in Scheme 2.3.^{25, 26}



Scheme 2.3: Synthesis of **HL₈₋₁₆**

Pale yellow oils were obtained for **HL₈** and **HL₁₀** and off-white solids were obtained for **HL₁₂**, **HL₁₄** and **HL₁₆**. **HL₈** and **HL₁₀** were purified by partitioning methanol solution of the crude material with hexane in a separatory funnel to remove any unreacted alkyl halide (86 and 82% yield respectively) while **HL₁₂**, **HL₁₄** and **HL₁₆** were purified by recrystallisation from chloroform and diethyl ether with respective yields of 82, 91 and 93%. All the imidazolium salts dissolve well in water and lower alcohols and have moderate solubility in chlorinated solvents. These proligands have been characterised by ¹H and ¹³C NMR spectroscopy, high-resolution mass spectrometry (HRMS) and their Critical Micelle Concentrations (CMC) evaluated. The ¹H NMR chemical shifts of the C2–H protons of **HL₈₋₁₆** are in the range 10.29 – 10.51 ppm (Figure 2.5) which are consistent with the general C2-H acidic proton shift of imidazolium salts (δ 8 – 10 ppm) reported by Herrmann and Köcher²⁷ while the hydrogen on C4 and C5 appear between 7.3 – 7.59 ppm. The peaks between 3.94 and 4.32 ppm are for the methyl and methylene group attached to the N1 and N3 nitrogen atoms on the imidazole ring. The ¹³C NMR shifts of the N-C-N sp² carbon for the two salts appear in the range 137.64 – 138.17 ppm (Figure 2.6). The high-resolution HRMS data of **HL₈₋₁₆** show peaks corresponding to the cationic fragment [(M-Br)⁺].

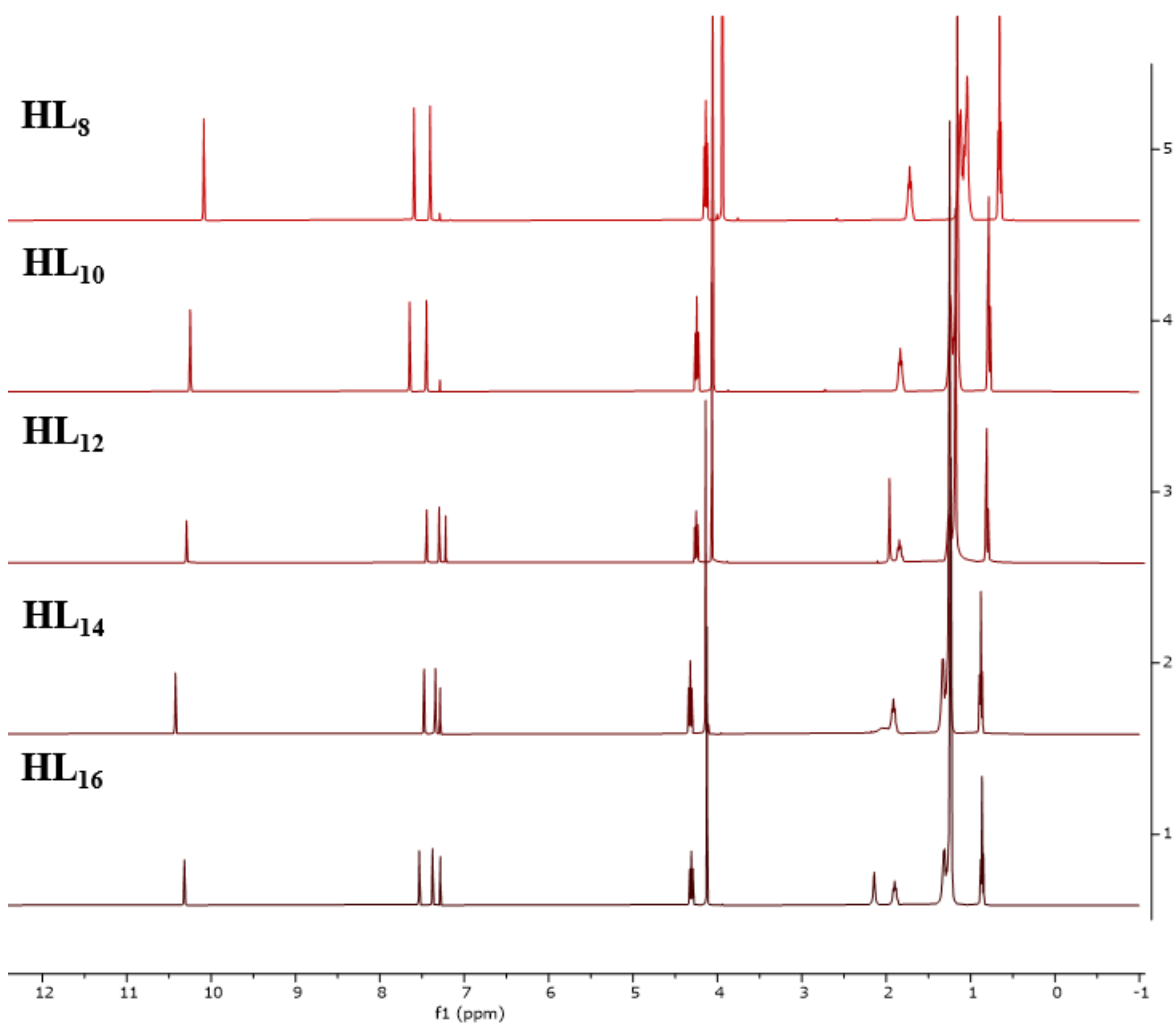


Figure 2.5: Stacked ¹H NMR spectra of HL₈₋₁₆ in CDCl₃ using Bruker 400 MHz spectrophotometer at room temperature

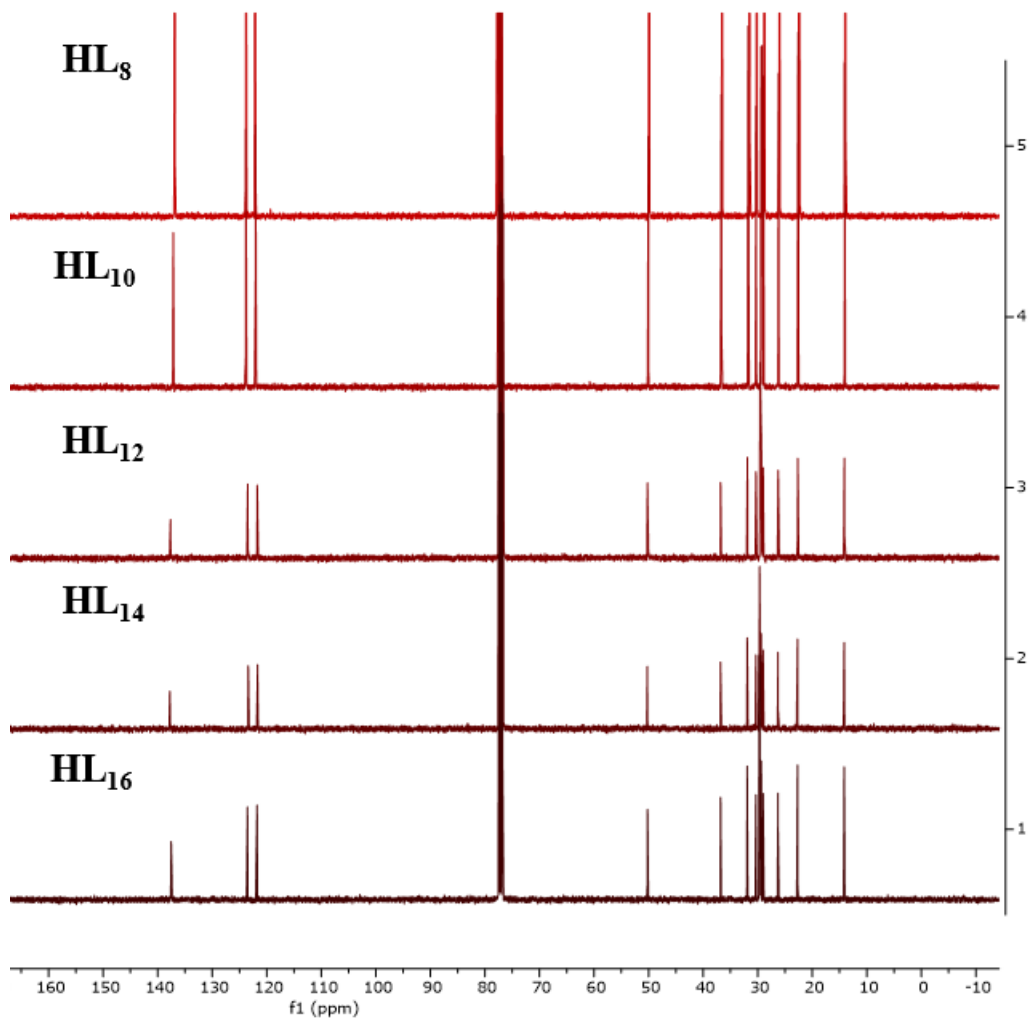


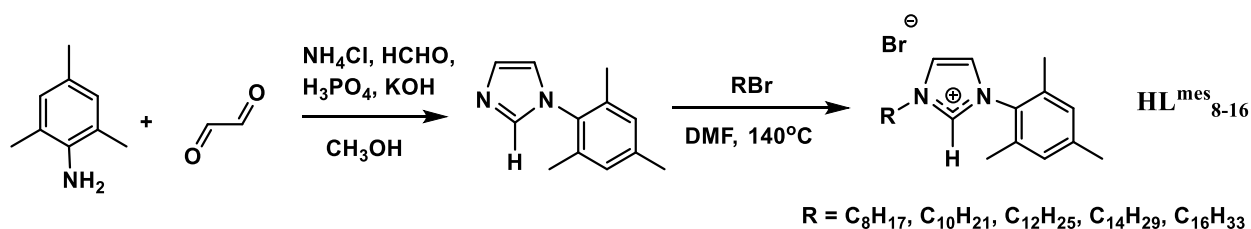
Figure 2.6: Stacked $^{13}\text{C}\{^1\text{H}\}$ NMR spectra of HL_{8-16} in CDCl_3 using Bruker spectrophotometer at room temperature

2.4.2. Synthesis of 1-(2,4,6-Trimethylphenyl)-1*H*-Imidazole

1-(2,4,6-Trimethylphenyl)-1*H*-imidazole was synthesized following a previously reported procedure (Scheme 2.4).²⁵

2.4.3. Synthesis of **HL**^{mes}₈₋₁₆

1-mesityl-3-alkyl-imidazolium bromide compounds (**HL**^{mes}₈₋₁₆) were synthesized following an established procedure²⁵ by the reaction of 1-(2,4,6-trimethylphenyl)-1*H*-imidazole with alkyl bromides with chain length ranging from 8 - 16 carbon atoms respectively as shown below in Scheme 2.4.

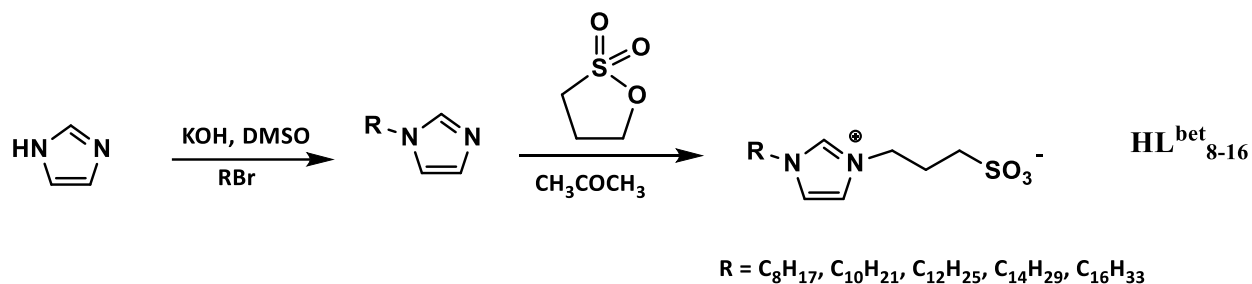


Scheme 2.4: Synthesis of **HL**^{mes}₈₋₁₆

Brown oils were isolated for **HL**^{mes}₈₋₁₆. The crude products were precipitated with cold diethyl ether to give off white, waxy solids in 74 – 79% yields. Just like the **HL**₈₋₁₆ salts, they dissolve well in water and lower alcohols with moderate solubility in chlorinated solvents. The ¹H NMR chemical shifts of the C2–H protons of **HL**^{mes}₈₋₁₆ are in the range 10.30 – 10.60 ppm while the signals of the hydrogen on the meta position of the mesityl group are between 6.95 – 7.03 ppm. The peaks between 4.66 and 4.78 ppm are for the methylene group attached to the N3 nitrogen atom on the imidazole ring. The ¹³C NMR shifts of the N-C-N sp² carbon appear in the range 137.80 – 138.37 ppm (Appendix B). The HRMS data of **HL**^{mes}₈₋₁₆ show peaks of the cationic fragment [(M-Br)⁺].

2.4.4. Synthesis of $\text{HL}^{\text{bet}}_{8-16}$

The preparation of these proligands has been previously described²⁸⁻³⁰ and it involves the use of 1,3-propane sultone as one of the alkylating agents.



Scheme 2.5: Synthesis of $\text{HL}^{\text{bet}}_{8-16}$

As depicted in Scheme 2.5, initial *N*-alkylation of imidazole was carried out using an alkyl bromide with chain lengths ranging from 8–16 carbons, followed by nucleophilic substitution of the *N*-alkyl imidazoles with 1,3-propane sultone to produce the sulfonate functionalized imidazolium zwitterions $\text{HL}^{\text{bet}}_{8-16}$. These zwitterions were characterized by ¹H and ¹³C NMR spectroscopy as well as HRMS. The ¹H and ¹³C NMR spectra are consistent with the structure of $\text{HL}^{\text{bet}}_{8-16}$. In the ¹H spectra of $\text{HL}^{\text{bet}}_{8-16}$, the imidazolium proton appears at approximately 10 ppm, which is consistent with the C₂-H proton of imidazolium salts. The ¹³C NMR spectra show the C₂ signal resonating at approximately 136 ppm (Appendix C). HRMS analyses of these zwitterions show the parent ion, [M+H⁺], respectively.

2.4.5. Synthesis of Gemini Amphiphilic Imidazolium Salts, $\mathbf{H_2G_{8-16}}$, $\mathbf{H_2G^{mes}_{8-16}}$ and $\mathbf{HG^{tma}_{8-16}}$

Gemini amphiphilic imidazolium salts were prepared by the route summarized in Scheme 2.6,³¹ starting from *N*-alkylation of imidazole (**1**) and followed by nucleophilic substitution of the *N*-alkyl imidazoles (**2**) with 1,3-dibromopropane to form **3** (bromopropyl alkyl imidazolium salts). Finally, the quarternary imidazolium salts were reacted with methylimidazole (**4**), mesitylimidazole (**5**) and trimethylamine (**6**) to form $\mathbf{H_2G_{8-16}}$, $\mathbf{H_2G^{mes}_{8-16}}$ and $\mathbf{HG^{tma}_{8-16}}$ respectively. To suppress the formation of symmetrical Gemini surfactants during the nucleophilic substitution of **2** with 1,3-dibromopropane, 1,3-dibromopropane was used in excess. Also, excess of **4**, **5** and **6** were used respectively to avoid any unreacted impurities of **3**, as it may be difficult to remove it from the target compounds. Formation of the series of asymmetrical dicationic imidazolium salts of $\mathbf{H_2G_{8-16}}$, $\mathbf{H_2G^{mes}_{8-16}}$ and $\mathbf{HG^{tma}_{8-16}}$ was confirmed by ^1H and ^{13}C NMR spectroscopy and HRMS. The spectra obtained were consistent with their molecular structure. The ^1H and ^{13}C NMR spectra of each of the series of asymmetrical dicationic imidazolium salts in Scheme 2.6 have common features, with minimal or no change in the chemical shifts of the signals (Appendixes D, E and F). This observation indicates that increasing the chain length of the alkyl group makes little or no difference to the chemical shifts. Generally, the ^1H NMR spectra of $\mathbf{H_2G_{8-16}}$ (Figure 2.11), $\mathbf{H_2G^{mes}_{8-16}}$ show two signals ranging from 10.22 to 9.69 ppm, while that of $\mathbf{HG^{tma}_{8-16}}$ show one resonance signal at approximately 10 ppm, which is consistent with the general C₂-H acidic proton shift of imidazolium salts (δ 8–10 ppm) and the ^{13}C NMR shifts of the N-C-N sp² carbon signal appear between 141.47 and 136.28 ppm (Figure 2.12 shows ^{13}C NMR of $\mathbf{H_2G_{8-16}}$). Analyses of these dicationic imidazolium salts with HRMS often revealed $[(\text{M}-2\text{Br})^{2+}]$, corresponding to the dicationic fragment.

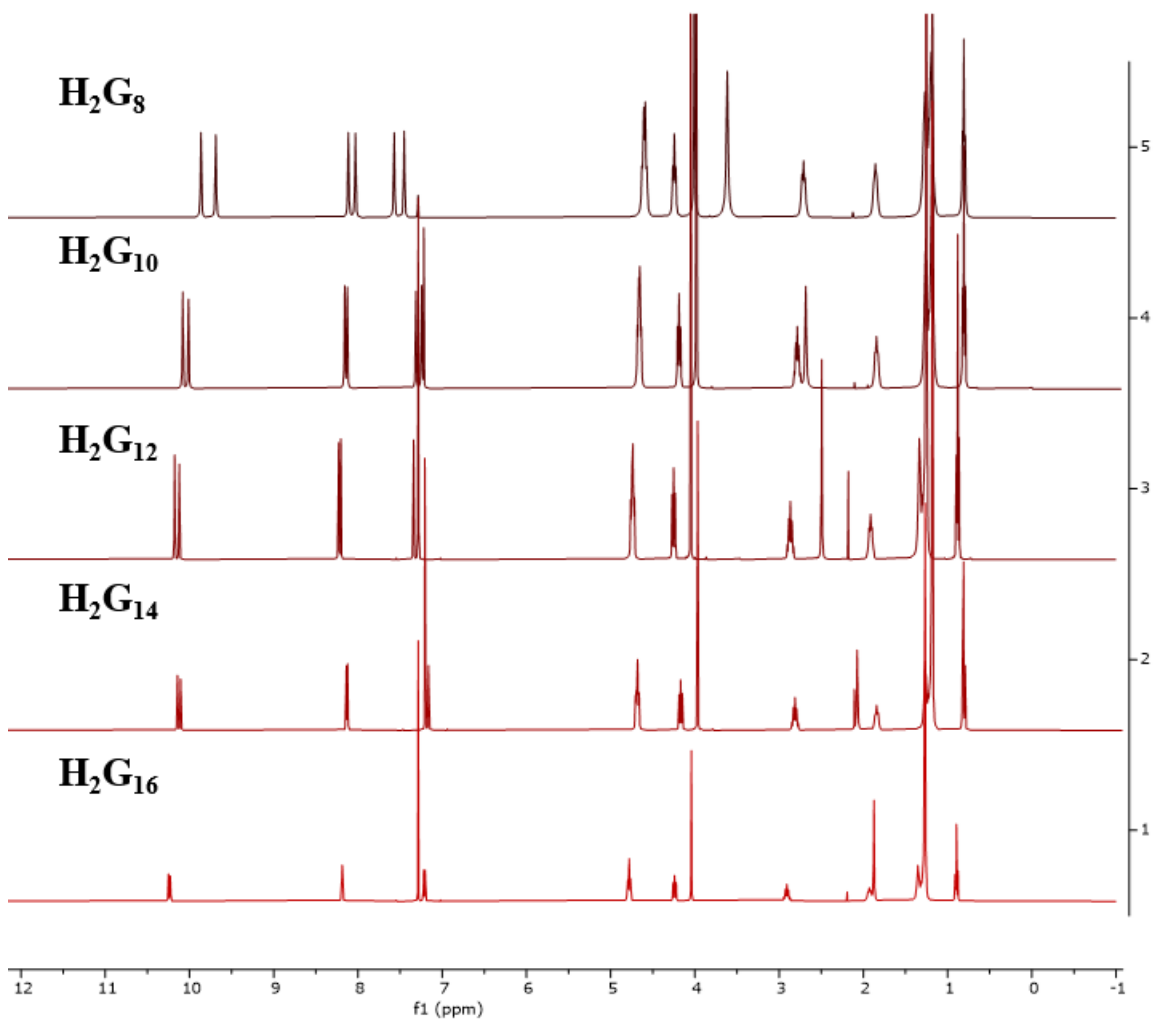
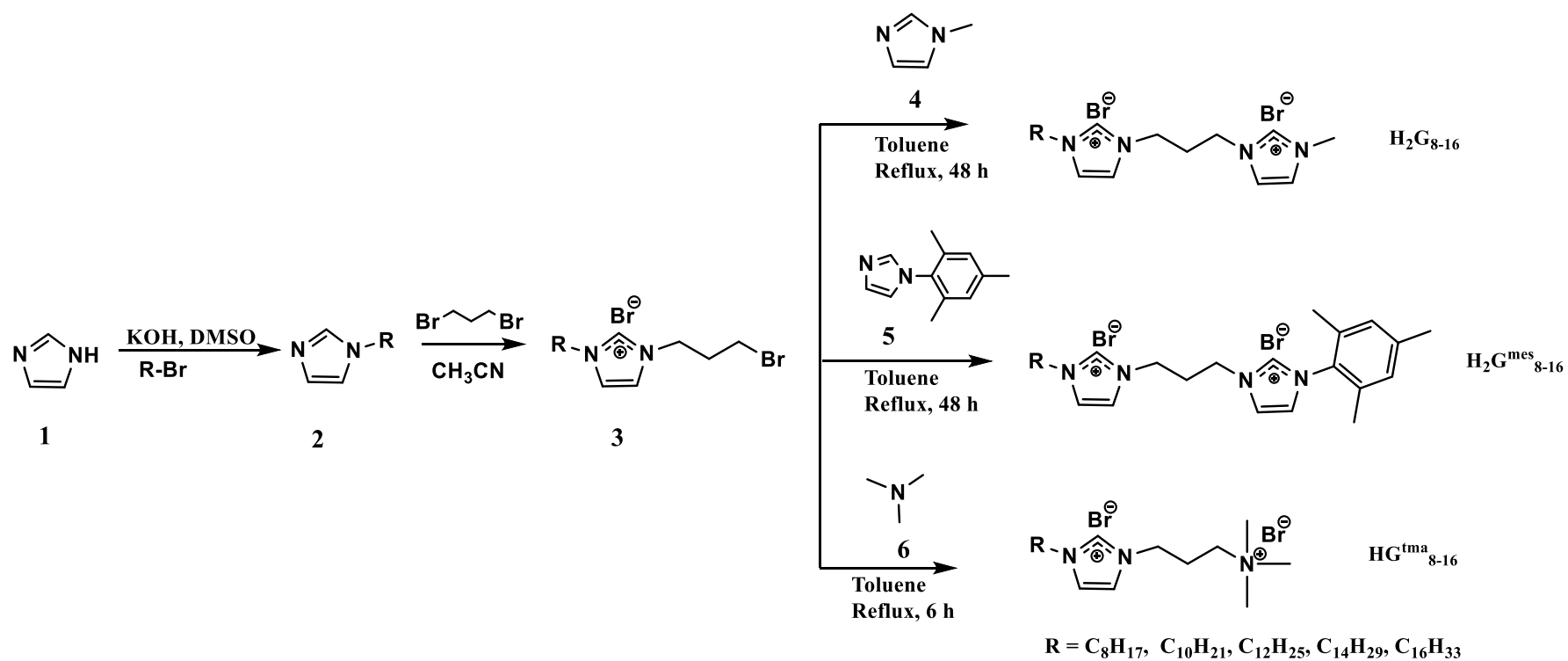


Figure 2.11: Stacked ^1H NMR spectra of $\text{H}_2\text{G}_{8-16}$ in CDCl_3 using Bruker 400 MHz spectrophotometer at room temperature



Scheme 2.6: Synthesis of hetero-gemini amphiphilic imidazolium salts

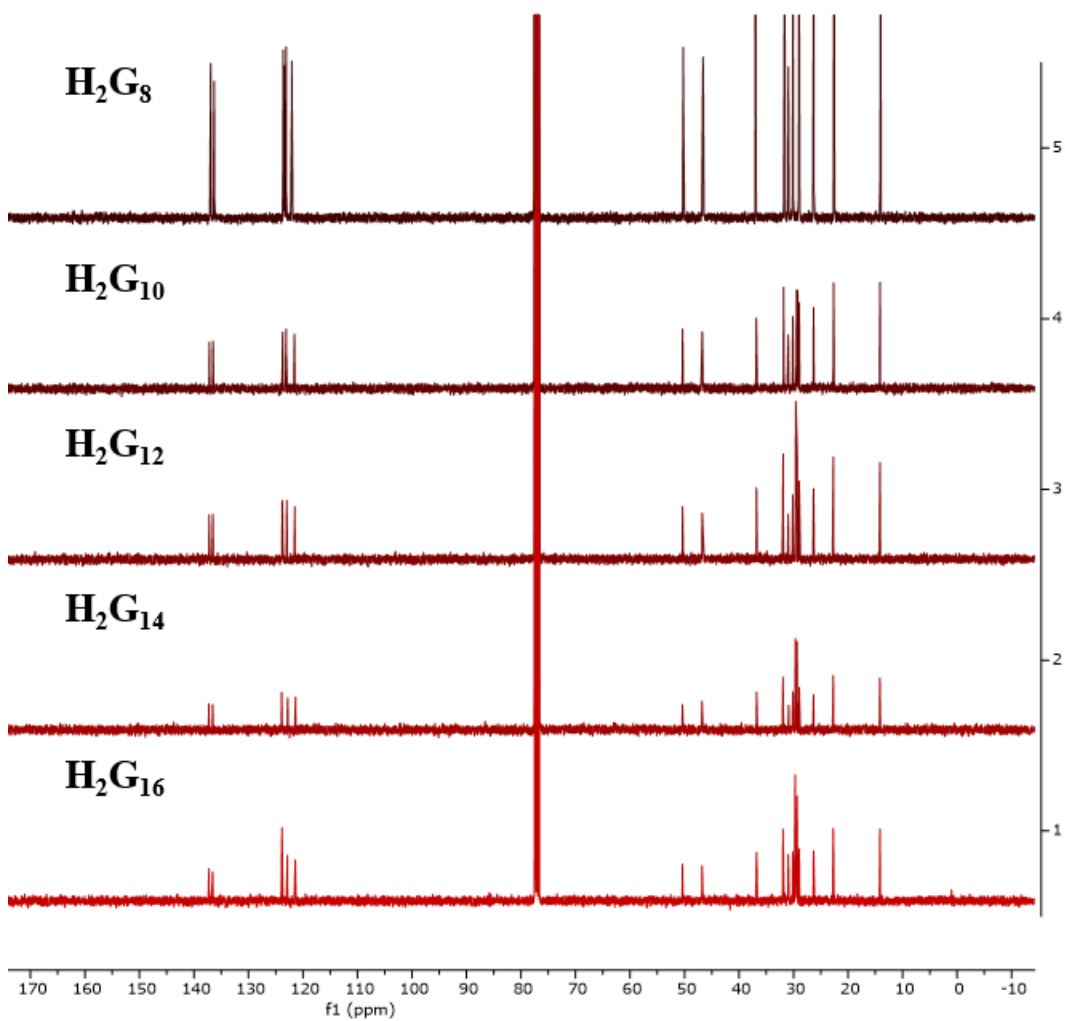


Figure 2.12: Stacked $^{13}\text{C}\{^1\text{H}\}$ NMR of $\text{H}_2\text{G}_{8-16}$ in CDCl_3 using Bruker spectrophotometer at room temperature

2.4.6. Determination of Critical Micelle Concentration (CMC)

Surfactants are amphiphilic molecules with hydrophobic tail and hydrophilic head (or *vice versa*) and by implication, they contain components that are water-soluble and oil soluble.^{25, 32} In water, surfactant molecules aggregate into organized molecular assemblies known as micelles and micelle formation is governed by electrostatic and hydrophobic interactions. The concentration above which this phenomenon occurs is called the critical micelle concentration (CMC) and the value of the CMC can be determined by the change in the physicochemical properties of the surfactant solutions as the concentration of the amphiphilic molecules is increased.^{33, 34} The CMC values of **HL**₈₋₁₆, **HL**^{mes}₈₋₁₆, **H₂G**₈₋₁₆ and **H₂G**^{mes}₈₋₁₆ were determined by conductometry, which is one of the common electrochemical techniques owing to its accuracy and relatively good agreement between values obtained by other methods,³² using a Mettler Toledo Conductivity Meter (InLab 738 model). Various concentrations of surfactant molecules were prepared by dilution method in aqueous solution and the conductivity of these solutions was measured at 298 K.

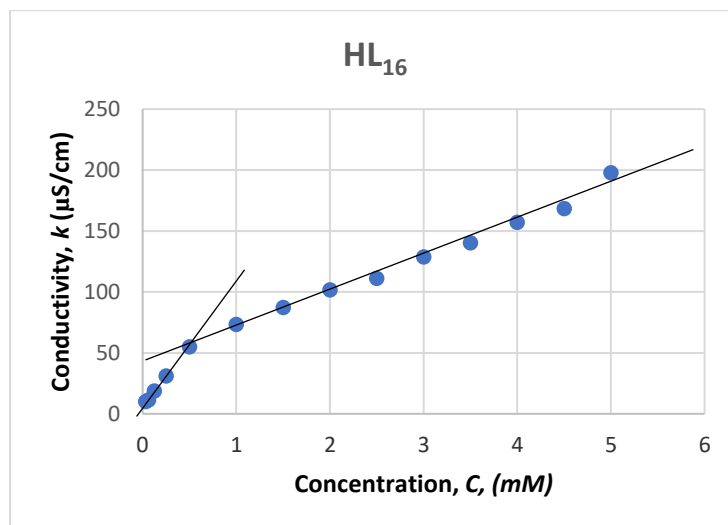


Figure 2.17: Plot of specific conductivity, k , against **HL**₁₆ concentration, c , at 25°C in water

An example of how CMC is evaluated from a plot of conductivity, k , as a function of concentration, c , of **HL**₁₆ is as shown in Figure 2.17. The value of k increases almost linearly with an increase in the concentration of **HL**₁₆ and the slope changes steeply at a certain concentration. The slope of the first and second lines are 96.12 and 28.50 $\mu\text{S}/\text{mM}$ respectively, this implies an effective loss of ionic charges because a fraction of the counterions is confined to the micellar surface.³⁵ It is obvious that the results fit into two straight lines of different slopes and this steep change of the slope in k as a function of c plot indicates the onset of molecular aggregates at the concentration corresponding to the breakpoint. From the location of the abrupt change of the slopes, 0.60 mM was derived for the CMC in the k against c plot in Figure 2.11 and other CMCs derived by this method are listed in Table 1 for **HL**₈₋₁₆, **HL**^{mes}₈₋₁₆, **H₂G**₈₋₁₆ and **H₂G**^{mes}₈₋₁₆ (Appendix H) respectively at 25°C.

2.4.7. Structural Effects of Monocationic and Dicationic Ionic Surfactants on Critical Micelle Concentration

From the results in Table 1, the cationic head and the alkyl chain are found to affect the CMC of the surfactants. The CMC values of **HL**₈₋₁₆, **HL**^{mes}₈₋₁₆, **H₂G**₈₋₁₆ and **H₂G**^{mes}₈₋₁₆ decrease by 262-, 58-, 19- and 14-fold respectively as the alkyl chain length increases from 8-16 in each homologous series. Comparatively, the effect of the cationic heads between the two monocationic surfactants, **HL**₈₋₁₆ and **HL**^{mes}₈₋₁₆ led to 6.80-, 4.20-, 3.70-, 4.20- and 1.50-fold decrease and 2.60-, 2.40-, 1.80-, 1.40- and 1.20-fold decrease between the dicationic surfactant series comprising of **H₂G**₈₋₁₆ and **H₂G**^{mes}₈₋₁₆ for 8, 10, 12, 14 and 16 alkyl chain lengths respectively. Consequently, the alkyl chain has a more profound effect on the CMC than the cationic heads and the longer the chain length, the lower the CMC value. Furthermore, the CMC values of surfactants with mesityl-imidazole and mesityl-imidazole-tethered-to-imidazole heads are lower than that of methyl-imidazole and methyl-imidazole-tethered-to-imidazole respectively.

Table 2.1.: Critical Micelle Concentration of **HL**₈₋₁₆, **HL**^{mes}₈₋₁₆, **HL**^{mes}₈₋₁₆ and **H₂G**₈₋₁₆

| Compound | CMC (mM) | Compound | CMC (mM) | Compound | CMC (mM) | Compound | CMC (mM) |
|------------------|---------------------|---------------------------------|-------------------|--------------------------------|----------|---|----------|
| HL ₈ | 157.00 | HL ^{mes} ₈ | 23.00 | H ₂ G ₈ | - | H ₂ G ^{mes} ₈ | 39.00 |
| HL ₁₀ | 37.40 ^a | HL ^{mes} ₁₀ | 9.00 | H ₂ G ₁₀ | - | H ₂ G ^{mes} ₁₀ | 19.00 |
| HL ₁₂ | 9.60 ^{a,b} | HL ^{mes} ₁₂ | 2.62 ^c | H ₂ G ₁₂ | 17.90 | H ₂ G ^{mes} ₁₂ | 10.00 |
| HL ₁₄ | 2.40 ^{a,b} | HL ^{mes} ₁₄ | 0.57 ^c | H ₂ G ₁₄ | 7.00 | H ₂ G ^{mes} ₁₄ | 5.00 |
| HL ₁₆ | 0.60 ^{a,b} | HL ^{mes} ₁₆ | 0.40 | H ₂ G ₁₆ | 3.30 | H ₂ G ^{mes} ₁₆ | 2.80 |

^a Reported in Ref. 3³ ^b Reported in Ref. 28.²⁸ ^c Reported in Ref. 24²⁴.

2.4.8. Comparison of Critical Micelle Concentration Values of Monocationic and Dicationic Surfactants

A comparison of the CMC values between the monocationic series (**HL**₈₋₁₆ and **HL**^{mes}₈₋₁₆) and dicationic series (**H₂G**₈₋₁₆ and **H₂G**^{mes}₈₋₁₆) from Table 1 reveals that the monocationic surfactants possess lower CMC values than the dicationic surfactants for 14 and 16 alkyl chain lengths, **HL**^{mes}_{14,16} < **HL**₈₋₁₂ < **H₂G**^{mes}_{14,16} < **H₂G**_{14,16}. However, the CMC values of the surfactants (both mono and dicationic) bearing 8, 10 and 12 alkyl chain lengths did not follow the above trend, rather the CMC values increases in the following order: **HL**^{mes}₈₋₁₂ < **H₂G**^{mes}₈₋₁₂ < **HL**₈₋₁₂ < **H₂G**₁₂.

2.5. Experimental

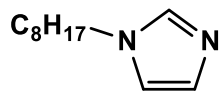
General

All reactions were carried out under aerobic conditions unless otherwise specified and all reagents were purchased from commercial sources and used without further purification. ^1H and ^{13}C NMR spectra were recorded on a Bruker 400 MHz or 500 MHz spectrophotometers and recorded in deuterated solvents and the chemical shifts are given in ppm. Coupling constants J are given in hertz (Hz). High-resolution mass spectra were obtained as appropriate (in positive and negative modes) using a Waters LCT Premier XE instrument and are reported as m/z (relative intensity), and conductance measurements were determined by Mettler Toledo Conductivity Meter (InLab 738 model).

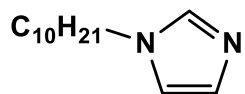
General procedure for the preparation of *N*-alkylimidazole

A mixture of imidazole (73 mmol), potassium hydroxide (80 mmol) and dimethyl sulfoxide (5 mL) was placed in a 250 mL round bottom flask. After vigorous stirring for 2 h at 50°C, the mixture was cooled to room temperature after which, 1-bromoalkane (70 mmol) was added slowly with a dropping funnel into the above reaction mixture and stirred for additional 4 h. Upon completion, distilled water (150 mL) was poured into the flask followed by extraction with chloroform (5×20 mL) in a separatory funnel. Combined organic layers were collected, dried over anhydrous magnesium sulfate, filtered, and the solvent evaporated. The residue was subjected to flash chromatography with ethyl acetate as eluent to give the *N*-alkylimidazole.

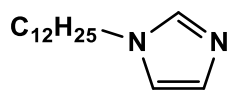
N-Octylimidazole, C8Im



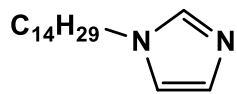
Yield: 77%; ^1H NMR (δ ppm, 400 MHz, CDCl_3): 0.80 (t, $^3J=8.0$ Hz, 3H), 1.12- 1.25 (m, 10H), 1.68 (m, 2H), 3.83 (t, $^3J = 8.0$ Hz, 2H), 6.82 (s, 1H), 6.96 (s, 1H), 7.37 (s, 1H), $^{13}\text{C}\{^1\text{H}\}$ NMR (δ ppm, 100 MHz, CDCl_3): 14.00 (CH_3), 22.54 (CH_2), 26.46 (CH_2), 28.96 (CH_2), 29.03 (CH_3), 31.02 (CH_3), 31.65 (CH_2), 46.94 (NCH_2), 118.71 (C_5), 129.24 (C_4), 136.99 (C_2), HRMS (ESI): m/z found 181.1711 [(M+H) $^+$, ($\text{C}_{11}\text{H}_{20}\text{N}_2^+$), 100%], expected 181.1626.

N-Decyllimidazole, C10Im

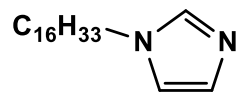
Yield: 78%; ^1H NMR (δ ppm, 400 MHz, CDCl_3): 0.81 (t, $^3\text{J}=8.0$ Hz, 3H), 1.25- 1.13 (m, 14H), 1.71 (m, 2H), 3.83 (t, $^3\text{J} = 8.0$ Hz, 2H), 6.96 (s, 1H), 6.81 (s, 1H), 7.39 (s, 1H), $^{13}\text{C}\{^1\text{H}\}$ NMR (δ ppm, 100 MHz, CDCl_3): 14.12 (CH₃), 22.67 (CH₂), 26.55 (CH₂), 29.07 (CH₂), 29.29 (CH₃), 29.26 (CH₂), 29.43 (CH₂), 29.48 (CH₂), 31.09 (CH₃), 31.85 (CH₂), 47.04 (NCH₂), 118.77 (C₅), 129.36 (C₄), 137.07 (C₂), HRMS (ESI): m/z found 209.2018 [(M+H)⁺, (C₁₃H₂₄N₂⁺), 100%], expected 209.2012.

N-Dodecylimidazole, C12Im

Yield: 72%; ^1H NMR (δ ppm, 400 MHz, CDCl_3): 0.80 (t, $^3\text{J}=8.0$ Hz, 3H), 1.25- 1.13 (m, 18H), 1.68 (m, 2H), 3.83 (t, $^3\text{J} = 8.0$ Hz, 2H), 6.81 (s, 1H), 6.96 (s, 1H), 7.37 (s, 1H), $^{13}\text{C}\{^1\text{H}\}$ NMR (δ ppm, 100 MHz, CDCl_3): 14.23 (CH₃), 22.63 (CH₂), 26.48 (CH₂), 29.02 (CH₂), 29.29 (CH₃), 29.38 (CH₂), 29.47 (CH₂), 29.55 (CH₂), 31.04 (CH₃), 31.85 (CH₂), 46.94 (NCH₂), 118.69 (C₅), 129.28 (C₄), 136.99 (C₂), HRMS (ESI): m/z found 237.2323 [(M+H)⁺, (C₁₃H₂₈N₂⁺), 100%], expected 237.2325 .

N-Tetradecylimidazole, C14Im

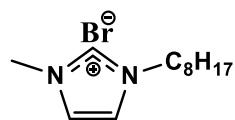
Yield: 75%; ^1H NMR (δ ppm, 400 MHz, CDCl_3): 0.80 (t, $^3\text{J}=8.0$ Hz, 3H), 1.15-1.25 (m, 22H), 1.66 (m, 2H), 3.83 (t, $^3\text{J} = 8.0$ Hz, 2H), 6.80 (s, 1H), 6.94 (s, 1H), 7.40 (s, 1H), $^{13}\text{C}\{^1\text{H}\}$ NMR (δ ppm, 100 MHz, CDCl_3): 14.01 (CH₃), 22.59 (CH₂), 26.42 (CH₂), 28.97 (CH₂), 29.27 (CH₂), 29.34 (CH₂), 29.43 (CH₃), 29.51 (CH₂), 29.55 (CH₂), 29.59 (CH₂), 30.99 (CH₃), 31.83 (CH₂), 46.85 (NCH₂), 118.59 (C₅), 129.19 (C₄), 136.89 (C₂), HRMS (ESI): m/z found 265.2640 [(M+H)⁺, (C₁₅H₃₂N₂⁺), 100%], expected 265.2638.

N-Hexadecylimidazole, C16Im

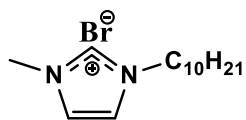
Yield: 83%; ^1H NMR (δ ppm, 400 MHz, CDCl_3): 0.88 (t, $^3\text{J}=8.0$ Hz, 3H), 1.22- 1.32 (m, 26H), 1.76 (m, 2H), 3.91 (t, $^3\text{J} = 8.0$ Hz, 2H), 6.90 (s, 1H), 7.05 (s, 1H), 7.45 (s, 1H), $^{13}\text{C}\{^1\text{H}\}$ NMR (δ ppm, 100 MHz, CDCl_3): 14.13 (CH₃), 22.70 (CH₂), 26.55 (CH₂), 29.08 (CH₂), 29.44 (CH₃), 29.53 (CH₂), 29.61 (CH₂), 29.64 (CH₂) 29.66 (CH₂), 29.68 (CH₂), 29.69 (CH₂), 29.70 (CH₂) 31.10 (CH₃), 31.93 (CH₂), 47.02 (NCH₂), 118.74 (C₅), 129.38 (C₄), 137.07 (C₂), HRMS (ESI): m/z found 293.2962 [(M+H)⁺, (C₁₇H₃₆N₂⁺), 100%], expected 293.2951.

General procedure for the preparation of HL₈₋₁₆

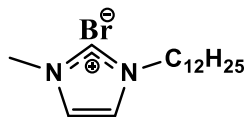
N-methylimidazole (60 mmol) and 1-alkyl bromide (61 mmol) (alkyl = octyl, decyl, dodecyl, tetradecyl and hexadecyl) were charged into a round bottom flask without solvent and stirred at 100°C for 16 h. At the end of the reaction, the crude product was dissolved in hot chloroform and precipitated out by adding petroleum ether. Pale-yellow oils were obtained for C₈ and C₁₀ derivatives and C₁₂, C₁₄ and C₁₆ derivatives were isolated as off-white solids.

HL₈

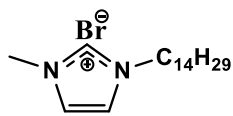
Yield: 86%; ^1H NMR (δ ppm, 400 MHz, CDCl_3): 0.66 (t, $^3\text{J}= 8.0$ Hz, 3H), 1.00-1.20 (m, 10H), 1.72 (m, 2H), 3.94 (s, 3H), 4.14 (t, $^3\text{J}= 8.0$ Hz, 2H), 7.40 (s, 1H), 7.59 (s, 1H), 10.09 (s, 1H). $^{13}\text{C}\{^1\text{H}\}$ NMR (δ ppm, 100 MHz, CDCl_3): 13.91 (CH₃), 22.38 (CH₂), 26.04 (CH₂), 28.76 (CH₂), 28.83 (CH₂), 30.18 (CH₂), 31.47 (CH₂), 36.54 (NCH₃), 49.90 (NCH₂), 122.09 (C₄), 123.82 (C₅) 136.86 (C₂). HRMS (ESI) (m/z): found 195.1869 [(M-Br)⁺, (C₁₂H₂₃N₂⁺), 100%], expected 195.1856.

HL₁₀

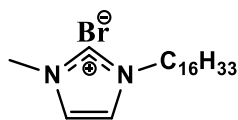
Yield: 82%; ¹H NMR (δ ppm, 400 MHz, CDCl₃): 0.88 (t, ³J= 8.0 Hz, 3H), 1.20-1.40 (m, 14H), 1.92 (m, 2H), 4.14 (s, 3H), 4.32 (t, ³J= 8.0 Hz, 2H), 7.36 (s, 1H), 7.51 (s, 1H), 10.51 (s, 1H). ¹³C{¹H} NMR (δ ppm, 100 MHz, CDCl₃): 14.04 (CH₃), 22.57 (CH₂), 26.17 (CH₂), 28.92 (CH₂), 29.15 (CH₂), 29.29 (CH₂), 29.36 (CH₂), 30.28 (CH₂), 31.74 (CH₂), 36.65 (NCH₃), 50.04 (NCH₂), 122.05 (C₄), 123.82 (C₅), 137.10 (C₂). HRMS (ESI) (*m/z*): found 223.2183 [(M-Br)⁺, (C₁₄H₂₇N₂⁺), 100%], expected 223.2169.

HL₁₂

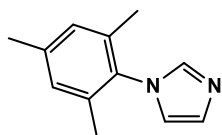
Yield: 82%; ¹H NMR (δ ppm, 400 MHz, CDCl₃): 0.81 (t, ³J= 8.0 Hz, 3H), 1.10-1.29 (m, 18H), 1.85 (m, 2H), 4.07 (s, 3H), 4.25 (t, ³J= 8.0 Hz, 2H), 7.30 (s, 1H), 7.44 (s, 1H), 10.29 (s, 1H). ¹³C{¹H} NMR (δ ppm, 100 MHz, CDCl₃): 14.10 (CH₃), 22.66 (CH₂), 26.26 (CH₂), 28.98 (CH₂), 29.30 (CH₂), 29.36 (CH₂), 29.48 (CH₂), 29.57 (CH₂), 30.30 (CH₂), 31.88 (CH₂), 36.80 (NCH₃), 50.21 (NCH₂), 121.74 (C₄), 123.48 (C₅), 137.64 (C₂). HRMS (ESI) (*m/z*): found 251.2495 [(M-Br)⁺, (C₁₆H₃₁N₂⁺), 100%], expected 251.2482.

HL₁₄

Yield: 91%; ¹H NMR (δ ppm, 400 MHz, CDCl₃): 0.88 (t, ³J= 8.0 Hz, 3H), 1.20-1.40 (m, 22H), 1.92 (m, J= 8, 2H), 4.14 (s, 3H), 4.32 (t, ³J= 8.0 Hz, 2H), 7.34 (s, 1H), 7.48 (s, 1H), 10.42 (s, 1H). ¹³C{¹H} NMR (δ ppm, 100 MHz, CDCl₃): 14.14 (CH₃), 22.69 (CH₂), 26.27 (CH₂), 29.00 (CH₂), 29.36 (CH₂), 29.38 (CH₂), 29.51 (CH₂), 29.60 (CH₂), 29.65 (CH₂), 29.68 (CH₂), 30.32 (CH₂), 31.92 (CH₂), 36.78 (NCH₃), 50.23 (NCH₂), 121.67 (C₄), 123.39 (C₅), 137.75 (C₂). HRMS (ESI) (*m/z*): found 279.2807 [(M-Br)⁺, (C₁₈H₃₅N₂⁺), 100%], expected 279.2795.

HL₁₆

Yield: 93%; ¹H NMR (δ ppm, 400 MHz, CDCl₃): 0.87 (t, ³J= 8.0 Hz, 3H), 1.29 (m, 26H) 1.93 (m, 2H), 4.13 (s, 3H), 4.31 (t, ³J= 8.0 Hz, 2H), 7.36 (s, 1H), 7.51 (s, 1H), 10.42 (s, 1H). ¹³C{¹H} NMR (δ ppm, 100 MHz, CDCl₃): 14.13 (CH₃), 22.69 (CH₂), 26.27 (CH₂), 29.00 (CH₂), 29.36 (CH₂), 29.38 (CH₂), 29.51 (CH₂), 29.60 (CH₂), 29.65 (CH₂), 29.69 (CH₂), 30.33 (CH₂), 31.92 (CH₂), 36.78 (NCH₃), 50.20 (NCH₂), 121.76 (C₄), 123.51 (C₅) 137.64 (C₂). HRMS (ESI) (*m/z*): found 307.3120 [(M-Br)⁺, (C₂₀H₃₉N₂)⁺, 100%], expected 307.3108.

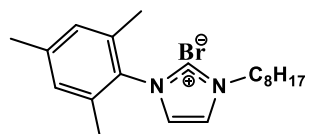
Synthesis of 1-(2,4,6-Trimethylphenyl)-1H-Imidazole

2,4,6-trimethylaniline (6.8 g, 0.05 mol) in MeOH (25 mL) was stirred with 30 % aqueous glyoxal (8.1 mL, 0.05 mol) for 16 h at room temperature. A bright yellow mixture was formed. Then, NH₄Cl (5.4 g, 0.1 mol) was added followed by 37 % aqueous formaldehyde (8 mL, 0.1 mol). The mixture was diluted with MeOH (200 mL) and the resulting mixture was refluxed for 1 h. H₃PO₄ (7 mL, 85 % soln.) was added for 10 min. The resulting mixture was then stirred at reflux overnight. After removal of the solvent, the dark residue was poured onto ice (100 g) and neutralised with 40 % KOH solution until pH 9. The resulting mixture was extracted with EtOAc (2 × 100 mL). The organic phases were combined and washed with H₂O, brine and dried with anhydrous MgSO₄. After filtering, the solvent was removed and the residue was purified by distillation on a Kugelrohr under vacuum (70 mbar) at 140 °C (some unreacted 2,4,6-trimethylaniline initially distills as a colourless oil at a lower temperature).

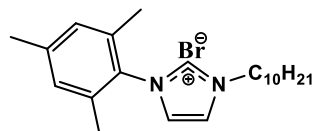
General procedure for the preparation of HL^{mes}₈₋₁₆

1-(2,4,6-Trimethylphenyl)-1H-Imidazole (27 mmol) and 1-alkyl bromide (28 mmol) (alkyl = C₈H₁₇, C₁₀H₂₁, C₁₂H₂₅, C₁₄H₂₉, and C₁₆H₃₃) were mixed in DMF at 140 °C for 48 h. The solvent

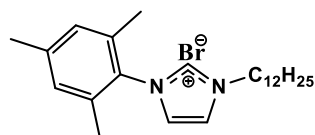
was removed under vacuum and brown, transparent, viscous oil was obtained. Afterwards, the crude products were precipitated with cold diethyl ether to give off white solids.

HL^{mes}₈

Yield: 76%; ¹H NMR (δ ppm, 400 MHz, CDCl₃): 0.88 (t, ³J= 8.0 Hz, 3H), 1.20-1.40 (m, 10H), 2.00 (m, 2H), 2.09 (s, 6H), 2.35 (s, 3H), 4.75 (t, ³J= 8.0 Hz, 2H), 7.02 (s, 2H), 7.20 (d, 1H), 7.70 (s, 1H), 10.48 (s, 1H). ¹³C{¹H} NMR (δ ppm, 100 MHz, CDCl₃): 14.09 (CH₃), 17.69 (CH₂), 21.13 (CH₂), 22.60 (CH₂), 26.12 (CH₂), 29.01 (CH₃), 29.06 (CH₃), 30.57 (CH₃), 31.67 (CH₂), 50.50 (NCH₂), 122.45 (C₅), 123.07 (C₄), 129.92 (*ipso*-mesityl), 130.67 (*m*-mesityl), 134.21 (*o*-mesityl), 138.37 (C₂), 141.37 (*p*-mesityl). HRMS (ESI) (*m/z*): found 299.2493 [(M-Br)⁺, (C₂₀H₃₁N₂)⁺, 100%], expected 299.2482.

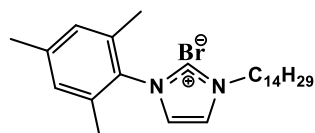
HL^{mes}₁₀

Yield: 74%; ¹H NMR (δ ppm, 400 MHz, CDCl₃): 0.89 (t, ³J= 8.0 Hz, 3H), 1.20-1.45 (m, 14H), 1.98 (m, 2H), 2.09 (s, 6H), 2.36 (s, 3H), 4.75 (t, ³J= 8.0 Hz, 2H), 7.02 (s, 2H), 7.20 (d, 1H), 7.69 (s, 1H), 10.47 (s, 1H). ¹³C{¹H} NMR (δ ppm, 100 MHz, CDCl₃): 14.13 (CH₃), 17.70 (CH₂), 21.13 (CH₂), 22.67 (CH₃), 26.14 (CH₂), 29.06 (CH₂), 29.27 (CH₂), 29.41 (CH₂), 29.45 (CH₃), 30.57 (CH₂), 31.86 (CH₃), 50.53 (NCH₂), 122.43 (C₅), 123.06 (C₄), 129.92 (*ipso*-mesityl), 130.66 (*m*-mesityl), 134.21 (*o*-mesityl), 138.36 (C₂), 141.38 (*p*-mesityl). HRMS (ESI) (*m/z*): found 327.2806 [(M-Br)⁺, (C₂₂H₃₅N₂)⁺, 100%], expected 327.2795.

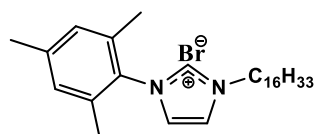
HL^{mes}₁₂

Yield: 79%; ¹H NMR (δ ppm, 400 MHz, CDCl₃): 0.90 (t, ³J= 8.0 Hz, 3H), 1.20-1.45 (m, 18H), 2.01 (m, 2H), 2.11 (s, 6H), 2.37 (s, 3H), 4.78 (t, ³J= 8.0 Hz, 2H), 7.03 (s, 2H), 7.17 (s, 1H), 7.58 (s, 1H), 10.60 (s, 1H). ¹³C{¹H} NMR (δ ppm, 100 MHz, CDCl₃): 14.12 (CH₃), 17.68 (CH₂), 21.11 (CH₂), 22.68 (CH₂), 26.14 (CH₃), 29.06 (CH₂), 29.33 (CH₃), 29.42 (CH₂), 29.49 (CH₂), 29.60 (CH₂), 30.55

(CH₃), 31.90 (CH₂), 50.53 (NCH₂), 122.57 (C₅), 123.12 (C₄), 129.90 (*ipso*-mesityl), 130.67 (*m*-mesityl), 134.21 (*o*-mesityl), 138.24 (C₂), 141.35(*p*-mesityl). HRMS (ESI) (*m/z*): 355.3119 [(M-Br)⁺, (C₂₄H₃₉N₂⁺), 100%] expected 355.3108.

HL^{mes}₁₄

Yield: 77%; ¹H NMR (δ ppm, 400 MHz, CDCl₃): 0.84 (t, ³J= 8.0 Hz, 3H), 1.15-1.35 (m, 22H), 1.95 (m, 2H), 2.03 (s, 6H), 2.30 (s, 3H), 4.66 (t, ³J= 8.0 Hz, 2H), 6.95 (s, 2H), 7.25 (s, 1H), 7.95 (s, 1H), 10.30 (s, 1H). ¹³C{¹H} NMR (δ ppm, 100 MHz, CDCl₃): 14.10 (CH₃), 17.62 (CH₂), 21.07 (CH₂), 22.65 (CH₂), 26.10 (CH₂), 29.04 (CH₃), 29.32 (CH₃), 29.41 (CH₃), 29.48 (CH₃), 29.59 (CH₂), 29.61 (CH₂), 29.62 (CH₂), 29.65 (CH₂), 30.55 (CH₃), 31.88 (CH₂), 50.33 (NCH₂), 122.76 (C₅), 123.19 (C₄), 129.80 (*ipso*-mesityl), 130.72 (*m*-mesityl), 134.17 (*o*-mesityl), 137.80 (C₂), 141.14 (*p*-mesityl). HRMS (ESI) (*m/z*): found 383.3421 [(M-Br)⁺, (C₂₆H₄₃N₂⁺), 100%], expected 383.3421.

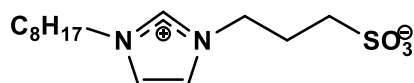
HL^{mes}₁₆

Yield: 75%; ¹H NMR (δ ppm, 400 MHz, CDCl₃): 0.86 (t, ³J= 8.0 Hz, 3H), 1.15-1.35 (m, 26H), 1.96 (m, 2H) 2.05 (s, 6H), 2.31 (s, 3H), 4.68 (t, ³J= 8.0 Hz, 2H), 6.97 (s, 2H), 7.24 (s, 1H), 7.91 (s, 1H), 10.31 (s, 1H). ¹³C{¹H} NMR (δ ppm, 100 MHz, CDCl₃): 14.11 (CH₃), 17.63 (CH₂), 21.08 (CH₂), 22.67 (CH₃), 26.11 (CH₂), 29.05 (CH₃), 29.34 (CH₃), 29.42 (CH₃), 29.50 (CH₂), 29.61 (CH₂), 29.64 (CH₂), 29.68 (CH₂), 30.55 (CH₃), 31.90 (CH₃), 50.38 (NCH₂), 123.10 (C₅), 123.35 (C₄), 129.82 (*ipso*-mesityl), 130.72 (*m*-mesityl), 134.19 (*o*-mesityl), 137.88 (C₂), 141.19 (*p*-mesityl). HRMS (ESI) (*m/z*): found 411.3739 [(M-Br)⁺, (C₂₈H₄₇N₂⁺), 100%], expected 411.3734.

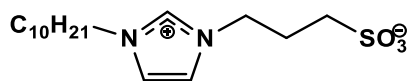
General procedure for the preparation of sulfonated imidazolium zwitterions, HL^{bet}₈₋₁₆

To a solution of propane sultone (3.00 mmol) in acetone (10 mL) the corresponding alkyl imidazole (2.00 mmol) was added and the reaction solution was left stirring overnight. As the

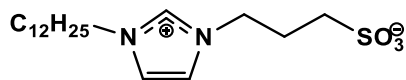
product forms, it separates from the acetone solution either as a solid (C₁₂, C₁₄ and C₁₆ derivatives) or viscous liquid (C₈ and C₁₀ derivatives). The product was isolated by separation from the supernatant acetone and purified by further washings with acetone (2 x 10 mL).

HL^{bet}₈

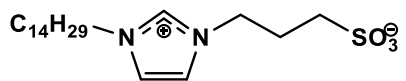
Yield: 91%; ¹H NMR (400 MHz, CDCl₃): δ 0.87 (t, ³J = 7.6 Hz, 3H), 1.24 – 1.38 (br, 10H), 1.86 (m, 2H), 2.38 (m, 8, 2H), 2.84 (t, ³J = 7.0 Hz, 2H), 4.27 (t, ³J = 7.4 Hz, 2H), 4.55 (t, ³J = 7.0 Hz, 2H), 7.32 (s, 1H), 7.69 (s, 1H), 9.52 (s, 1H). ¹³C{¹H} NMR (100 MHz, CDCl₃): δ 14.09 (CH₃), 22.60 (CH₂), 26.30 (CH₂), 26.57 (CH₂), 28.99 (CH₂), 29.05 (CH₂), 30.22 (CH₂), 31.71 (CH₂), 47.49 (CH₂), 48.46 (CH₂), 50.02 (CH₂), 121.71 (CH), 122.99 (CH), 137.09 (NCHN). HRMS (ESI⁺) m/z: Found 303.1736 [(M+H)⁺], (C₁₄H₂₇N₂O₃S⁺), 100%], expected 303.1737.

HL^{bet}₁₀

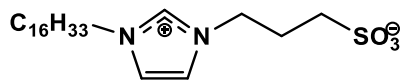
Yield: 90%; ¹H NMR (400 MHz, CDCl₃): δ 0.88 (t, ³J = 7.0 Hz, 3H), 1.20 – 1.38 (br, 18H), 1.96 (m, 2H), 2.37 (m, 2H), 2.83 (t, ³J = 7.7 Hz, 2H), 4.24 (t, ³J = 7.0 Hz, 2H), 4.54 (t, ³J = 7.4 Hz, 2H), 7.29 (s, 1H), 7.69 (s, 1H), 9.48 (s, 1H). ¹³C{¹H} NMR (100 MHz, CDCl₃): δ 14.13 (CH₃), 22.67 (CH₂), 26.33 (CH₂), 26.55 (CH₂), 29.07 (CH₂), 29.28 (CH₂), 29.42 (CH₂), 29.51 (2C, CH₂), 30.22 (CH₂), 31.86 (CH₂), 47.51 (CH₂), 48.46 (CH₂), 50.01 (CH₂), 121.72 (CH), 123.00 (CH), 137.02 (NCHN). HRMS (ESI⁺) m/z: Found 331.2057 [(M+H)⁺], (C₁₆H₂₉N₂O₃S⁺), 100%], expected 331.2050.

HL^{bet}₁₂

Yield: 89%; ¹H NMR (400 MHz, CDCl₃): δ 0.89 (t, ³J = 7.0 Hz, 3H), 1.24 – 1.38 (br, 18H), 1.89 (m, 2H), 2.42 (m, 2H), 2.87 (t, ³J = 6.9 Hz, 2H), 4.27 (t, ³J = 7.5 Hz, 2H), 4.60 (t, ³J = 7.0 Hz, 2H), 7.22 (s, 1H), 7.57 (s, 1H), 9.72 (s, 1H). ¹³C{¹H} NMR (100 MHz, CDCl₃): δ 14.15 (CH₃), 22.70 (CH₂), 26.31 (CH₂), 26.64 (CH₂), 29.03 (CH₂), 29.35 (CH₂), 29.39 (CH₂), 29.53 (CH₂), 29.61 (2C, CH₂), 30.26 (CH₂), 31.92 (CH₂), 47.35(CH₂), 48.62 (CH₂), 50.14 (CH₂), 121.35 (CH), 122.64 (CH), 137.72 (NCHN). HRMS (ESI+) m/z: Found 359.2376 [(M+H)⁺, (C₁₈H₃₅N₂O₃S⁺), 100%], expected 359.2363.

HL^{bet}₁₄

Yield: 89%; ¹H NMR (400 MHz, CDCl₃): δ 0.87 (t, ³J = 6.7 Hz, 3H), 1.24 – 1.38 (br, 22H), 1.89 (m, 2H), 2.42 (m, 2H), 2.87 (t, ³J = 6.9 Hz, 2H), 4.26 (t, ³J = 7.4 Hz, 2H), 4.59 (t, ³J = 7.0 Hz, 2H), 7.29 (s, 1H), 7.63 (s, 1H), 9.70 (s, 1H). ¹³C{¹H} NMR (100 MHz, CDCl₃): δ 14.15 (CH₃), 22.71 (CH₂), 26.32 (CH₂), 26.68 (CH₂), 29.05 (CH₂), 29.38 (CH₂), 29.41 (CH₂), 29.55 (CH₂), 29.63 (CH₂), 29.67 (2C, CH₂), 29.70 (CH₂), 31.93 (CH₂), 47.35(CH₂), 48.62 (CH₂), 50.14 (CH₂), 121.40 (CH), 122.82 (CH), 137.58 (NCHN). HRMS (ESI+) m/z: Found 387.2683 [(M+H)⁺, (C₂₀H₃₉N₂O₃S⁺), 100%], expected 387.2676.

HL^{bet}₁₆

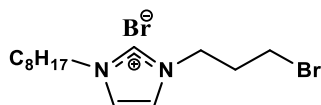
Yield: 93%; ¹H NMR (400 MHz, CDCl₃): δ 0.89 (t, ³J = 7.0 Hz, 3H), 1.20 – 1.40 (br, 26H), 1.89 (m, 2H), 2.42 (m, 2H), 2.87 (t, ³J = 6.9 Hz, 2H), 4.27 (t, ³J = 7.5 Hz, 2H), 4.59 (t, ³J = 7.0 Hz, 2H), 7.23 (s, 1H), 7.56 (s, 1H), 9.68 (s, 1H). ¹³C{¹H} NMR (100 MHz, CDCl₃): δ 14.16 (CH₃), 22.71 (CH₂), 26.32 (CH₂), 26.59 (CH₂), 29.05 (CH₂),

29.39 (CH₂), 29.41 (CH₂), 29.56 (CH₂), 29.64 (CH₂), 29.69 (CH₂), 29.72 (2C, CH₂), 30.25 (CH₂), 31.94 (CH₂), 47.34 (CH₂), 48.61 (CH₂), 50.14 (CH₂), 121.39 (CH), 122.60 (CH), 137.64 (NCHN). HRMS (ESI+) *m/z*: Found 415.2991 [(M+H)⁺, (C₂₂H₄₃N₂O₃S⁺), 100%], expected 415.2989.

General procedure for the preparation of 1-(3-Bromopropyl)-3-alkylimidazolium bromide

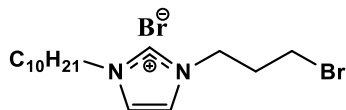
N-alkyl imidazole (alkyl = C₈H₁₇, C₁₀H₂₁, C₁₂H₂₅, C₁₄H₂₉, and C₁₆H₃₃) (30 mmol) was reacted with a large excess (more than 3-fold) of 1,3-dibromopropane in acetonitrile (70 mL) at 50°C. At the end of the reaction, the solvent was removed under reduced pressure and unreacted 1,3-dibromopropane was removed by partitioning methanol solution of the crude with hexane in a separatory funnel. The resulting viscous pale-yellow oil was purified by silica column chromatography (CH₃COCH₃:CH₃OH=10:1) to afford 1-(3-bromopropyl)-3-alkylimidazolium bromide salts as a pale-yellow viscous oil.

C8ImPrBr



Yield: 68%; ¹H NMR (δ ppm, 400 MHz, CDCl₃): 0.85 (t, ³J = 8.0 Hz, 3H) 1.20-1.35 (m, 10H), 1.91 (m, 2H), 2.56 (m, 2H), 3.48 (t, ³J = 8.0 Hz, 2H), 4.33 (t, ³J = 8.0 Hz, 2H), 4.62 (t, ³J = 8.0 Hz, 2H), 7.46 (s, 1H), 7.67 (s, 1H), 10.44 (s, 1H), ¹³C{¹H} NMR (δ ppm, 100 MHz, CDCl₃): 14.05 (CH₃), 22.55 (CH₂), 26.25 (CH₂), 28.91 (CH₂) 29.00 (CH₂), 29.21 (CH₃), 30.24 (CH₂), 30.31 (CH₂), 31.64 (CH₂), 32.75 (CH₂Br), 48.36 (NCH₂), 50.31 (NCH₂), 121.98 (C₅), 122.86 (C₄), 137.08 (C₂), HRMS (ESI) *m/z*: found 301.1288 [(M-Br)⁺, (C₁₄H₂₅BrN₂⁺)], expected 301.1274.

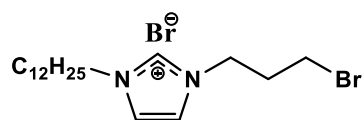
C10ImPrBr



Yield: 71%; ¹H NMR (δ ppm, 400 MHz, CDCl₃): 0.81 (t, ³J = 8.0 Hz, 3H) 1.15-1.32 (m, 14H), 1.86 (m, 2H), 2.53 (m, 2H), 3.43 (t, ³J = 8.0 Hz, 2H), 4.26 (t, ³J = 8.0 Hz, 2H), 4.57 (t, ³J = 8.0 Hz,

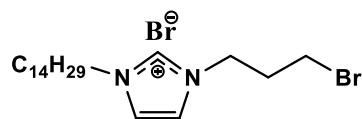
2H), 7.40 (s, 1H), 7.61 (s, 1H), 10.38 (s, 1H), $^{13}\text{C}\{^1\text{H}\}$ NMR (δ ppm, 100 MHz, CDCl_3): 14.11 (CH₃), 22.64 (CH₂), 26.27 (CH₂), 28.97 (CH₂), 29.22 (CH₂), 29.25 (CH₂), 29.36 (CH₃), 29.43 (CH₂), 30.25 (CH₂), 31.82 (CH₂), 32.74 (CH₂), 41.01 (CH₂Br), 48.36 (NCH₂), 50.33 (NCH₂), 121.94 (C₅), 122.84 (C₄), 137.21 (C₂), HRMS (ESI) m/z : 329.1602 [(M-Br)⁺, (C₁₆H₂₉BrN₂⁺)], expected 329.1587.

C12ImPrBr

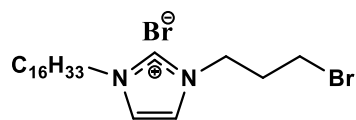


Yield: 77%; ^1H NMR (δ ppm, 400 MHz, CDCl_3): 0.87 (t, $^3\text{J} = 8.0$ Hz, 3H) 1.20-1.37 (m, 18H), 1.92 (m, 2H), 2.59 (m, 2H), 3.48 (t, $^3\text{J} = 8.0$ Hz, 2H), 4.32 (t, $^3\text{J} = 8.0$ Hz, 2H), 4.63 (t, $^3\text{J} = 8.0$ Hz, 2H), 7.43 (s, 1H), 7.64 (s, 1H), 10.49 (s, 1H), $^{13}\text{C}\{^1\text{H}\}$ NMR (δ ppm, 100 MHz, CDCl_3): 14.11 (CH₃), 22.66 (CH₂), 26.28 (CH₂), 28.98 (CH₂), 29.23 (CH₂), 29.31 (CH₂), 29.37 (CH₂), 29.48 (CH₃), 29.57 (2C, CH₂), 30.25 (CH₂), 31.88 (CH₂), 32.74 (CH₂Br), 48.38 (NCH₂), 50.35 (NCH₂), 121.86 (C₅), 122.80 (C₄), 137.33 (C₂), HRMS (ESI) m/z : 357.1898 [(M-Br)⁺, (C₁₈H₃₃BrN₂⁺)], expected 357.1900.

C14ImPrBr



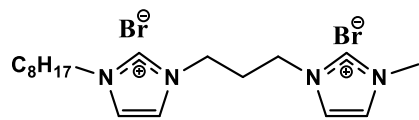
Yield: 65%; ^1H NMR (δ ppm, 400 MHz, CDCl_3): 0.90 (t, $^3\text{J} = 8.0$ Hz, 3H) 1.25-1.40 (m, 22H), 1.95 (m, 2H), 2.64 (m, 2H), 3.51 (t, $^3\text{J} = 8.0$ Hz, 2H), 4.33 (t, $^3\text{J} = 8.0$ Hz, 2H), 4.66 (t, $^3\text{J} = 8.0$ Hz, 2H), 7.25 (s, 1H), 7.40 (s, 1H), 10.89 (s, 1H), $^{13}\text{C}\{^1\text{H}\}$ NMR (δ ppm, 100 MHz, CDCl_3): 14.14 (CH₃), 22.70 (CH₂), 26.30 (CH₂), 28.96 (CH₂), 29.57 (CH₂), 29.48 (CH₂), 29.59 (CH₂), 29.65 (CH₃), 29.68 (CH₂), 30.22 (CH₂), 31.93 (CH₂), 29.32 (CH₂), 32.36 (CH₂Br), 48.36 (NCH₂), 50.31 (NCH₂), 121.21 (C₅), 122.36 (C₄), 138.19 (C₂), HRMS (ESI) m/z : 385.2237 [(M-Br)⁺, (C₂₀H₃₇BrN₂⁺)], expected 385.2213.

C16ImPrBr

Yield: 72%; ^1H NMR (δ ppm, 400 MHz, CDCl_3): 0.86 (t, $^3\text{J} = 8.0$ Hz, 3H) 1.22-1.40 (m, 26H), 1.93 (m, 2H), 2.60 (m, 2H), 3.50 (t, $^3\text{J} = 8.0$ Hz, 2H), 4.32 (t, $^3\text{J} = 8.0$ Hz, 2H), 4.64 (t, $^3\text{J} = 8.0$ Hz, 2H), 7.37 (s, 1H), 7.57 (s, 1H), 10.59 (s, 1H), $^{13}\text{C}\{^1\text{H}\}$ NMR (δ ppm, 100 MHz, CDCl_3): 14.05 (CH_3), 22.69 (CH_2), 26.29 (CH_2), 28.98 (CH_2), 29.26 (CH_2), 29.36 (CH_2), 29.38 (CH_2), 29.50 (CH_2), 29.60 (CH_2), 29.65 (CH_3), 29.69 (CH_2), 30.24 (CH_2), 31.92 (CH_2), 32.71 (CH_2Br), 48.40 (NCH_2), 50.40 (NCH_2), 121.66 (C_5), 122.65 (C_4), 137.58 (C_2), HRMS (ESI) m/z : 413.2537 [(M-Br) $^+$, ($\text{C}_{22}\text{H}_{41}\text{BrN}_2^+$)], expected 413.2526.

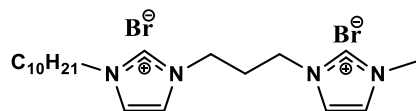
General procedure for the preparation of dicationic imidazolium salts, $\text{H}_2\text{G}_{8-16}$, $\text{H}_2\text{G}^{\text{mes}}_{8-16}$ and $\text{HG}^{\text{ima}}_{8-16}$

1-(3-bromopropyl)-3-alkylimidazolium bromide (1 mmol) (alkyl = C_8H_{17} , $\text{C}_{10}\text{H}_{21}$, $\text{C}_{12}\text{H}_{25}$, $\text{C}_{14}\text{H}_{29}$, and $\text{C}_{16}\text{H}_{33}$) was reacted with (1.5 mmol) of *N*-methyl imidazole, *N*-mesityl imidazole and trimethylamine respectively in toluene (40 mL) under reflux for 48 h. At the end of the reaction, the solution was cooled down to give two immiscible layers. The top layer was decanted carefully, and the thick oily product was precipitated with acetone. The crude product was recrystallized in acetone and dried under vacuum to yield white solid.

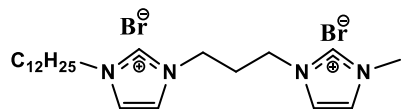
 H_2G_8 

Yield: 88%; ^1H NMR (δ ppm, 400 MHz, CDCl_3): 0.81 (t, $^3\text{J} = 7.0$ Hz, 3H), 1.12-1.35 (m, 10H), 1.86 (m, 2H) 2.71 (m, 2H), 4.00 (s, 3H, CH_3N), 4.24 (t, $^3\text{J} = 7.5$ Hz, 2H), 4.61 (m, 4H), 7.45 (s, 1H), 7.57 (s, 1H), 8.03 (s, 1H), 8.11 (s, 1H), 9.69 (s, 1H), 9.86 (s, 1H), $^{13}\text{C}\{^1\text{H}\}$ NMR (δ ppm, 100 MHz, CDCl_3): 14.06 (CH_3), 22.54 (CH_2), 26.30 (CH_2), 28.94 (CH_2), 29.01 (CH_2), 30.09 (CH_2), 30.95 (CH_3), 31.65 (CH_2), 36.97 (CH_2), 46.59 (CH_2), 46.63 (CH_2), 50.22 (NCH_2), 122.05 (C_5), 123.09 (C_5'), 123.45 (C_4), 123.64 (C_4'), 136.28 (C_2), 136.92 (C_2'), HRMS (ESI) m/z : found

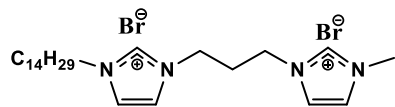
383.1800 [(M-Br)⁺, (C₁₈H₃₀BrN₄)⁺, 100%], expected 383.1628, found 152.1689 [(M-2Br)²⁺, (C₁₈H₃₀N₄)²⁺, 10%], expected 151.6247.

H₂G₁₀

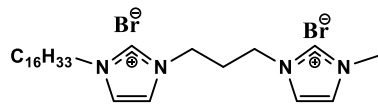
Yield: 89%; ¹H NMR (δ ppm, 400 MHz, CDCl₃): 0.81 (t, ³J = 7.0 Hz, 3H), 1.12-1.35 (m, 14H), 1.84 (m, 2H), 2.78 (m, 2H), 3.98 (s, 3H, CH₃N), 4.19 (t, ³J = 7.5 Hz, 2H), 4.65 (m, 4H), 7.24 (s, 1H), 7.31 (s, 1H), 8.13 (s, 1H), 8.16 (s, 1H), 10.01 (s, 1H), 10.08 (s, 1H), ¹³C{¹H} NMR (δ ppm, 100 MHz, CDCl₃): 14.13 (CH₃), 22.66 (CH₂), 26.32 (CH₂), 28.97 (CH₃), 29.23 (CH₂), 29.36 (CH₂), 29.44 (CH₂), 30.12 (CH₂), 30.96 (CH₃), 31.83 (CH₂), 36.83 (CH₂), 46.69 (CH₂), 46.74 (CH₂), 50.35 (NCH₂), 121.57 (C₅), 123.07 (C₅'), 123.71 (C₄), 123.79 (C₄'), 136.51 (C₂), 137.18 (C₂'),. HRMS (ESI) *m/z*: found 411.2130 [(M-Br)⁺, (C₂₀H₃₄BrN₄)⁺, 100%], expected 411.1941, found 166.1473 [(M-2Br)²⁺, (C₂₀H₃₄N₄)²⁺, 8%], expected 165.1386.

H₂G₁₂

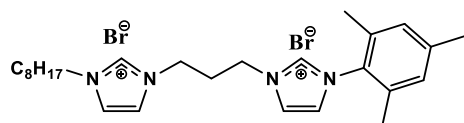
Yield: 86%; ¹H NMR (δ ppm, 400 MHz, CDCl₃): 0.88 (t, ³J = 7.1 Hz, 3H), 1.22-1.35 (m, 18H), 1.90 (m, 2H), 2.87 (m, 2H), 4.05 (s, 3H, CH₃N), 4.25 (t, ³J = 7.8 Hz, 2H), 4.74 (m, 4H), 7.28 (s, 1H), 7.34 (s, 1H), 8.20 (s, 1H), 8.23 (s, 1H), 10.12 (s, 1H), 10.18 (s, 1H), ¹³C{¹H} NMR (δ ppm, 100 MHz, CDCl₃): 14.14 (CH₃), 22.69 (CH₂), 26.32 (CH₂), 28.97 (CH₂), 29.33 (CH₃), 29.37 (CH₂), 29.50 (CH₂), 29.59 (2C, CH₂), 30.12 (CH₂), 30.96 (CH₃), 31.90 (CH₂), 36.81 (CH₂), 46.70 (CH₂), 46.76 (CH₂), 50.36 (NCH₂), 121.49 (C₅), 122.97 (C₅'), 123.79 (C₄), 123.83 (C₄'), 136.53 (C₂), 137.20 (C₂'),. HRMS (ESI) *m/z*: found 180.1689 [(M-2Br)²⁺, (C₂₂H₃₈N₄)²⁺], expected 179.1543, found 439.2441 [(M-Br)⁺, (C₂₂H₃₈BrN₄)⁺, 20%], expected 439.2254.

H₂G₁₄

Yield: 92%; ¹H NMR (δ ppm, 400 MHz, CDCl₃): 0.81 (t, ³J = 8.0 Hz, 3H), 1.15-1.30 (m, 22H), 1.84 (m, 2H) 2.81 (m, 2H), 3.97 (s, 3H, CH₃N), 4.17 (t, ³J = 7.0 Hz, 2H), 4.68 (m, 4H), 7.28 (s, 1H), 7.34 (s, 1H), 8.12 (s, 1H), 8.13 (s, 1H), 10.11 (s, 1H), 10.14 (s, 1H), ¹³C{¹H} NMR (δ ppm, 100 MHz, CDCl₃): 14.50 (CH₃), 22.70 (CH₂), 26.32 (CH₂), 28.97 (CH₃), 29.37 (2C, CH₂), 29.50 (CH₃), 29.60 (CH₂), 29.65 (2C, CH₂), 29.69 (CH₂), 30.12 (CH₂), 30.90 (CH₃), 31.93 (CH₂), 36.78 (CH₂), 46.73 (CH₂), 46.81 (CH₂), 50.39 (NCH₂), 121.36 (C₅), 122.80 (C_{5'}), 123.90 (C₄), 123.91 (C_{4'}), 136.57 (C₂), 137.26 (C_{2'}),. HRMS (ESI) *m/z*: found 194.1768 [(M-2Br)²⁺, (C₂₄H₄₂N₄)²⁺, 100%], expected 193.1699, found 467.2742 [(M-Br)⁺, (C₂₄H₄₂BrN₄)⁺, 50%], expected 467.2567.

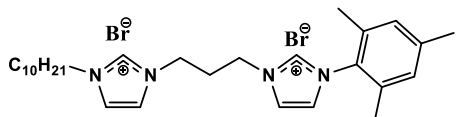
H₂G₁₆

Yield: 90.1%; ¹H NMR (δ ppm, 400 MHz, CDCl₃): 0.90 (t, ³J = 7.1 Hz, 3H), 1.22-1.40 (m, 26H), 1.93 (m, 2H) 2.91 (m, 2H), 4.04 (s, 3H, CH₃N), 4.24 (t, ³J = 7.5 Hz, 2H), 4.79 (m, 4H), 7.19 (s, 1H), 7.21 (s, 1H), 8.16 (s, 1H), 8.17 (s, 1H), 10.20 (s, 1H), 10.22 (s, 1H), ¹³C{¹H} NMR (δ ppm, 100 MHz, CDCl₃): 14.15 (CH₃), 22.70 (CH₂), 26.32 (CH₂), 28.97 (CH₃), 29.37 (2C, CH₂), 29.51 (CH₃), 29.60 (CH₂), 29.66 (2C, CH₂), 29.70 (2C, CH₂), 30.12 (CH₂), 30.89 (CH₂), 30.97 (CH₃), 31.93 (CH₂), 36.79 (CH₂), 46.71 (CH₂), 46.79 (CH₂), 121.42 (C₅), 122.87 (C_{5'}), 123.86 (C₄), 123.86 (C_{4'}), 136.57 (C₂), 137.25 (C_{2'}),. HRMS (ESI) *m/z*: found 208.1897 [(M-2Br)²⁺, (C₂₆H₄₆N₄)²⁺, 100%], expected 207.1856, found 495.3053 [(M-Br)⁺, (C₂₆H₄₆BrN₄)⁺, 95%], expected 495.2880.

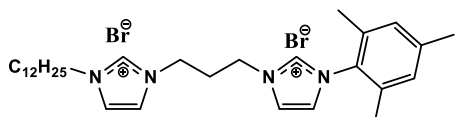
H₂G^{mes}₈

Yield: 91%; ¹H NMR (δ ppm, 500 MHz, CDCl₃): 0.87 (t, ³J = 7.0 Hz, 3H), 1.20-1.40 (m, 12H), 1.27 (m, 6H), 1.91 (m, 2H), 2.05 (s, 6H), 2.33 (s, 3H), 3.04 (m, 2H), 4.25 (t,

$^3J = 7.5$ Hz, 2H), 4.78 (t, $^3J = 7.2$ Hz, 2H), 4.95 (t, $^3J = 8.0$ Hz, 2H), 6.99 (s, 2H), 7.11 (s, 1H), 7.24 (s, 1H), 8.22 (s, 1H), 8.70 (s, 1H), 10.07 (s, 1H), 10.22 (s, 1H), $^{13}\text{C}\{^1\text{H}\}$ NMR (δ ppm, 125 MHz, CDCl_3): 14.04 (CH_3), 17.63 (CH_2), 21.09 (CH_2), 22.55 (CH_2), 26.27 (CH_3), 28.87 (CH_2), 28.97 (CH_3), 30.11 (CH_3), 31.52 (CH_2), 31.63 (CH_2), 46.98 (CH_2), 47.00 (CH_2), 50.32 (NCH_2), 121.30 (C_5), 122.89 (C_5'), 124.17 (C_4), 124.76 (C_4'), 129.87 (2C, *m*-mesityl), 130.62 (*p*-mesityl), 134.15 (2C, *o*-mesityl), 136.47 (C_2), 137.21 (C_2'), 141.36(*ipso*-mesityl). HRMS (ESI) m/z : found 204.1592 [(M-2Br) $^{2+}$, ($\text{C}_{26}\text{H}_{38}\text{N}_4$) $^{2+}$, 30%], expected 203.1543, found 485.2433 [(M-Br) $^+$, ($\text{C}_{26}\text{H}_{38}\text{BrN}_4$) $^+$, 35%], expected 485.2275.

H₂G^{mes}₁₀

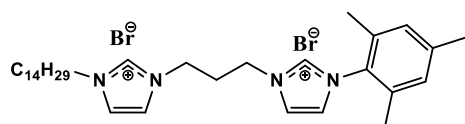
Yield: 93%; ^1H NMR (δ ppm, 500 MHz, CDCl_3): 0.88 (t, $^3J = 6.8$ Hz, 3H), 1.24-1.40 (m, 12H), 1.27 (m, 6H), 1.92 (m, 2H), 2.06 (s, 6H), 2.37 (s, 3H), 3.05 (m, 2H), 4.25 (t, $^3J = 7.5$ Hz, 2H), 4.79 (t, $^3J = 7.3$ Hz, 2H), 4.96 (t, $^3J = 8.0$ Hz, 2H), 7.00 (s, 2H), 7.11 (s, 1H), 7.23 (s, 1H), 8.21 (s, 1H), 8.69 (s, 1H), 10.07 (s, 1H), 10.20 (s, 1H), $^{13}\text{C}\{^1\text{H}\}$ NMR (δ ppm, 125 MHz, CDCl_3): 14.10 (CH_3), 17.63 (CH_2), 21.10 (CH_2), 22.65 (CH_2), 26.29 (CH_3), 28.93 (CH_2), 29.21 (CH_3), 29.33 (CH_2), 29.42 (CH_2), 30.12 (CH_2), 30.29 (CH_3), 31.57 (CH_2), 31.82 (CH_2), 32.45 (CH_2), 46.99 (CH_2), 50.35 (NCH_2), 121.23 (C_5), 122.89 (C_5'), 124.20 (C_4), 124.76 (C_4'), 129.89 (2C, *m*-mesityl), 130.62 (*p*-mesityl), 134.16 (2C, *o*-mesityl), 136.47 (C_2), 137.20 (C_2'), 141.39(*ipso*-mesityl). HRMS (ESI) m/z : found 218.1742 [(M-2Br) $^{2+}$, ($\text{C}_{28}\text{H}_{42}\text{N}_4$) $^{2+}$, 50%], expected 217.1699, found 515.2733 [(M-Br) $^+$, ($\text{C}_{28}\text{H}_{42}\text{BrN}_4$) $^+$, 25%], expected 515.2567.

H₂G^{mes}₁₂

Yield: 89%; ^1H NMR (δ ppm, 500 MHz, CDCl_3): 0.81 (t, $^3J = 7.0$ Hz, 3H), 1.24-1.15 (m, 18H), 1.85 (m, 2H), 1.98 (s, 6H), 2.28 (s, 3H), 2.99 (m, 2H), 4.16 (t, $^3J = 7.5$ Hz, 2H), 4.75 (t, $^3J = 7.3$ Hz, 2H), 4.90 (t, $^3J = 8.0$ Hz, 2H), 6.94 (s, 2H), 7.02 (s, 1H), 7.09 (s, 1H), 8.06 (s, 1H), 8.56 (s, 1H), 9.97 (s, 1H), 10.14 (s, 1H), $^{13}\text{C}\{^1\text{H}\}$ NMR (δ ppm, 125 MHz, CDCl_3): 14.12 (CH_3), 17.61 (CH_2), 21.11 (CH_2), 22.68 (CH_2), 26.30 (CH_3), 28.93 (CH_2), 29.32 (CH_3), 29.47

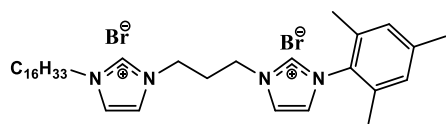
(CH₂), 29.57 (CH₂), 29.58 (CH₂), 30.12 (CH₂), 30.94 (CH₃), 31.48 (CH₂), 31.90 (CH₂), 47.01 (CH₂), 47.07 (CH₂), 50.57 (NCH₂), 121.08 (C₅), 122.87 (C_{5'}), 124.20 (C₄), 124.69 (C_{4'}), 129.92 (2C, *m*-mesityl), 130.58 (*p*-mesityl), 134.13 (2C, *o*-mesityl), 136.52 (C₂), 137.19 (C_{2'}), 141.47(*ipso*-mesityl). HRMS (ESI) *m/z*: found 232.1882 [(M-2Br)²⁺, (C₃₀H₄₆N₄)²⁺, 85%], expected 231.1856, found 541.3055 [(M-Br)⁺, (C₃₀H₄₆BrN₄)⁺, 55%], expected 541.2901.

H₂G^{mes}₁₄



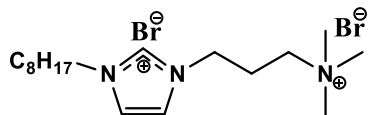
Yield: 86%; ¹H NMR (δ ppm, 500 MHz, CDCl₃): 0.89 (t, ³J = 7.0 Hz, 3H), 1.20-1.38 (m, 22H), 1.93 (m, 2H), 2.07 (s, 6H), 2.36 (s, 3H), 3.07 (m, 2H), 4.25 (t, ³J = 7.5 Hz, 2H), 4.82 (t, ³J = 7.2 Hz, 2H), 4.98 (t, ³J = 8.0 Hz, 2H), 7.02 (s, 2H), 7.10 (s, 1H), 7.18 (s, 1H), 8.17 (s, 1H), 8.66 (s, 1H), 10.05 (s, 1H), 10.21 (s, 1H), ¹³C{¹H} NMR (δ ppm, 125 MHz, CDCl₃): 14.13 (CH₃), 17.62 (CH₂), 21.10 (CH₂), 22.69 (CH₂), 26.31 (CH₃), 27.91 (CH₂), 28.94 (CH₂), 29.35 (2C, CH₃), 29.48 (CH₂), 29.57 (CH₂), 29.64 (2C, CH₂), 29.67 (CH₂), 30.12 (CH₂), 31.46 (CH₂), 31.92 (CH₂), 47.01 (CH₂), 47.06 (CH₂), 50.39 (NCH₂), 121.14 (C₅), 122.87 (C_{5'}), 124.18 (C₄), 124.71 (C_{4'}), 129.91 (2C, *m*-mesityl), 130.59 (*p*-mesityl), 134.14 (2C, *o*-mesityl), 136.52 (C₂), 137.21 (C_{2'}), 141.45(*ipso*-mesityl). HRMS (ESI) *m/z*: found 246.2079 [(M-2Br)²⁺, (C₃₂H₅₀N₄)²⁺, 100%], expected 245.2012, found 571.3361 [(M-Br)⁺, (C₃₂H₅₀BrN₄)⁺, 20%], expected 571.3193.

H₂G^{mes}₁₆

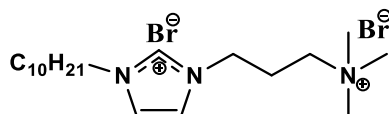


Yield: 92%; ¹H NMR (δ ppm, 500 MHz, CDCl₃): 0.86 (t, ³J = 7.1 Hz, 3H), 1.20-1.35 (m, 26H), 1.88 (m, 2H), 2.04 (s, 6H), 2.32 (s, 3H), 3.01 (m, 2H), 4.24 (t, ³J = 7.5 Hz, 2H), 4.76 (t, ³J = 7.2 Hz, 2H), 4.93 (t, ³J = 8.0 Hz, 2H), 6.98 (s, 2H), 7.11 (s, 1H), 7.24 (s, 1H), 8.24 (s, 1H), 8.69 (s, 1H), 10.03 (s, 1H), 10.12 (s, 1H), ¹³C{¹H} NMR (δ ppm, 125 MHz, CDCl₃): 14.11 (CH₃), 17.64 (CH₂), 21.08 (CH₂), 21.44 (CH₂), 22.67 (CH₂), 26.30 (CH₃), 28.95 (CH₂), 29.34 (2C, CH₃), 29.35 (CH₂), 29.48 (CH₂), 29.63 (2C, CH₂), 29.67 (2C, CH₂), 29.68 (CH₂), 30.12 (CH₂), 31.59 (CH₂), 31.90 (CH₂), 46.92 (CH₂), 47.00 (CH₂), 50.29 (NCH₂), 121.35 (C₅), 122.91 (C_{5'}),

124.15 (C₄), 124.78 (C₄'), 129.85 (2C, *m*-mesityl), 130.64 (*p*-mesityl), 134.17 (2C, *o*-mesityl), 136.42 (C₂), 137.20 (C₂'), 141.31 (*ipso*-mesityl). HRMS (ESI) *m/z*: found 260.2238 [(M-2Br)²⁺, (C₃₄H₅₄N₄)²⁺, 20%], expected 259.2169, found 599.3655 [(M-Br)⁺, (C₃₄H₅₄BrN₄)⁺, 5%], expected 599.3506.

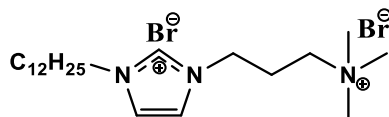
HG^{tma}₈

Yield: 81%; ¹H NMR (400 MHz, CDCl₃): δ 0.86 (t, ³J = 6.3 Hz, 3H), 1.20 – 1.40 (m, 26H), 1.93 (m, 2H), 2.81 (m, 2H), 3.47 (s, 9H), 4.03 (t, ³J = 8.0 Hz, 2H), 4.26 (t, ³J = 7.5 Hz, 2H), 4.71 (t, ³J = 7.3 Hz, 2H), 7.39 (s, 1H), 8.24 (s, 1H), 10.02 (s, 1H). ¹³C{¹H} NMR (δ ppm, 100 MHz, CDCl₃): δ 14.15 (CH₃), 22.70 (2C, CH₂), 24.72 (CH₂), 26.40 (CH₂), 29.04 (CH₂), 29.38 (CH₂), 29.44 (CH₂), 29.56 (CH₂), 29.65 (CH₂), 29.67 (CH₂), 29.69 (CH₂), 29.72 (3C, CH₃), 30.07 (CH₂), 31.93 (2C, CH₂), 46.65 (CH₂), 50.44 (CH₂), 54.07 (CH₂), 62.73 (CH₂), 121.80 (C₅), 123.72 (C₄), 136.48 (C₂). HRMS (ESI+) *m/z*: Found 140.6431 [(M-2Br)²⁺, (C₂₅H₅₁N₃)²⁺, 60%], expected 140.1371.

HG^{tma}₁₀

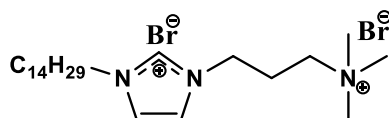
Yield: 86%; ¹H NMR (400 MHz, CDCl₃): δ 0.80 (t, ³J = 6.6 Hz, 3H), 1.10 – 1.30 (m, 26H), 1.86 (m, 2H), 2.68 (m, 2H), 3.41 (s, 9H), 3.88 (t, ³J = 8.0 Hz, 2H), 4.22 (t, ³J = 7.5 Hz, 2H), 4.60 (t, ³J = 7.4 Hz, 2H), 7.44 (s, 1H), 8.15 (s, 1H), 9.85 (s, 1H).

¹³C{¹H} NMR (δ ppm, 100 MHz, CDCl₃): δ 14.11 (CH₃), 22.63 (CH₂), 24.55 (CH₂), 26.37 (CH₂), 29.03 (CH₂), 29.24 (CH₂), 29.41 (CH₂), 29.47 (CH₂), 30.05 (CH₂), 31.82 (3C, CH₃), 46.62 (CH₂), 50.34 (CH₂), 53.83 (CH₂), 62.65 (CH₂), 122.08 (C₅), 123.51 (C₄), 136.35 (C₂). HRMS (ESI+) *m/z*: Found 388.2320 [(M-Br)⁺, (C₁₉H₃₉BrN₃)⁺, 80%], expected 387.2244.

HG^{tma}₁₂

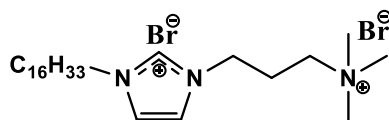
Yield: 81%; ¹H NMR (400 MHz, CDCl₃): δ 0.86 (t, ³J = 7.1 Hz, 3H), 1.20 – 1.40 (m, 26H), 1.93 (m, 2H), 2.81 (m, 2H), 3.47 (s, 9H), 4.03 (t, ³J = 8.0 Hz, 2H), 4.26 (t, ³J = 7.6 Hz, 2H), 4.71 (t, ³J = 7.4 Hz, 2H), 7.39 (s, 1H), 8.24 (s, 1H), 10.02 (s, 1H).

¹³C{¹H} NMR (δ ppm, 100 MHz, CDCl₃): δ 14.15 (CH₃), 22.70 (2C, CH₂), 24.72 (CH₂), 26.40 (CH₂), 29.04 (CH₂), 29.38 (CH₂), 29.44 (CH₂), 29.56 (CH₂), 29.65 (CH₂), 29.67 (CH₂), 29.69 (CH₂), 29.72 (3C, CH₃), 30.07 (CH₂), 31.93 (2C, CH₂), 46.65 (CH₂), 50.44 (CH₂), 54.07 (CH₂), 62.73 (CH₂), 121.80 (C₅), 123.72 (C₄), 136.48 (C₂). HRMS (ESI+) m/z: Found 416.2624 [(M-Br)⁺, (C₂₁H₄₃BrN₃)⁺, 55%], expected 415.2557.

HG^{tma}₁₄

Yield: 88%; ¹H NMR (400 MHz, CDCl₃): δ 0.86 (t, ³J = 6.7 Hz, 3H), 1.20 – 1.40 (m, 26H), 1.93 (m, 2H), 2.81 (m, 2H), 3.47 (s, 9H), 4.03 (t, ³J = 8.0 Hz, 2H), 4.26 (t, ³J = 7.6 Hz, 2H), 4.71 (t, ³J = 7.3 Hz, 2H), 7.39 (s, 1H), 8.24 (s, 1H), 10.02 (s, 1H).

¹³C{¹H} NMR (δ ppm, 100 MHz, CDCl₃): δ 14.15 (CH₃), 22.70 (2C, CH₂), 24.72 (CH₂), 26.40 (CH₂), 29.04 (CH₂), 29.38 (CH₂), 29.44 (CH₂), 29.56 (CH₂), 29.65 (CH₂), 29.67 (CH₂), 29.69 (CH₂), 29.72 (3C, CH₃), 30.07 (CH₂), 31.93 (2C, CH₂), 46.65 (CH₂), 50.44 (CH₂), 54.07 (CH₂), 62.73 (CH₂), 121.80 (C₅), 123.72 (C₄), 136.48 (C₂). HRMS (ESI+) m/z: Found 182.6956 [(M-2Br)²⁺, (C₂₃H₄₇N₃)²⁺, 100%], expected 182.1841.

HG^{tma}₁₆

Yield: 86%; ¹H NMR (400 MHz, CDCl₃): δ 0.86 (t, ³J = 7.1 Hz, 3H), 1.20 – 1.40 (m, 26H), 1.93 (m, 2H), 2.81 (m, 2H), 3.47 (s, 9H), 4.03 (t, ³J = 8.0 Hz, 2H), 4.26 (t, ³J = 7.6 Hz, 2H), 4.71 (t, ³J = 7.3 Hz, 2H), 7.39 (s, 1H), 8.24 (s, 1H), 10.02 (s, 1H).

¹³C{¹H} NMR (δ ppm, 100 MHz, CDCl₃): δ 14.15 (CH₃), 22.70 (2C, CH₂), 24.72 (CH₂), 26.40

(CH₂), 29.04 (CH₂), 29.38 (CH₂), 29.44 (CH₂), 29.56 (CH₂), 29.65 (CH₂), 29.67 (CH₂), 29.69 (CH₂), 29.72 (3C, CH₃), 30.07 (CH₂), 31.93 (2C, CH₂), 46.65 (CH₂), 50.44 (CH₂), 54.07 (CH₂), 62.73 (CH₂), 121.80 (C₅), 123.72 (C₄), 136.48 (C₂). MS (ESI+) m/z: Found 196.7123 [(M-2Br)²⁺, (C₂₅H₅₁N₃)²⁺, 100%], expected 196.1997.

Electrical Conductivity Measurements

The specific conductivities of the solutions were measured at (298.15 ± 0.1) K using Mettler Toledo Conductivity Meter (InLab 738 model) with a cell constant of 1.00 cm⁻¹ and having a sensitivity of 0.1 μS·cm⁻¹. Temperature was maintained constant within 0.1 K using a constant temperature bath and the dip type conductivity probe provided with the instrument has an inbuilt temperature probe. Prior to measurements, this probe was calibrated with standard aqueous KCl solution (1413 μS/cm). The CMC values of **HL**₈₋₁₆, **HL**^{mes}₈₋₁₆, **H₂G**₈₋₁₆ and **H₂G**^{mes}₈₋₁₆ were determined by preparing various concentrations of surfactant molecules by dilution method in aqueous solution and the conductivity of these solutions were measured at 298 K after thorough mixing. Three measurements were made for each concentration and only the mean values were taken into consideration.

2.6. References

1. S. N. Riduan and Y. Zhang, *Chem. Soc. Rev.*, 2013, **42**, 9055.
2. X. Zeng, X. Yang, Y. Zhang, C. Qing and H. Zhang, *Bioorg. Med. Chem. Lett.*, 2010, **20**, 1844-1847.
3. T. Inoue, H. Ebina, B. Dong and L. Zheng, *J. Coll. Interf. Sci.*, 2007, **314**, 236-241.
4. A. S. Larsen, J. D. Holbrey, F. S. Tham and C. A. Reed, *J. Am. Chem. Soc.*, 2000, **122**, 7264-7272.
5. J. E. Bara, E. S. Hatakeyama, B. R. Wiesenauer, X. Zeng, R. D. Noble and D. L. Gin, *Liq. Cryst.*, 2010, **37**, 1587-1599.
6. A. Sorrenti, O. Illa and R. M. Ortuño, *Chem. Soc. Rev.*, 2013, **42**, 8200-8219.
7. X. Han and D. W. Armstrong, *Org. Lett.*, 2005, **7**, 4205-4208.
8. J.-H. Fuhrhop and J. Koning, *Membranes and molecular assemblies: the synkinetic approach*, Roy. Soc. Chem., 2007, 20-44.
9. J. H. Fuhrhop and W. Helfrich, *Chem. Rev.*, 1993, **93**, 1565-1582.
10. R. Zana, *Dynamics of surfactant self-assemblies: micelles, microemulsions, vesicles and lyotropic phases*, CRC press, 2005, 1-75.
11. R. Nagarajan and E. Ruckenstein, *J. Coll. Interf. Sci.*, 1979, **71**, 580-604.
12. J. N. Israelachvili, *Intermolecular and surface forces*, press, 2015, 635-660.
13. P. Bonhote, A.-P. Dias, N. Papageorgiou, K. Kalyanasundaram and M. Grätzel, *Inorg. chem.*, 1996, **35**, 1168-1178.
14. M. Lee, Z. Niu, C. Slebodnick and H. W. Gibson, *The J. Phys. Chem. B*, 2010, **114**, 7312-7319.

15. A. A. Gridnev and I. M. Mihaltseva, *Synth. Comm.*, 1994, **24**, 1547-1555.
16. R. T. Huang, K. Peng, H. Shih, G. Lin, T. Chang, S. Hsu, T. S. Hsu and I. J. Lin, *Soft Matt.*, 2011, **7**, 8392-8400.
17. E. P. Çoban, R. Fırıncı, H. Biyik and M. E. Günay, *Braz. J. Pharm. Sci.*, 2017, **53**, 1-10.
18. O. A. El Seoud, P. A. R. Pires, T. Abdel-Moghny and E. L. Bastos, *J. Coll. Interf. Sci.*, 2007, **313**, 296-304.
19. B. Findlay, G. G. Zhanel and F. Schweizer, *Antimicro. Agents Chemoth.*, 2010, **54**, 4049-4058.
20. A. Getsis and A.-V. Mudring, *Acta Crystall. Sec. E Struc. Rep.*, 2005, **61**, o2945-o2946.
21. D. C. Apperley, C. Hardacre, P. Licence, R. W. Murphy, N. V. Plechkova, K. R. Seddon, G. Srinivasan, M. Swadźba-Kwaśny and I. J. Villar-Garcia, *Dalton Trans.*, 2010, **39**, 8679-8687.
22. Y. V. Nelyubina, A. S. Shaplov, E. I. Lozinskaya, M. I. Buzin and Y. S. Vygodskii, *J. Am. Chem. Soc.*, 2016, **138**, 10076-10079.
23. Z. Wei, X. Wei, S. Fu, J. Liu and D. Zhang, *Acta Crystall. Sect. E Struct. Rep.*, 2009, **65**, o1159-o1159.
24. B. Dong, N. Li, L. Zheng, L. Yu and T. Inoue, *Langmuir*, 2007, **23**, 4178-4182.
25. L. Shi, N. Li, H. Yan, Y. a. Gao and L. Zheng, *Langmuir*, 2011, **27**, 1618-1625.
26. R. Vanyúr, L. Biczók and Z. Miskolczy, *Coll. and Surf. A: Physico. Eng. Asp.*, 2007, **299**, 256-261.
27. W. A. Herrmann and C. Köcher, *Angew. Chem. Int. Ed.*, 1997, **36**, 2162-2187.
28. R. Rondla, J. C. Y. Lin, C. T. Yang and I. J. B. Lin, *Langmuir*, 2013, **29**, 11779-11785.
29. H. Nan, K. Kuroda, K. Takahashi and J. L. Anderson, *J. Chromat. A*, 2019, **1603**, 288-296.

30. P. Sun, F. Lu, A. Wu, L. Shi and L. Zheng, *Soft Matt.*, 2017, **13**, 2543-2548.
31. X.-h. Zhao and Z.-w. Ye, *Chin. J. Chem. Phys.*, 2016, **29**, 249-254.
32. K. Nesměrák and I. Němcová, *Analyt. Lett.*, 2006, **39**, 1023-1040.
33. H. Ritacco, J. Kovensky, A. Fernández-Cirelli and M. J. L. Castro, *J. Chem. Educ.*, 2001, **78**, 347-348.
34. U. More, Z. Vaid, P. Bhamoria, A. Kumar and N. I. Malek, *J. Sol. Chem.*, 2015, **44**, 850-874.
35. Z. Miskolczy, K. Sebők-Nagy, L. Biczók and S. Göktürk, *Chem. Phys. Lett.*, 2004, **400**, 296-300.

Chapter

3

Synthesis and Characterisation of silver (I) *N*-heterocyclic carbenes

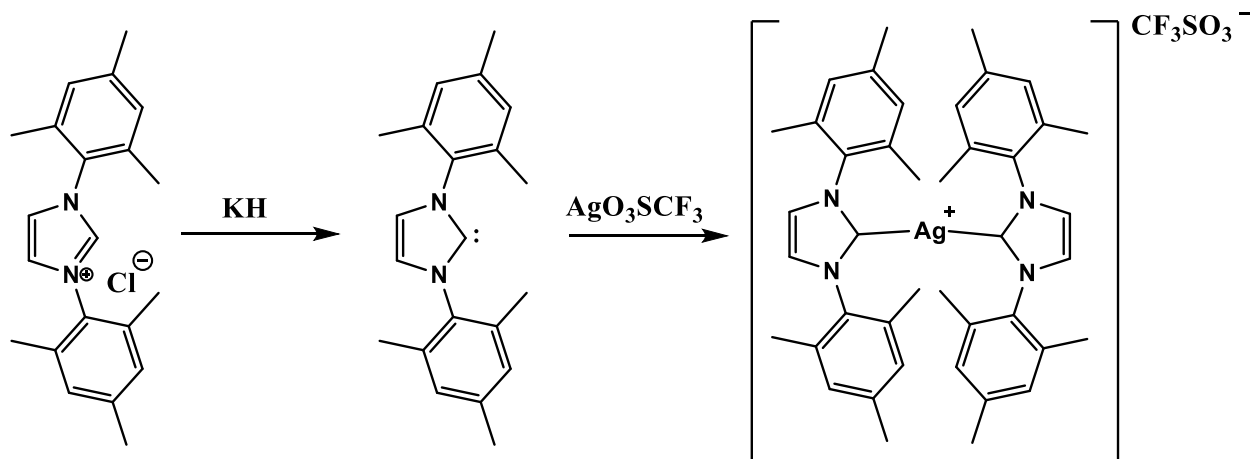
| | |
|--|------------|
| 3.0. Synthesis and Characterisation of silver (I) <i>N</i>-heterocyclic carbenes..... | 81 |
| 3.1. Introduction..... | 82 |
| 3.2. Aims..... | 84 |
| 3.3. Results and Discussion..... | 88 |
| 3.3.1. Synthesis of silver(I) <i>N</i> -heterocyclic carbene complexes..... | 88 |
| 3.3.2. ¹ H and ¹³ C NMR study of silver(I) complexes..... | 91 |
| 3.3.3. HRMS study of silver(I) complexes..... | 98 |
| 3.4. Experimental..... | 105 |
| 3.5. References..... | 115 |

Chapter 3

Synthesis and Characterisation of Silver (I) N-Heterocyclic Carbenes

3.1. Introduction

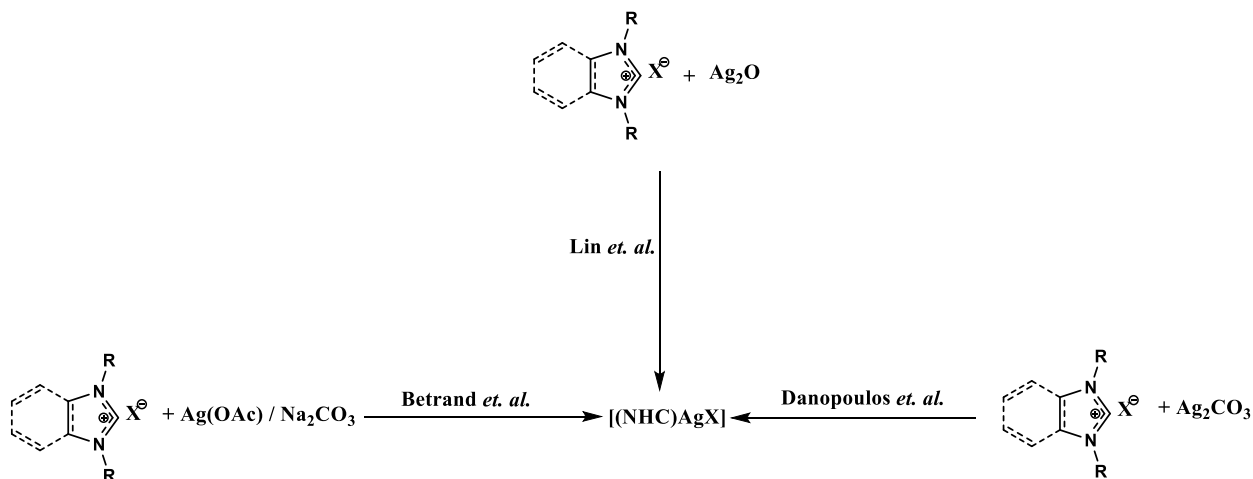
NHCs act as excellent strong σ -donors and can be used as ligands for both transition^{1,2} and main group metals.³ Research activities on the metal complexes of NHCs are on the rise because of their chemistry and wide area of applications.³⁻¹⁰ Amongst the metal complexes of NHCs, Ag(I)-NHCs have enjoyed considerable interest due to their diverse structures in the solid-state, their use as carbene transfer reagents^{9, 11, 12} and their application as antimicrobial⁸ and antitumor agents.¹³ Arduengo *et. al.*, in 1993, synthesized the first Ag(I)-NHC from a free carbene route by deprotonating 1,3-dimesityl imidazolium salt with KH and subsequent reaction of the free carbene with AgO_3SCF_3 (Scheme 3.1).¹⁴ One of the problems associated with this method is the difficulty of generating



Scheme 3.1: First example of Ag-NHC

free carbenes due to their high reactivity and sensitivity to moisture, air and heat.¹¹ The pioneering efforts of Arduengo and coworkers in 1993 and the challenges thereof, spurred other scientists on

and this has led to the development of other synthetic methods that are relatively easier and some of these methods involve *in-situ* deprotonation of the azolium salt with a basic silver (I) salt independently reported by Bertrand *et. al.*¹⁵ in 1997, Lin *et. al.*¹⁶ in 1998 and Danopoulos *et. al.*¹⁷ in 2000 as depicted in Scheme 3.2 below.



Scheme 3.2: Preparation of Ag(I)-NHCs by *in-situ* deprotonation of NHCs with basic silver salts

The use of Ag_2O has made the preparation of silver(I)-NHC complexes easier and the reactions can be performed at room temperature, in a variety of solvents including water with little work up.¹⁸⁻²⁰ Of all the available synthetic methods, the method proposed by Lin and coworkers is by far the easiest and the fact that this procedure can be carried out in water suggests that the deprotonation of the azolium salt and its coordination to silver(I) is a concerted process and does not involve generation of free carbene at any point owing to its sensitivity to moisture and air.^{2, 18} Complexes of Ag(I)-NHC have been found to show diverse structures in the solid-state and this depends on the ratio of silver reagent to the imidazolium salts used in the synthesis, the nature of the NHC ligand, the source of the silver, counter anions, solvent and temperature.^{2, 21} Based on the available research publications on monocationic and dicationic azolium salts with coordinating (halides) and non-coordinating anions, varying solid state structures of Ag(I)-NHCs have been observed as shown in Scheme 3.3.^{2, 7, 16, 20, 22-26} Lin and coworkers in 2007 compared the structures obtained from Ag(I)-NHCs derived from a short chain and long chain azolium, benzimidazolium

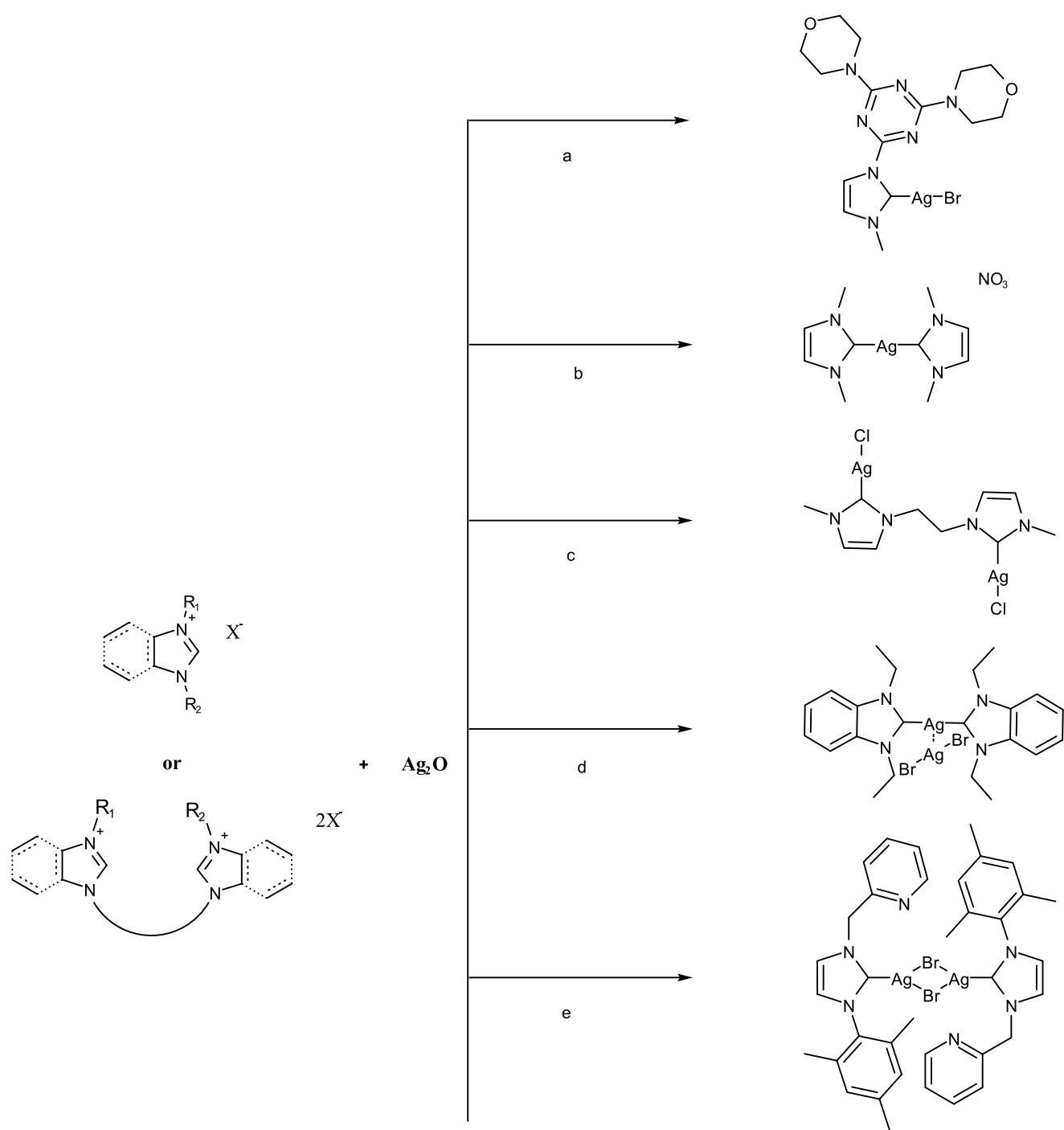
and triazolium halides. Extended Ag---Ag interactions were observed to be dominant and in some cases Ag---halide interactions extended the moiety to form an infinite one-dimensional polymer of Ag(I)-NHCs with short-chains, while chain-chain interactions were found to dominate Ag(I)-NHCs derived from long-chain azolium, benzimidazolium and triazolium halides.²¹ The nature of the chemical bond in Ag(I)-NHCs are about 65% electrostatic and approximately 35% covalent and is the weakest among the group 11 triad.²⁷ Lack of ^{107,109}Ag-¹³C coupling in ¹³C NMR spectrum enabled Lin *et. al.* to conclude that Ag(I)-NHCs are labile in solution and established their role as NHC transfer agents in the development of many other metal-NHCs.¹⁶ Besides the use of Ag(I)-NHCs as transmetallating agents, they have found use in catalysis^{28, 29} and pharmaceutical applications.^{9, 30} Initial synthetic effort in our group showed that Ag(I)-NHCs exhibited high activity against methicillin-resistant *S. aureus* (MRSA) NCTC 13277 and moderate activity against *S. aureus* NCTC 6571, *P. aeruginosa* NCTC 10662, and *P. mirabilis* NCTC 11938.⁹

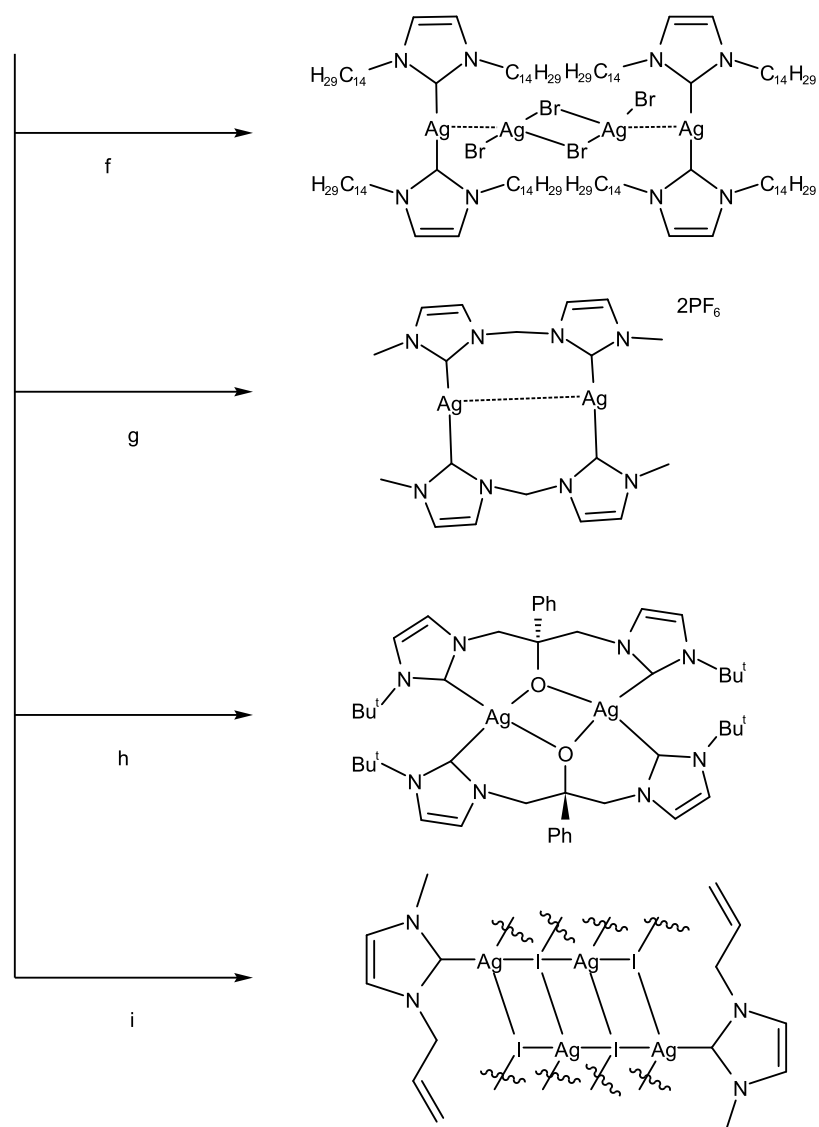
3.2. Aims

The aim of this chapter was to prepare five series of new Ag(I)-NHC complexes of general composition [NHC-Ag-Br] and Na⁺[NHC-Ag-Cl]⁻ derived from amphiphilic imidazolium proligands, **HL**₈₋₁₆, **HL**^{mes}₈₋₁₆, **HG**₈₋₁₆, **HG**^{mes}₈₋₁₆ and **HL**^{bet}₈₋₁₆ respectively, described in chapter 2.

In order to sustain the development of new and more efficient silver-based antibacterial agents and to raise the existing ability to treat infectious diseases, especially those caused by multidrug-resistant organisms, we have designed five series of Ag(I)NHCs, **L**₈₋₁₆-Ag-Br, **L**^{mes}₈₋₁₆-Ag-Br, Na[**L**^{bet}₈₋₁₆-Ag-Cl], **G**₈₋₁₆-Ag-Br and **G**^{mes}₈₋₁₆-Ag-Br.

All the Ag(I)-NHC complexes described herein were characterised by ¹H and ¹³C NMR spectroscopy and HRMS.





Scheme 3.3: Common solid-state structures of Ag(I)-NHCs obtained from monocationic and dicationic azolium salts

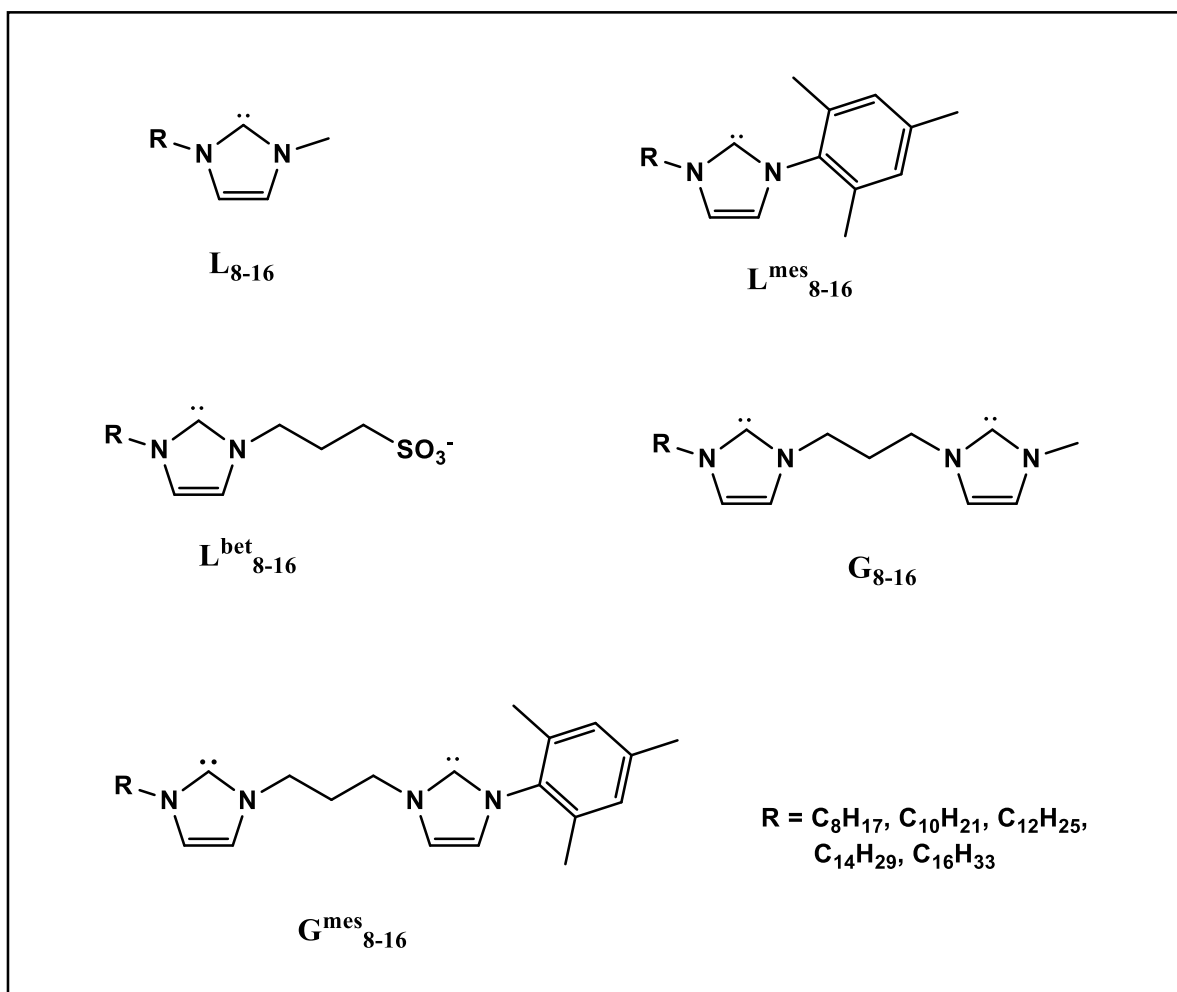
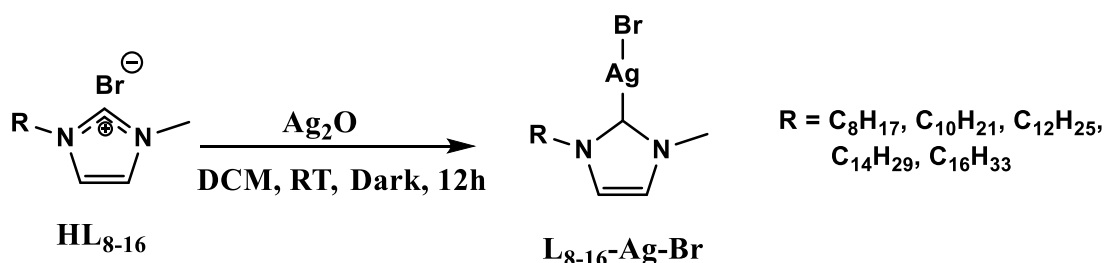


Figure 3.2: NHC ligands used in this study (the synthesis of their salt precursors is discussed in Chapter 2)

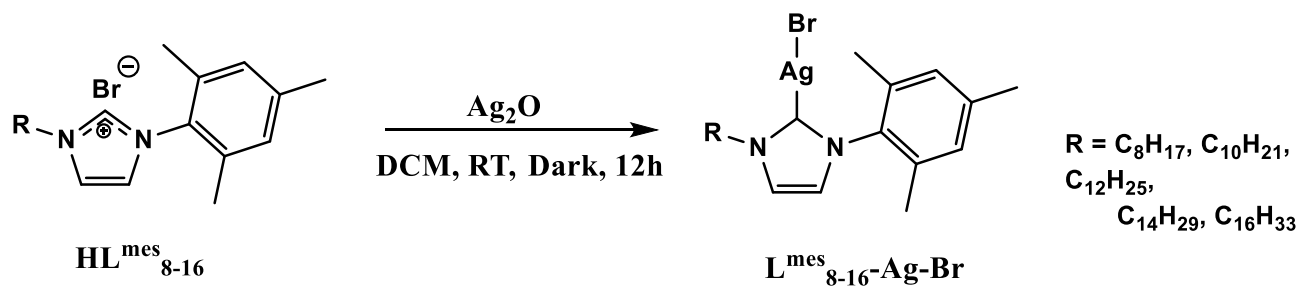
3.3. Results and Discussion

3.3.1. Synthesis of Silver(I) *N*-Heterocyclic Carbene Complexes

Ag(I)-NHCs derived from imidazolium salts (proligands) **HL**₈₋₁₆ and **HL**^{mes}₈₋₁₆, bearing alkyl groups with carbon chains ranging from eight to sixteen on the *N*1 nitrogen of the imidazole ring and with methyl and mesityl attached to the *N*3 nitrogen respectively, were prepared by an established method described in the literature that involves the use of basic Ag₂O.¹⁶ The reaction of **HL**₈₋₁₆ and **HL**^{mes}₈₋₁₆ with a slight excess of silver(I) oxide in dichloromethane at room temperature for about 12 h afforded **L**₈₋₁₆-Ag-Br and **L**^{mes}₈₋₁₆-Ag-Br in good yields respectively (Schemes 3.4 and 3.5).

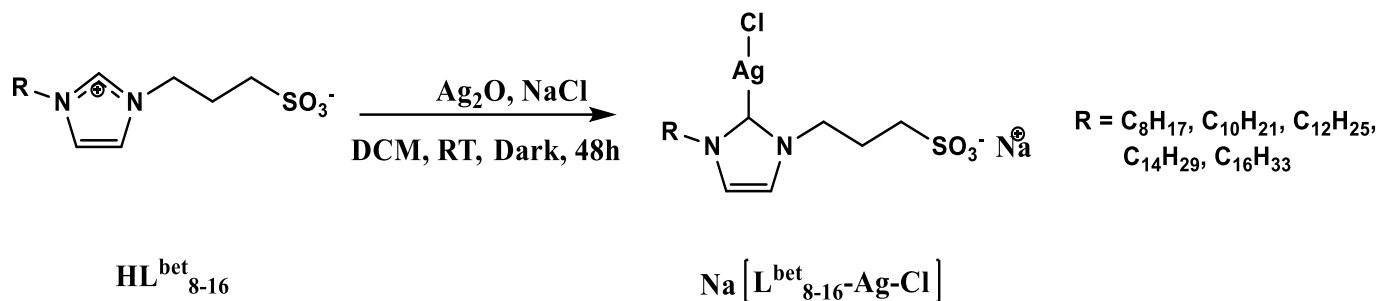


Scheme 3.4: Synthesis of **L**₈₋₁₆-Ag-Br



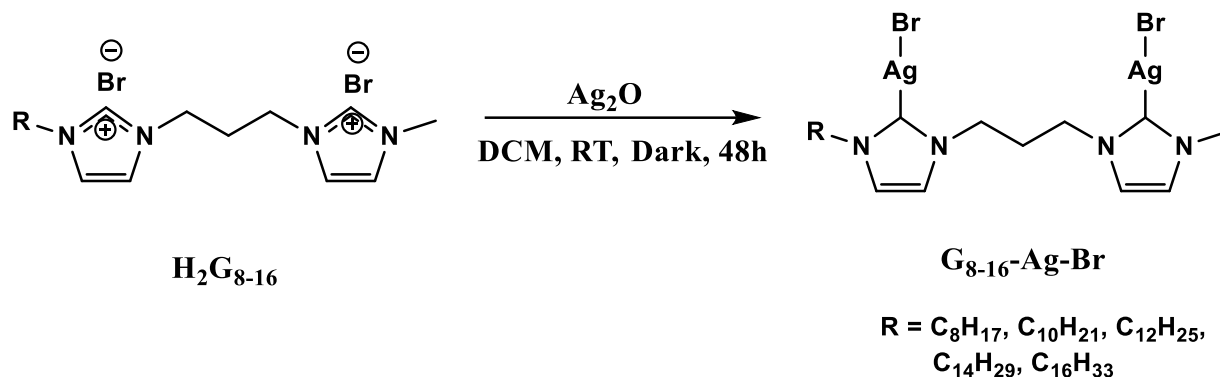
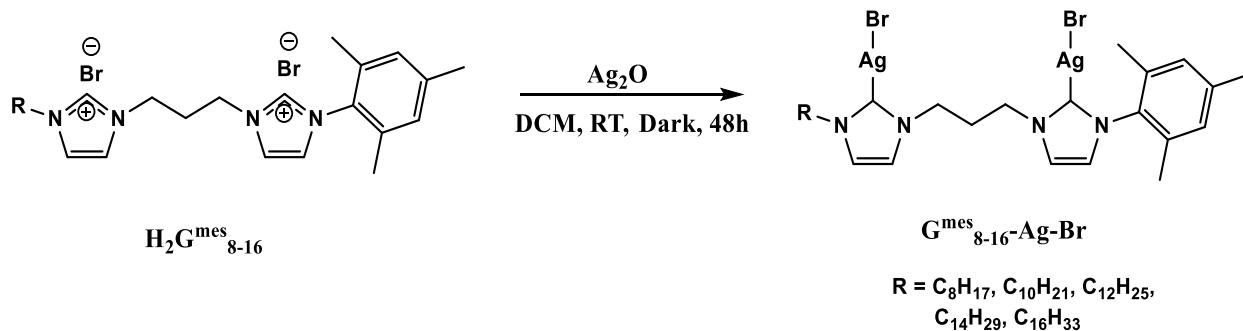
Scheme 3.5: Synthesis of **L**^{mes}₈₋₁₆-Ag-Br

With the same procedure and reaction conditions described in Schemes 3.4 and 3.5 for **L**₈₋₁₆-**Ag-Br** and **L**^{mes}₈₋₁₆-**Ag-Br** above, a mixture of the salts **HL**^{bet}₈₋₁₆ and Ag₂O was stirred at room temperature for 1h after which appropriate amount of NaCl was added to the mixture. The reaction was stopped after 12 h and the desired NHC complexes [**L**^{bet}₈₋₁₆-**Ag-Cl**]⁻ Na⁺ were obtained with about ~65% yield (reaction was monitored by the disappearance of the acidic proton in the imidazolium precursor by ¹H NMR spectroscopy) alongside the starting salts **HL**^{bet}₈₋₁₆ (~35%). To improve the yield of the desired Ag(I)-NHC complexes and make their isolation easier, the reaction time was increased from 12 h to 48 h, after which total conversion to [**L**^{bet}₈₋₁₆-**Ag-Cl**]⁻ Na⁺ was achieved (Scheme 3.6).



Scheme 3.6: Synthesis of Na[L^{bet}₈₋₁₆-Ag-Cl]

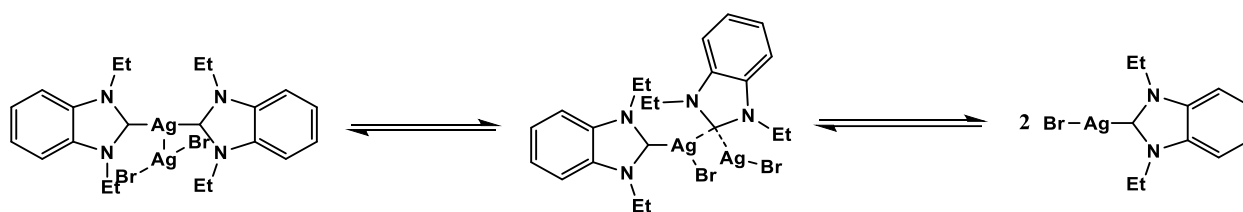
Similarly, the two series of dinuclear Ag(I)-NHCs derived from **H**₂**G**₈₋₁₆ and **H**₂**G**^{mes}₈₋₁₆ require a longer reaction time (2 days) to obtain good yields. **G**₈₋₁₆-**Ag-Br** and **G**^{mes}₈₋₁₆-**Ag-Br** were prepared as highlighted in Schemes 3.7 and 3.8.

Scheme 3.7: Synthesis of **G₈₋₁₆-Ag-Br**Scheme 3.8: Synthesis of **G^{mes}₈₋₁₆-Ag-Br**

All the Ag(I)-NHC complexes prepared were manipulated in the dark to avoid interaction of Ag(I) with light during the syntheses. The reactions were worked up by filtration through a pad of celite and the filtrates were dried under vacuum to obtain off-white solids, or waxy-like material in the case of **L^{mes}₈₋₁₆-Ag-Br**. The products were purified by precipitation from the slow addition of diethyl ether into concentrated chloroform solutions of the crude products. The complexes are generally stable to moisture and light however, [**L^{bet}₈₋₁₆-Ag-Cl**]⁻ Na⁺ derived from **L^{bet}₈₋₁₆** were found to decompose after a few days. The compounds turned grey and sticky, and the ¹H NMR analysis confirmed the presence of some zwitterionic precursors.

3.3.2. ^1H and ^{13}C NMR study of silver(I) complexes

^1H and ^{13}C NMR spectroscopy are two of many characterization techniques heavily relied upon by organometallic chemists in the analysis of Ag(I)-NHC complexes. The progress of the reaction between the NHC precursor and Ag_2O can be monitored by ^1H NMR spectroscopy following the disappearance of the acidic proton on C2 of the imidazolium precursor. However, the use of protic NMR solvents could pose a challenge because of the deuterium exchange with the C2 proton. This could lead to misinterpretation of the ^1H NMR spectra due to the apparent absence of the C2 proton in this case. ^{13}C NMR measurements complement the information provided by ^1H NMR and reveal more information on the bonding nature of Ag-NHCs in solution. For instance, silver isotopes, ^{107}Ag and ^{109}Ag , are NMR active, with a nuclear spin of $\frac{1}{2}$ each. As a result, the splitting pattern of the ^{13}C resonance of the carbenic carbon bound to the Ag(I) ion is expected to give a pair of doublet with different chemical shifts which is actually a singlet with $^{107/109}\text{Ag}$ satellites.² However, very few of the Ag(I)-NHC complexes reported to date exhibit this coupling pattern with the majority producing sharp single peaks and others showing no resonance at all for the carbenic carbon. This observation guided Lin and coworkers to propose that Ag(I)-NHCs are dynamic in solution with a plausible fluxional behaviour between mono- and bis-carbenes as shown in Scheme 3.9 for halogeno Ag(I)-NHC complexes.^{2, 16, 17}



Scheme 3.9: Fluxional behaviour of Ag(I)-NHCs in solution

Formation of the series of $\text{L}_{8-16}\text{-Ag-Br}$, $\text{L}^{\text{mes}}_{8-16}\text{-Ag-Br}$ and $\text{L}^{\text{bet}}_{8-16}\text{-Ag-Br}$ was confirmed by the disappearance of the resonance at approximately 10 ppm in the ^1H NMR spectra and this affirms the deprotonation of the acidic hydrogen of the imidazolium moieties. Additionally, the protons

on the C4 and C5 carbons on the imidazole ring were shifted upfield with resonances at 7.00 and 7.01, 6.97 and 7.19, and 7.52 ppm for **L8-16-Ag-Br** in CDCl₃, **L^{mes}8-16-Ag-Br** in CDCl₃ and **L^{bet}8-16-Ag-Br** in *d*⁶-dmsO respectively (Appendixes A, B and C) as a result of coordination to Ag(I). For example, Figure 3.3 show the stacked ¹H NMR spectra of the proligands with C₁₂H₂₅ alkyl side chain of **HL₁₂** and its corresponding Ag(I)-NHC, **L₁₂-Ag-Br**.

The most significant feature of the ¹³C NMR spectra of **L8-16-Ag-Br**, is the resonance signal around 180 ppm corresponding to the carbenic carbon atom (NCN-Ag) (Table 3.1), which appears in the typical range of other 5-membered NHC complexes of Ag(I),^{2, 36} and the loss of the resonance signal around 137 ppm in the ¹³C NMR spectra of proligands as can be seen in the stacked ¹³C NMR spectra of **HL₁₂** and **L₁₂-Ag-Br** in Figure 3.4. The ¹³C NMR spectra of **L^{mes}8-16-Ag-Br** and **L^{bet}8-16-Ag-Br** did not show a low field resonance signal that can be attributed to NCN-Ag, however, the disappearance of the C2 peak between 136-140 ppm confirmed the formation of the desired Ag(I)-NHC complexes.

The ¹H NMR spectra of the two series of Ag(I)-NHCs derived from Gemini imidazolium salts, **G8-16-Ag-Br** and **G^{mes}8-16-Ag-Br** in *d*⁶-dmsO show four resonance signals attributed to C4, C4', C5 and C5' of the two imidazolium motifs around 7.50-7.65 and 7.40-7.90 ppm respectively (Appendixes E and F). Furthermore, the absence of the two peaks due to the acidic hydrogens on C2 and C2' confirmed the formation of **G8-16-Ag-Br** and **G^{mes}8-16-Ag-Br** (Figure 3.5 shows stacked ¹H NMR spectra of **H₂G₁₂** and **L₁₂-Ag-Br**). The ¹³C NMR spectra show the loss of the resonance peaks of the two N-C-N sp² carbon between 141.47 and 136.28 ppm and two low field signals, attributed to the two carbenic carbon between 179-182 ppm (Table 3.1 and Figure 3.6 which shows stacked ¹³C NMR spectra of **H₂G₁₂** and **L₁₂-Ag-Br**). Just like **L8-16-Ag-Br**, **L^{mes}8-16-Ag-Br** and **L^{bet}8-16-Ag-Br**, the dinuclear Ag(I)-NHCs, **G8-16-Ag-Br** and **G^{mes}8-16-Ag-Br** did not show any coupling between carbenic carbon and silver isotopes, ¹⁰⁷Ag and ¹⁰⁹Ag. The lack of coupling between carbenic carbon and silver isotopes in all the Ag(I)-NHCs suggests these complexes are dynamic in solution with labile Ag-C_{carbene} bond(s) which enhance(s) the formation of equilibrium between mononuclear and dinuclear species (Scheme 3.9).^{2, 37}

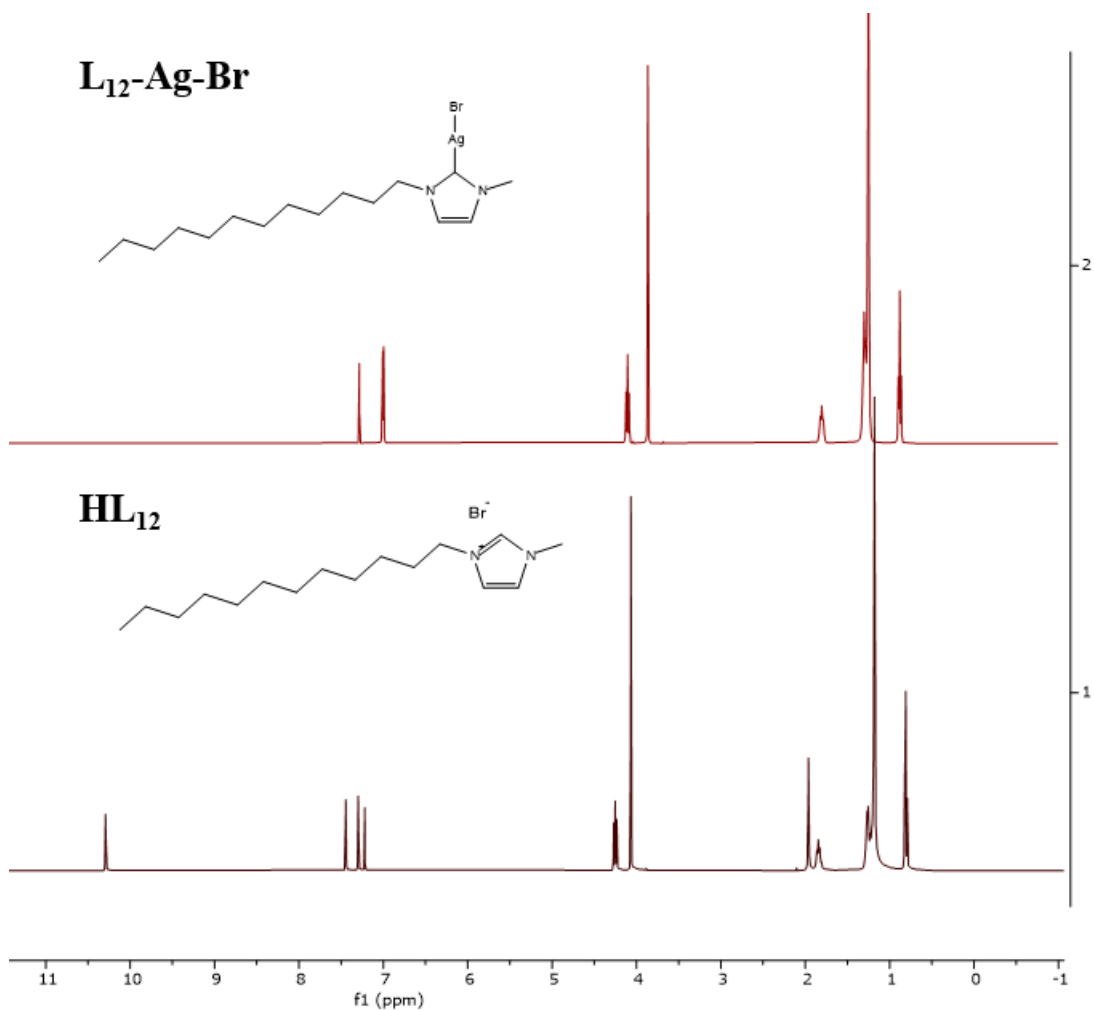


Figure 3.3: Stacked ¹H NMR spectra of **HL₁₂** and **L₁₂-Ag-Br** in CDCl₃ using Bruker 400 MHz at room temperature

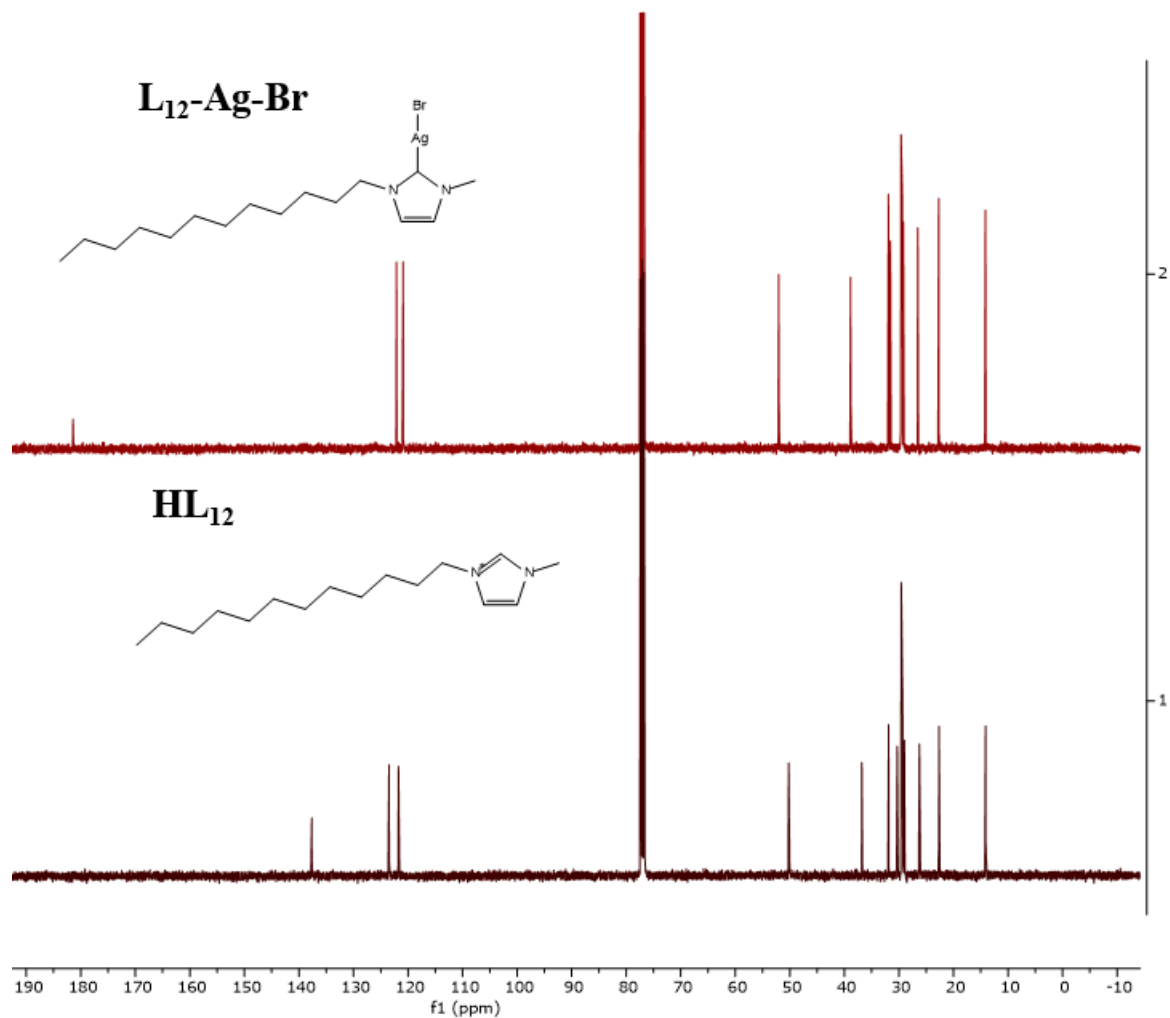


Figure 3.4: Stacked $^{13}\text{C}\{^1\text{H}\}$ NMR spectra of HL_{12} and $\text{L}_{12}\text{-Ag-Br}$ in CDCl_3 using Bruker 400 MHz at room temperature

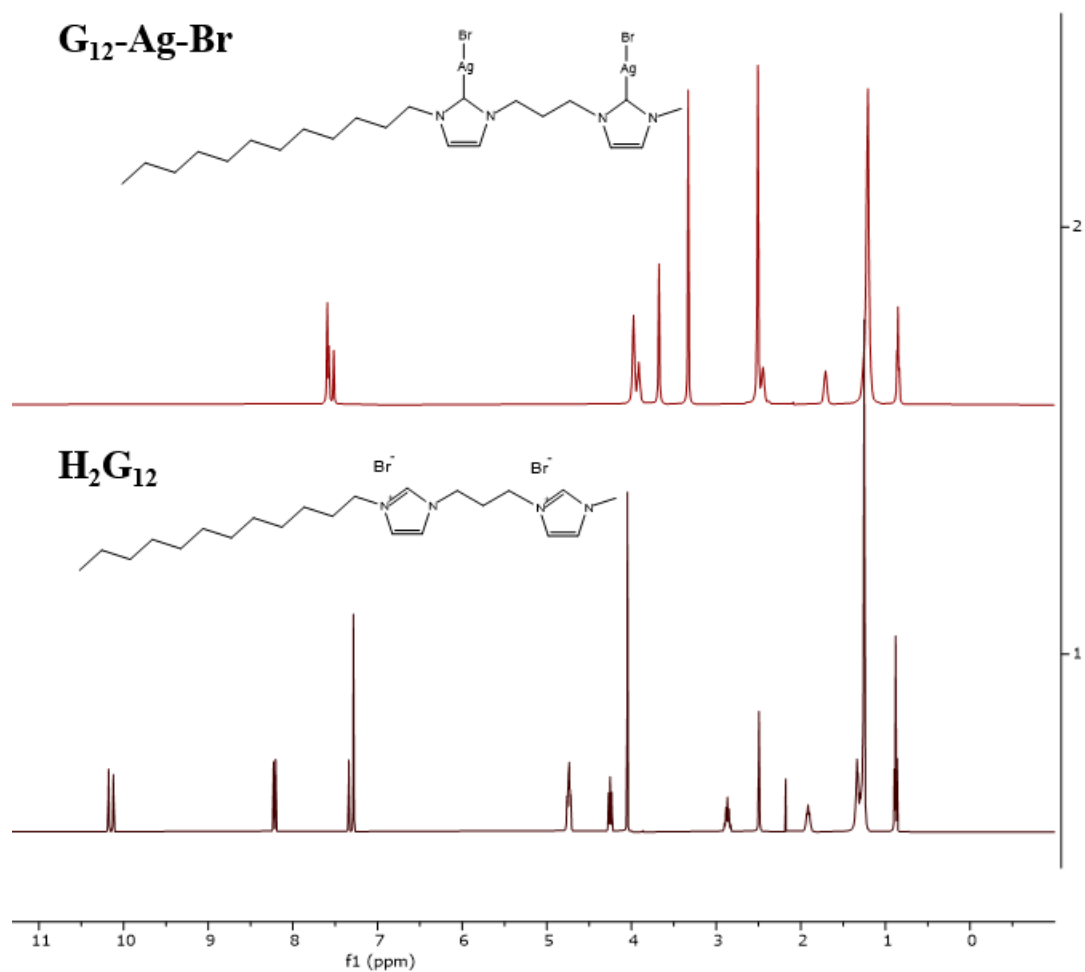


Figure 3.5: Stacked ^1H NMR spectra of H_2G_{12} in CDCl_3 and $\text{G}_{12}\text{-Ag-Br}$ in $d^6\text{-DMSO}$ using Bruker 400 MHz at room temperature

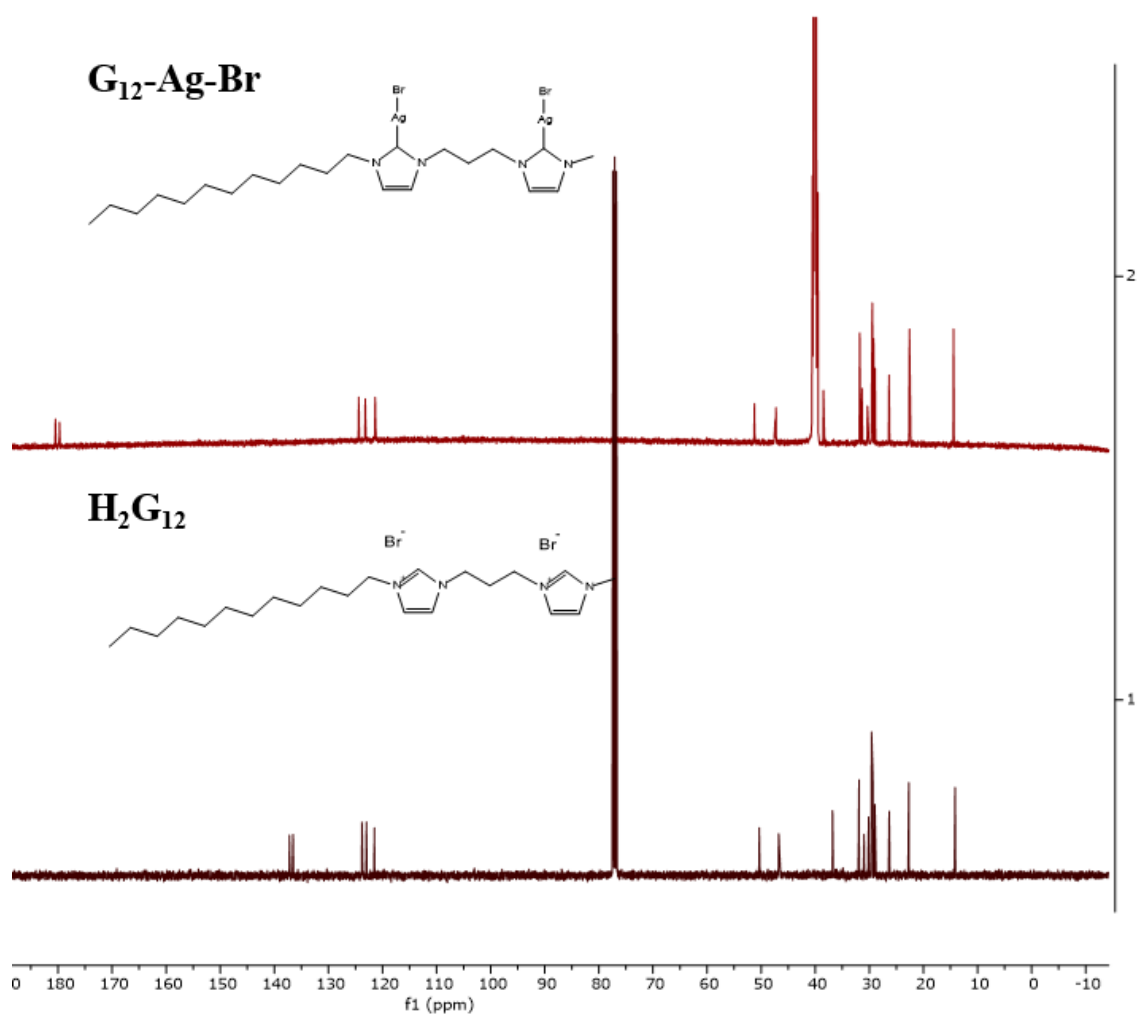


Figure 3.6: Stacked $^{13}\text{C}\{^1\text{H}\}$ NMR spectra of H_2G_{12} in CDCl_3 and $\text{G}_{12}\text{-Ag-Br}$ in $d^6\text{-DMSO}$ using Bruker 400 MHz at room temperature

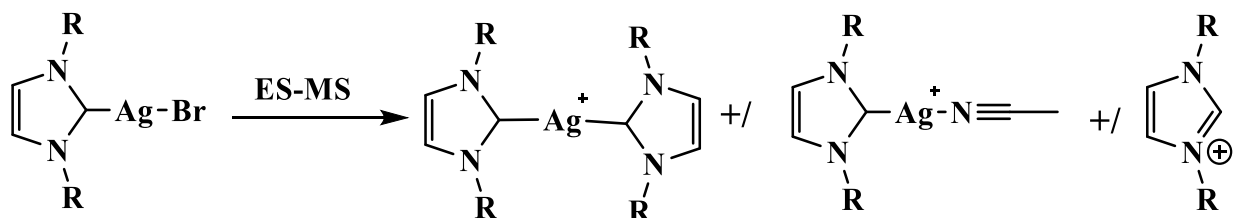
Table 3.1: $^{13}\text{C}\{^1\text{H}\}$ NMR Chemical Shifts of the Carbenic Carbon of the Ag-NHC Complexes

| Complex | Solvent | δ (Ag-C) | Appearance of signal |
|---------------------------------------|-----------------------------|--------------------|----------------------|
| L ₈ -Ag-Br | CDCl ₃ | 181.35 | Singlet |
| L ₁₀ -Ag-Br | CDCl ₃ | 181.38 | Singlet |
| L ₁₂ -Ag-Br | CDCl ₃ | 181.43 | Singlet |
| L ₁₄ -Ag-Br | CDCl ₃ | 181.43 | Singlet |
| L ₁₆ -Ag-Br | CDCl ₃ | 181.47 | Singlet |
| L ^{mes} ₈ -Ag-Br | CDCl ₃ | ---- ^{a)} | ---- |
| L ^{mes} ₁₀ -Ag-Br | CDCl ₃ | ---- | ---- |
| L ^{mes} ₁₂ -Ag-Br | CDCl ₃ | ---- | ---- |
| L ^{mes} ₁₄ -Ag-Br | CDCl ₃ | ---- | ---- |
| L ^{mes} ₁₆ -Ag-Br | CDCl ₃ | ---- | ---- |
| L ^{bet} ₈ -Ag-Br | <i>d</i> ⁶ -DMSO | ---- | ---- |
| L ^{bet} ₁₀ -Ag-Br | <i>d</i> ⁶ -DMSO | 176.23 | Singlet |
| L ^{bet} ₁₂ -Ag-Br | <i>d</i> ⁶ -DMSO | ---- | ---- |
| L ^{bet} ₁₄ -Ag-Br | <i>d</i> ⁶ -DMSO | 179.25 | Singlet |
| L ^{bet} ₁₆ -Ag-Br | <i>d</i> ⁶ -DMSO | ---- | ---- |
| G ₈ -Ag-Br | <i>d</i> ⁶ -DMSO | 179.60, 180.37 | Singlet |
| G ₁₀ -Ag-Br | <i>d</i> ⁶ -DMSO | 179.82, 180.55 | Singlet |
| G ₁₂ -Ag-Br | <i>d</i> ⁶ -DMSO | 179.72, 180.48 | Singlet |
| G ₁₄ -Ag-Br | <i>d</i> ⁶ -DMSO | 179.88, 180.64 | Singlet |
| G ₁₆ -Ag-Br | <i>d</i> ⁶ -DMSO | ---- | ---- |
| G ^{mes} ₈ -Ag-Br | <i>d</i> ⁶ -DMSO | 179.49, 181.17 | Singlet |
| G ^{mes} ₁₀ -Ag-Br | <i>d</i> ⁶ -DMSO | 179.60, 181.27 | Singlet |
| G ^{mes} ₁₂ -Ag-Br | <i>d</i> ⁶ -DMSO | 179.44, 181.13 | Singlet |
| G ^{mes} ₁₄ -Ag-Br | <i>d</i> ⁶ -DMSO | 179.36, 181.02 | Singlet |
| G ^{mes} ₁₆ -Ag-Br | <i>d</i> ⁶ -DMSO | 179.57, 181.23 | Singlet |

¹J(^{107/109}Ag-C) Hz, not observed; a) not observed.

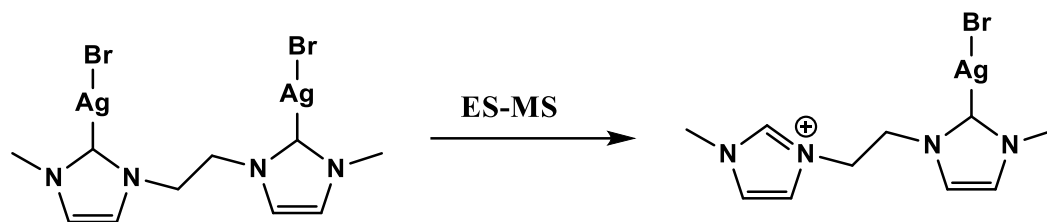
3.3.3. HRMS study of silver(I) complexes

Mass spectrometry is one of the techniques that has been used to analyse Ag(I)-NHCs and of all the modes of ionization, electrospray ionization mass spectrometry (ES-MS), seems to be the mode of choice for the characterization of Ag(I)-NHC complexes.² Danopoulos *et. al.*, were the first to report the analysis of Ag(I)-NHCs by ES-MS and in their work, they found that Ag(I)-NHCs with halide ligand with solid-state motifs of [NHC-Ag-X] form biscarbenes [NHC-Ag-NHC]⁺ in the gas phase (Scheme 3.10).¹⁷



Scheme 3.10: Observed splitting and rearrangement pattern of halogeno silver-NHC complexes, C-Ag-X, in the gas phase

Douthwaite and coworkers and Pellei and coworkers also reported the formation of biscarbenes and imidazolium cations in the gas phase^{38, 39} while several others reported only the formation of biscarbenes for Ag(I)-NHCs whose solid-state structure is of the type [NHC-Ag-X].^{9, 40, 41} Furthermore, [M-AgBr + H]⁺ was reported for dinuclear [NHC-Ag₂-Br₂] by Castro *et. al.* (Scheme 3.11).⁴²



Scheme 3.11: Observed splitting and rearrangement pattern of dinuclear halogeno silver NHC complexes, bisNHC-Ag₂-X₂, in the gas phase

In addition to ¹H and ¹³C NMR spectroscopy, ES-HRMS was used to analyse all the Ag(I)-NHC complexes prepared in this project. The fragmentation and isotopic pattern were carefully examined and studied in detail. **L₈₋₁₆-Ag-Br**, **L^{mes}₈₋₁₆-Ag-Br** and **L^{bet}₈₋₁₆-Ag-Br** show three major peaks with [Ag(NHC)₂]⁺ as the base peak, [NHC-Ag-NCCH₃]⁺ and the corresponding imidazolium cation (NHC-H) fragment ions (Figures 3.7, 3.8 and 3.9 show some examples). The fragment ions observed in the ES-HRMS contains acetonitrile because it is one of the commonly used solvents for ES-HRMS analysis. Largely, the fragment ions observed are similar to what has been reported in the literature for halogeno NHC-Ag-X type of Ag(I)-NHC complexes.

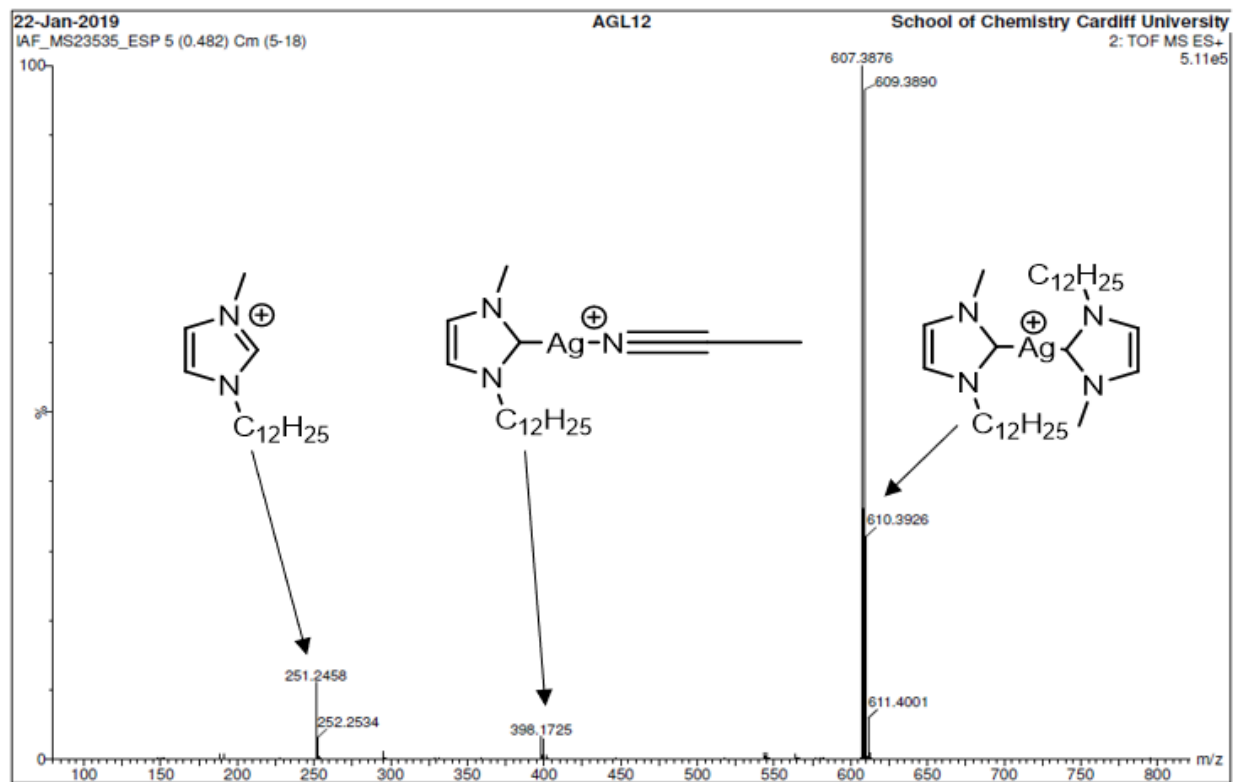


Figure 3.7: ES-HRMS (positive mode) spectrum of **L₁₂-Ag-Br**

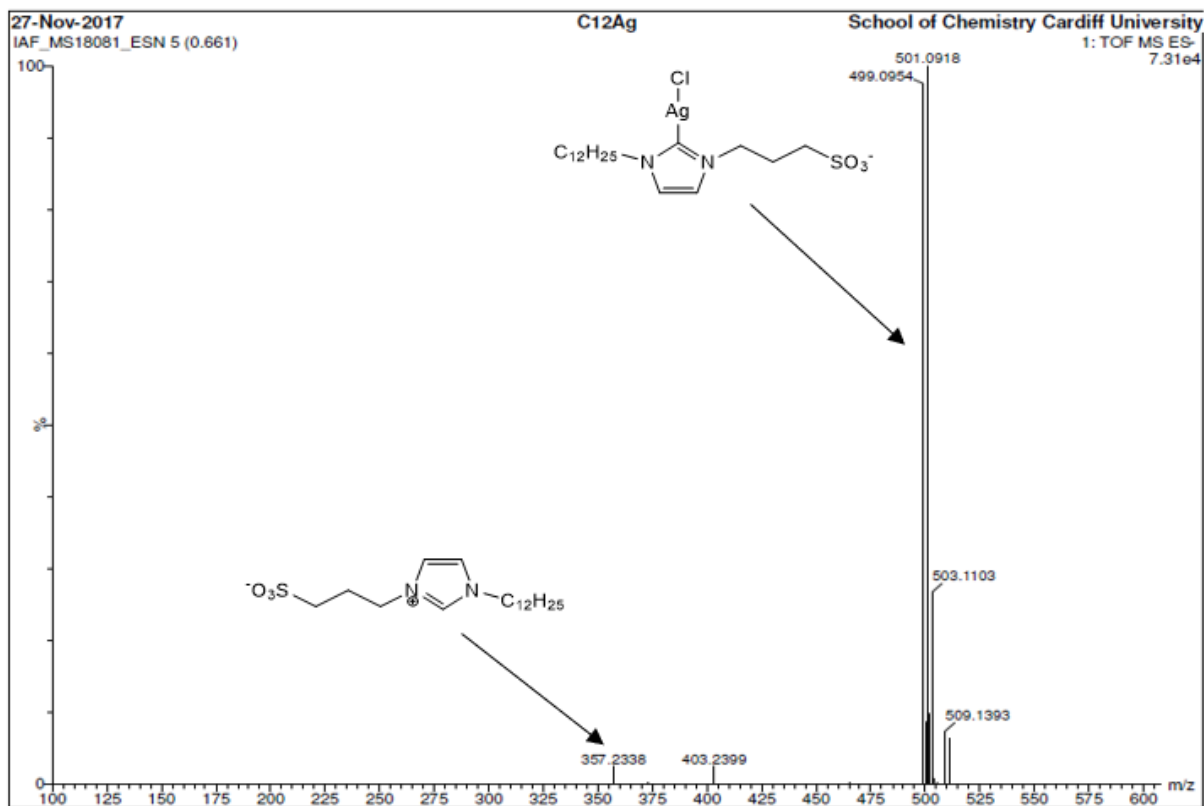


Figure 3.8: ES-HRMS (negative mode) spectrum of $L^{\text{mes}}_{12}\text{-Ag-Br}$

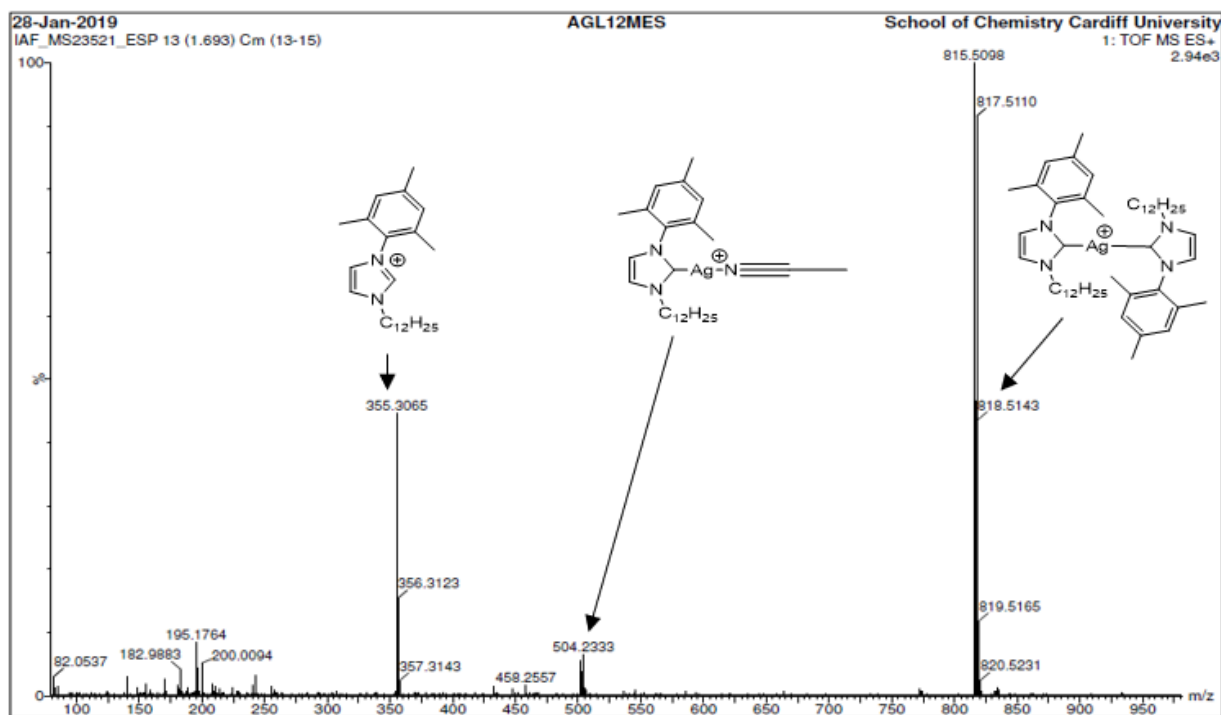


Figure 3.9: ES-HRMS (positive mode) spectrum of $L^{\text{bet}}_{12}\text{-Ag-Br}$

The spectra of **G₈₋₁₆-Ag-Br** and **G^{mes}₈₋₁₆-Ag-Br** have peaks corresponding to the imidazolium cation (bis-NHC-H) fragment ions as the base peak respectively (some examples are depicted in Figures 3.10 and 3.11). Also, the spectra of these complexes show peaks that are attributed to the free bis-carbenes (bis-NHC), [(bis-NHC)₂-Ag₂]²⁺, [bis-NHC-Ag₂-Br]⁺ and [bis-NHC-Ag-Br]⁺ fragment ions respectively. This is in agreement with the ES-MS data of dinuclear halogeno [bis-NHC-Ag₂-Br₂] reported by Castro and coworkers⁴² and Dervisi *et al.*⁷

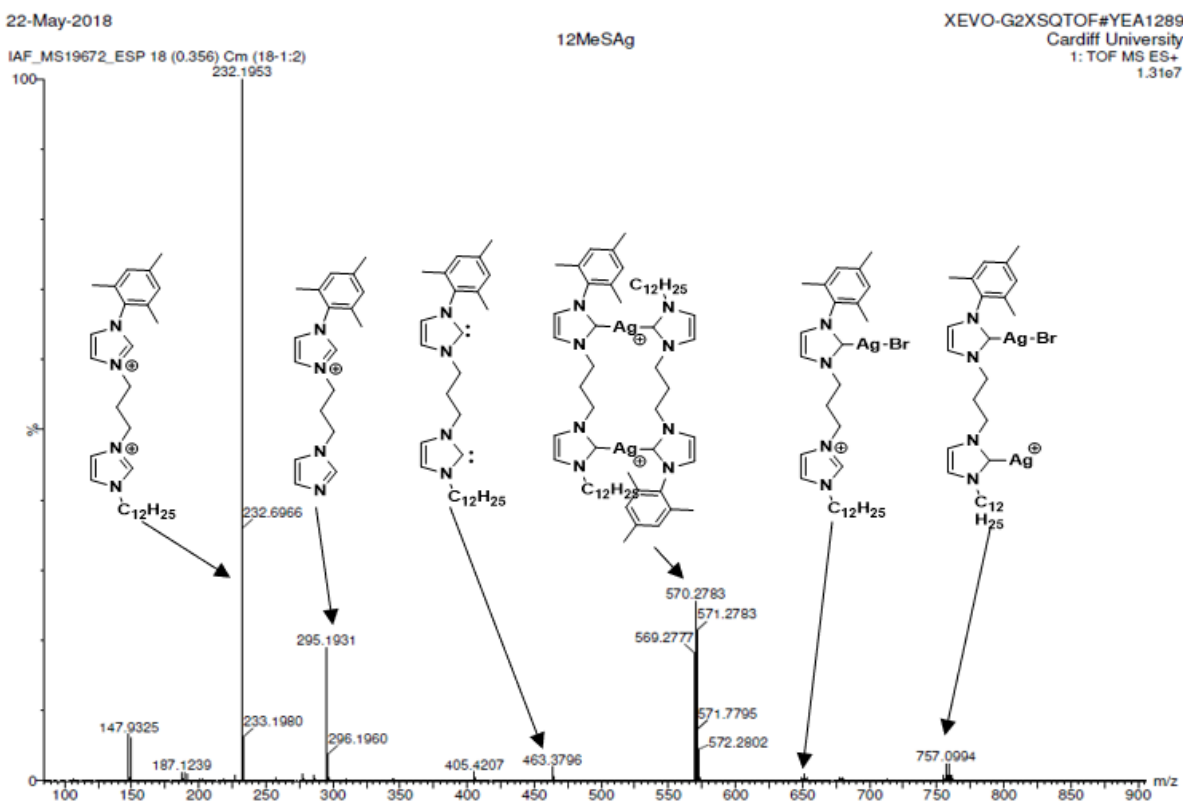


Figure 3.10: ES-HRMS (positive mode) spectrum of **G₁₂-Ag₂-Br₂**

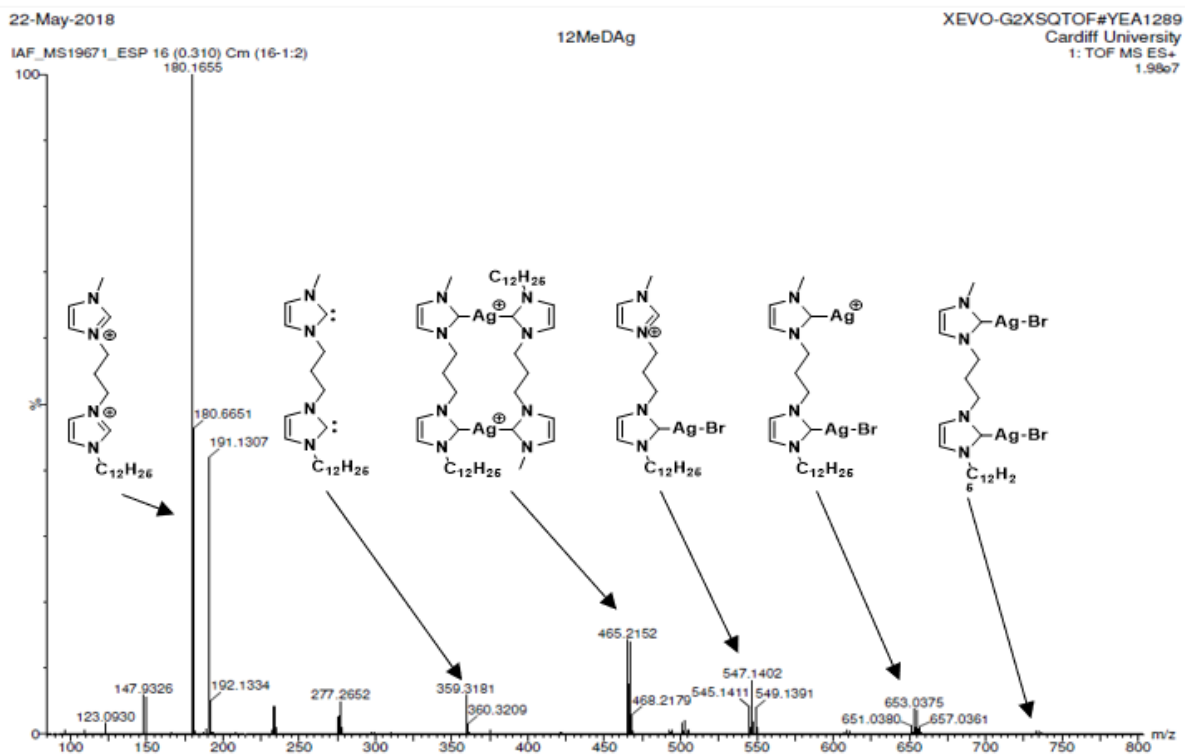


Figure 3.11: ES-HRMS (positive mode) spectrum of $G^{\text{mes}}_{12}\text{-Ag}_2\text{-Br}_2$

3.4. Experimental

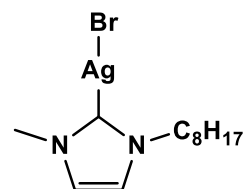
General Remark

All reactions were carried out under aerobic conditions unless otherwise specified and all reagents were purchased from commercial sources and used without further purification. ^1H and ^{13}C NMR spectra were recorded on a Bruker 400 MHz or 500 MHz spectrophotometer and recorded in deuterated solvents and the chemical shifts are given in ppm. Coupling constants J are given in hertz (Hz). High-resolution mass spectra were obtained as appropriate (in positive and negative modes) using a Waters LCT Premier XE instrument and are reported as m/z (relative intensity),

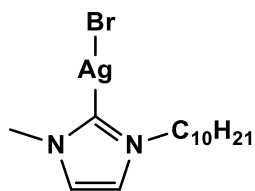
General procedure for the synthesis of Ag(I)-NHCs

The appropriate imidazolium salts or zwitterions (2 mmol) and Ag_2O (1.2 equivalent) were dissolved and suspended respectively in 50 mL of CH_2Cl_2 and the mixture was stirred at room temperature under darkness to avoid interaction with light for 12 and 48 h respectively for **L8-16-Ag-Br**, **L^{mes}8-16-Ag-Br** and **Na[L^{bet}8-16-Ag-Cl]**, **G12-Ag2-Br2**, **G^{mes}12-Ag2-Br2**. Appropriate amount of NaCl was added in the case of **Na[L^{bet}8-16-Ag-Cl]**. After which, the mixture was passed through a short Celite pad to remove unreacted Ag_2O and the collected washings were concentrated under vacuum and precipitated with Et_2O to afford the silver complex as off white solid for **L8-16-Ag-Br**, **Na[L^{bet}8-16-Ag-Cl]**, **G12-Ag2-Br2** and **G^{mes}12-Ag2-Br2** and waxy-like solid for **L^{mes}8-16-Ag-Br**.

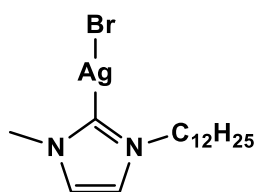
L8-Ag-Br



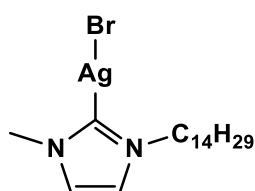
Yield: 71%; ^1H NMR (δ ppm, 400 MHz, CDCl_3): 0.90 (t, $^3J= 8.0$ Hz, 3H), 1.25-1.35 (m, 10H) 1.83 (m, 2H), 4.09 (s, 3H), 4.35 (t, $^3J= 8.0$ Hz, 2H), 6.99 (s, 2H). $^{13}\text{C}\{^1\text{H}\}$ NMR (δ ppm, 100 MHz, CDCl_3): 14.09 (CH_3), 22.61 (CH_2), 26.48 (CH_2), 29.12 (CH_2), 31.53 (CH_2), 31.72 (CH_2), 38.82 (NCH_3), 52.01 (NCH_2), 120.92 (C_4), 122.11 (C_5) 181.35 (C_2). HRMS (ESI) (m/z): found 495.2631 [$\text{Ag}(\text{C}_{12}\text{H}_{22}\text{N}_2)_2^+$, 100%], expected 495.2611.

L₁₀-Ag-Br

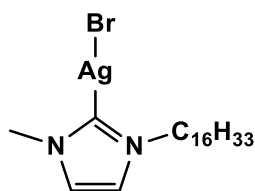
Yield: 82%; ¹H NMR (δ ppm, 400 MHz, CDCl₃): 0.89 (t, ³J= 8.0 Hz, 3H), 1.25-1.35 (m, 14H) 1.81 (m, 2H), 3.85 (s, 3H), 4.09 (t, ³J= 8.0 Hz, 2H), 6.98 (s, 2H). ¹³C{¹H} NMR (δ ppm, 100 MHz, CDCl₃): 14.14 (CH₃), 22.68 (CH₂), 26.28 (CH₂), 29.16 (CH₂), 29.28 (CH₂), 29.44 (CH₂), 29.49 (CH₂), 31.86 (CH₂), 38.79 (NCH₃), 52.04 (NCH₂), 120.88 (C₄), 122.02 (C₅) 181.38 (C₂). HRMS (ESI) (*m/z*): found 553.3129 [Ag(C₁₄H₂₆N₂)₂]⁺, 100%], expected 553.3237.

L₁₂-Ag-Br

Yield: 76%; ¹H NMR (δ ppm, 400 MHz, CDCl₃): 0.88 (t, ³J= 8.0 Hz, 3H), 1.22-1.35 (m, 18H) 1.80 (m, 2H), 3.86 (s, 3H), 4.11 (t, ³J= 8.0 Hz, 2H), 7.00 (s, 1H), 7.01 (s, 1H). ¹³C{¹H} NMR (δ ppm, 100 MHz, CDCl₃): 14.14 (CH₃), 22.69 (CH₂), 26.52 (CH₂), 29.19 (CH₂), 29.34 (CH₂), 29.46 (CH₂), 29.54 (CH₂), 29.61 (CH₂), 29.62 (CH₂), 31.91 (CH₂), 38.85 (NCH₃), 52.02 (NCH₂), 120.90 (C₄), 122.11 (C₅) 181.43 (C₂). HRMS (ESI) (*m/z*): found 607.3876 [Ag(C₁₆H₃₀N₂)₂]⁺, 100%], expected 607.3863.

L₁₄-Ag-Br

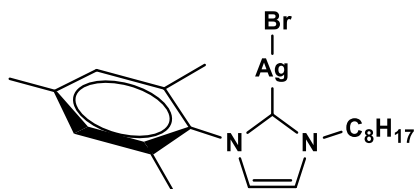
Yield: 79%; ¹H NMR (δ ppm, 400 MHz, CDCl₃): 0.89 (t, ³J= 8.0 Hz, 3H), 1.30 (m, 22H) 1.81 (m, 2H), 3.85 (s, 3H), 4.09 (t, ³J= 8.0 Hz, 2H), 6.99 (s, 2H). ¹³C{¹H} NMR (δ ppm, 100 MHz, CDCl₃): 14.15 (CH₃), 22.71 (CH₂), 26.50 (CH₂), 29.18 (CH₂), 29.37 (CH₂), 29.45 (CH₂), 29.54 (CH₂), 29.63 (CH₂), 29.66 (CH₂), 29.70 (CH₂), 31.54 (CH₂), 31.93 (CH₂), 38.80 (NCH₃), 52.04 (NCH₂), 120.88 (C₄), 122.03 (C₅) 181.43 (C₂). HRMS (ESI) (*m/z*): found 665.4359 [Ag(C₁₈H₃₄N₂)₂]⁺, 100%], expected 665.4487.

L₁₆-Ag-Br

Yield: 74%; ¹H NMR (δ ppm, 400 MHz, CDCl₃): 0.88 (t, ³J= 8.0 Hz, 3H), 1.30 (m, 26H) 1.80 (m, 2H), 3.85 (s, 3H), 4.09 (t, ³J= 8.0 Hz, 2H), 6.99 (s, 2H). ¹³C{¹H} NMR (δ ppm, 100 MHz, CDCl₃): 14.13 (CH₃), 22.69 (CH₂),

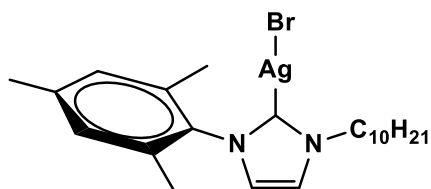
26.50 (CH₂), 29.17 (CH₂), 29.36 (CH₂), 29.45 (CH₂), 29.54, 29.62 (CH₂), 29.66 (CH₂), 29.70 (CH₂), 31.54 (CH₂), 31.92 (CH₂), 38.81 (NCH₃), 52.03 (NCH₂), 120.89 (C₄), 122.05 (C₅) 181.47 (C₂). HRMS (ESI) (*m/z*): found 719.5130 [Ag(C₂₀H₃₈N₂)₂⁺, 100%], expected 719.5115.

L^{mes}₈-Ag-Br



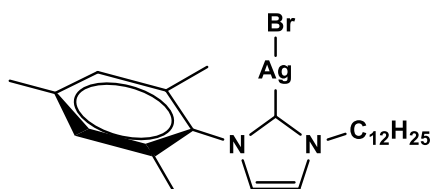
Yield: 75%; ¹H NMR (δ ppm, 400 MHz, CDCl₃): 0.81 (t, ³J= 8.0 Hz, 3H), 1.15-1.30 (m, 10H), 1.80 (m, 2H), 1.89 (s, 6H), 2.26 (s, 3H), 4.13 (t, ³J= 8.0 Hz, 2H), 6.88 (s, 3H), 7.12 (s, 1H). ¹³C{¹H} NMR (δ ppm, 100 MHz, CDCl₃): 14.11 (CH₃), 17.68 (CH₂), 21.09 (CH₂), 22.63 (CH₂), 26.38 (CH₂), 29.09 (CH₂), 29.12 (CH₃), 31.45 (CH₃), 31.69 (CH₃), 52.13 (NCH₂), 120.79 (C₄), 122.71 (C₅) 129.44 (*ipso*-mesityl), 134.70 (*m*-mesityl), 135.39 (*o*-mesityl), 139.51 (*p*-mesityl). HRMS (ESI) (*m/z*): found 703.3083 [Ag(C₂₀H₃₀N₂)₂⁺, 100%], expected 703.3863.

L^{mes}₁₀-Ag-Br



Yield: 79%; ¹H NMR (δ ppm, 400 MHz, CDCl₃): 0.81 (t, ³J= 8.0 Hz, 3H), 1.15-1.30 (m, 14H), 1.80 (m, 2H), 1.89 (s, 6H), 2.27 (s, 3H), 4.13 (t, ³J= 8.0 Hz, 2H), 6.88 (s, 3H), 7.13 (s, 1H). ¹³C{¹H} NMR (δ ppm, 100 MHz, CDCl₃): 14.14 (CH₃), 17.68 (CH₂), 21.10 (CH₂), 22.68 (CH₃), 26.39 (CH₂), 29.15 (CH₂), 29.29 (CH₂), 29.46 (CH₂), 31.46 (CH₃), 31.87 (CH₃), 52.13 (NCH₂), 120.79 (C₄), 122.70 (C₅) 129.43 (*ipso*-mesityl), 134.70 (*m*-mesityl), 135.40 (*o*-mesityl), 139.50 (*p*-mesityl). HRMS (ESI) (*m/z*): found 759.4510 [Ag(C₂₂H₃₄N₂)₂⁺, 100%], expected 759.4489.

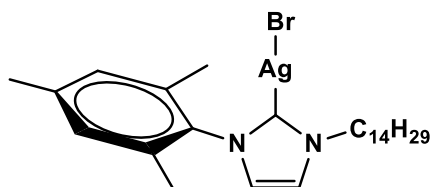
L^{mes}₁₂-Ag-Br



Yield: 75%; ¹H NMR (δ ppm, 400 MHz, CDCl₃): 0.89 (t, ³J= 8.0 Hz), 1.20-1.40 (m, 18H), 1.89 (m, 2H), 1.98 (s, 6H), 2.35 (s, 3H), 4.23 (t, ³J= 8.0 Hz, 2H), 6.95 (s, 2H), 6.97 (s, 1H), 7.19 (s, 1H). ¹³C{¹H} NMR (δ ppm, 100 MHz, CDCl₃): 14.14 (CH₃), 17.68 (CH₂), 21.09 (CH₂), 22.70 (CH₃), 26.40 (CH₂), 29.15 (CH₂), 29.35 (CH₂), 29.46

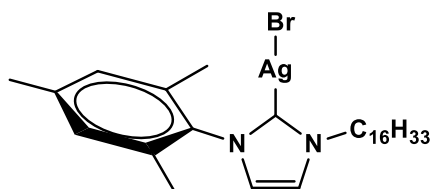
(CH₂), 29.51 (CH₂), 29.63 (CH₃), 31.46 (CH₃), 31.92 (CH₃), 52.14 (NCH₂), 120.68 (C₄), 122.67 (C₅) 129.46 (*ipso*-mesityl), 134.69 (*m*-mesityl), 135.39 (*o*-mesityl), 139.53 (*p*-mesityl). HRMS (ESI) (*m/z*): found 815.5098 [Ag(C₂₄H₃₈N₂)₂⁺, 100%], expected 815.5115.

L^{mes}₁₄-Ag-Br



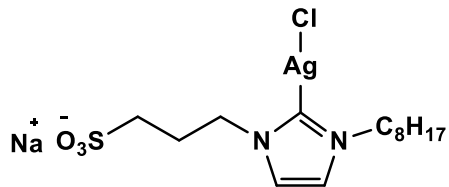
Yield: 75%; ¹H NMR (δ ppm, 400 MHz, CDCl₃): 0.81 (t, ³J= 8.0 Hz, 3H), 1.15-1.30 (m, 22H), 1.79 (m, 2H), 1.88 (s, 6H), 2.26 (s, 3H), 4.12 (t, ³J= 8.0 Hz, 2H), 6.87 (s, 2H), 6.88 (s, 1H), 7.13 (s, 1H). ¹³C{¹H} NMR (δ ppm, 100 MHz, CDCl₃): 14.12 (CH₃), 17.30 (CH₂), 17.66 (CH₂), 21.08 (CH₂), 22.69 (CH₃), 26.39 (CH₂), 29.14 (CH₃), 29.35 (CH₃), 29.46 (CH₃), 29.51 (CH₂), 29.63 (CH₂), 29.65 (CH₂), 29.68 (CH₃), 31.45 (CH₃), 31.92 (CH₃), 52.11 (NCH₂), 120.85 (C₄), 122.69 (C₅) 129.42 (*ipso*-mesityl), 134.70 (*m*-mesityl), 135.41 (*o*-mesityl), 139.47 (*p*-mesityl). HRMS (ESI) (*m/z*): found 871.5765 [Ag(C₂₆H₄₂N₂)₂⁺, 100%], expected 871.5741.

L^{mes}₁₆-Ag-Br



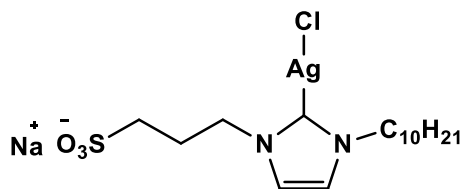
Yield: 75%; ¹H NMR (δ ppm, 400 MHz, CDCl₃): 0.89 (t, ³J= 8.0 Hz, 3H), 1.25-1.35 (m, 26H), 1.88 (m, 2H), 2.00 (s, 6H), 2.34 (s, 3H), 4.22 (t, ³J= 8.0 Hz, 2H), 6.95 (s, 2H), 6.96 (s, 1H), 7.19 (s, 1H). ¹³C{¹H} NMR (δ ppm, 100 MHz, CDCl₃): 14.16 (CH₃), 17.68 (CH₂), 21.09 (CH₂), 22.71 (CH₃), 26.40 (CH₂), 29.16 (CH₃), 29.39 (CH₃), 29.47 (CH₃), 29.52 (CH₂), 29.64 (CH₂), 29.68 (CH₂), 29.72 (CH₃), 31.47 (CH₃), 31.94 (CH₃), 52.16 (NCH₂), 120.74 (C₄), 122.70 (C₅) 129.45 (*ipso*-mesityl), 134.70 (*m*-mesityl), 135.39 (*o*-mesityl), 139.52 (*p*-mesityl). HRMS (ESI) (*m/z*): found 927.6313 [Ag(C₂₈H₄₆N₂)₂⁺, 100%], expected 927.6367.

Na[L^{bet}₈-Ag-Cl]



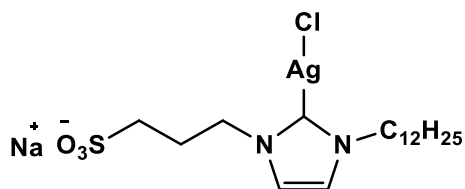
Yield 75%; ¹H NMR (δ ppm, 400 MHz, d⁶-dmsO): 0.82 (t, ³J = 7.4 Hz, 3H), 1.15-1.30 (m, 10H), 1.78 (m, 2H), 2.08 (m, 2H), 2.40 (t, ³J = 7.3 Hz, 2H), 4.14 (t, ³J = 6.6 Hz, 2H), 4.27 (t, ³J = 7.0 Hz, 2H), 7.80 (s, 2H). ¹³C{¹H} NMR (δ ppm, 100 MHz, d⁶-dmsO): 14.41 (CH₃), 22.53 (CH₂), 26.38 (CH₂), 28.30 (CH₂), 29.02 (CH₂), 29.08 (CH₂), 31.60 (CH₂), 31.68 (CH₂), 48.25 (CH₂), 50.31 (CH₂), 51.40 (CH₂), 122.25 (CH), 122.46 (CH). HRMS (ES⁻, CH₃OH): found 443.0461 [Ag(C₁₄H₂₅ClN₂O₃S)⁻, (30%)], expected 443.0331.

Na[L^{bet}₁₀-Ag-Cl]

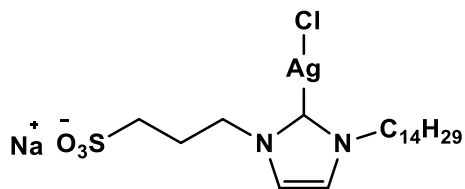


Yield 78%; ¹H NMR (δ ppm, 400 MHz, d⁶-dmsO): 0.84 (t, ³J = 7.0 Hz, 3H), 1.15-1.30 (br, 14H), 1.77 (m, 2H), 2.06 (m, 2H), 2.39 (t, ³J = 8.0 Hz, 2H), 4.11 (t, ³J = 7.0 Hz, 2H), 4.24 (t, ³J = 6.8 Hz, 2H), 7.51 (q, J = 1.8 Hz, 2H). ¹³C{¹H} NMR (δ ppm, 100 MHz, d⁶-dmsO): 14.43 (CH₃), 22.57 (CH₂), 23.94 (CH₂), 26.34 (CH₂), 28.25 (CH₂), 29.04 (CH₂), 29.16 (CH₂), 29.43 (CH₂), 31.51 (CH₂), 31.77 (CH₂), 48.30 (CH₂), 50.34 (CH₂), 51.38 (CH₂), 122.20 (CH), 122.44 (CH), 176.23 (Ag-C). HRMS (ES⁻, CH₃OH): found 767.3010 [Ag(C₁₆H₂₉ClN₂O₃S)⁻, (100%)], expected 767.3005.

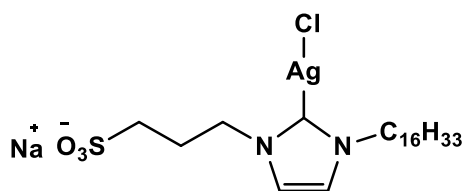
Na[L^{bet}₁₂-Ag-Cl]



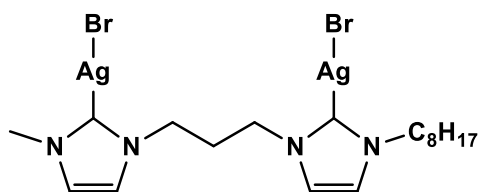
Yield 70%; ¹H NMR (δ ppm, 400 MHz, d⁶-dmsO): 0.85 (t, ³J = 7.1 Hz, 3H), 1.15-1.30 (m, 18H), 1.79 (m, 2H), 2.09 (m, 2H), 2.40 (t, ³J = 7.7 Hz, 2H), 4.14 (t, ³J = 7.0 Hz, 2H), 4.27 (t, ³J = 6.8 Hz, 2H), 7.51 (q, J = 1.8 Hz, 2H). ¹³C{¹H} NMR (δ ppm, 100 MHz, d⁶-dmsO): 14.43 (CH₃), 22.58 (CH₂), 26.41 (CH₂), 28.32 (CH₂), 29.09 (CH₂), 29.21 (CH₂), 29.46 (CH₂), 29.52 (CH₂), 31.61 (CH₂), 31.78 (CH₂), 48.26 (CH₂), 50.32 (CH₂), 51.41 (CH₂), 122.22 (CH), 122.47 (CH). HRMS (ES⁻, CH₃OH): found 499.0954 [Ag(C₁₈H₃₃ClN₂O₃S)⁻, (100%)], expected 499.0957.

Na[L^{bet}₁₄-Ag-Cl]

Yield 80%; ¹H NMR (δ ppm, 500 MHz, d⁶-dmsO): 0.85 (t, ³J = 6.9 Hz, 3H), 1.15-1.30 (m, 22H), 1.78 (m, 2H), 2.09 (m, 2H), 2.41 (t, ³J = 7.2 Hz, 2H), 4.13 (t, ³J = 7.4 Hz, 2H), 4.27 (t, ³J = 8.0 Hz, 2H), 7.50 (s, 2H). ¹³C{¹H} NMR (δ ppm, 125 MHz, d⁶-dmsO): 14.41 (CH₃), 22.57 (CH₂), 26.42 (CH₂), 28.27 (CH₂), 29.11 (CH₂), 29.20 (CH₂), 29.46 (CH₂), 29.50 (CH₂), 29.52 (CH₂), 29.55 (CH₂), 31.60 (CH₂), 31.78 (CH₂), 48.16 (CH₂), 50.23 (CH₂), 51.41 (CH₂), 122.21 (CH), 122.41 (CH), 179.25 (Ag-C). HRMS (ES⁻, CH₃OH): found 879.4180 [Ag(C₂₀H₃₈ClN₂O₃S)₂]⁻, (100%), expected 879.4257.

Na[L^{bet}₁₆-Ag-Cl]

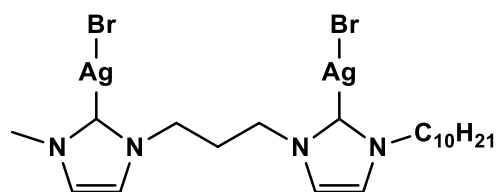
Yield: 76%; ¹H NMR (δ ppm, 500 MHz, d⁶-dmsO): 0.86 (t, ³J = 7.1 Hz, 3H), 1.15-1.30 (m, 26H), 1.78 (m, 2H), 2.06 (m, 2H), 2.37 (t, ³J = 7.8 Hz, 2H), 4.12 (t, ³J = 7.0 Hz, 2H), 4.24 (t, ³J = 6.8 Hz, 2H), 7.49 (d, ³J = 1.8 Hz, 1H), 7.51 (d, ³J = 1.8 Hz, 1H). ¹³C{¹H} NMR (δ ppm, 125 MHz, d⁶-dmsO): 14.42 (CH₃), 22.57 (CH₂), 26.38 (CH₂), 28.31 (CH₂), 29.06 (CH₂), 29.19 (CH₂), 29.44 (CH₂), 29.49 (CH₂), 29.54 (CH₂), 31.53 (CH₂), 31.77 (CH₂), 48.32 (CH₂), 50.36 (CH₂), 51.41 (CH₂), 122.16 (CH), 122.45 (CH). HRMS (ES⁻, CH₃OH): found 935.4771 [Ag(C₂₂H₄₂ClN₂O₃S)₂]⁻, (100%), expected 935.4883.

G₈-Ag₂-Br₂

Yield: 76%; ¹H NMR (δ ppm, 500 MHz, d⁶-dmsO): 0.83 (t, *J* = 6.8 Hz, 3H), 1.15-1.24 (m, 10H), 1.70 (m, 2H), 2.50 (m, 2H), 3.66 (s, 3H, CH₃N), 3.89 (t, *J* = 6.8 Hz, 2H), 4.00 (m, 4H), 7.54 (d, ³J = 1.8 Hz, 1H), 7.60 (d, ³J = 1.8 Hz, 1H), 7.62 (s, 2H). ¹³C{¹H} NMR (δ ppm, 125 MHz, d⁶-dmsO): 14.41 (CH₃), 22.52 (CH₂), 26.33 (CH₂), 28.85 (CH₂), 29.06 (CH₃), 30.27 (CH₂), 31.37 (NCH₃), 31.63 (CH₂), 38.41 (CH₂), 47.25

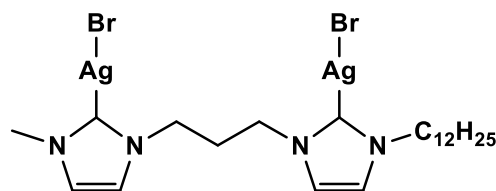
(NCH₂), 47.41 (NCH₂), 51.18 (NCH₂), 121.39 (C₅), 121.45 (C₅'), 123.30 (C₄), 124.49 (C₄'), 179.60 (C₂), 180.37 (C₂'). HRMS (ESI) (*m/z*): found 409.1527 [Ag₂(C₃₆H₆₀N₈)²⁺, 20%], expected 409.1516.

G₁₀-Ag₂-Br₂



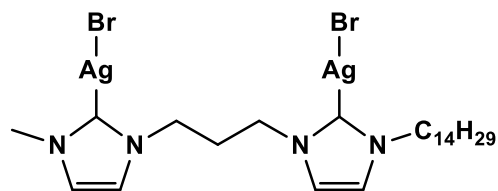
Yield: 82%; ¹H NMR (δ ppm, 500 MHz, d⁶-dms_o): 0.85 (t, *J* = 6.8 Hz, 3H), 1.12-1.34 (m, 14H), 1.71 (m, 2H), 2.44 (m, 2H), 3.68 (s, 3H, CH₃N), 3.91 (t, *J* = 8.0 Hz, 2H), 3.98 (m, 4H), 7.51 (s, 1H), 7.57 (s, 1H), 7.59 (s, 2H), ¹³C{¹H} NMR (δ ppm, 125 MHz, d⁶-dms_o): 14.45 (CH₃), 22.57 (CH₂), 26.36 (CH₂), 28.93 (CH₂), 29.16 (CH₂), 29.39 (CH₂), 29.43 (CH₂), 30.42 (CH₂), 31.35 (NCH₃), 31.76 (CH₂), 38.52 (CH₂), 47.31 (NCH₂), 47.44 (NCH₂), 51.24 (NCH₂), 121.30 (C₅), 121.36 (C₅'), 123.15 (C₄), 124.38 (C₄'), 179.82 (C₂), 180.55 (C₂'). HRMS (ESI) (*m/z*): found 437.1830 [Ag₂(C₄₀H₆₈N₈)²⁺, 20%], expected 437.1829.

G₁₂-Ag₂-Br₂



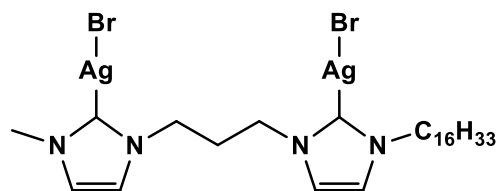
Yield: 86%; ¹H NMR (δ ppm, 500 MHz, d⁶-dms_o): 0.85 (t, *J* = 6.8 Hz, 3H), 1.12-1.30 (m, 18H), 1.71 (m, 2H), 2.45 (m, 2H), 3.61 (s, 3H, CH₃N), 3.91 (t, *J* = 8.0 Hz, 2H), 3.98 (m, 4H), 7.52 (s, 1H), 7.57 (s, 1H), 7.59 (s, 2H), ¹³C{¹H} NMR (δ ppm, 125 MHz, d⁶-dms_o): 14.44 (CH₃), 22.57 (CH₂), 26.35 (CH₂), 28.93 (CH₂), 29.20 (CH₃), 29.44 (CH₂), 29.49 (CH₃), 29.52 (CH₂), 30.33 (CH₂), 31.35 (NCH₃), 31.77 (CH₂), 38.49 (CH₂), 47.26 (NCH₂), 47.40 (NCH₂), 51.23 (NCH₂), 121.29 (C₅), 121.36 (C₅'), 123.19 (C₄), 124.41 (C₄'), 179.72 (C₂), 180.48 (C₂'). HRMS (ESI) (*m/z*): found 465.2152 [Ag₂(C₄₄H₇₆N₈)²⁺, 15%], expected 465.2142.

G₁₄-Ag₂-Br₂



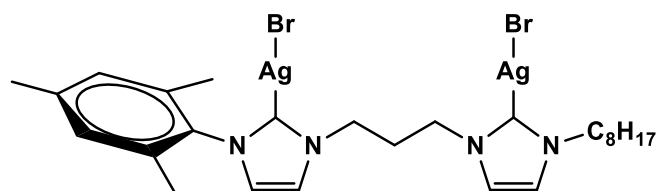
Yield: 92%; ¹H NMR (δ ppm, 500 MHz, d⁶-dms_o): 0.91 (t, *J* = 6.8 Hz, 3H), 1.22-1.34 (m, 24H), 1.77 (m, 2H), 2.50 (m, 2H), 3.73 (s, 3H, CH₃N), 3.98 (t, *J* = 8.0 Hz, 2H), 4.05 (m, 4H), 7.57 (s, 1H), 7.62 (s, 1H), 7.65 (s, 2H), ¹³C{¹H} NMR (δ ppm, 125 MHz, d⁶-dms_o): 14.42 (CH₃), 22.59 (CH₂), 26.41 (CH₂), 29.00 (CH₂), 29.22 (CH₃), 29.48 (CH₂), 29.49 (CH₃), 29.53 (CH₂), 29.56 (CH₂), 29.58 (CH₂), 30.56 (CH₂), 31.40 (NCH₃), 31.79 (CH₂), 38.51 (CH₂), 47.37 (NCH₂), 47.50 (NCH₂), 51.25 (NCH₂), 121.29 (C₅), 121.35 (C₅''), 123.07 (C₄), 124.31 (C₄''), 179.88 (C₂), 180.64 (C₂''). MS (ESI⁺) *m/z*: Found 493.2471 [Ag₂(C₄₈H₈₄N₈)²⁺, 15%], expected 493.2455.

G₁₆-Ag₂-Br₂



Yield: 87%; ¹H NMR (δ ppm, 500 MHz, d⁶-dms_o): 0.86 (t, *J* = 6.8 Hz, 3H), 1.12-1.34 (m, 24H), 1.70 (m, 2H), 2.64 (m, 2H), 2.50 (m, 2H), 3.64 (s, 3H, CH₃N), 3.89 (t, *J* = 8.0 Hz, 2H), 4.00 (m, 4H), 7.54 (s, 1H), 7.60 (s, 1H), 7.62 (s, 2H), HRMS (ESI) (*m/z*): found 523.2780 [Ag₂(C₅₂H₉₂N₈)²⁺, 15%], expected 522.7783.

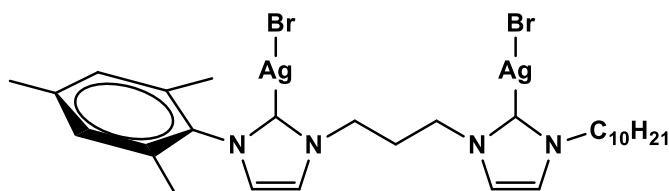
G^{mes}₈-Ag₂-Br₂



Yield: 88%; ¹H NMR (δ ppm, 500 MHz, d⁶-dms_o): 0.73 (t, ³*J* = 7.1 Hz, 3H), 0.99, (m, 2H), 1.08-1.17 (m, 20H), 1.52 (m, 2H), 1.79 (s, 6H), 2.24 (m, 3H), 2.31 (m, 2H), 3.77 (m, 2H), 4.07 (t, ³*J* = 7.3 Hz, 2H), 4.18 (t, ³*J* = 7.1 Hz, 2H), 6.94 (s, 2H), 7.42 (d, ³*J* = 1.8 Hz, 1H), 7.45 (t, *J* = 2.0 Hz, 2H), 7.67 (d, ³*J* = 1.8 Hz, 1H), ¹³C{¹H} NMR (δ ppm, 125 MHz, d⁶-dms_o): 14.42 (CH₃), 17.84 (2C, CH₂), 21.13 (CH₂), 22.52 (2C, CH₃), 26.28 (CH₂), 28.98 (CH₃), 29.04 (CH₃), 31.22 (CH₃), 31.93 (CH₃), 32.56 (NCH₂), 48.96 (NCH₂), 51.31 (NCH₂), 121.87 (C₅), 122.35 (C₅''), 122.76 (C₄), 124.21 (C₄''), 129.35 (2C, *m*-mesityl), 135.00 (2C, *o*-mesityl), 136.12

(*p*-mesityl), 139.06 (*ipso*-mesityl), 179.49 (C₂), 181.17 (C₂'). HRMS (ESI) (*m/z*): found 514.2156 [Ag₂(C₅₂H₇₆N₈)²⁺, 30%], expected 514.7157.

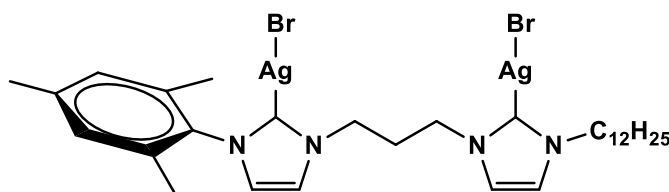
G^{mes}₁₀-Ag₂-Br₂



Yield: 86%; ¹H NMR (δ ppm, 500 MHz, d⁶-dmsO): 0.94 (t, ³J = 7.1 Hz, 3H), 1.19, (m, 2H), 1.25-1.40 (m, 20H), 1.71 (m, 2H), 1.98 (s, 6H), 2.40 (s, 3H), 2.51 (m,

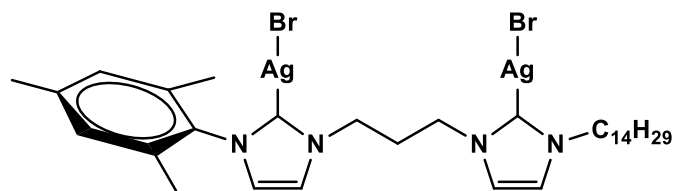
2H), 3.97 (m, 2H), 4.26 (t, ³J = 7.3 Hz, 2H), 4.37 (t, ³J = 7.1 Hz, 2H), 7.12 (s, 2H), 7.61 (d, ³J = 1.8 Hz, 1H), 7.63 (d, ³J = 1.8 Hz, 1H), 7.64 (d, ³J = 1.8 Hz, 1H), 7.87 (d, ³J = 1.8 Hz, 1H), ¹³C{¹H} NMR (δ ppm, 125 MHz, d⁶-dmsO): 14.43 (CH₃), 17.85 (CH₂), 21.13 (CH₂), 22.56 (CH₂), 26.29 (CH₃), 29.04 (CH₂), 29.13 (CH₂), 29.37 (CH₂), 29.40 (CH₂), 31.25 (CH₃), 31.74 (CH₂), 32.56 (CH₂), 48.95 (CH₂), 51.33 (NCH₂), 121.84 (C₅), 122.34 (C₅'), 122.75 (C₄), 124.19 (C₄'), 129.34 (2C, *m*-mesityl), 134.99 (2C, *o*-mesityl), 136.12 (*p*-mesityl), 139.03 (*ipso*-mesityl), 179.60 (C₂), 181.27 (C₂'). HRMS (ESI) (*m/z*): found 542.2473 [Ag₂(C₅₆H₈₄N₈)²⁺, 25%], expected 542.7470.

G^{mes}₁₂-Ag₂-Br₂



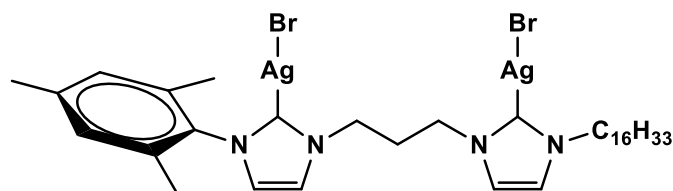
Yield: 77%; ¹H NMR (δ ppm, 500 MHz, d⁶-dmsO): 0.85 (t, ³J = 7.1 Hz, 3H), 1.08 (m, 2H), 1.15-1.30 (m, 16H), 1.62 (m, 2H), 1.87 (s, 6H), 2.33 (m, 3H), 2.42 (m,

2H), 3.87 (m, 2H), 4.16 (t, ³J = 7.3 Hz, 2H), 4.27 (t, ³J = 7.1 Hz, 2H), 7.02 (s, 2H), 7.52 (d, ³J = 1.8 Hz, 1H), 7.54 (t, *J* = 2.0 Hz, 2H), 7.77 (d, ³J = 1.8 Hz, 1H), ¹³C{¹H} NMR (δ ppm, 125 MHz, d⁶-dmsO): 14.45 (CH₃), 17.84 (CH₂), 21.13 (CH₂), 22.58 (CH₂), 26.30 (CH₃), 29.06 (CH₂), 29.19 (CH₂), 29.42 (CH₃), 29.48 (CH₂), 29.49 (CH₂), 31.25 (CH₃), 31.77 (CH₂), 32.52 (CH₂), 48.95 (CH₂), 51.30 (NCH₂), 121.86 (C₅), 122.35 (C₅'), 122.79 (C₄), 124.23 (C₄'), 129.35 (2C, *m*-mesityl), 136.09 (*p*-mesityl), 134.98 (2C, *o*-mesityl), 139.05 (*ipso*-mesityl), 179.44 (C₂), 181.13 (C₂'). HRMS (ESI) (*m/z*): found 570.2783 [Ag₂(C₆₀H₉₂N₈)²⁺, 30%], expected 570.7783.

G^{mes}₁₄-Ag₂-Br₂

Yield: 78%; ¹H NMR (δ ppm, 500 MHz, d⁶-dmsO): 0.85 (t, ³J = 7.1 Hz, 3H), 1.09, (m, 2H), 1.15-1.30 (m, 20H), 1.61 (m, 2H), 1.87 (s, 6H), 2.32 (m, 3H), 2.40 (m,

2H), 3.86 (m, 2H), 4.16 (t, ³J = 7.3 Hz, 2H), 4.26 (t, ³J = 7.1 Hz, 2H), 7.02 (s, 2H), 7.52 (d, ³J = 1.8 Hz, 1H), 7.54 (t, J = 2.0 Hz, 2H), 7.76 (d, ³J = 1.8 Hz, 1H), ¹³C{¹H} NMR (δ ppm, 125 MHz, d⁶-dmsO): 14.43 (CH₃), 17.82 (CH₂), 21.12 (CH₂), 22.57 (CH₂), 26.31 (CH₃), 29.05 (CH₂), 29.18 (CH₂), 29.40 (CH₂), 29.42 (CH₃), 29.48 (CH₂), 29.50 (CH₂), 29.52 (CH₂), 31.26 (CH₃), 31.76 (CH₂), 32.53 (CH₂), 49.01 (CH₂), 51.35 (NCH₂), 121.87 (C₅), 122.36 (C₅'), 122.80 (C₄), 124.24 (C₄'), 129.35 (2C, *m*-mesityl), 136.09 (*p*-mesityl), 134.97 (2C, *o*-mesityl), 139.06 (*ipso*-mesityl), 179.36 (C₂), 181.02 (C₂'). HRMS (ESI+) m/z: Found 598.3093 [Ag₂(C₆₄H₁₀₀N₈)²⁺, 20%], expected 598.8096.

G^{mes}₁₆-Ag₂-Br₂

Yield: 86%; ¹H NMR (δ ppm, 500 MHz, d⁶-dmsO): 0.85 (br 3H), 0.95-1.30 (m, 26H), 1.62 (m, 2H), 1.87 (s, 6H), 2.33 (m, 3H), 2.40 (m, 2H), 3.88 (m, 2H), 4.16 (br

2H), 4.27 (br, 2H), 7.01 (s, 2H), 7.52 (s, 3H), 7.76 (s, 1H), ¹³C{¹H} NMR (δ ppm, 125 MHz, d⁶-dmsO): 14.43 (CH₃), 17.84 (CH₃), 21.12 (CH₂), 22.57 (CH₃), 26.33 (CH₃), 29.08 (CH₂), 29.19 (CH₂), 29.52 (7C, CH₂), 31.30 (CH₃), 31.78 (CH₃), 32.57 (NCH₂), 48.98 (NCH₂), 51.33 (NCH₂), 121.85 (C₅), 122.35 (C₅'), 122.76 (C₄), 124.19 (C₄'), 129.33 (2C, *m*-mesityl), 134.97 (2C, *o*-mesityl), 136.09 (*p*-mesityl), 139.03 (*ipso*-mesityl), 179.57 (C₂), 181.23 (C₂'). HRMS (ESI+) m/z: Found 626.4002. [Ag₂(C₆₄H₁₀₀N₈)²⁺, 20%], expected 626.8409.

3.4. References

1. A. J. Arduengo Iii, H. V. R. Dias, R. L. Harlow and M. Kline, *J. Am. Chem. Soc.*, 1992, **114**, 5530-5534.
2. J. C. Garrison and W. J. Youngs, *Chem. Rev.*, 2005, **105**, 3978-4008.
3. A. Sidiropoulos, C. Jones, A. Stasch, S. Klein and G. Frenking, *Angew. Chem.*, 2009, **121**, 9881-9884.
4. C. Cao, R. Sun, Q. Chen, L. Lv, Y. Shi and G. Pang, *Transit. Met. Chem.*, 2013, **38**, 351-358.
5. C. Carcedo, J. C. Knight, S. J. A. Pope, I. A. Fallis and A. Dervisi, *Organometallics*, 2011, **30**, 2553-2562.
6. C. Hu, X. Li, W. Wang, R. Zhang and L. Deng, *Curr. Med. Chem.*, 2014, **21**, 1220-1230.
7. P. Marshall, R. L. Jenkins, W. Clegg, R. W. Harrington, S. K. Callear, S. J. Coles, I. A. Fallis and A. Dervisi, *Dalton Trans.*, 2012, **41**, 12839-12846.
8. A. G. Tennyson, E. L. Rosen, M. S. Collins, V. M. Lynch and C. W. Bielawski, *Inorg. Chem.*, 2009, **48**, 6924-6933.
9. F. Almalioti, J. MacDougall, S. Hughes, M. M. Hasson, R. L. Jenkins, B. D. Ward, G. J. Tizzard, S. J. Coles, D. W. Williams, S. Bamford, I. A. Fallis and A. Dervisi, *Dalton Trans.*, 2013, **42**, 12370-12380.
10. W. Liu and R. Gust, *Chem. Soc. Rev.*, 2013, **42**, 755-773.
11. I. J. B. Lin and C. S. Vasam, *Coord. Chem. Rev.*, 2007, **251**, 642-670.
12. P. de Frémont, N. Marion and S. P. Nolan, *Coord. Chem. Rev.*, 2009, **253**, 862-892.
13. L. Eloy, A.-S. Jarrouse, M.-L. Teysot, A. Gautier, L. Morel, C. Jolival, T. Cresteil and S. Roland, *Chem Med Chem*, 2012, **7**, 805-814.

14. A. J. Arduengo, H. V. R. Dias, J. C. Calabrese and F. Davidson, *Organometallics*, 1993, **12**, 3405-3409.
15. O. Guerret, S. Solé, H. Gornitzka, M. Teichert, G. Trinquier and G. Bertrand, *J. Am. Chem. Soc.*, 1997, **119**, 6668-6669.
16. H. M. J. Wang and I. J. B. Lin, *Organometallics*, 1998, **17**, 972-975.
17. A. A. D. Tulloch, A. A. Danopoulos, S. Winston, S. Kleinhenz and G. Eastham, *Dalton Trans.*, 2000, 4499-4506.
18. J. C. Garrison, R. S. Simons, C. A. Tessier and W. J. Youngs, *J. Organomet. Chem.*, 2003, **673**, 1-4.
19. A. Kascatan-Nebioglu, M. J. Panzner, J. C. Garrison, C. A. Tessier and W. J. Youngs, *Organometallics*, 2004, **23**, 1928-1931.
20. C. A. Quezada, J. C. Garrison, M. J. Panzner, C. A. Tessier and W. J. Youngs, *Organometallics*, 2004, **23**, 4846-4848.
21. I. J. B. Lin and C. S. Vasam, *Comm. on Inorg. Chem.*, 2004, **25**, 75-129.
22. Q.-X. Liu, F.-B. Xu, Q.-S. Li, X.-S. Zeng, X.-B. Leng, Y. L. Chou and Z.-Z. Zhang, *Organometallics*, 2003, **22**, 309-314.
23. C. K. Lee, K. M. Lee and I. J. B. Lin, *Organometallics*, 2002, **21**, 10-12.
24. P. L. Arnold, A. C. Scarisbrick, A. J. Blake and C. Wilson, *Chem. Comm.*, 2001, 2340-2341.
25. I. S. Edworthy, M. Rodden, S. A. Mungur, K. M. Davis, A. J. Blake, C. Wilson, M. Schröder and P. L. Arnold, *J. Organomet. Chem.*, 2005, **690**, 5710-5719.
26. W. Chen, B. Wu and K. Matsumoto, *J. Organomet. Chem.*, 2002, **654**, 233-236.
27. D. Nemcsok, K. Wichmann and G. Frenking, *Organometallics*, 2004, **23**, 3640-3646.

28. A. C. Sentman, S. Csihony, R. M. Waymouth and J. L. Hedrick, *The J. Org. Chem.*, 2005, **70**, 2391-2393.
29. A. Melaiye and W. J. Youngs, *Expert Opin. Ther. Pat.*, 2005, **15**, 125-130.
30. S. Silver, *FEMS Microbiol. Rev.*, 2003, **27**, 341-353.
31. T. R. Neu, *Microbiol. Rev.*, 1996, **60**, 151-166.
32. E. P. Çoban, R. Fırıncı, H. Biyik and M. E. Günay, *Brazilian J. Pharm. Sci.*, 2017, **53**, 1-10.
33. O. A. El Seoud, P. A. R. Pires, T. Abdel-Moghny and E. L. Bastos, *J. Coll. Interf. Sci.*, 2007, **313**, 296-304.
34. R. Zana, M. Benrraou and R. Rueff, *Langmuir*, 1991, **7**, 1072-1075.
35. W. A. Herrmann and C. Köcher, *Angew. Chem. Int. Ed.*, 1997, **36**, 2162-2187.
36. W. A. Herrmann, S. K. Schneider, K. Öfele, M. Sakamoto and E. Herdtweck, *J. Organomet. Chem.*, 2004, **689**, 2441-2449.
37. L. G. Bonnet, R. E. Douthwaite, R. Hodgson, J. Houghton, B. M. Kariuki and S. Simonovic, *Dalton Trans.*, 2004, 3528-3535.
38. V. Gandin, M. Pelli, M. Marinelli, C. Marzano, A. Dolmella, M. Giorgetti and C. Santini, *J. Inorg. Biochem.*, 2013, **129**, 135-144.
39. J. Berding, H. Kooijman, A. L. Spek and E. Bouwman, *J. Organomet. Chem.*, 2009, **694**, 2217-2221.
40. S. Dastgir, K. S. Coleman and M. L. H. Green, *Dalton Trans.*, 2011, **40**, 661-672.
41. O. Sanchez, S. González, M. Fernández, A. R. Higuera-Padilla, Y. Leon, D. Coll, A. Vidal, P. Taylor, I. Urdanibia, M. C. Goite and W. Castro, *Inorg. Chimic. Act.*, 2015, **437**, 143-151.

Chapter

4

In vitro Antimicrobial screening of Ag(I)-NHCs against planktonic and biofilm cells

| | |
|---|------------|
| 4.0. <i>In vitro</i> Antimicrobial screening of Ag(I)-NHCs against planktonic and biofilm cells..... | 118 |
| 4.1. Introduction..... | 119 |
| 4.2. Aims..... | 121 |
| 4.3. Results and Discussion..... | 123 |
| 4.3.1. Preliminary antimicrobial screening..... | 123 |
| 4.3.2. Determination of MIC, MBC and MBEC..... | 123 |
| 4.3.2.1. HL ₈₋₁₆ and L ₈₋₁₆ -Ag-Br..... | 123 |
| 4.3.2.2. HL ^{mes} ₁₀₋₁₆ and L ^{mes} ₁₀₋₁₆ -Ag-Br..... | 128 |
| 4.3.2.3. H ₂ G ₈₋₁₆ and G ₈₋₁₆ -Ag ₂ -Br ₂ | 132 |
| 4.3.2.4. H ₂ G ^{mes} ₈₋₁₆ and G ^{mes} ₈₋₁₆ -Ag ₂ -Br ₂ | 136 |
| 4.4. Conclusions..... | 139 |
| 4.5. Experimental..... | 142 |
| 4.5.1. Biological Activity..... | 142 |
| 4.5.1.1. MIC and MBC Determinations..... | 142 |
| 4.5.1.2. Biofilm Cells Susceptibility Test..... | 142 |
| 4.6. References..... | 143 |

Chapter 4

***In vitro* Antimicrobial Screening of Ag(I)-NHCs Against Planktonic and Biofilm Cells**

4.1. Introduction

For many centuries, silver has been used extensively for a variety of medical purposes and as a major therapeutic agent for infectious diseases, including surgical infections and in 1800, there was a wide acceptance that silver vessels be used to store products like wine, water, milk and vinegar.^{1,2} Before the scientific understanding of disease-causing pathogenic organisms was brought to light in 1683 by Anton van Leeuwenhoek, when he used his new microscope to visualize bacteria among the ‘animalcules’ harvested from his own teeth, silver nitrate has been in use for various medical treatments and treatment of infectious diseases.^{3,4} It has been found and established that the bioactive form of silver is the silver(I) ion, and that pure metallic silver does not interact chemically with human tissue or is poisonous to microorganisms. However, the widespread use of silver has led to bacterial resistance as has been observed in burn wound wards of hospitals using silver salts (silver nitrate and silver sulfadiazine) for topical treatment and in hospitals that utilize silver-coated catheters.^{4,5} One of the mechanisms of silver resistance by some strains of bacteria has been shown to involve the use of a superfamily of transport proteins called P-type ATPases that are driven by ATP hydrolysis which ensures the transport of heavy metal cations from the cytoplasm to the periplasm by efflux.⁶

The Infectious Diseases Society of America (IDSA) in 2009, expressed their concern about the slow pace of development for novel therapeutics to treat drug-resistant infections, especially those caused by gram-negative pathogens.⁷ This view was reinforced by World Health Organisation (WHO) in their recent report on analysis of antibacterial drugs undergoing clinical development and from the report, most of the drugs are modifications of existing classes of antibiotics and as such, they are only short-term solutions.⁸

The use of transition metal complexes of N-heterocyclic carbenes (NHCs) for applications other than catalysis has been gaining attention in recent years.⁹ Much of this interest stems from recent studies demonstrating the exceptional antimicrobial efficacy of some of these complexes against a broad spectrum of both gram-positive and gram-negative bacteria, fungi and as chemotherapeutic agents.^{10,11} Among the metal N-heterocyclic carbene (NHC) complexes, there is growing interest

in silver(I) N-heterocyclic carbene (Ag(I)-NHC) complexes, due to the rich history of silver for its antimicrobial properties and application as carbene transfer agents in the synthesis of both transition and inner transition metal-NHC complexes.⁵

Youngs et al. pioneered the use of Ag(I)-NHCs as antimicrobials in 2003, and in their report, alcohol functionalized Ag(I)-NHCs (Figure 4.1A) show a better bacteriostatic effect than AgNO₃ against *E. coli*, *P. aeruginosa* and *S. aureus*.¹² In our group, we have investigated the activity of Ag(I)-NHC in Figure 4.1B against methicillin-resistant *Staphylococcus aureus* (MRSA) NCTC 13277, *S. aureus* NCTC 6571, *Pseudomonas aeruginosa* NCTC 10662, and *Proteus mirabilis* NCTC 11938 and the fungal organism, *Candida albicans* ATCC 90028. This complex showed good activity against MRSA and moderate activity against all other tested microbes.¹⁰

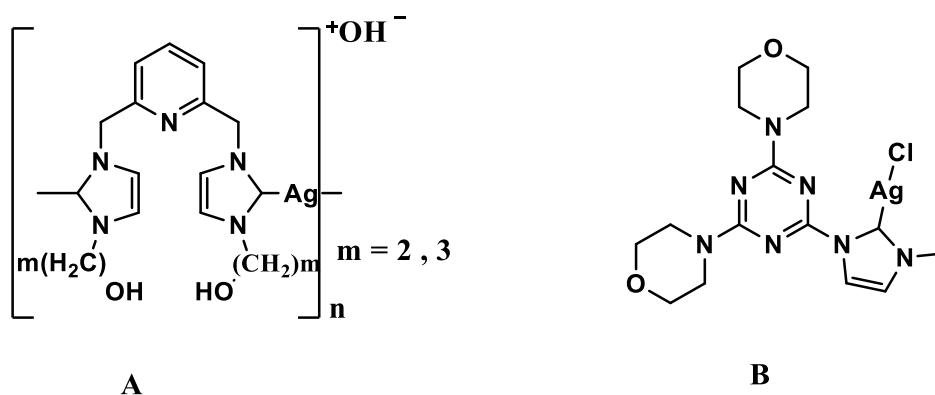


Figure 4.1: Structure of Ag(I)-NHC antimicrobials reported by Youngs et al (A) and Fallis et al (B)

One of the advantages of using Ag(I)-NHCs as antimicrobials is that the NHC precursor (quaternary ammonium ion) and silver ion tethered to it are both active biologically.^{1,2,13-15} Interestingly, the proligands (imidazolium salts) used in this work are amphiphilic in nature and they have been found to bind to the cell surfaces of bacteria by chemisorption,¹⁵ and their ability to penetrate and disrupt the membrane of bacteria has also been documented.¹⁶⁻¹⁸ The bacterial and fungal strains used in this study have been confirmed to form biofilm cells,^{19,20} which are a complex organization of communal bacterial/fungal cells, which anchor to various biological and

non-biological surfaces and have been implicated in the pathogenesis of recalcitrant chronic infections associated with indwelling medical devices such as catheters.²¹ Bacteria within biofilms are protected by extracellular polymer matrices (EPS) that are impervious to antibiotics, which is one of the major factors that cause antibiotic resistance.²² This work investigated the susceptibility of bacterial/fungal planktonic and biofilm cells to the synthesized proligands and their corresponding Ag-NHCs (Figure 4.2) with the aim of obtaining a potential lead compound that can be incorporated into a urinary catheter, thereby generating a catheter surface that could inhibit the growth and swarming of pathogenic microorganisms.

4.2. Aims

The aim of this chapter was to explore the activity of the synthesized proligands, (**HL₈₋₁₆**, **HL^{mes}₈₋₁₆**, **H₂G₈₋₁₆** and **H₂G^{mes}₈₋₁₆**) and the Ag(I)-NHCs, (**L₈₋₁₆-Ag-Br**, **L^{mes}₈₋₁₆-Ag-Br**, **G₈₋₁₆-Ag₂-Br₂** and **G^{mes}₈₋₁₆-Ag₂-Br₂**) described in chapters 2 and 3 against *Escherichia coli* NCTC 12923, *Staphylococcus aureus* NCTC 6571, *Staphylococcus aureus* NCIMB 9518, *Pseudomonas aeruginosa* ATCC 15692, *Staphylococcus epidermidis* ATCC 14990, *Staphylococcus epidermidis* ATCC RP62A and *Candida albicans* ATCC 90028.

Preliminary screening of the proligands and the Ag(I)-NHCs were carried out *in vitro* against planktonic and biofilm cells of the above-mentioned organisms and their activities expressed as minimal inhibitory concentration (MIC), defined as the lowest concentration of an antibacterial compound that suppresses the visible growth of the microorganisms; minimal bactericidal concentration (MBC), defined as the lowest concentration of antibacterial agent that reduces the viability of the initial bacterial inoculum by $\geq 99.9\%$; and minimal biofilm eradication concentration (MBEC), defined as the lowest concentration of antimicrobial agent required to eradicate already grown biofilm¹⁹ and their activities are compared to triclosan (5-chloro-2-(2,4-dichlorophenoxy)phenol) and AgNO₃.

Lastly, the relationship between the antimicrobial activities and the molecular structures of the proligands and the Ag(I)-NHCs was explored.

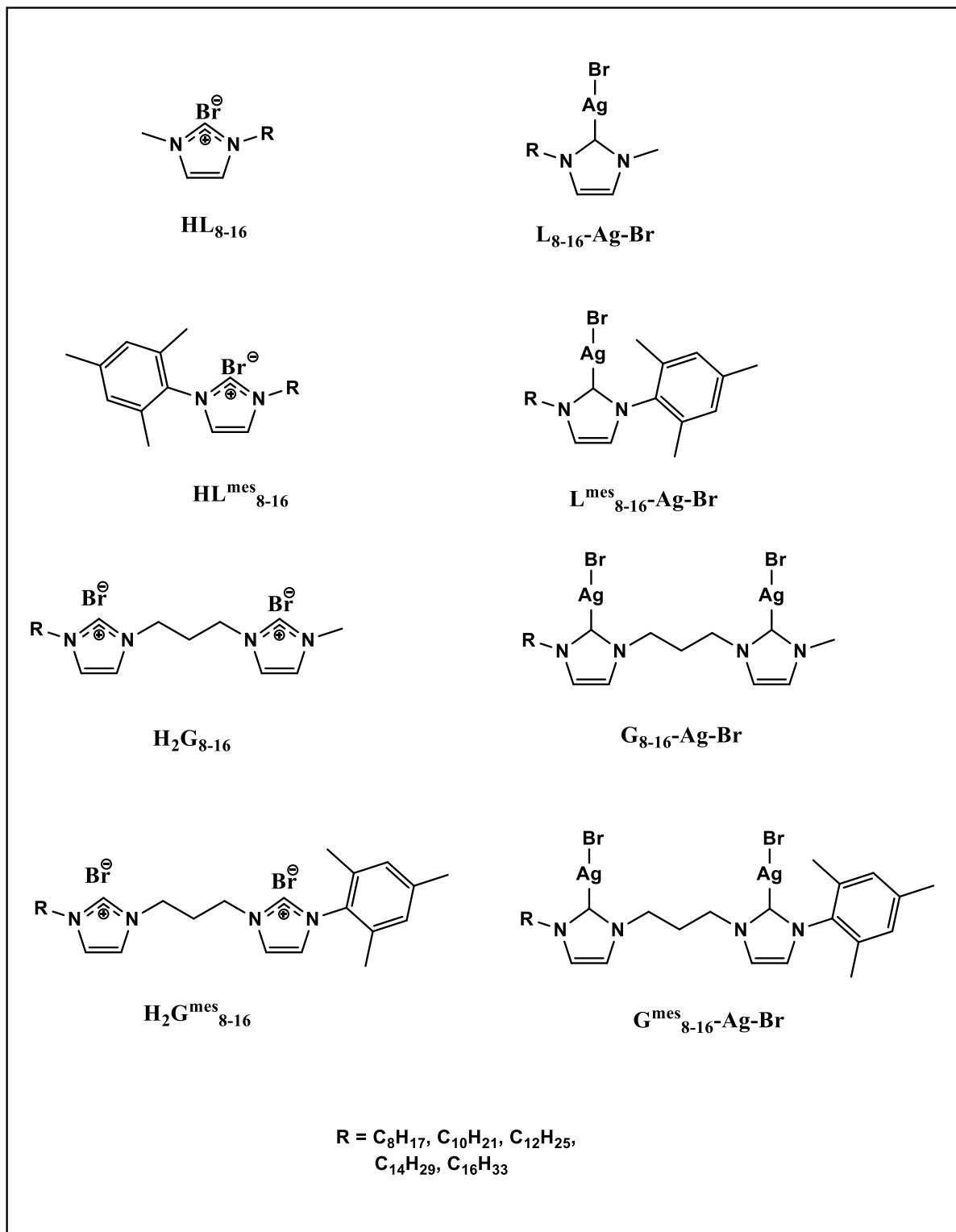


Figure 4.2: NHC precursors and the Ag(I)-NHCs used in this study (their syntheses are discussed in Chapters 2 and 3)

4.3. Results and Discussion

4.3.1. Preliminary antimicrobial screening

4.3.2. Determination of MIC, MBC and MBEC

The MIC and MBC were determined using the microbroth dilution method according to the Clinical and Laboratory Standards Institute (CLSI)²⁴ and MBEC was evaluated as described elsewhere.¹⁹ Results presented in tables are averages of three replicates.

4.3.2.1. HL₈₋₁₆ and L₈₋₁₆-Ag-Br

From Table 4.1, the MIC of **HL₁₂**, **HL₁₄**, **HL₁₆** and **L₈₋₁₆-Ag-Br** against the four gram-positive bacterial strains range from 6.25-<0.78125 µg/mL respectively while that of **HL₁₀** is in the range 12.5-25 µg/mL and **HL₈** broadly shows no activity. **HL₁₄**, **HL₁₆**, and **L₁₂-Ag-Br**, **L₁₄-Ag-Br**, **L₁₆-Ag-Br** show moderate activity with MIC ranging from 50-100 µg/mL respectively against *Pseudomonas aeruginosa* NCTC 10662, while **HL₈**, **HL₁₀**, **HL₁₂**, and **L₈-Ag-Br** and **L₁₀-Ag-Br** did not show any activity. **HL₈₋₁₆** and **L₈₋₁₆-Ag-Br** show moderate activity against *Escherichia coli* NCTC 12923 with MIC ranging from 12.5-50 and 12.5-25 µg/mL respectively. For the fungal strain, *Candida albicans* ATCC 90028, **HL₁₂**, **HL₁₄**, **HL₁₆** and **L₈-Ag-Br**, **L₁₂-Ag-Br**, **L₁₄-Ag-Br**, **L₁₆-Ag-Br** show good activity with MIC ranging from 1.5625-6.25 µg/mL respectively and **HL₁₀** and **L₁₀-Ag-Br** show moderate activity with MIC values of 25 µg/mL respectively. *Candida albicans* ATCC 90028 however tolerated **HL₈**.

The activity of **HL₁₂**, **HL₁₄**, **HL₁₆** and **L₈₋₁₆-Ag-Br** are found to be bactericidal against the four gram-positive bacteria strains with MBC values (Table 4.2) ranging from 1.5625-100 and <0.78125-50 µg/mL respectively. The activity of **HL₈** and **HL₁₀** can be described as bacteriostatic where they have been found to have inhibited any of the four gram-positive bacteria. Furthermore, the activity of **HL₁₄**, **HL₁₆** and **L₁₂-Ag-Br**, **L₁₄-Ag-Br**, **L₁₆-Ag-Br** tend to be bactericidal against *Pseudomonas aeruginosa* NCTC 10662 with MBC values of 100 and 50-100 µg/mL respectively. **HL₁₀₋₁₆** and **L₁₀₋₁₆-Ag-Br**, show bactericidal activity with moderate MBC values ranging from

12.5-100 µg/mL respectively against *Escherichia coli* NCTC 12923. Lastly, the activity of **HL**₁₂₋₁₆ and **L**₈₋₁₆-**Ag-Br** are found to be bactericidal against *Candida albicans* ATCC 90028 with MBC values ranging from 3.125-6.25 and 1.5625-25 µg/mL respectively while **HL**₈ is fungistatic.

Overall, the proligands **HL**₁₂, **HL**₁₄ and **HL**₁₆ and the Ag-NHCs (**L**₈₋₁₆-**Ag-Br**) show good activity against all the gram-positive bacterial and fungal strains, moderate activity towards the gram-negative strains and their inhibitory activity were found to be bactericidal and fungicidal.


Results of Biofilm susceptibility test with the isolates described above are presented in Table 4.3. Unlike the MIC and MBC results, all the proligands (**HL**₈₋₁₆) were found to have no activity (in the concentration range used in this work) against all the bacteria strains tested, while **HL**₁₂, **HL**₁₄ and **HL**₁₆ have MBEC values ranging from 100-300 µg/mL against *Candida albicans* ATCC 90028 biofilm. Equally, the two gram-negative bacteria biofilms show resistance against the Ag-NHCs (**L**₈₋₁₆-**Ag-Br**). **L**₁₄-**Ag-Br**, however, is active against all the four stains of gram-positive bacteria biofilms with MBEC values ranging from 200-300 µg/mL. Also, *Staphylococcus aureus* NCTC 6571 and *Staphylococcus aureus* NCIMB 9518 biofilms were found to be susceptible to **L**₁₂-**Ag-Br** and **L**₁₆-**Ag-Br** with MBEC values of 300 and 400 µg/mL respectively. *Candida albicans* ATCC 90028 biofilm was found to be susceptible to **L**₈₋₁₆-**Ag-Br** and with **L**₁₄-**Ag-Br** and **L**₁₆-**Ag-Br** showing good activity with MBEC value of <50 µg/mL respectively.


Although, there is no clear-cut difference in the activity of **HL**₁₂₋₁₆ and **L**₈₋₁₆-**Ag-Br** against planktonic cells, all the biofilm cells tested tolerated **HL**₁₂₋₁₆. Based on the result of the silver nitrate used as one of the standards, we can infer that the amphiphilic imidazolium scaffolds enhanced the antibiofilm activity of the silver ion. Therefore, the activity of **L**₁₂-**Ag-Br** against *Staphylococcus aureus* NCTC 6571, **L**₁₄-**Ag-Br** against *Staphylococcus aureus* NCTC 6571, *Staphylococcus aureus* NCIMB 9518, *Staphylococcus epidermidis* ATCC 14990 and *Staphylococcus epidermidis* ATCC RP62A and **L**₁₆-**Ag-Br** against *Staphylococcus aureus* NCIMB 9518 biofilm cells, can be primarily attributed to the silver functionality.

Table 4.1: Minimum Inhibitory Concentrations (MIC) of HL₈₋₁₆ and L₈₋₁₆-Ag-Br

| MIC ($\mu\text{g/mL}$) | HL ₈ | L ₈ -Ag-Br | HL ₁₀ | L ₁₀ -Ag-Br | HL ₁₂ | L ₁₂ -Ag-Br | HL ₁₄ | L ₁₄ -Ag-Br | HL ₁₆ | L ₁₆ -Ag-Br | Triclosan | AgNO ₃ |
|----------------------------|-----------------|-----------------------|------------------|------------------------|------------------|------------------------|------------------|------------------------|------------------|------------------------|-----------|-------------------|
| S aureus 6571 | R | 6.25 | 25 | 6.25 | 3.125 | 3.125 | 6.25 | <0.78125 | <0.78125 | <0.78125 | <0.78125 | 25 |
| S aureus 9518 | R | 3.125 | 25 | 6.25 | 3.125 | 3.125 | 6.25 | <0.78125 | <0.78125 | <0.78125 | <0.78125 | 12.5 |
| S epidermidis 14990 | 100 | 1.5625 | 12.5 | 6.25 | 1.5625 | <0.78125 | <0.78125 | <0.78125 | <0.78125 | <0.78125 | <0.78125 | 6.25 |
| S epidermidis RP62A | R | 3.125 | 12.5 | 6.25 | 1.5625 | 1.5625 | <0.78125 | <0.78125 | <0.78125 | <0.78125 | <0.78125 | 3.125 |
| P aeruginosa 15692 | R | R | R | R | R | 100 | 100 | 50 | 50 | 50 | R | 3.125 |
| E coli 12923 | R | 25 | 50 | 25 | 25 | 25 | 12.5 | 12.5 | 12.5 | 12.5 | 1.5625 | 6.25 |
| C. albicans 90028 | R | 6.25 | 25 | 25 | 6.25 | 1.5625 | 1.5625 | 1.5625 | 1.5625 | 1.5625 | <0.78125 | 3.125 |

Key

 No activity

 Moderate activity (12.5-100 $\mu\text{g/mL}$)




 Good activity (6.25-<0.78125 $\mu\text{g/mL}$)

Table 4.2: Minimum Bactericidal Concentration (MBC) of HL8-16 and L8-16-Ag-Br

| MBC ($\mu\text{g/mL}$) | HL ₈ | L ₈ -Ag-Br | HL ₁₀ | L ₁₀ -Ag-Br | HL ₁₂ | L ₁₂ -Ag-Br | HL ₁₄ | L ₁₄ -Ag-Br | HL ₁₆ | L ₁₆ -Ag-Br | Triclosan | AgNO ₃ |
|----------------------------|-----------------|-----------------------|------------------|------------------------|------------------|------------------------|------------------|------------------------|------------------|------------------------|-----------|-------------------|
| S aureus 6571 | R | 6.25 | R | 50 | 25 | 25 | 100 | 6.25 | 3.125 | 6.25 | 12.5 | 25 |
| S aureus 9518 | R | 6.25 | R | 25 | 12.5 | 12.5 | 12.5 | 3.125 | 3.125 | 1.5625 | 12.5 | 25 |
| S epidermidis 14990 | R | 6.25 | 100 | 25 | 6.25 | 6.25 | 3.125 | 3.125 | 1.5625 | <0.78125 | 12.5 | 12.5 |
| S epidermidis RP62A | R | 3.125 | R | 25 | 12.5 | 12.5 | 3.125 | 3.125 | 1.5625 | <0.78125 | 12.5 | 12.5 |
| P aeruginosa 15692 | R | R | R | R | R | 100 | 100 | 100 | 100 | 50 | R | 12.5 |
| E coli 12923 | R | R | 100 | 100 | 25 | 50 | 25 | 25 | 12.5 | 12.5 | 25 | 12.5 |
| C. albicans 90028 | R | 12.5 | R | 25 | 6.25 | 3.125 | 3.125 | 1.5625 | 3.125 | 1.5625 | <0.78125 | |

Key

 No activity

 Moderate activity (12.5-100 $\mu\text{g/mL}$)




 Good activity (6.25-<0.78125 $\mu\text{g/mL}$)


Table 4.3: Minimum Biofilm Eradication Concentrations (MBEC) of HL₈₋₁₆ and L₈₋₁₆-Ag-Br

| MBEC (µg/mL) | HL ₈ | L ₈ -Ag-Br | HL ₁₀ | L ₁₀ -Ag-Br | HL ₁₂ | L ₁₂ -Ag-Br | HL ₁₄ | L ₁₄ -Ag-Br | HL ₁₆ | L ₁₆ -Ag-Br | Triclosan | AgNO ₃ |
|-----------------------------|-----------------|-----------------------|------------------|------------------------|------------------|------------------------|------------------|------------------------|------------------|------------------------|-----------|-------------------|
| S. aureus 6571 | R | R | R | R | R | 300 | R | 200 | R | R | R | R |
| S. aureus 9518 | R | R | R | R | R | R | R | 250 | R | 400 | R | 400 |
| S. epidermidis 14990 | R | R | R | R | R | R | R | 300 | R | R | R | R |
| S. epidermidis RP62A | R | R | R | R | R | R | R | 300 | R | R | R | 300 |
| P. aeruginosa 15692 | R | R | R | R | R | R | R | R | R | R | R | R |
| E. coli 12923 | R | R | R | R | R | R | R | R | R | R | R | R |
| C. albicans 90028 | R | 250 | R | 350 | 300 | 200 | 100 | <50 | 200 | <50 | <50 | 400 |

Key

 No activity

 Moderate activity (100-400 µg/mL)

 Good activity (<50 µg/mL)

4.3.2.2. **HL^{mes}₁₀₋₁₆ and L^{mes}₁₀₋₁₆-Ag-Br**

The MIC of **HL^{mes}₁₀₋₁₆** and **L^{mes}₁₀₋₁₆-Ag-Br** against the four gram-positive bacterial strains (Table 4.4) ranges from 6.25-<0.78125 µg/mL respectively and that of **HL^{mes}₈** and **L^{mes}₈-Ag-Br** are 25 and 12.5 µg/mL respectively against *Staphylococcus aureus* NCTC 6571. Except for **HL^{mes}₈** and **HL^{mes}₁₀** with no activity, **HL^{mes}₁₂₋₁₆** and **L^{mes}₈₋₁₆-Ag-Br** show moderate activity with MIC ranging from 50-100 µg/mL respectively against *Pseudomonas aeruginosa* NCTC 10662. **L^{mes}₁₂₋₁₆-Ag-Br** and **HL^{mes}₈₋₁₆**, **L^{mes}₈-Ag-Br**, **L^{mes}₁₀-Ag-Br** show good and moderate activity with MIC ranging from 3.125-6.25 and 12.5-100 µg/mL respectively against *Escherichia coli* NCTC 12923. The fungal strain, *Candida albicans* ATCC 90028, is susceptible to **HL^{mes}₈₋₁₆** and **L^{mes}₈₋₁₆-Ag-Br**, besides **HL^{mes}₈** with MIC of 25 µg/mL, the rest of the compounds show good activity with MIC values ranging <0.78125-6.25 µg/mL.

The activity of **HL^{mes}₁₀₋₁₆** and **L^{mes}₈₋₁₆-Ag-Br** are found to be bactericidal against the four gram-positive bacterial strains with MBC values ranging from 1.5625-50 and 1.5625-100 µg/mL respectively. However, the activity of **HL^{mes}₈** is bacteriostatic. In addition, the activity of **HL^{mes}₁₀₋₁₆**, and **L^{mes}₁₂₋₁₆-Ag-Br** tend to be bactericidal against *Pseudomonas aeruginosa* NCTC 10662 with moderate MBC values (Table 4.5) ranging from 50-100 and 100 µg/mL respectively, while the activity of **L^{mes}₈-Ag-Br** is bacteriostatic. And lastly, the activity of **HL^{mes}₁₀₋₁₆**, and **L^{mes}₁₀₋₁₆-Ag-Br** are bactericidal as well with MBC values ranging from 25-50 and 6.25-100 µg/mL respectively against *Escherichia coli* NCTC 12923. **HL^{mes}₈₋₁₆** and **L^{mes}₈₋₁₆-Ag-Br** show fungicidal activity towards *Candida albicans* ATCC 90028 with MBC values ranging from 1.5625-100 and <0.78125-6.25 µg/mL respectively.


Just like **HL₈₋₁₆** and **L₈₋₁₆-Ag-Br**, the activity of **HL^{mes}₈₋₁₆** and **L^{mes}₈₋₁₆-Ag-Br** ranges generally from good to moderate against all the planktonic microbial strains tested and their inhibitory activity was found largely to be bactericidal and fungicidal.

Table 4.4: Minimum Inhibitory Concentrations (MIC) of HL^{mes}₈₋₁₆ and L^{mes}₈₋₁₆-Ag-Br

| MIC (µg/mL) | HL ^{mes} ₈ | L ^{mes} ₈ -Ag-Br | HL ^{mes} ₁₀ | L ^{mes} ₁₀ -Ag-Br | HL ^{mes} ₁₂ | L ^{mes} ₁₂ -Ag-Br | HL ^{mes} ₁₄ | L ^{mes} ₁₄ -Ag-Br | HL ^{mes} ₁₆ | L ^{mes} ₁₆ -Ag-Br | Triclosan | AgNO ₃ |
|-----------------------------|--------------------------------|--------------------------------------|---------------------------------|---------------------------------------|---------------------------------|---------------------------------------|---------------------------------|---------------------------------------|---------------------------------|---------------------------------------|-----------|-------------------|
| S. aureus 6571 | 25 | 12.5 | 6.25 | 1.5625 | 1.5625 | <0.78125 | <0.78125 | <0.78125 | <0.78125 | <0.78125 | <0.78125 | 25 |
| S. aureus 9518 | 6.25 | 6.25 | 3.125 | 1.5625 | <0.78125 | <0.78125 | <0.78125 | <0.78125 | <0.78125 | <0.78125 | <0.78125 | 12.5 |
| S. epidermidis 14990 | 3.125 | 3.125 | 1.5625 | <0.78125 | 1.5625 | <0.78125 | <0.78125 | <0.78125 | <0.78125 | <0.78125 | <0.78125 | 6.25 |
| S. epidermidis RP62A | 6.25 | 6.25 | 3.125 | 1.5625 | 1.5625 | <0.78125 | <0.78125 | <0.78125 | <0.78125 | <0.78125 | <0.78125 | 3.125 |
| P. aeruginosa 15692 | R | 50 | R | 50 | 50 | 25 | 50 | 25 | 50 | 6.25 | R | 3.125 |
| E. coli 12923 | 100 | 50 | 50 | 25 | 12.5 | 6.25 | 12.5 | 3.125 | 12.5 | 3.125 | 1.5625 | 6.25 |
| C. albicans 90028 | 25 | 6.25 | 3.125 | 1.5625 | 1.5625 | 1.5625 | 1.5625 | <0.78125 | 1.5625 | <0.78125 | <0.78125 | 3.125 |

Key

 No activity

 Moderate activity (12.5-100 µg/mL)




 Good activity (6.25-<0.78125 µg/mL)

Table 4.5: Minimum Bactericidal Concentration (MBC) of HL^{mes}₈₋₁₆ and L^{mes}₈₋₁₆-Ag-Br

| MBC ($\mu\text{g/mL}$) | HL ^{mes} ₈ | L ^{mes} ₈ -Ag-Br | HL ^{mes} ₁₀ | L ^{mes} ₁₀ -Ag-Br | HL ^{mes} ₁₂ | L ^{mes} ₁₂ -Ag-Br | HL ^{mes} ₁₄ | L ^{mes} ₁₄ -Ag-Br | HL ^{mes} ₁₆ | L ^{mes} ₁₆ -Ag-Br | Triclosan | AgNO ₃ |
|--------------------------|--------------------------------|--------------------------------------|---------------------------------|---------------------------------------|---------------------------------|---------------------------------------|---------------------------------|---------------------------------------|---------------------------------|---------------------------------------|-----------|-------------------|
| S. aureus 6571 | R | 100 | 25 | 6.25 | 6.25 | 1.5625 | 50 | 6.25 | 6.25 | 3.125 | 12.5 | 25 |
| S. aureus 9518 | R | 50 | 25 | 25 | 3.125 | 6.25 | 50 | 3.125 | 12.5 | 3.125 | 12.5 | 25 |
| S. epidermidis 14990 | R | 50 | 12.5 | 6.25 | 1.5625 | 1.5625 | 6.25 | 1.5625 | 1.5625 | 1.5625 | 12.5 | 12.5 |
| S. epidermidis RP62A | R | 50 | 25 | 3.125 | 1.5625 | 1.5625 | 6.25 | 1.5625 | 3.125 | 3.125 | 12.5 | 12.5 |
| P. aeruginosa 15692 | R | R | R | 100 | 100 | 50 | 100 | 100 | 100 | 50 | R | 12.5 |
| E. coli 12923 | R | R | 50 | 100 | 25 | 50 | 50 | 12.5 | 50 | 6.25 | 25 | 12.5 |
| C. albicans 90028 | 100 | 6.25 | 25 | 3.125 | 3.125 | 1.5625 | 1.5625 | <0.78125 | 6.25 | 1.5625 | <0.78125 | |

Key

 No activity

 Moderate activity (12.5-100 $\mu\text{g/mL}$)




 Good activity (6.25-<0.78125 $\mu\text{g/mL}$)

Table 4.6: Minimum Biofilm Eradication Concentrations (MBEC) of HL^{mes}₈₋₁₆ and L^{mes}₈₋₁₆-Ag-Br

| MBEC ($\mu\text{g/mL}$) | HL ^{mes} ₈ | L ^{mes} ₈ -Ag-Br | HL ^{mes} ₁₀ | L ^{mes} ₁₀ -Ag-Br | HL ^{mes} ₁₂ | L ^{mes} ₁₂ -Ag-Br | HL ^{mes} ₁₄ | L ^{mes} ₁₄ -Ag-Br | HL ^{mes} ₁₆ | L ^{mes} ₁₆ -Ag-Br | Triclosan | AgNO ₃ |
|-----------------------------|--------------------------------|--------------------------------------|---------------------------------|---------------------------------------|---------------------------------|---------------------------------------|---------------------------------|---------------------------------------|---------------------------------|---------------------------------------|-----------|-------------------|
| <i>S. aureus</i> 6571 | R | R | R | R | R | 200 | R | 300 | R | 300 | R | R |
| <i>S. aureus</i> 9518 | R | R | R | R | R | 200 | R | 200 | R | 350 | R | 400 |
| <i>S. epidermidis</i> 14990 | R | R | R | R | R | 400 | R | 300 | R | 400 | R | R |
| <i>S. epidermidis</i> RP62A | R | R | R | R | R | R | R | R | R | R | R | 300 |
| <i>P. aeruginosa</i> 15692 | R | R | R | R | R | R | R | R | R | R | R | R |
| <i>E. coli</i> 12923 | R | R | R | R | R | 200 | R | 300 | R | 300 | R | R |
| <i>C. albicans</i> 90028 | R | 250 | R | 100 | 350 | <50 | <50 | <50 | <50 | <50 | <50 | 400 |

Key

 No activity

 Moderate activity (100-400 $\mu\text{g/mL}$)

 Good activity (<50 $\mu\text{g/mL}$)

Biofilm susceptibility screening was also conducted with the isolates described above and the results are presented in Table 4.6. Except for **HL^{mes}₈** and **HL^{mes}₁₀** with no activity against *Candida albicans* ATCC 90028 biofilm, **HL^{mes}₁₂** show moderate activity with MBEC value of 350 µg/mL while **HL^{mes}₁₄** and **HL^{mes}₁₆** have MBEC values of <50 µg/mL. **L^{mes}₁₂₋₁₆-Ag-Br** show moderate biofilm activity against two gram-positive bacteria (*Staphylococcus aureus* NCTC 6571 and *Staphylococcus aureus* NCIMB 9518) and one gram-negative bacteria (*Escherichia coli* NCTC 12923) with MBEC values ranging from 200-400 and 200-300 µg/mL respectively. **HL^{mes}₈₋₁₆** were found to have no activity against the biofilms of all the bacteria strains tested. *Pseudomonas aeruginosa* NCTC 10662 and *Staphylococcus epidermidis* ATCC RP62A biofilms show resistance against all of **L^{mes}₈₋₁₆-Ag-Br**.

Generally, the activity of **HL^{mes}₈₋₁₆** and **L^{mes}₈₋₁₆-Ag-Br** against planktonic cells ranges from moderate to good activity with no significant difference between the proligands, **HL^{mes}₈₋₁₆** and their Ag-NHCs, **L^{mes}₈₋₁₆-Ag-Br**. Relative to the result of the silver nitrate used as one of the standards, we can infer that the amphiphilic imidazolium scaffolds enhanced the antibiofilm activity of silver ion and therefore the antibiofilm activity of **L^{mes}₁₂-Ag-Br**, **L^{mes}₁₄-Ag-Br** and **L^{mes}₁₆-Ag-Br** against *Staphylococcus aureus* NCTC 6571, *Staphylococcus aureus* NCIMB 9518 and *Escherichia coli* NCTC 12923 can therefore, be primarily attributed to the silver functionality.

4.3.2.3. **H₂G₈₋₁₆ and G₈₋₁₆-Ag₂-Br₂**

The MIC of **H₂G₁₄** and **H₂G₁₆** ranges from 1.5625-6.25 µg/mL against all the gram-positive bacteria respectively while **H₂G₁₂** show good (6.25 µg/mL) and moderate (12.5 µg/mL) activity against *Staphylococcus aureus* NCTC 6571, *Staphylococcus aureus* NCIMB 9518 and *Staphylococcus epidermidis* ATCC 14990, *Staphylococcus epidermidis* ATCC RP62A respectively (Table 4.7). The activity of **H₂G₁₂**, **H₂G₁₄** and **H₂G₁₆** against *Escherichia coli* NCTC 12923 ranges from 12.5-50 µg/mL respectively but they all show no activity against *Pseudomonas aeruginosa* NCTC 10662. **H₂G₁₀** is also found to show moderate activity with 50 µg/mL against *Staphylococcus epidermidis* ATCC 14990 and *Staphylococcus epidermidis* ATCC RP62A respectively. **H₂G₈** show no activity against all the microbial strains. **H₂G₁₀** exhibits no activity against *Staphylococcus aureus* NCTC 6571, *Staphylococcus aureus* NCIMB 9518, *Pseudomonas*


aeruginosa NCTC 10662 and *Escherichia coli* NCTC 12923 respectively. For the Ag-NHCs, **G8-Ag2-Br2**, **G10-Ag2-Br2** and **G16-Ag2-Br2** show moderate activity with MIC ranging from 12.5-100 µg/mL against all the bacterial strains respectively. The MIC values of **G12-Ag2-Br2** against *Staphylococcus aureus* NCTC 6571, *Staphylococcus aureus* NCIMB 9518 and *Staphylococcus epidermidis* ATCC 14990, *Staphylococcus epidermidis* ATCC RP62A and *Pseudomonas aeruginosa* NCTC 10662, *Escherichia coli* NCTC 12923 are 25 and 6.25 and 50 µg/mL respectively, while **G14-Ag2-Br2** shows no activity against *Pseudomonas aeruginosa* NCTC 10662. **G14-Ag2-Br2** exhibits MIC values of 6.25 µg/mL against *Staphylococcus aureus* NCTC 6571 and *Staphylococcus aureus* NCIMB 9518 respectively, 3.125 µg/mL against *Staphylococcus epidermidis* ATCC 14990 and *Staphylococcus epidermidis* ATCC RP62A respectively and 25 µg/mL against *Escherichia coli* NCTC 12923. The fungal strain, *Candida albicans* ATCC 90028, is susceptible to **H2G10** and **H2G12** with MIC ranging from 12.5-50 µg/mL respectively, 3.125 µg/mL for **H2G16** and **G16-Ag2-Br2** respectively and <0.78125 µg/mL for **G8-16-Ag2-Br2** and **H2G14** respectively.


The activity of **H2G12**, **H2G14**, **H2G16** and **G8-16-Ag2-Br2** are found to be bactericidal against the four gram-positive bacterial strains with MBC values ranging from 12.5-50 and 3.125-100 µg/mL respectively (Table 4.8). **H2G12** is bacteriostatic against *Staphylococcus aureus* NCIMB 9518 and *Pseudomonas aeruginosa* NCTC 10662 respectively. In addition, the activity of **H2G12-16**, and **G8-16-Ag2-Br2** are found to be bactericidal as well with MBC values ranging from 50-100 µg/mL respectively against *Escherichia coli* NCTC 12923. The activity of **G8-Ag2-Br2** and **G10-Ag2-Br2** are found to be bactericidal while that of **G12-Ag2-Br2** and **G14-Ag2-Br2** are bacteriostatic against *Pseudomonas aeruginosa* NCTC 10662. **H2G10-16** and **G8-16-Ag2-Br2** are also able to kill 99.9% of *Candida albicans* ATCC 90028 with MBC values of 6.25 µg/mL for **H2G14**, **H2G16**, **G8-Ag2-Br2** and **G16-Ag2-Br2** respectively, 1.5625 µg/mL for **G10-Ag2-Br2**, 25 µg/mL for **H2G12**, 50 µg/mL for **H2G10** and <0.78125 µg/mL for **G12-Ag2-Br2**, and **G14-Ag2-Br2** respectively.

Table 4.7: Minimum Inhibitory Concentrations (MIC) of H₂G₈₋₁₆ and G₈₋₁₆-Ag₂-Br₂

| MIC (µg/mL) | H ₂ G ₈ | G ₈ -Ag ₂ -Br ₂ | H ₂ G ₁₀ | G ₁₀ -Ag ₂ -Br ₂ | H ₂ G ₁₂ | G ₁₂ -Ag ₂ -Br ₂ | H ₂ G ₁₄ | G ₁₄ -Ag ₂ -Br ₂ | H ₂ G ₁₆ | G ₁₆ -Ag ₂ -Br ₂ | Triclosan | AgNO ₃ |
|---------------------|-------------------------------|--|--------------------------------|---|--------------------------------|---|--------------------------------|---|--------------------------------|---|-----------|-------------------|
| S aureus 6571 | R | 100 | R | 50 | 12.5 | 25 | 3.125 | 6.25 | 6.25 | 25 | <0.78125 | 25 |
| S aureus 9518 | R | 100 | R | 50 | 12.5 | 25 | 6.25 | 6.25 | 6.25 | 50 | <0.78125 | 12.5 |
| S epidermidis 14990 | R | 50 | 50 | 50 | 6.25 | 6.25 | 1.5625 | 3.125 | 1.5625 | 12.5 | <0.78125 | 6.25 |
| S epidermidis RP62A | R | 50 | 50 | 50 | 6.25 | 6.25 | 1.5625 | 3.125 | 1.5625 | 12.5 | <0.78125 | 3.125 |
| P aeruginosa 15692 | R | 50 | R | 50 | R | 50 | R | R | R | 100 | R | 3.125 |
| E coli 12923 | R | 50 | R | 100 | 50 | 50 | 12.5 | 25 | 25 | 100 | 1.5625 | 6.25 |
| C. albicans 90028 | R | <0.78125 | 50 | <0.78125 | 12.5 | <0.78125 | <0.78125 | <0.78125 | 3.125 | 3.125 | <0.78125 | 3.125 |

Key

 No activity

 Moderate activity (12.5-100 µg/mL)




 Good activity (6.25-<0.78125 µg/mL)


Table 4.8: Minimum Bactericidal Concentration (MBC) of H₂G₈₋₁₆ and G₈₋₁₆-Ag₂-Br₂

| MBC (µg/mL) | H ₂ G ₈ | G ₈ -Ag ₂ -Br ₂ | H ₂ G ₁₀ | G ₁₀ -Ag ₂ -Br ₂ | H ₂ G ₁₂ | G ₁₂ -Ag ₂ -Br ₂ | H ₂ G ₁₄ | G ₁₄ -Ag ₂ -Br ₂ | H ₂ G ₁₆ | G ₁₆ -Ag ₂ -Br ₂ | Triclosan | AgNO ₃ |
|---------------------|-------------------------------|--|--------------------------------|---|--------------------------------|---|--------------------------------|---|--------------------------------|---|-----------|-------------------|
| S aureus 6571 | R | 100 | R | 100 | 50 | 25 | 12.5 | 12.5 | 12.5 | 100 | 12.5 | 25 |
| S aureus 9518 | R | 100 | R | 100 | R | 25 | 25 | 12.5 | 12.5 | 100 | 12.5 | 25 |
| S epidermidis 14990 | R | 100 | 100 | 50 | 12.5 | 12.5 | 6.25 | 6.25 | 12.5 | 25 | 12.5 | 12.5 |
| S epidermidis RP62A | R | 100 | 100 | 50 | 12.5 | 6.25 | 3.125 | 3.125 | 6.25 | 25 | 12.5 | 12.5 |
| P aeruginosa 15692 | R | 50 | R | 50 | R | R | R | R | R | R | R | 12.5 |
| E coli 12923 | R | 50 | R | 50 | 100 | 100 | 50 | 50 | 100 | 100 | 25 | 12.5 |
| C. albicans 90028 | R | 6.25 | 50 | 1.56 | 25 | <0.78125 | 6.25 | <0.78125 | 6.25 | 6.25 | <0.78125 | |

Key

 No activity

 Moderate activity (12.5-100 µg/mL)

 Good activity (6.25-<0.78125 µg/mL)

4.3.2.4. $\text{H}_2\text{G}^{\text{mes}}_{8-16}$ and $\text{G}^{\text{mes}}_{8-16}\text{-Ag}_2\text{-Br}_2$


The MIC of $\text{H}_2\text{G}^{\text{mes}}_8$ and $\text{G}^{\text{mes}}_8\text{-Ag}_2\text{-Br}_2$ ranges from 25-100 $\mu\text{g/mL}$ and that of $\text{H}_2\text{G}^{\text{mes}}_{10-16}$ and $\text{G}^{\text{mes}}_{10-16}\text{-Ag}_2\text{-Br}_2$ from <0.78125 -6.25 $\mu\text{g/mL}$ respectively against all the gram-positive bacteria (Table 4.9). $\text{H}_2\text{G}^{\text{mes}}_8$ has no activity against the two gram-negative bacteria while *Pseudomonas aeruginosa* NCTC 10662 tolerates $\text{H}_2\text{G}^{\text{mes}}_{10}$, $\text{H}_2\text{G}^{\text{mes}}_{16}$ and $\text{G}^{\text{mes}}_{14}\text{-Ag}_2\text{-Br}_2$ respectively. Equally, the MIC values of $\text{H}_2\text{G}^{\text{mes}}_{12}$ and $\text{H}_2\text{G}^{\text{mes}}_{14}$ are 100 $\mu\text{g/mL}$ respectively while that of $\text{G}^{\text{mes}}_{8-12}\text{-Ag}_2\text{-Br}_2$ and $\text{G}^{\text{mes}}_{16}\text{-Ag}_2\text{-Br}_2$ are 50 $\mu\text{g/mL}$ respectively against *Pseudomonas aeruginosa* NCTC 10662. *Escherichia coli* NCTC 12923 is susceptible to $\text{H}_2\text{G}^{\text{mes}}_{10-16}$ and $\text{G}^{\text{mes}}_{8-16}\text{-Ag}_2\text{-Br}_2$ with MIC values ranging from 12.5-100 $\mu\text{g/mL}$ respectively. The activity of $\text{H}_2\text{G}^{\text{mes}}_8$, $\text{H}_2\text{G}^{\text{mes}}_{10}$, $\text{H}_2\text{G}^{\text{mes}}_{12}$ and $\text{H}_2\text{G}^{\text{mes}}_{14}$ and $\text{H}_2\text{G}^{\text{mes}}_{16}$ are found to have MIC values of 50, 12.5, 3.125, <0.78125 and <0.78125 $\mu\text{g/mL}$ respectively against the fungal strain, *Candida albicans* ATCC 90028, and $\text{G}^{\text{mes}}_{8-16}\text{-Ag}_2\text{-Br}_2$ with <0.78125 $\mu\text{g/mL}$ respectively.


Except for $\text{G}^{\text{mes}}_8\text{-Ag}_2\text{-Br}_2$ which is bacteriostatic towards *Staphylococcus aureus* NCIMB 9518 (Table 4.10), the activity of $\text{H}_2\text{G}^{\text{mes}}_{8-16}$ and $\text{G}^{\text{mes}}_{8-16}\text{-Ag}_2\text{-Br}_2$ are found to be bactericidal against the four gram-positive bacterial strains with MBC values ranging from <0.78125 -100 $\mu\text{g/mL}$ respectively. The activity of $\text{H}_2\text{G}^{\text{mes}}_{10-16}$ and $\text{G}^{\text{mes}}_{8-16}\text{-Ag}_2\text{-Br}_2$ are bactericidal against *Escherichia coli* NCTC 12923 with MBCs ranging from 25-100 and 50-100 $\mu\text{g/mL}$ respectively. The activity of $\text{G}^{\text{mes}}_{10}\text{-Ag}_2\text{-Br}_2$, and $\text{G}^{\text{mes}}_{16}\text{-Ag}_2\text{-Br}_2$ are found to be bactericidal (100 $\mu\text{g/mL}$ respectively) and that of $\text{H}_2\text{G}^{\text{mes}}_{12}$, $\text{H}_2\text{G}^{\text{mes}}_{14}$, $\text{G}^{\text{mes}}_8\text{-Ag}_2\text{-Br}_2$ and $\text{G}^{\text{mes}}_{12}\text{-Ag}_2\text{-Br}_2$ are bacteriostatic against *Pseudomonas aeruginosa* NCTC 10662. Lastly, $\text{H}_2\text{G}^{\text{mes}}_{8-16}$ and $\text{G}^{\text{mes}}_{8-16}\text{-Ag}_2\text{-Br}_2$ are able to kill 99.9% of *Candida albicans* ATCC 90028 with MBC values of 100 $\mu\text{g/mL}$ for $\text{H}_2\text{G}^{\text{mes}}_8$, 12.5 $\mu\text{g/mL}$ for $\text{H}_2\text{G}^{\text{mes}}_{10}$, 3.125 $\mu\text{g/mL}$ for $\text{G}^{\text{mes}}_8\text{-Ag}_2\text{-Br}_2$ and $\text{G}^{\text{mes}}_{10}\text{-Ag}_2\text{-Br}_2$ respectively, 1.5625 $\mu\text{g/mL}$ for $\text{H}_2\text{G}^{\text{mes}}_{12}$, $\text{H}_2\text{G}^{\text{mes}}_{14}$, $\text{G}^{\text{mes}}_{12}\text{-Ag}_2\text{-Br}_2$, $\text{G}^{\text{mes}}_{14}\text{-Ag}_2\text{-Br}_2$ and $\text{G}^{\text{mes}}_{16}\text{-Ag}_2\text{-Br}_2$ respectively and <0.78125 $\mu\text{g/mL}$ for $\text{H}_2\text{G}^{\text{mes}}_{16}$.

Table 4.9: Minimum Inhibitory Concentrations (MIC) of H₂G^{mes}₈₋₁₆ and G^{mes}₈₋₁₆-Ag₂-Br₂

| MIC (µg/mL) | H ₂ G ^{mes} ₈ | G ^{mes} ₈ -Ag ₂ -Br ₂ | H ₂ G ^{mes} ₁₀ | G ^{mes} ₁₀ -Ag ₂ -Br ₂ | H ₂ G ^{mes} ₁₂ | G ^{mes} ₁₂ -Ag ₂ -Br ₂ | H ₂ G ^{mes} ₁₄ | G ^{mes} ₁₄ -Ag ₂ -Br ₂ | H ₂ G ^{mes} ₁₆ | G ^{mes} ₁₆ -Ag ₂ -Br ₂ | Triclosan | AgNO ₃ |
|----------------------|--|---|---|--|---|--|---|--|---|--|-----------|-------------------|
| S. aureus 6571 | 100 | 50 | 6.25 | 6.25 | 3.125 | 3.125 | 1.5625 | 3.125 | 3.125 | 6.25 | <0.78125 | 25 |
| S. aureus 9518 | 100 | 50 | 12.5 | 6.25 | 3.125 | 3.125 | 1.5625 | 3.125 | 1.5625 | 3.125 | <0.78125 | 12.5 |
| S. epidermidis 14990 | 25 | 25 | 3.125 | 3.125 | <0.78125 | <0.78125 | <0.78125 | <0.78125 | <0.78125 | <0.78125 | <0.78125 | 6.25 |
| S. epidermidis RP62A | 50 | 25 | 3.125 | 3.125 | <0.78125 | 1.5625 | <0.78125 | <0.78125 | <0.78125 | <0.78125 | <0.78125 | 3.125 |
| P. aeruginosa 15692 | R | 50 | R | 50 | 100 | 50 | 100 | R | R | 50 | R | 3.125 |
| E. coli 12923 | R | 100 | 100 | 25 | 25 | 25 | 12.5 | 12.5 | 25 | 50 | 1.5625 | 6.25 |
| C. albicans 90028 | 50 | <0.78125 | 12.5 | <0.78125 | 3.125 | <0.78125 | <0.78125 | <0.78125 | <0.78125 | <0.78125 | <0.78125 | 3.125 |

Key

 No activity

 Moderate activity (12.5-100 µg/mL)




 Good activity (6.25-<0.78125 µg/mL)

Table 4.10: Minimum Bactericidal Concentration (MBC) of H₂G^{mes}₈₋₁₆ and G^{mes}₈₋₁₆-Ag₂-Br₂

| MBC (µg/mL) | H ₂ G ^{mes} ₈ | G ^{mes} ₈ -Ag ₂ -Br ₂ | H ₂ G ^{mes} ₁₀ | G ^{mes} ₁₀ -Ag ₂ -Br ₂ | H ₂ G ^{mes} ₁₂ | G ^{mes} ₁₂ -Ag ₂ -Br ₂ | H ₂ G ^{mes} ₁₄ | G ^{mes} ₁₄ -Ag ₂ -Br ₂ | H ₂ G ^{mes} ₁₆ | G ^{mes} ₁₆ -Ag ₂ -Br ₂ | Triclosan | AgNO ₃ |
|----------------------|--|---|---|--|---|--|---|--|---|--|-----------|-------------------|
| S. aureus 6571 | 100 | 100 | 12.5 | 12.5 | 3.125 | 3.125 | 3.125 | 3.125 | 6.25 | 50 | 12.5 | 25 |
| S. aureus 9518 | 100 | R | 12.5 | 50 | 3.125 | 12.5 | 3.125 | 12.5 | 6.25 | 25 | 12.5 | 25 |
| S. epidermidis 14990 | 50 | 50 | 6.25 | 3.125 | 1.5625 | 1.5625 | <0.78125 | 1.5625 | 1.5625 | 6.25 | 12.5 | 12.5 |
| S. epidermidis RP62A | 50 | 25 | 6.25 | 6.25 | 1.5625 | 1.5625 | <0.78125 | 3.125 | <0.78125 | 6.25 | 12.5 | 12.5 |
| P. aeruginosa 15692 | R | R | R | 100 | R | R | R | R | R | 100 | R | 12.5 |
| E. coli 12923 | R | 100 | 100 | 50 | 25 | 100 | 50 | 50 | 50 | 50 | 25 | 12.5 |
| C. albicans 90028 | 100 | 3.125 | 12.5 | 3.125 | 1.5625 | 1.5625 | 1.5625 | 1.5625 | <0.78125 | 1.5625 | <0.78125 | |

Key

 No activity

 Moderate activity (100-400 µg/mL)

 Good activity (<50 µg/mL)

The results of the dicationic imidazolium salts, **H₂G₈₋₁₆** and **H₂G^{mes}₈₋₁₆** and their corresponding Ag-NHCs, **G₈₋₁₆-Ag₂-Br₂** and **G^{mes}₈₋₁₆-Ag₂-Br₂**, largely vary from good to moderate against all the planktonic microbial strains tested just like the results of monocationic proligands, **HL₈₋₁₆** and **HL^{mes}₈₋₁₆** and their Ag-NHCs, **L₈₋₁₆-Ag-Br** and **L^{mes}₈₋₁₆-Ag-Br**, albeit, with a slightly lower biological activity and most of their inhibitory activity are also found to be bactericidal and fungicidal respectively. Due to poor solubility at the concentration range required for the in vitro screening, we could not assess the activity of **G₈₋₁₆-Ag₂-Br₂** and **G^{mes}₈₋₁₆-Ag₂-Br₂** against biofilm cells.

4.4. Conclusions

The antimicrobial activities of all the mononuclear Ag(I)NHCs were found to strongly depend upon their molecular structure as seen in the plot of MIC against chain length in Figures 4.3, 4.4, 4.5 and 4.6. Generally, for each bacterial and fungal strain, the MIC values decrease (increased antimicrobial activity) as the aliphatic chain length of the Ag(I)NHCs increases from C₈ – C₁₆. Furthermore, Ag(I)NHCs with mesityl group on one of the N atoms in the imidazolium moiety show better activity than that with methyl group and these observations are in line with the observation that increasing hydrophobicity increases the biological activity of compounds derived from an imidazolium moiety.²⁵⁻²⁹ The dinuclear Ag(I)NHCs show similar trends as described above. Many of the published reports on the antimicrobial activities of Ag(I)NHC complexes have attributed the observed activity to the slow release of Ag(I) ions from the Ag(I)-NHC complexes.^{5,30-33} Except for **L^{mes}₈₋₁₆-Ag-Br** with no low field resonance signals that can be attributed to the carbenic carbon in the ¹³C NMR spectra (Table 3.1), **L₈₋₁₆-Ag-Br**, **G₈₋₁₆-Ag₂-Br₂** and **G^{mes}₈₋₁₆-Ag₂-Br₂** have similar signals at approximately 180 ppm and the implication of this is that the NCN-Ag bond are of the same nature.³⁴ With these observations, we would expect the antimicrobial activity of the mononuclear Ag(I)-NHCs to be the same irrespective of the ligand structure and the dinuclear Ag(I)-NHC complexes to have better activity relative to the mononuclear Ag(I)-NHCs. We can therefore conclude that the antimicrobial activities and the mode of action of these Ag(I)-NHCs are strongly due to the combination of Ag(I) ion and the bioactive proligand scaffolds.

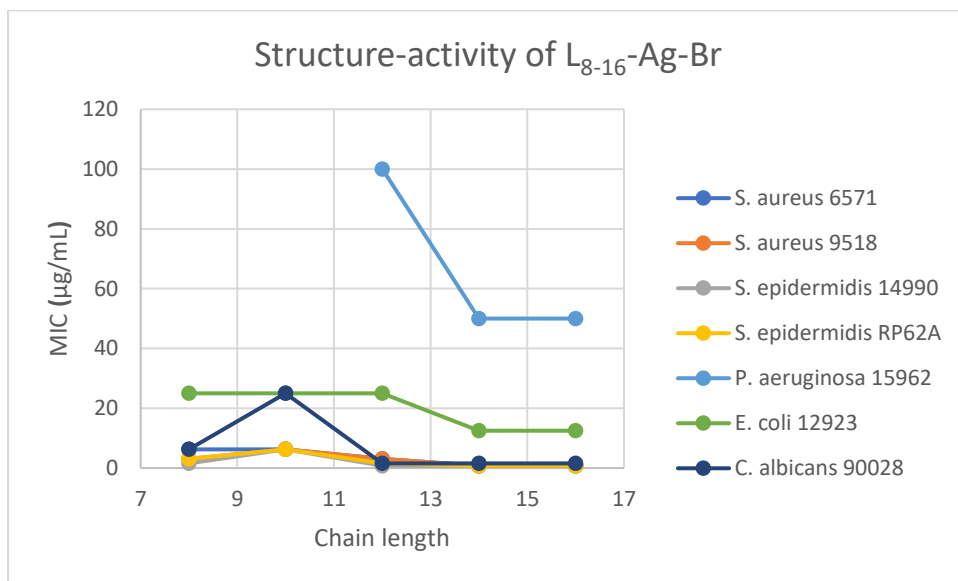


Figure 4.3: Structure-activity relationship of L_{8-16} -Ag-Br

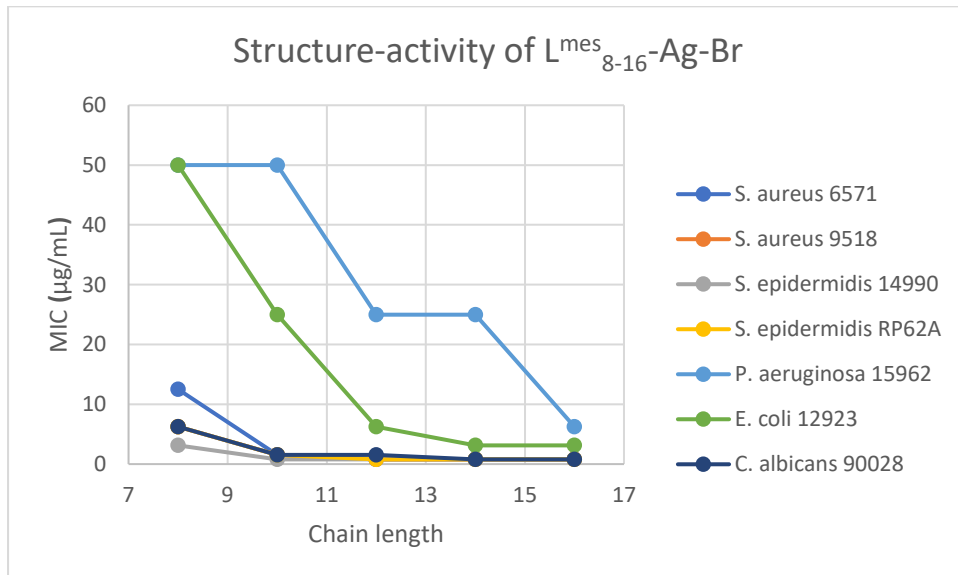


Figure 4.4: Structure-activity relationship of L_{8-16}^{mes} -Ag-Br

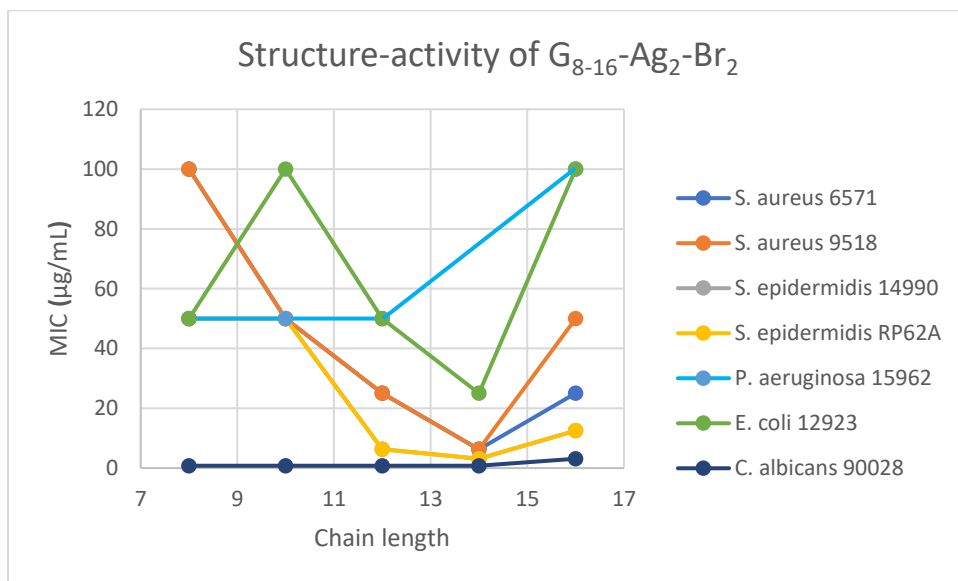


Figure 4.5: Structure-activity relationship of $G_{8-16}-Ag_2-Br_2$

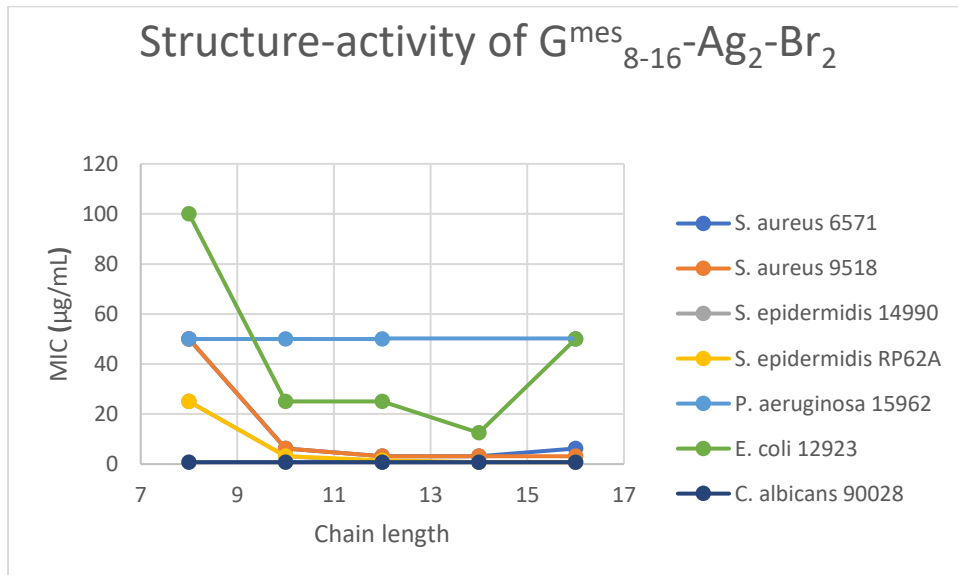


Figure 4.6: Structure-activity relationship of $G^{mes}_{8-16}-Ag_2-Br_2$

4.5. Experimental

4.5.1. Biological Activity

4.5.1.1. MIC and MBC Determinations

Overnight cultures of test isolates were prepared in Mueller-Hinton broth (MHB) for bacterial strains and in Roswell Park Memorial Institute (RPMI) broth for fungal strain. Bacterial and fungal cultures were adjusted to 0.1 and 1.0 McFarland standards (approximately 10^8 cells mL^{-1}) respectively, diluted 1000-fold and serial dilutions of the antimicrobial agents were prepared in appropriate media. A 100- μL volume of each dilution of antimicrobial agent was added to an equal volume of a microbial suspension, giving antimicrobial concentrations ranging from 100-0.78125 $\mu\text{g}/\text{mL}$. Controls included bacterial suspensions containing no antimicrobial agent and uninoculated culture medium. The test isolates and antimicrobial agent were coincubated aerobically in 96-well microtiter plates for 24 h at 37°C. Microbial growth was determined by spectrophotometric analysis at 620 nm. Absorbance readings were standardized against microbial-free antimicrobial agent controls. All experiments were performed in triplicate on three separate occasions.

4.5.1.2. Biofilm Cells Susceptibility Test

Isolates were incubated as described above but without agitation to allow biofilm formation. Culture medium was removed, and the biofilms were washed with 100 μL phosphate-buffered saline (PBS) to remove planktonic cells. Fresh culture medium (100 μL) containing an antimicrobial agent at concentrations ranging from 400-50 $\mu\text{g}/\text{mL}$ was added to each well. Controls prepared as already described were also included. Biofilms were incubated in the presence of an antimicrobial agent for 24 h without agitation under the conditions described above before the supernatant was removed and the biofilm was washed once with PBS. Fresh culture medium (100 μL) that did not contain any antimicrobial agent was added to the biofilms, which were disrupted by repeated pipetting. After 24 h, the incubated, disrupted biofilm cells were then plated onto the appropriate agar medium and were incubated for 24 h at 37°C. All experiments were performed in triplicate.

4.6. References

1. J. W. Alexander, *Surgical Infect.*, 2009, **10**, 289-292.
2. H. J. Klasen, *Burns*, 2000, **26**, 131-138.
3. J. Lederberg, *Science*, 2000, **288**, 287-293.
4. A. Melaiye and W. J. Youngs, *Expert Opin. Ther. Pat.*, 2005, **15**, 125-130.
5. B. D. Wright, P. N. Shah, L. J. McDonald, M. L. Shaeffer, P. O. Wagers, M. J. Panzner, J. Smolen, J. Tagaev, C. A. Tessier, C. L. Cannon and W. J. Youngs, *Dalton Trans.*, 2012, **41**, 6500-6506.
6. D. H. Nies, *FEMS Microbiol. Rev.*, 2003, **27**, 313-339.
7. Helen W. Boucher, George H. Talbot, John S. Bradley, John E. Edwards, D. Gilbert, Louis B. Rice, M. Scheld, B. Spellberg and J. Bartlett, *Clin. Infect. Dis.*, 2009, **48**, 1-12.
8. World-Health-Organization, *Antibacterial agents in clinical development: an analysis of the antibacterial clinical development pipeline, including tuberculosis*, 2017, 1-48.
9. K. M. Hindi, T. J. Siciliano, S. Durmus, M. J. Panzner, D. A. Medvetz, D. V. Reddy, L. A. Hogue, C. E. Hovis, J. K. Hilliard, R. J. Mallet and others, *J. med. chem.*, 2008, **51**, 1577-1583.
10. F. Almalioti, J. MacDougall, S. Hughes, M. M. Hasson, R. L. Jenkins, B. D. Ward, G. J. Tizzard, S. J. Coles, D. W. Williams, S. Bamford, I. A. Fallis and A. Dervisi, *Dalton Trans.*, 2013, **42**, 12370-12380.
11. M. J. Panzner, K. M. Hindi, B. D. Wright, J. B. Taylor, D. S. Han, W. J. Youngs and C. L. Cannon, *Dalton Trans.*, 2009, 7308-7313.
12. A. Melaiye, R. S. Simons, A. Milsted, F. Pingitore, C. Wesdemiotis, C. A. Tessier and W. J. Youngs, *J. Med. Chem.*, 2004, **47**, 973-977.

13. S. Kanjilal, S. Sunitha, P. S. Reddy, K. P. Kumar, U. S. N. Murty and R. B. N. Prasad, *Eur. J. Lip. Sci. Tech.*, 2009, **111**, 941-948.
14. P. Marshall, R. L. Jenkins, W. Clegg, R. W. Harrington, S. K. Callear, S. J. Coles, I. A. Fallis and A. Dervisi, *Dalton Trans.*, 2012, **41**, 12839-12846.
15. T. R. Neu, *Microbiol. Rev.*, 1996, **60**, 151-166.
16. E. P. Çoban, R. Fırıncı, H. Biyik and M. E. Günay, *Braz. J. Pharm. Sci.*, 2017, **53**, 1-10.
17. O. A. El Seoud, P. A. R. Pires, T. Abdel-Moghny and E. L. Bastos, *J. Coll. Interf. Sci.*, 2007, **313**, 296-304.
18. R. Zana, M. Benrraou and R. Rueff, *Langmuir*, 1991, **7**, 1072-1075.
19. S. Malic, R. P. C. Jordan, M. G. J. Waters, D. J. Stickler and D. W. Williams, *Antimicrob. Agents Chemoth.*, 2014, **58**, 1192-1194.
20. D. Mack, *J. Hospit. Infect.*, 1999, **43**, S113-S125.
21. R. M. Donlan and J. W. Costerton, *Clin. Microbiol. Rev.*, 2002, **15**, 167-193.
22. G. H. De Zoysa, A. J. Cameron, V. V. Hegde, S. Raghothama and V. Sarojini, *J. Med. Chem.*, 2015, **58**, 625-639.
23. C. Schmidt, B. Karge, R. Misgeld, A. Prokop, R. Franke, M. Brönstrup and I. Ott, *Chem. - A Eur. J.*, 2017, **23**, 1869-1880.
24. R. M. Humphries, J. Amber, S. L. Mitchell, M Castanheira, T. Dingle, J. A. Hindler, L. Koeth, K. Sei, CLSI Methods Development and Standardisation Working Group of the Subcommittee on Antimicrobial Susceptibility Testing, *J. Clin. Microbiol.*, 2018, **56**, 1-10.
25. A. Cornellas, L. Perez, F. Comelles, I. Ribosa, A. Manresa and M. T. Garcia, *J. Coll. Interf. Sci.*, 2011, **355**, 164-171.
26. K. M. Docherty and J. C. F. Kulpa, *Green Chem.*, 2005, **7**, 185-189.

27. J. Ranke, K. Mölter, F. Stock, U. Bottin-Weber, J. Poczobutt, J. Hoffmann, B. Ondruschka, J. Filser and B. Jastorff, *Ecotoxicol. Environ. Saf.*, 2004, **58**, 396-404.
28. İ. Özdemir, E. Ö. Özcan, S. Günal and N. Gürbüz, *Molecules*, 2010, **15**, 2499-2508.
29. R. A. Haque, P. O. Asekunowo, M. R. Razali and F. Mohamad, *Heteroatom Chem.*, 2014, **25**, 194-204.
30. R. Sakamoto, S. Morozumi, Y. Yanagawa, M. Toyama, A. Takayama, N. C. Kasuga and K. Nomiya, *J. Inorg. Biochem.*, 2016, **163**, 110-117.
31. A. Kascatan-Nebioglu, M. J. Panzner, C. A. Tessier, C. L. Cannon and W. J. Youngs, *Coord. Chem. Rev.*, 2007, **251**, 884-895.
32. K. M. Hindi, M. J. Panzner, C. A. Tessier, C. L. Cannon and W. J. Youngs, *Chem. Rev.*, 2009, **109**, 3859-3884.
33. A. Kascatan-Nebioglu, A. Melaiye, K. Hindi, S. Durmus, M. J. Panzner, L. A. Hogue, R. J. Mallett, C. E. Hovis, M. Coughenour, S. D. Crosby, A. Milsted, D. L. Ely, C. A. Tessier, C. L. Cannon and W. J. Youngs, *J. Med. Chem.*, 2006, **49**, 6811-6818.
34. J. C. Garrison and W. J. Youngs, *Chem. Rev.*, 2005, **105**, 3978-4008.

Chapter

5

Synthesis and characterisation of surface-active platinum(II) *N*-heterocyclic carbenes

| | |
|--|------------|
| 5.0. Synthesis and characterisation of surface-active platinum(II) <i>N</i>-heterocyclic carbenes..... | 146 |
| 5.1. Introduction..... | 147 |
| 5.2. Aims..... | 153 |
| 5.3. Results and Discussion..... | 154 |
| 5.3.1. Synthesis of surface-active platinum(II) <i>N</i> -heterocyclic carbene complexes..... | 154 |
| 5.3.2. Catalytic application of Na[PtL ^{bet} ₈₋₁₆ dmsocCl ₂] in Hydrosilylation of terminal alkenes and alkyne in water..... | 157 |
| 5.3.2.1. Hydrosilylation of 1-octene with PhMe ₂ SiH, Et ₃ SiH and ClMe ₂ SiH in water..... | 157 |
| 5.3.2.2. Hydrosilylation of styrene with PhMe ₂ SiH and ClMe ₂ SiH in water..... | 161 |
| 5.3.2.3. Hydrosilylation of 1-octyne with PhMe ₂ SiH, Et ₃ SiH and ClMe ₂ SiH in water..... | 166 |
| 5.3.2.4. Structure-activity relationship..... | 169 |
| 5.4. Experimental..... | 171 |
| 5.5. References..... | 175 |

Chapter 5

Synthesis and Characterisation of Surface-Active Platinum(II) N-Heterocyclic Carbenes

5.1. Introduction

Two of the unique features that set N-heterocyclic carbenes apart from other ligands in organometallics/coordination chemistry are their strong σ -donor and relatively weak π -acceptor properties.¹ The ease with which libraries of NHCs can be created by varying the substituents attached to the ring heteroatoms and/or backbone consequently dictate the steric and electronic features displayed by NHCs.^{2,3} The strong σ -donor and weak π -acceptor ability of NHCs result in a thermodynamically stable and strong metal-ligand bonds characterised by high bond dissociation energies and short metal–ligand bond lengths.⁴ These attractive features of NHC-metal bond have led to a wide range of different areas of applications such as catalysis for various organic reactions, medicinal, luminescent and functional materials.⁵⁻⁷ Herrman and co-workers pioneered the use NHC-metal complexes in homogeneous catalysis when they reported their findings on Pd(II)-NHCs (A and B) (Figure 5.1) catalysed Heck coupling of aryl halides. Due to the exceptional stability displayed by these catalysts, they suggested that NHCs could be derivatized into stable water-soluble catalysts.⁸

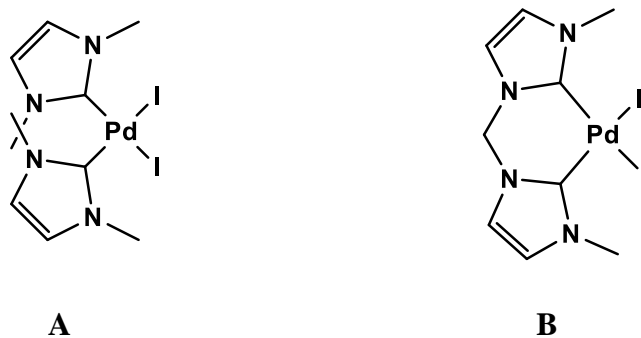
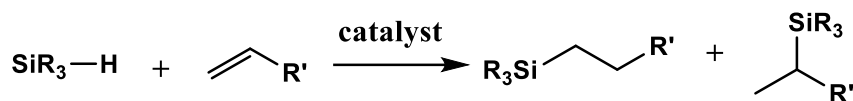
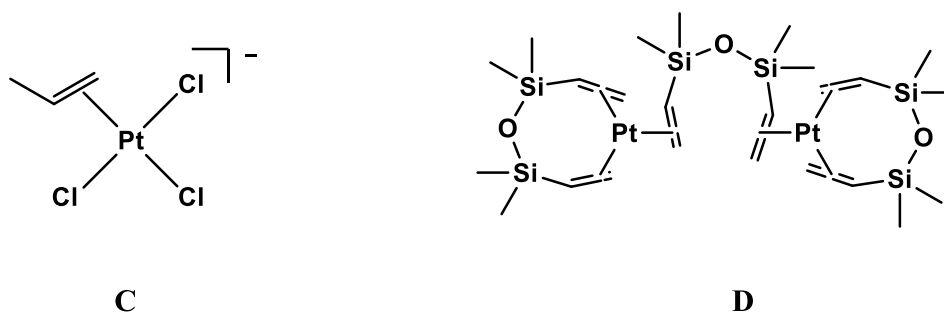


Figure 5.1: First reported metal-NHCs as transition metal catalysts

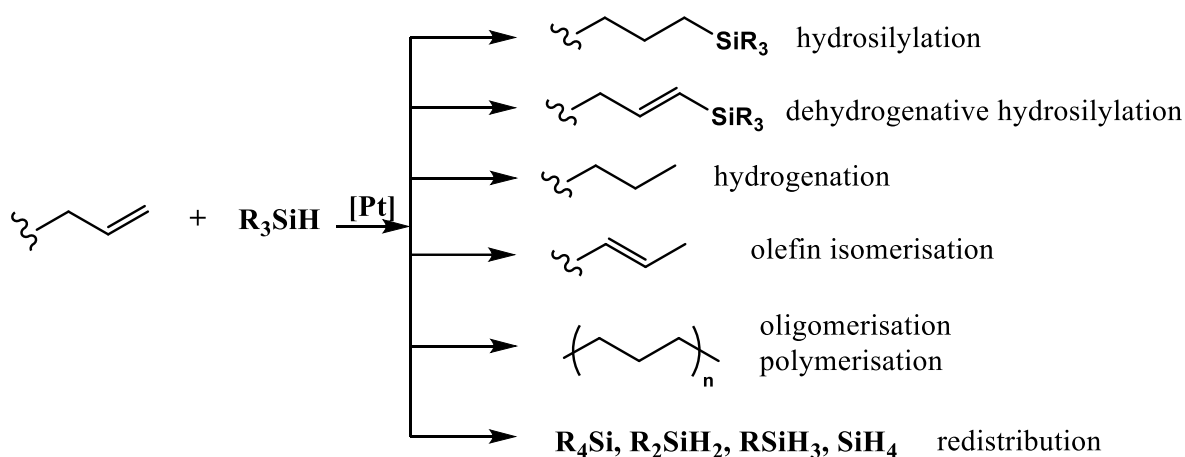
One of the most important uses of homogeneous catalysis in the laboratory and in industry is in the synthesis of organosilicon molecules by the addition of hydrosilanes to unsaturated substrates and this reaction is known as hydrosilylation (Scheme 5.1).^{9,10}

**Scheme 5.1:** The hydrosilylation reaction

The hydrosilylation reaction has enabled the production of silicon polymers used in silicon rubbers, urinary catheters, paper release coatings, and pressure-sensitive adhesives and platinum complexes have been widely employed as catalysts for this process.^{7, 11} The two leading platinum-based catalysts employed for the hydrosilylation reaction in industry are Speier's catalyst¹² (C) and the Karstedt catalyst (D) (Figure 5.2).¹³

**Figure 5.2:** Speier's catalyst (C) and the Karstedt catalyst (D)

In spite of the high activities exhibited by these catalysts, they are quite sensitive to moisture and form colloidal platinum particles which results in undesired side reactions such as dehydrogenative silylation, hydrogenation of olefins, isomerization of olefins, olefin oligomerization and redistribution of hydrosilanes (Scheme 5.2) and colouration of the final product.^{11, 14} Therefore, research efforts to develop a well-defined catalyst system with higher selectivity and activity are still very active in order to improve upon the methodology and make it more economical and environmentally friendly.



Scheme 5.2: Hydrosilylation and other side reactions of olefins with hydrosilane in the presence of a catalyst

In 2002, after learning that the divinyltetramethylsiloxane (dvtms) ligand in the Karstedt catalyst appears to be too labile and dissociates rapidly, leading to colloidal Pt species, Marko and coworkers reported the synthesis of a Pt(0)-NHC complex derived from Karstedt catalyst by treating Karstedt catalyst with an N-heterocyclic carbene ligand. The resulting Pt(0)-NHC complex (E) (Figure 5.3) was found to catalyse the hydrosilylation of octene with “remarkable efficiency and exquisite selectivity”. This catalyst was found to be remarkably stable with no formation of colloidal platinum species thereby reducing the amount of undesired by-products.¹¹

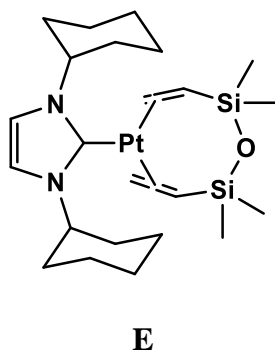
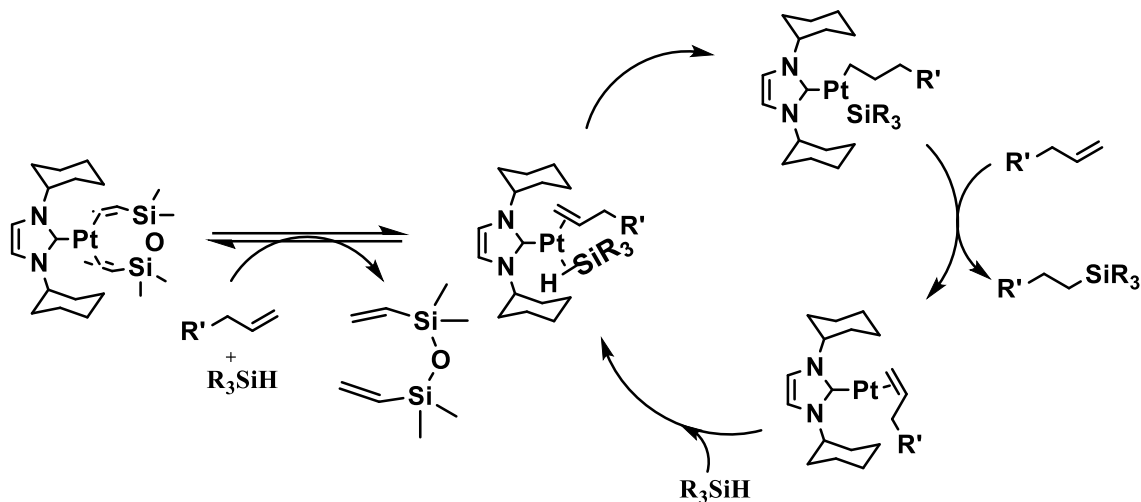


Figure 5.3: Chemical structure of $[Pt(NHC)(dvtms)]$ (E) by Marko *et al.*

A catalytic cycle was proposed after a detailed kinetic study and the dissociation of the labile dtvms ligand was found to initiate the catalytic cycle (Scheme 5.3) and this agrees with the Chalk-Harrod mechanism.^{9, 11}



Scheme 5.3: Proposed mechanism for the platinum-carbene catalysed hydrosilylation

Shortly after the findings by Marko *et al.*, Cavell and co-workers reported Pt(0)-NHC complex (F) (Figure 5.4) coordinated with sterically demanding and strong σ -donating 6-membered NHC ligands. The catalysts were found to have excellent activity comparable to that of Karstedt (D) and Marko (E) catalysts only for the reaction between bis(trimethylsiloxy)methylsilane and 1-octene.¹⁵

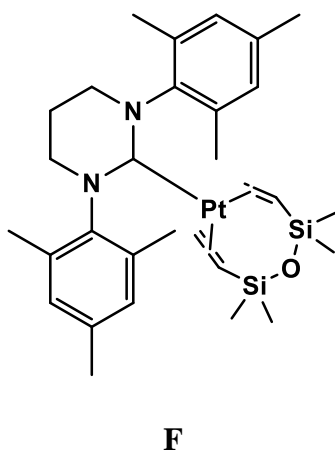


Figure 5.4: Chemical structure of [Pt(NHC)(dvtms)] (F) by Cavell *et al.*

Chelating biscarbene ligands were found to increase the stability of Pt-NHC catalyst systems and the activity of biscarbene-Pt(II), G, was found to be comparable to that of the Karstedt catalyst with less by-products (Figure 5.5).¹⁶

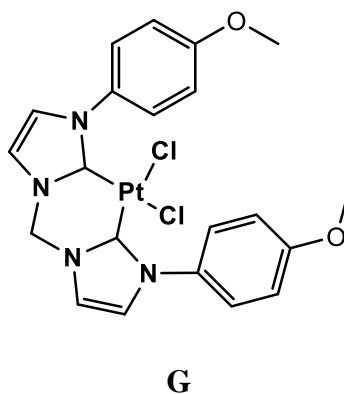


Figure 5.5: Chemical structure of [Pt(bis-NHC)Cl₂] (G) by Strassner *et al.*

De Jesus and co-workers in 2012 demonstrated the stability of water-soluble Pt(0)-NHC complexes in D₂O at room temperature (at least 1 month) and at 70 °C (at least 3 days) and this stability has been attributed to their strong α -donating property and high steric hindrance. Furthermore, Pt(0)-NHC complexes containing sulfonated N-heterocyclic carbene ligands (Figure 5.6, H and I) were found to be active catalysts that can activate the hydrosilylation of some terminal alkynes at room temperature in water.¹⁷

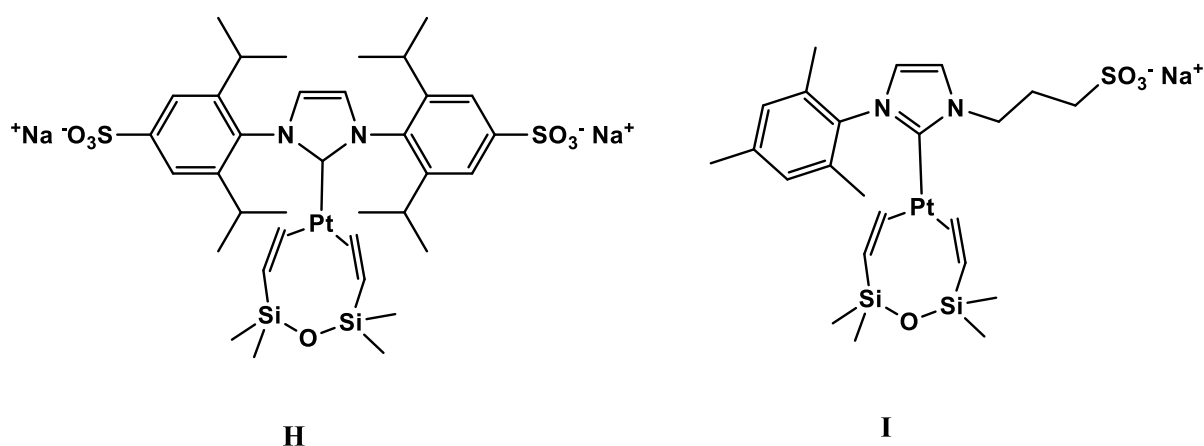


Figure 5.6: Chemical structures of water-soluble [Pt(NHC)(dvtms)] (H and I) by de Jesus *et al.*

Water is becoming an important alternative as a medium for chemical transformation to traditional organic solvents due to environmental concerns.¹⁸ Recently, a call has been made on the need to make chemical transformations more sustainable by transitioning from high dependence on organic media to aqueous media such that chemical reactions can be done under environmentally responsible conditions.¹⁹ Chemical reactions driven by catalysts can be adapted to aqueous media by the addition of surfactants providing a large interface for the immiscible organic reactants.²⁰ Surfactants are functional compounds containing hydrophilic head and hydrophobic tail attached to each other in one molecule and metallosurfactants represent a refined way of infusing other important properties beyond amphiphilicity into surfactant molecules. Polarz et al., recently published an article on the activity of metallosurfactant bearing NHC ligand system and Cu(I) metal centre (J) as the head group and hydrophobic tails comprising of dodecylbenzene (Figure 5.7) as a catalyst for the polymerization of methyl methacrylate (MMA).²¹

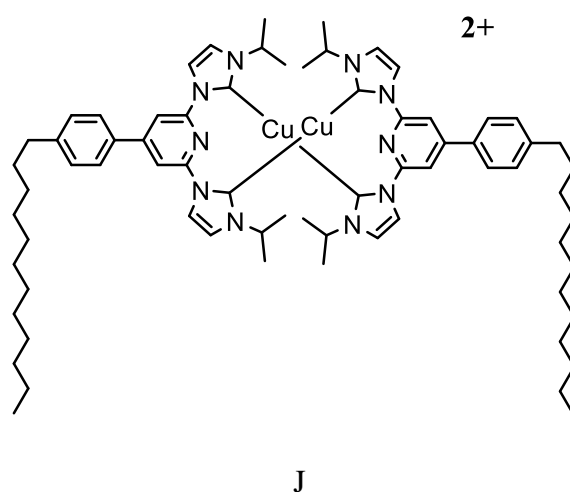


Figure 5.7: Chemical structure of metallosurfactant (J) with NHC ligand system by Polarz *et al.*

5.2. Aims

This chapter aimed to synthesise a series of new Pt(II)-NHC metallosurfactants. These complexes have general composition $\text{Na}[\text{PtL}^{\text{bet}}_{8-16}\text{dmsOCl}_2]$ and are derived from zwitterionic amphiphilic imidazolium proligands, $\text{HL}^{\text{bet}}_{8-16}$ described in chapter 2.

We have designed a series of water-soluble Pt(II)-NHCs that are surface-active to serve as catalysts in the formation of organosilanes both in-water and on-water in order to accommodate both hydrophilic and hydrophobic substrates.

These new set of novel metallosurfactants with a Pt(II) metal centre as the head group and the NHC ligand system ($\text{L}^{\text{bet}}_{8-16}$, Figure 5.8. synthesis discussed in chapter 2) bearing the hydrophobic tail (C_{8-16}). These metallosurfactants were characterised by ^1H and ^{13}C NMR spectroscopy, HRMS and their application as catalysts for the hydrosilylation of terminal alkenes and alkynes with three different hydrosilanes in water was explored.

Lastly, the correlation between the catalytic activity and the molecular structure of these metallosurfactants was explored.

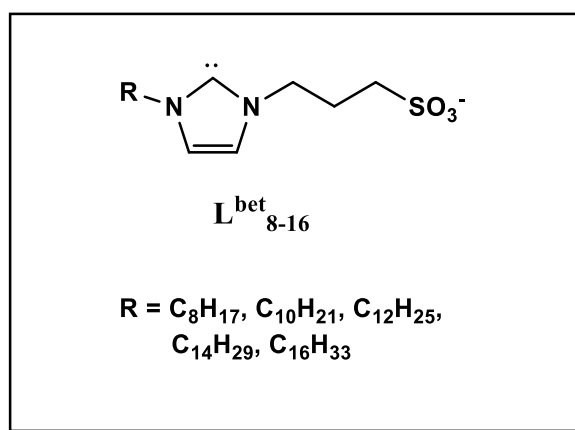
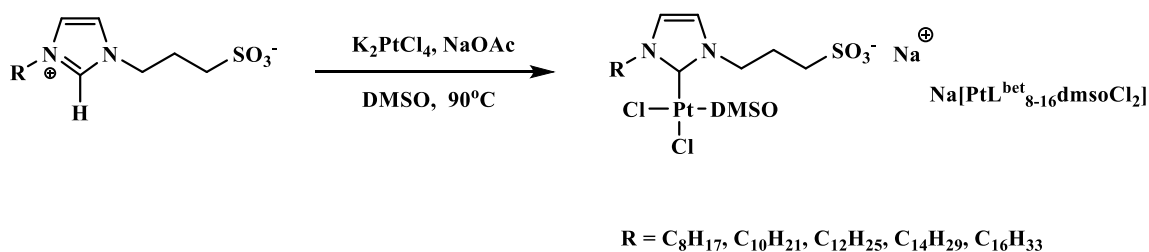


Figure 5.8: Betaine NHC ligands used in this study (synthesis discussed in chapter 2)

5.3. Results and Discussion

5.3.1. Synthesis of surface-active platinum(II) N-heterocyclic carbene complexes

The complexes $\text{Na}[\text{PtL}^{\text{bet}}_{8-16}\text{dmsOCl}_2]$ were obtained by a method described by Marshall and co-workers.²² This was achieved by the direct reaction of $\text{K}_2[\text{PtCl}_4]$ with sulfonate functionalized imidazolium zwitterions, $\text{HL}^{\text{bet}}_{8-16}$ in dimethyl sulfoxide at 90°C for 3 days using sodium acetate as the deprotonating agent. This procedure yielded complexes $\text{Na}[\text{PtL}^{\text{bet}}_{8-16}\text{dmsOCl}_2]$ as analytically pure solids in good yields (Scheme 5.4). It is important to note that the use of excess ligands has no effect on the nature of the complex formed because of competition from dimethyl sulfoxide (in excess) which functions as solvent and as ligand during the reaction.²³ This set of surface-active Pt(II)-NHC complexes were characterised by ^1H , ^{13}C and ^1H - ^{13}C HSQC NMR spectroscopy and mass spectrometry. The ESI-TOF mass spectra of these complexes were recorded in methanol in negative mode and showed intense peaks corresponding to the fragments $[(\text{M} - \text{Na})^-]$, with isotopic distributions matching the calculated patterns.



Scheme 5.4: Synthesis of $\text{Na}[\text{Pt}(\text{L}^{\text{bet}}_{8-16})(\text{dmsO})\text{Cl}_2]$

In the ^1H spectra, some characteristic changes were observed and as expected, the signals of the acidic protons at C2 of $\text{HL}^{\text{bet}}_{8-16}$ disappeared upon platinum coordination (Figures 5.9 and 5.10). The loss of the C2 resonance at approximately 136 ppm and the reappearance of a new signal at approximately 141 ppm signify the formation of platinum carbene complexes in the ^{13}C NMR spectra. Besides the loss of the C2 resonance signals, the ^1H NMR spectra of complex $\text{Na}[\text{PtL}^{\text{bet}}_{8-16}\text{dmsOCl}_2]$ are quite revealing (Appendix C). The presence of two different ligands

cis to the N-heterocyclic carbene moiety (dmsO and Cl⁻) makes the α methylene protons on the imidazole ring and the methyl groups on dmsO coordinated to Pt(II) center diastereotopic. Analysis of the cross peaks using ¹H-¹³C correlation spectroscopy revealed four proton signals between 4.15 and 4.60 ppm on the ¹H scale and between 48 and 51 ppm on the ¹³C scale and these resonance signals can be assigned to the four diastereotopic protons α to the two nitrogen atoms on the imidazole ring (Figures 5.10 and 5.11). The above observations can be rationalized if the stereochemistry of the square-planar metal environment is *cis*, with one of the chlorides *trans* to the dmsO and the other chloride *trans* to the carbene ligand (the carbene carbon signal at $\delta_c = 141$ ppm compares well with other Pt(II)-NHC complexes with similar architecture.).^{23, 24}

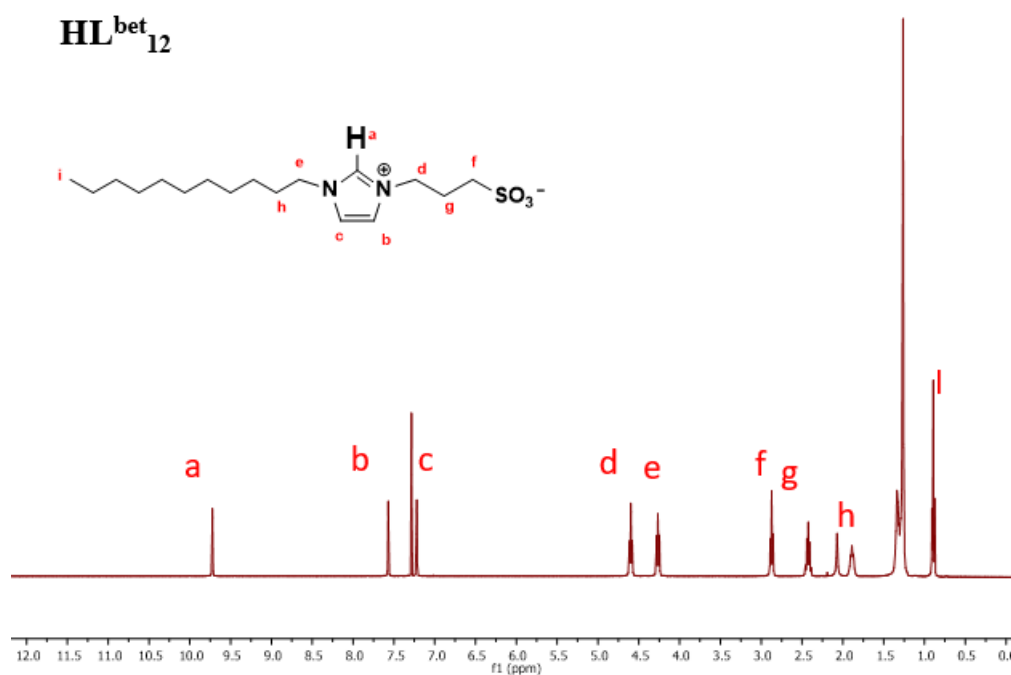


Figure 5.9: ¹H NMR spectrum of **HL^{bet}₁₂** in CDCl₃ using Bruker 400 MHz at room temperature

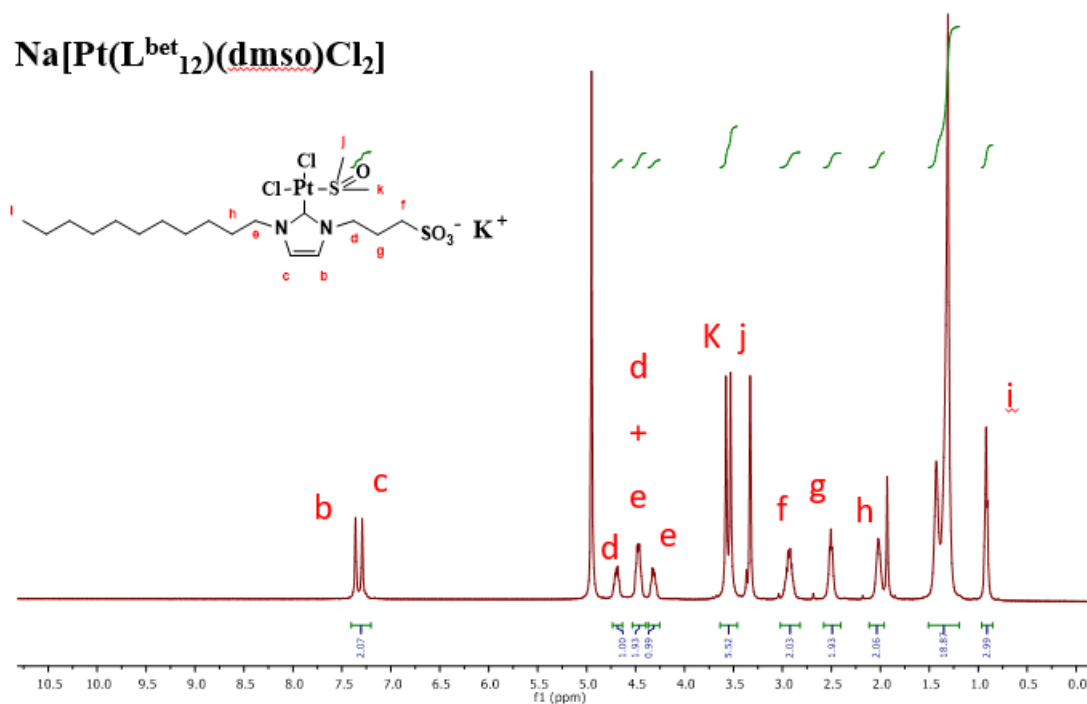


Figure 5.10: ¹H NMR spectrum of Na[Pt(L^{bet}₁₂)(dmsO)Cl₂] in CD₃OD using Bruker 400 MHz at room temperature

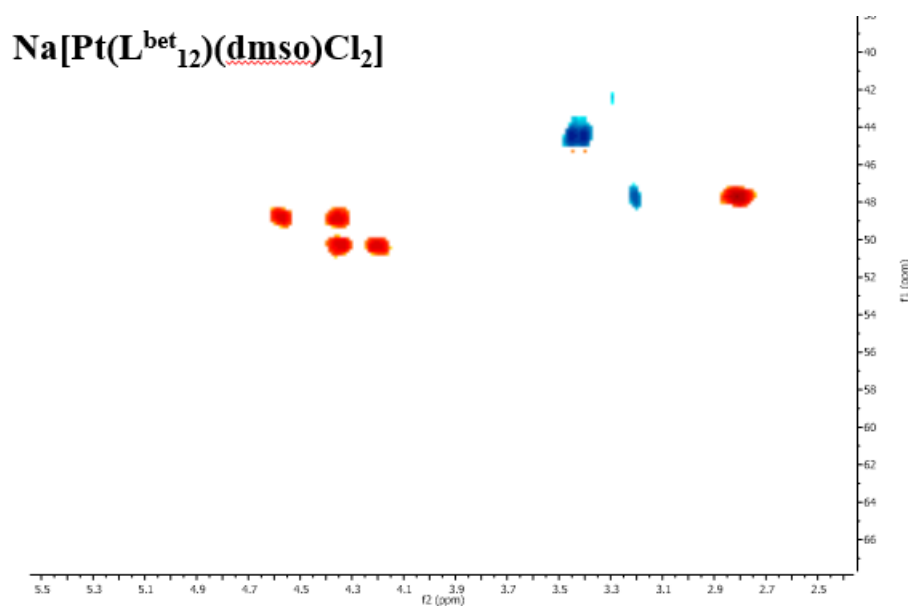


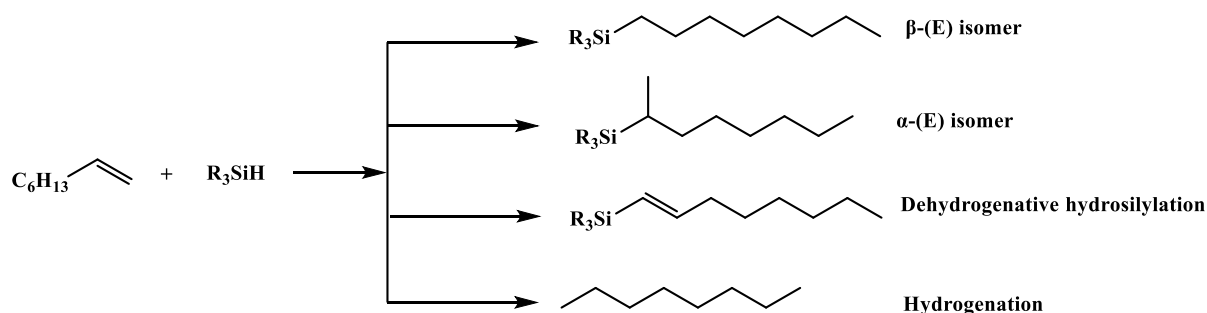
Figure 5.11: A cross section of HSQC of Na[PtL^{bet}₁₂dmsOCl₂] using Bruker 400 MHz at room temperature

5.3.2. Catalytic Application of $\text{Na}[\text{PtL}^{\text{bet}}_{8-16}\text{dmsOCl}_2]$ in Hydrosilylation of Terminal Alkenes and Alkyne in Water

The activity of $\text{Na}[\text{PtL}^{\text{bet}}_{8-16}\text{dmsOCl}_2]$ as catalysts in the hydrosilylation of terminal alkenes in water at 30°C at different concentrations and the effect of the alkyl chain lengths attached to these Pt(II)-NHC complexes on the conversion and regioselectivity was investigated. In this study, we employed three different hydrosilanes phenyldimethylsilane (PhMe_2SiH), triethylsilane (Et_3SiH) and chlorodimethylsilane (ClMe_2SiH), along with two alkenes (1-octene and styrene) and one alkyne (1-octyne).

5.3.2.1. Hydrosilylation of 1-Octene with PhMe_2SiH , Et_3SiH and ClMe_2SiH in Water

The newly synthesized and characterised surface-active and water-soluble Pt(II)-NHC complexes, $\text{Na}[\text{Pt}(\text{L}^{\text{bet}}_{8-16})(\text{dmsO})\text{Cl}_2]$, were screened as catalysts for the hydrosilylation reaction between 1-octene and PhMe_2SiH , Et_3SiH , and ClMe_2SiH respectively. The reaction solutions were stirred at 30°C in water with catalyst loading with respect to the tertiary silanes employed. Conversion of reactants to products was monitored by the disappearance of the Si-H and vinylic protons in the ^1H NMR spectra. The products and the stereochemistry of the products from the three catalysed reactions were confirmed by comparing the ^1H NMR spectra of the reaction before and after the reaction and by the analysis of the new peaks and their coupling constants respectively. Equally, under the reaction condition employed, we did not observe hydrolysis of ClMe_2SiH . It has been established that the hydrosilylation of 1-octene with hydrosilane substrate could yield four possible products as shown in scheme 5.5 and their ratio depends on the metal, the ligand, the alkene and the tertiary silane used.^{16, 25, 26}



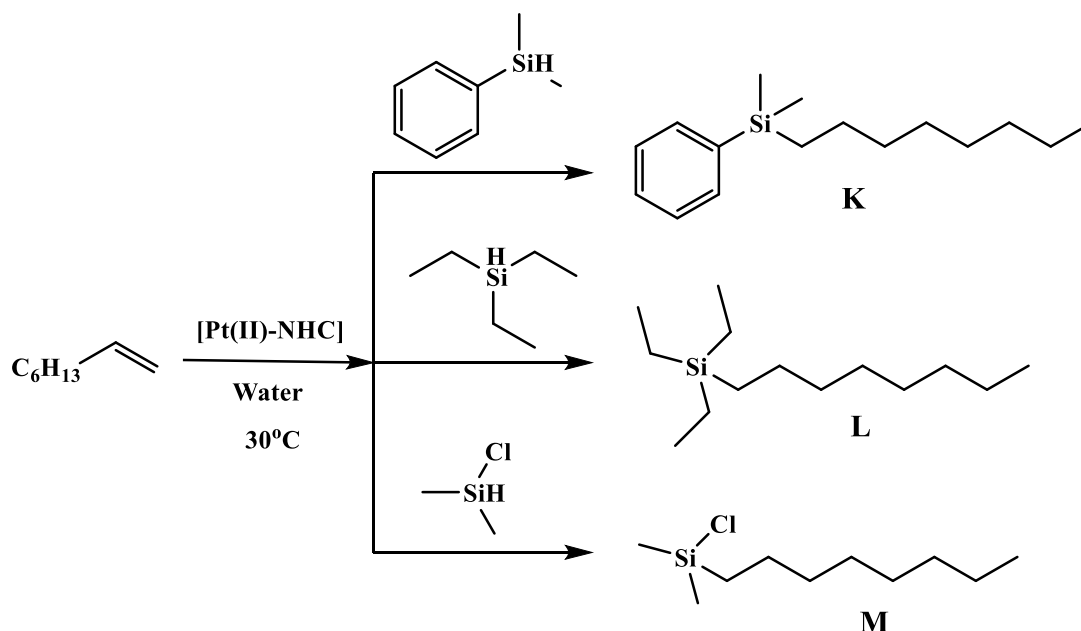
Scheme 5.5: Reported product distribution in the hydrosilylation of 1-octene

The hydrosilylation reaction between 1-octene and PhMe₂SiH, Et₃SiH, ClMe₂SiH respectively gave the β-(E) isomer (Figure 5.12 and scheme 5.6) and the ¹H NMR data is as highlighted below:

K: ¹H NMR (400 MHz, CDCl₃) δ 0.15 (s, 6H), 0.64 (m, 2H), 0.77 (t, *J* = 6.8 Hz, 3H), 1.15 (m, 12H), 7.46 – 7.37 (m, 1H), 7.29 – 7.19 (m, 2H).

L: ¹H NMR (400 MHz, CDCl₃) δ 0.42 (q, 2H, *J* = 8.0), 0.52 (qd, *J* = 8.0, 0.6 Hz, 8H), 0.85 (m, 4H), 0.90 (ddd, *J* = 8.0, Hz, 12H), 1.19 (m, 6H).

M: ¹H NMR (400 MHz, CDCl₃) δ 0.00 (s, 6H), 0.47 (dd, *J* = 9.4, 5.8 Hz, 2H), 0.85 (t, *J* = 6.6 Hz, 3H), 1.32-1.22 (m, 12H).

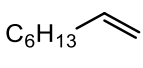
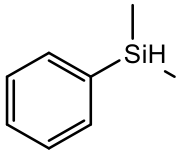
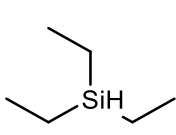
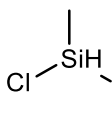


Scheme 5.6: Hydrosilylation of 1-octene with different tertiary silanes

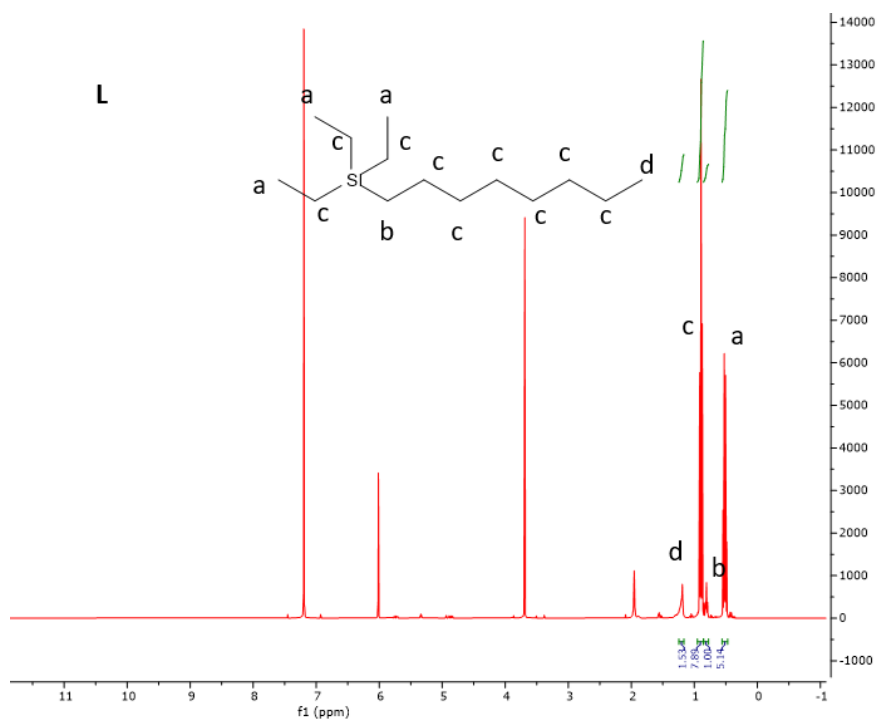
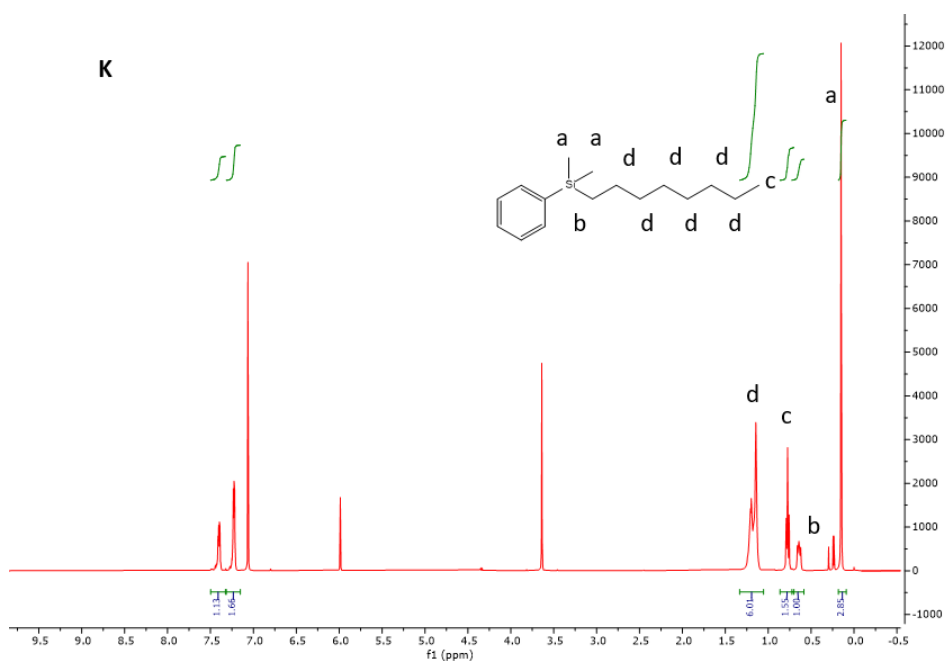
All the Pt(II)-NHC complexes used in this study catalysed the hydrosilylation in Scheme 5.6 with excellent conversions (Table 5.1) at varying catalyst loadings and with excellent regioselectivity for the anti-Markonikov products. This result is consistent with the Pt(0) catalysed hydrosilylation reaction bearing bulky NHC ligands reported by Pietraszuk and coworkers (catalyst loading = 0.001 mol%, yield = 98%, product ratio (β:α) = not available, reaction time = 24 h, solvent = toluene and reaction temperature = 80°C) for Et₃SiH and octene

and (catalyst loading = 1×10^{-5} mol%, conversion = 93%, product ratio (β : α) = 84:16, reaction time = 3 h, solvent = toluene and reaction temperature = 80°C) for PhMe_2SiH and octene.²⁶ The size of the tertiary silanes employed has no effect on the regioselectivity of the products and the summary of the results of these hydrosilylation reactions is presented in Table 5.1.

Table 5.1: Hydrosilylation of 1-octene with different tertiary silanes

| Entry | Catalyst | Catalyst Conc. (mol %) | Alkene | Silane | Time (h) | Conversion |
|-------|--|------------------------|---|--|----------|------------|
| 1 | $\text{Na}[\text{PtL}^{\text{bet}}_8\text{dmsOCl}_2]$ | 0.001 |  |  | 5 | 94 |
| 2 | $\text{Na}[\text{PtL}^{\text{bet}}_{10}\text{dmsOCl}_2]$ | | | | | 98 |
| 3 | $\text{Na}[\text{PtL}^{\text{bet}}_{12}\text{dmsOCl}_2]$ | | | | | 96 |
| 4 | $\text{Na}[\text{PtL}^{\text{bet}}_{14}\text{dmsOCl}_2]$ | | | | | 96 |
| 5 | $\text{Na}[\text{PtL}^{\text{bet}}_{16}\text{dmsOCl}_2]$ | | | | | 98 |
| 6 | $\text{Na}[\text{PtL}^{\text{bet}}_8\text{dmsOCl}_2]$ | 0.1 | |  | 8 | 96 |
| 7 | $\text{Na}[\text{PtL}^{\text{bet}}_{10}\text{dmsOCl}_2]$ | | | | | 96 |
| 8 | $\text{Na}[\text{PtL}^{\text{bet}}_{12}\text{dmsOCl}_2]$ | | | | | 96 |
| 9 | $\text{Na}[\text{PtL}^{\text{bet}}_{14}\text{dmsOCl}_2]$ | | | | | 96 |
| 10 | $\text{Na}[\text{PtL}^{\text{bet}}_{16}\text{dmsOCl}_2]$ | | | | | 96 |
| 11 | $\text{Na}[\text{PtL}^{\text{bet}}_8\text{dmsOCl}_2]$ | 0.001 | |  | 6 | 88 |
| 12 | $\text{Na}[\text{PtL}^{\text{bet}}_{10}\text{dmsOCl}_2]$ | | | | | 92 |
| 13 | $\text{Na}[\text{PtL}^{\text{bet}}_{12}\text{dmsOCl}_2]$ | | | | | 90 |
| 14 | $\text{Na}[\text{PtL}^{\text{bet}}_{14}\text{dmsOCl}_2]$ | | | | | 90 |
| 15 | $\text{Na}[\text{PtL}^{\text{bet}}_{16}\text{dmsOCl}_2]$ | | | | | 89 |

^a The conversion was determined by ^1H NMR analysis based on the disappearance of the alkene resonance. ^b The products and their stereochemistry were identified by ^1H NMR analysis of the product resonance peaks and their coupling constants. All reactions were carried out in water at 30°C



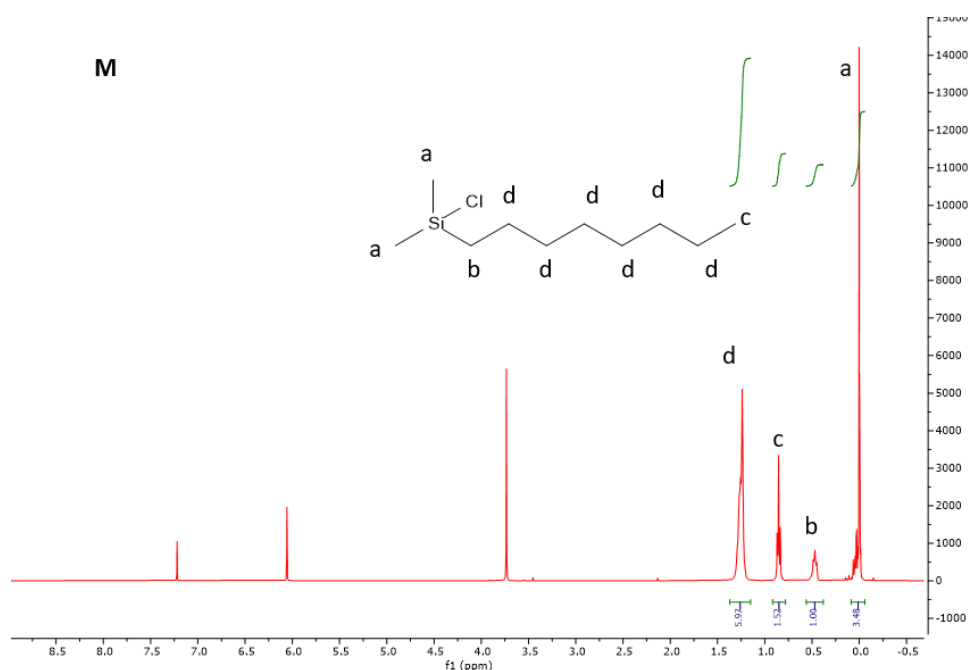


Figure 5.12: ^1H NMR spectrum of alkylsilanes K, L and M, (the reaction mixtures were extracted with CDCl_3 after completion), and trimethoxybenzene (standard used) in CDCl_3 using Bruker 400 MHz at room temperature

5.3.2.2. Hydrosilylation of Styrene with PhMe_2SiH , Et_3SiH and ClMe_2SiH in Water

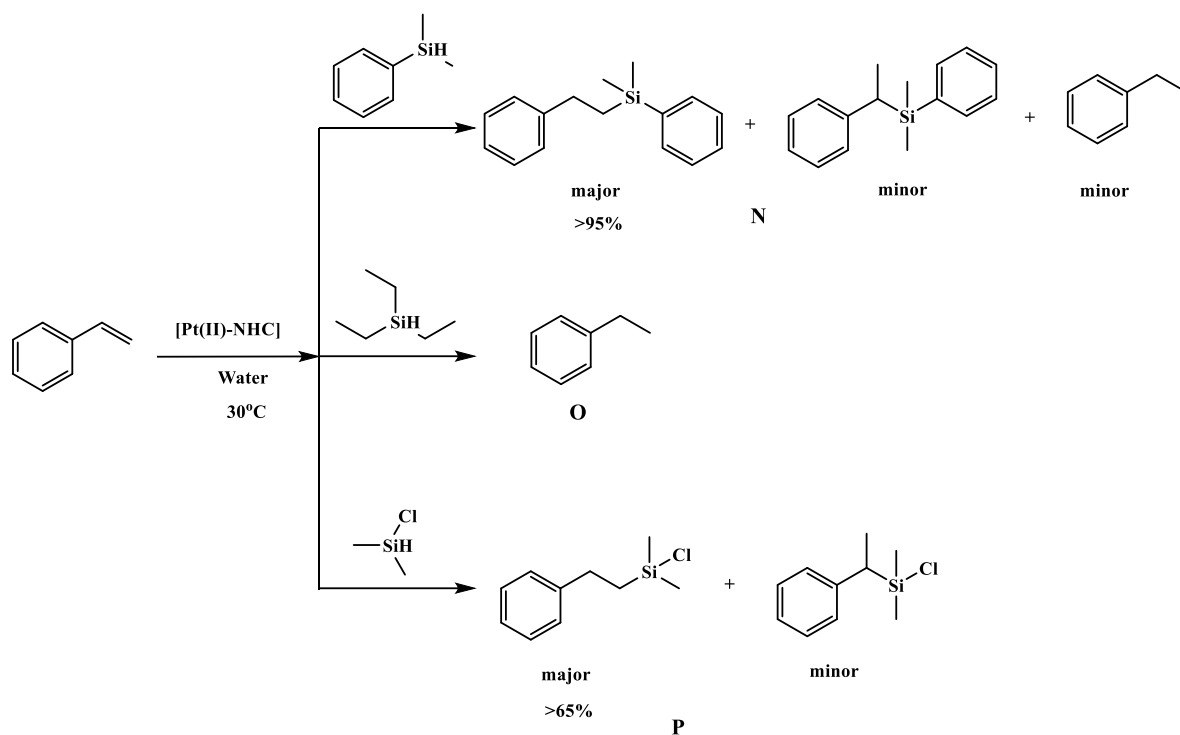
In the presence of the Pt(II)-NHCs, the hydrosilylation reaction between styrene and PhMe_2SiH , Et_3SiH , ClMe_2SiH respectively was also explored. The reaction solutions were stirred at 30°C in water with catalyst loading with respect to the tertiary silanes. The products and the stereochemistry of the products from the two catalysed reactions were confirmed as stated earlier and the important ^1H NMR peaks are highlighted below.

N: ^1H NMR (400 MHz, CDCl_3) δ 0.13 (s, 6H), 0.95 (m, 2H, due to β -(E) isomer), 1.09 (d, $J = 8.0$ Hz, 3H, due to α -(E) isomer), 2.48 (m, 2H, due to β -(E) isomer), 7.02 – 6.92 (m, 3H), 7.19 – 7.06 (m, 2H), 7.35 (m, 3H).

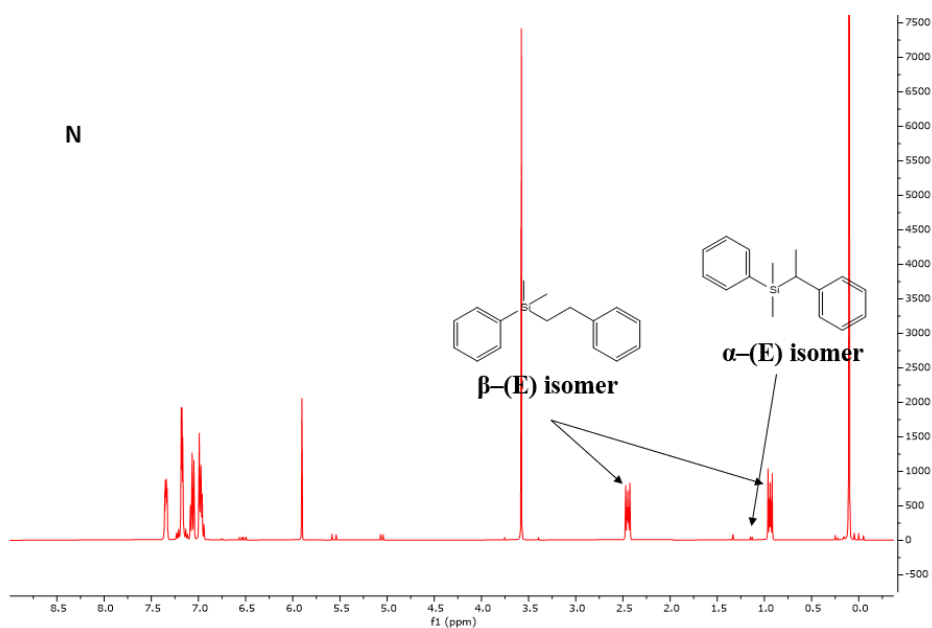
O: ^1H NMR (400 MHz, CDCl_3) δ 1.16 (t, $J = 7.6, 0.9$ Hz, 3H), 2.56 (q, $J = 7.6$ Hz, 2H), 7.24 (m, 2H), 7.10 (m, 3H).

P: ^1H NMR (400 MHz, CDCl_3) δ -0.09 (s, 6H, due to α -(E) isomer), 0.00 (s, 6H, due to β -(E) isomer), 0.81 (ddd, $J = 11.6, 5.3, 2.7$ Hz, 2H, due to β -(E) isomer). 1.28 (d, $J = 8.0$ Hz, 3H, due to α -(E) isomer), 2.56 (ddd, $J = 11.6, 5.3, 2.7$ Hz, 2H, due to β -(E) isomer), 7.20 (s, 5H).

The catalysed reaction between styrene and ClMe_2SiH or PhMe_2SiH gave the β -(E) isomers as the major product and α -(E) isomers as the minor product (Scheme 5.7). For the reaction with PhMe_2SiH , trace amounts of the hydrogenated product (ethylbenzene) was also obtained (Table 5.2). Reaction of styrene with Et_3SiH afforded no hydrosilylated products, rather, the styrene was hydrogenated to ethylbenzene with 52% conversion. Therefore, in the case of styrene, the size and electronic properties of the tertiary silanes employed played a great role on the regioselectivity of the products similar to what has been reported in literature.²⁵ The more hindered PhMe_2SiH formed the β -(E) isomer with >95% while >65% β -(E) isomer were observed for ClMe_2SiH (Figure 5.13). Equally, tertiary silanes with electron withdrawing groups gave the desired hydrosilylated products while Et_3SiH with electron releasing groups did not yield the desired hydrosilylated product. Comparatively, the result obtained with ClMe_2SiH is less favourable to that reported by Pregosin and Caseri (catalyst loading = 4×10^{-4} mol%, conversion = 93%, product ratio (β : α) = 84:16, reaction time = 5 mins, solvent = neat and reaction temperature = RT)²⁷, and Lai and coworkers (catalyst loading = 2.5×10^{-5} mol%, conversion = 99.9%, product ratio (β : α :others) = 94.1:1.4:4.5, reaction time = 3 h, solvent = neat and reaction temperature = 90°C)²⁸.



Scheme 5.7: Hydrosilylation of styrene with different tertiary silanes



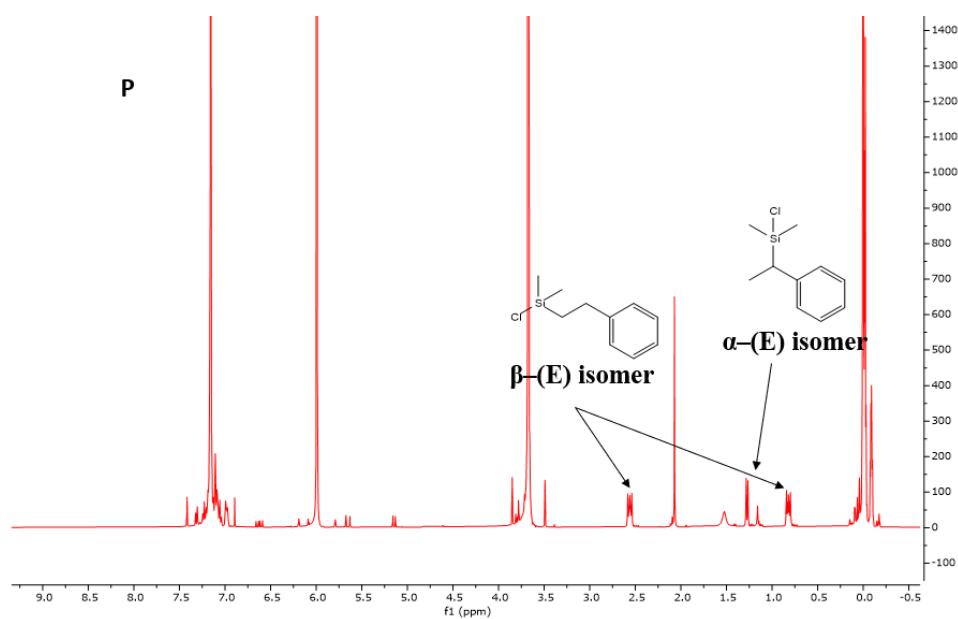
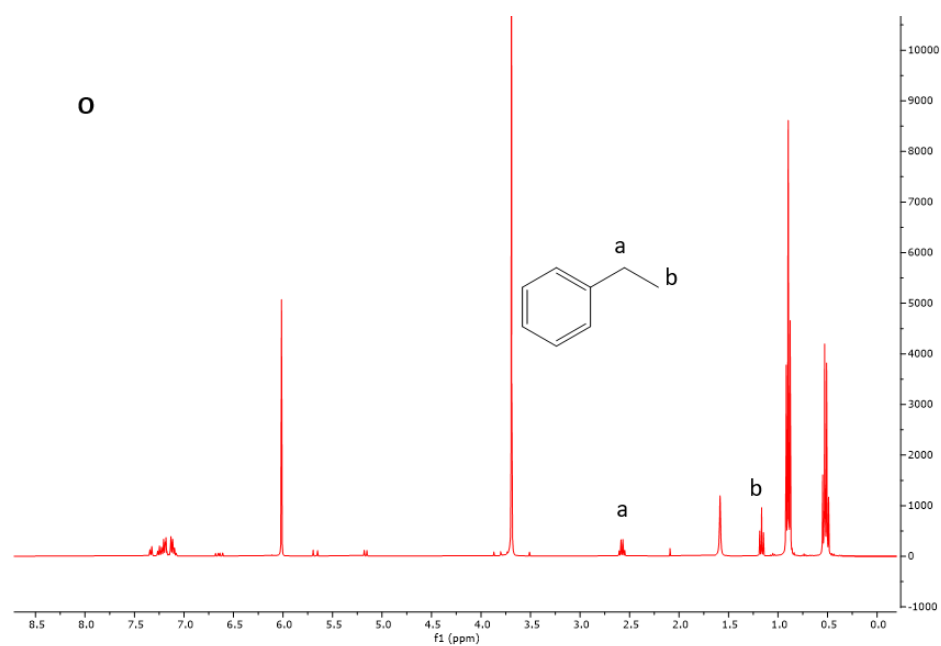
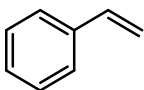
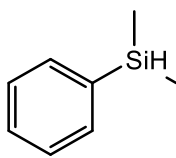
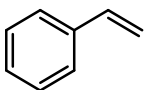
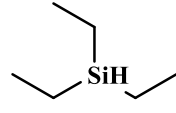
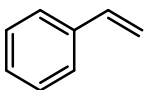
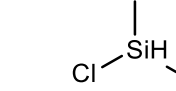


Figure 5.13: ^1H NMR spectrum of **N**, **O** and **P** showing the β -(E) and α -(E) isomers from the hydrosilylation reaction (the reaction mixture was extracted with CDCl_3 after completion), and trimethoxybenzene (standard used) in CDCl_3 using Bruker 400 MHz at room temperature

The result obtained for the hydrosilylation of styrene with PhMe_2SiH is particularly promising. PhMe_2SiH has been described as a less reactive silane compared to other silanes used in hydrosilylation reactions¹⁶ and the activity of the Pt(II)-NHCs used in this study compare favourably in terms of reaction time, reaction temperature, catalyst loading, conversion and selectivity with Karstedt's catalyst (catalyst loading = 0.5 mol%, conversion = 60%, product ratio ($\beta:\alpha$) = 96:4, reaction time = 6 h and reaction temperature = 101°C)¹⁶ and some other Pt(0)- and Pt(II)-NHCs by Strassner et al., (catalyst loading = 0.5 mol%, conversion = 68%, product ratio ($\beta:\alpha$) = 94:6, reaction time = 24 h, solvent = dioxane and reaction temperature = 101°C),¹⁶ Pietraszuk et al., (catalyst loading = 1×10^{-3} mol%, yield = 100%, product ratio ($\beta:\alpha$) = not available, reaction time = 24 h, solvent = toluene and reaction temperature = 80°C)²⁶, Peng et al., (catalyst loading = 0.02 mol%, conversion = 99.9%, product ratio ($\beta:\alpha$) = 100:0, reaction time = 10 h, solvent = neat and reaction temperature = 90°C)²⁹ and the vesicular self-assembled amphiphilic Pt(II)-NCN-pincer complex reported by Hamasaka and Uozumi³⁰ that have been used for this particular reaction (catalyst loading = 1 mol ppm, yield = 72%, product ratio ($\beta:\alpha$) = not available, reaction time = 12 h, solvent = H_2O and reaction temperature = 25°C).

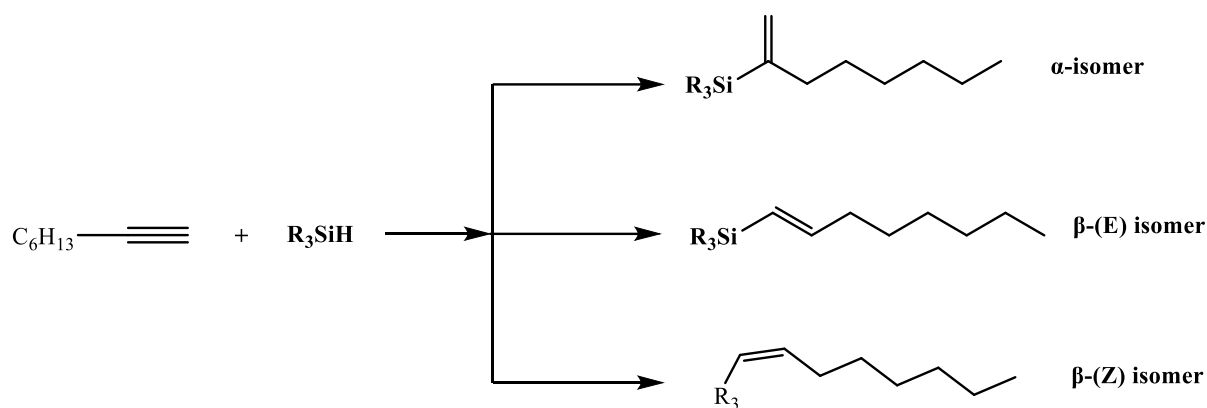
Table 5.2: Hydrosilylation of Styrene with PhMe₂SiH, Et₃SiH and ClMe₂SiH

| Entry | Catalyst | Catalyst Conc. (mol%) | Alkene | Silane | Time (h) | Conversion ^a | β:α ^b | | |
|-------|---|-----------------------|---|--|--|---|------------------|----|-------|
| 1 | Na[PtL ^{bet} ₈ dmsOCl ₂] | 0.001 |  |  | 5 | 94 | 96:4 | | |
| 2 | Na[PtL ^{bet} ₁₀ dmsOCl ₂] | | | | | 98 | 95:5 | | |
| 3 | Na[PtL ^{bet} ₁₂ dmsOCl ₂] | | | | | 96 | 94:6 | | |
| 4 | Na[PtL ^{bet} ₁₄ dmsOCl ₂] | | | | | 96 | 94:6 | | |
| 5 | Na[PtL ^{bet} ₁₆ dmsOCl ₂] | | | | | 98 | 96:4 | | |
| 6 | Na[PtL ^{bet} ₈ dmsOCl ₂] | 0.1 | |  |  | 8 | - | - | |
| 7 | Na[PtL ^{bet} ₁₀ dmsOCl ₂] | | | | | | - | - | |
| 8 | Na[PtL ^{bet} ₁₂ dmsOCl ₂] | | | | | | - | - | |
| 9 | Na[PtL ^{bet} ₁₄ dmsOCl ₂] | | | | | | - | - | |
| 10 | Na[PtL ^{bet} ₁₆ dmsOCl ₂] | | | | | | - | - | |
| 11 | Na[PtL ^{bet} ₈ dmsOCl ₂] | 0.001 | | |  |  | 8 | 62 | 65:35 |
| 12 | Na[PtL ^{bet} ₁₀ dmsOCl ₂] | | | | | | | 66 | 69:31 |
| 13 | Na[PtL ^{bet} ₁₂ dmsOCl ₂] | | | | | | | 69 | 62:38 |
| 14 | Na[PtL ^{bet} ₁₄ dmsOCl ₂] | | | | | | | 70 | 65:35 |
| 15 | Na[PtL ^{bet} ₁₆ dmsOCl ₂] | | | | | | | 71 | 65:35 |

^a The conversion was determined by ¹H NMR analysis based on the disappearance of the alkene resonance. ^bThe products and their stereochemistry were identified by ¹H NMR analysis of the product resonance peaks and their coupling constants. All reactions were carried out in water at 30°C

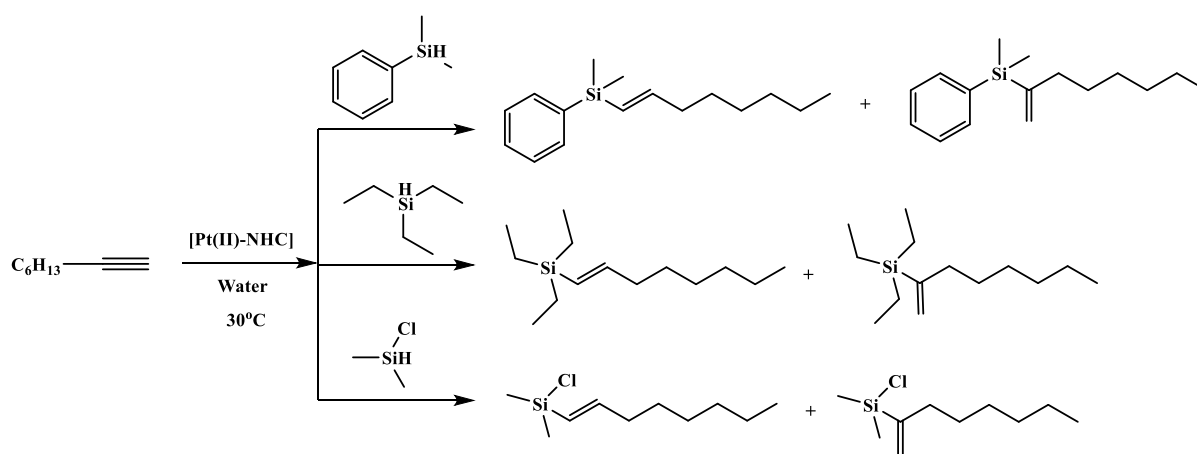
5.3.2.3. Hydrosilylation of 1-Octyne with PhMe₂SiH, Et₃SiH and ClMe₂SiH in Water

The hydrosilylation of 1-octyne with PhMe₂SiH, Et₃SiH and ClMe₂SiH respectively at a catalyst loading relative to the tertiary silanes were carried out to evaluate the catalytic activities of these Pt(II)-NHCs in the hydrosilylation of alkynes. It has been reported in many literary articles that the hydrosilylation of alkynes can lead to three regioisomers: the α, the β-(E), and the β-(Z) isomers (Scheme 5.8).²⁵



Scheme 5.8: Reported product distribution in the hydrosilylation of 1-octyne

The hydrosilylation of 1-octyne with $PhMe_2SiH$, Et_3SiH , $ClMe_2SiH$ gave good conversion within 24 h, generally yielding a mixture of α - and β -(E) isomers (Scheme 5.9) similar to other Pt(II)-NHCs that have been reported.^{17, 26} The catalysed hydrosilylation reaction afforded α - and β -(E) isomers with the β -(E) isomer as the major products. The formation of the products and the regioselectivity (β -(E)- relative to α -isomer) were confirmed by the disappearance of the Si-H proton resonance and the appearance of the corresponding vinylic protons in the 1H NMR spectrum (Figure 5.15).



Scheme 5.9: Hydrosilylation of 1-octyne with different tertiary silanes

Analysis of the product mixture by ^1H NMR spectroscopy showed two resonances for the alkenyl protons of the β -(E) isomer with chemical shifts at ~ 6.00 ppm (doublet of triplets with $^3J = 20.0$ Hz and $^4J = 8.0$ Hz) and ~ 5.50 ppm (a pair of multiplets with $^3J = 20.0$ Hz and $^4J = 2.0$ Hz) and a pair of multiplets (minor peaks) at ~ 5.55 and ~ 5.20 ppm corresponding to the α -isomer (Figure 5.15). The size of the tertiary silanes employed has no effect on the regioselectivity of the products and the summary of the results of these hydrosilylation reaction is presented in Table 5.3. The results obtained for the hydrosilylation of octyne compare favourably with that reported by de Jesus et al., (catalyst loading = 0.5 mol%, yield = 72%, product ratio (β : α) = 93:7, reaction time = 24 h, solvent = H_2O , and reaction temperature = 30°C)¹⁷, Kariuki et al., (catalyst loading = 0.005 mol%, yield = 82.7%, product ratio (β : α) = 89.5:10.5, reaction time = 3 h, solvent = *o*-xylene, and reaction temperature = 80°C)¹⁵ for the hydrosilylation reaction of Et_3SiH and octyne, Marko and coworkers (catalyst loading = 0.1 mol%, yield = 93%, product ratio (β : α) = 50:1, reaction time = 6 mins, solvent = neat, and reaction temperature = 60°C) for the hydrosilylation reaction of PhMe_2SiH and octyne.³¹

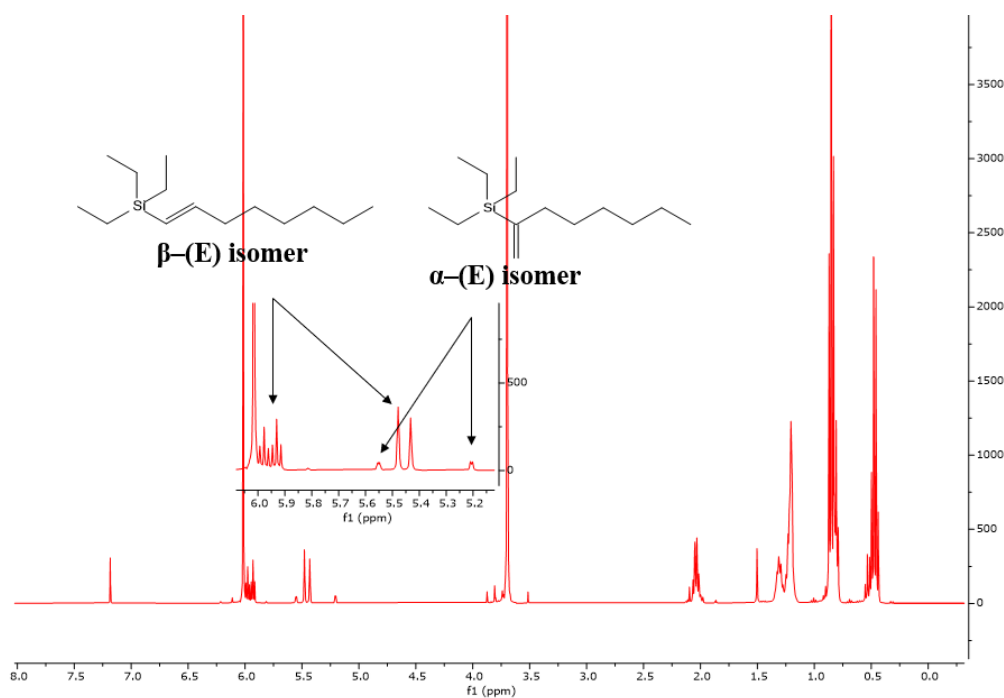


Figure 5.15: ^1H NMR spectrum of the β -(E) and α -isomers from the hydrosilylation of 1-octyne and Et_3SiH (the reaction mixture was extracted with CDCl_3 after completion), and trimethoxybenzene (standard used) in CDCl_3 using Bruker 400 MHz at room temperature

Table 5.3: Hydrosilylation of 1-octyne with Et₃SiH, PhMe₂SiH and ClMe₂SiH

| Entry | Catalyst | Catalyst Conc. (mol %) | Alkyne | Silane | Time (h) | Conversion ^a | β:α ^b | | |
|-------|---|------------------------|--------|--------|----------|-------------------------|------------------|-------|-------|
| 1 | Na[PtL ^{bet} ₈ dmsOCl ₂] | 0.01 | | | 24 | 74 | 72:28 | | |
| 2 | Na[PtL ^{bet} ₁₀ dmsOCl ₂] | | | | | 78 | 75:25 | | |
| 3 | Na[PtL ^{bet} ₁₂ dmsOCl ₂] | | | | | 76 | 77:23 | | |
| 4 | Na[PtL ^{bet} ₁₄ dmsOCl ₂] | | | | | 76 | 77:23 | | |
| 5 | Na[PtL ^{bet} ₁₆ dmsOCl ₂] | | | | | 78 | 74:26 | | |
| 6 | Na[PtL ^{bet} ₈ dmsOCl ₂] | 0.01 | | | | 24 | 88 | 85:15 | |
| 7 | Na[PtL ^{bet} ₁₀ dmsOCl ₂] | | | | | | 91 | 88:12 | |
| 8 | Na[PtL ^{bet} ₁₂ dmsOCl ₂] | | | | | | 93 | 85:15 | |
| 9 | Na[PtL ^{bet} ₁₄ dmsOCl ₂] | | | | | | 97 | 87:13 | |
| 10 | Na[PtL ^{bet} ₁₆ dmsOCl ₂] | | | | | | 96 | 82:18 | |
| 11 | Na[PtL ^{bet} ₈ dmsOCl ₂] | 0.01 | | | | | 24 | 62 | 81:19 |
| 12 | Na[PtL ^{bet} ₁₀ dmsOCl ₂] | | | | | | | 67 | 83:17 |
| 13 | Na[PtL ^{bet} ₁₂ dmsOCl ₂] | | | | | | | 65 | 83:17 |
| 14 | Na[PtL ^{bet} ₁₄ dmsOCl ₂] | | | | | | | 68 | 80:20 |
| 15 | Na[PtL ^{bet} ₁₆ dmsOCl ₂] | | | | | | | 68 | 80:20 |

^a The conversion was determined by ¹H NMR analysis based on the disappearance of the alkyne resonance. ^bThe products and their stereochemistry were identified by ¹H NMR analysis of the product resonance peaks and their coupling constants. All reactions were carried out in water at 30°C

5.3.2.4. Structure-Activity Relationship

The time dependence of the hydrosilylation reaction using Na[Pt(L^{bet}₁₆)(dmsO)Cl₂] at 0.001 mol % for PhMe₂SiH and 1-octene, 0.001 mol % for PhMe₂SiH and styrene and 0.01 mol % for PhMe₂SiH and 1-octyne respectively is as shown in Figure 5.16. The time-conversion plots for the hydrosilylation of PhMe₂SiH and 1-octene, PhMe₂SiH and styrene are similar in shape. The catalytic transformation of 1-octene and styrene to alkylsilane commenced rapidly giving full conversion within 5 and 6 h respectively. The transformation of 1-octyne to vinylsilane starts almost immediately but slows down as it progressed and got to full conversion at ~24 h (Figure 5.16).

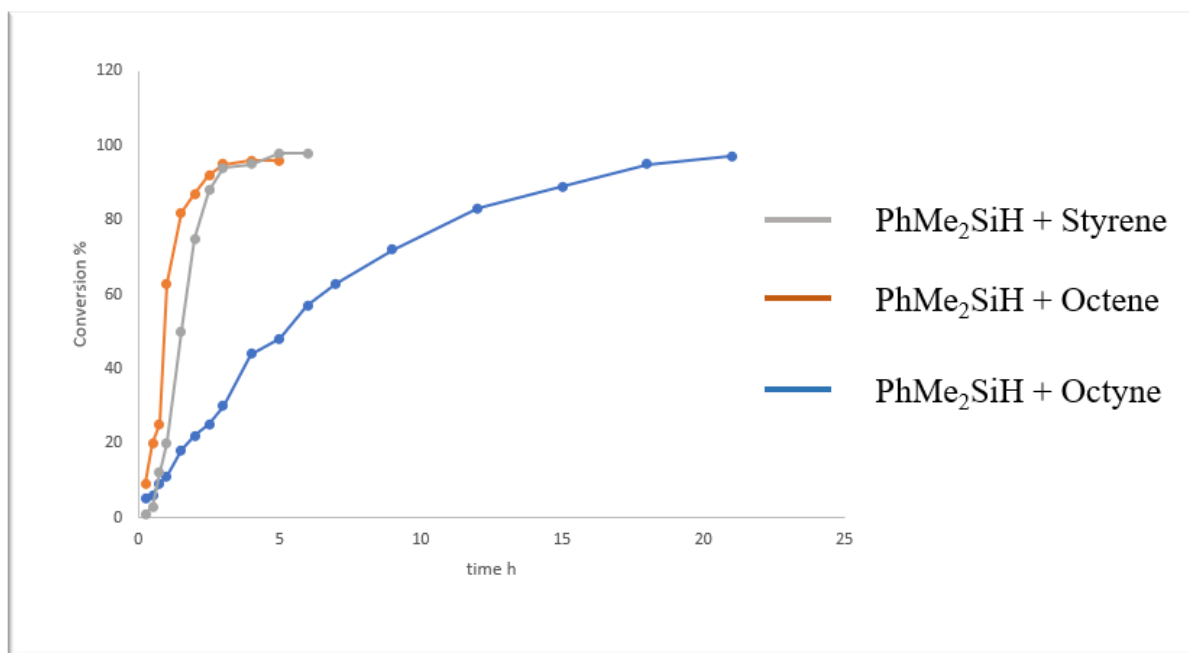


Figure 5.16: Time dependence of the hydrosilylation reaction between PhMe₂SiH and 1-octene, styrene, 1-octyne respectively catalysed by Na[PtL^{bet}₁₆dmsocCl₂]

Pt(0) has been found to be the catalytically active species with hydrosilanes acting as reducing agents in the hydrosilylation reaction.^{32, 33} We did not observe any induction periods in the kinetic curves and as a result we are not so sure what the active catalyst species is in this case. The time-conversion plots revealed these Pt(II)-NHCs show better activity towards the hydrosilylation of 1-octene and styrene with low catalyst loading and short conversion time than towards 1-octyne with high catalysts loading and long conversion time (Figure 5.16).

The effect of the chain length on reaction time, conversion, and catalyst loading was investigated in the hydrosilylation reaction between styrene and PhMe₂SiH and the result is presented in Figure 5.17. The stereo-electronic parameters have been found to influence the outcome of the hydrosilylation reactions^{25, 34} and from the time-conversion plot, the chain lengths appeared to have no influence on the reaction time, conversion, and catalyst loading. We can suggest from this result that varying the chain lengths on the surface-active Pt(II)-NHCs used in this study has little or no effect on the stereo-electronic properties of these complexes (Figure 5.17).

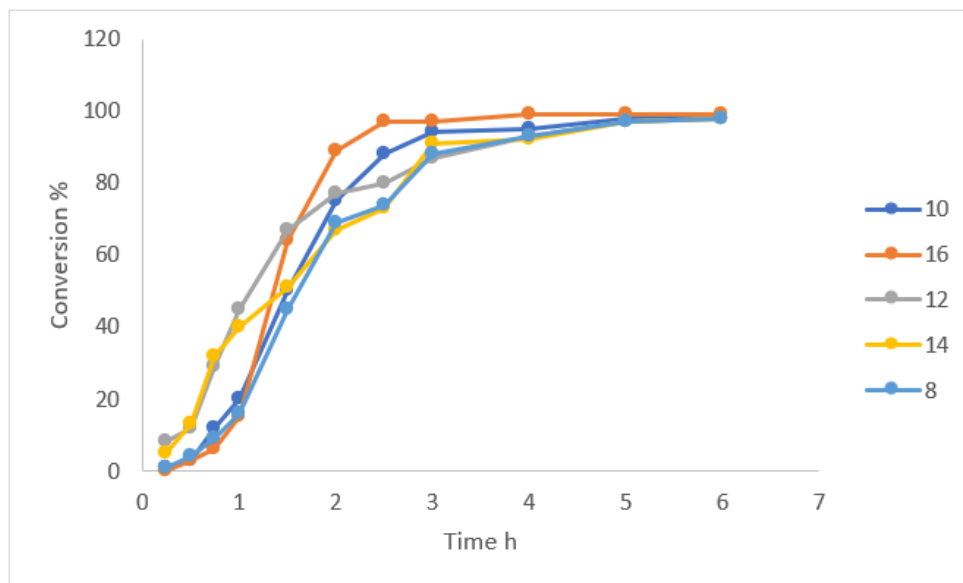


Figure 5.17: Time dependence of the hydrosilylation reaction between PhMe_2SiH and styrene catalysed by $\text{Na}[\text{PtL}^{\text{bet}}_{8-16}\text{dmsOCl}_2]$

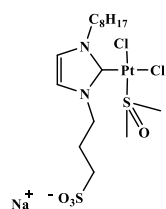
5.4. Experimental

General

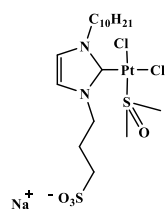
All reactions were carried out under aerobic conditions and all reagents were purchased from commercial sources and used without further purification. ^1H and ^{13}C NMR spectra were recorded on an NMR-FT Bruker 400 MHz or 500 MHz spectrophotometers and recorded in deuterated solvents and the chemical shifts are given in ppm. Coupling constants (J) are given in hertz. When required, two-dimensional ^1H - ^{13}C HSQC experiments were carried out for the unequivocal assignment of ^1H and ^{13}C resonances. High-resolution mass spectra were obtained as appropriate (in positive and negative modes) using a Waters LCT Premier XE instrument and are reported as m/z (relative intensity). Analytical thin layer chromatography was performed using Merck Silica gel F254 and the compounds were visualized with KMnO_4 . Column chromatography was performed on Merck Kieselgel 60 (0.040-0.063 mm) silica gel.

General Procedure for the Preparation of Surface-active Na[PtL^{bet}₈₋₁₆dmsOCl₂]

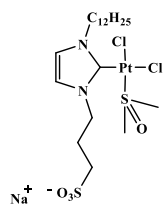
Imidazolium sulfonate (HL^{bet}₈₋₁₆) (0.33 mmol), K₂PtCl₄ (0.33 mmol) and sodium acetate (0.40 mmol) were dissolved in 5 mL of dmsO and heated to 90°C. The reaction mixture was stirred at that temperature for 3 days. The solution was dried under vacuum and the crude pale-yellow solid obtained was dissolved in methanol and transferred to a column chromatograph (Merck Kieselgel 60 (0.040-0.063 mm) silica gel) and the pure product was eluted with MeOH:CH₂Cl₂ (95:5) and subsequently dried under vacuum.

Na[PtL^{bet}₈dmsOCl₂]

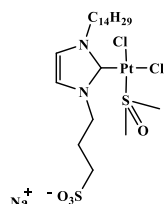
Yield: 74%; ¹H NMR (400 MHz, MeOH-d⁴): δ 0.80 (t, ³J= 8.0 Hz, 3H), 1.15-1.30 (br, 10H), 1.90 (m, 2H), 2.39 (m, 2H), 2.81 (m, 2H, CH₂S), 3.42 (s, 3H, Me₂SO), 3.46 (s, 3H, Me₂SO), 4.20 (m, 1H, NCH₂), 4.36 (m, 1H, NCH₂), 4.36 (m, 1H, NCH₂), 4.58 (m, 1H, NCH₂), 7.18 (d, ³J= 4.0 Hz, 1H, Imz), 7.24 (d, ³J= 4.0 Hz, 1H, Imz). ¹³C{¹H} NMR (100 MHz, MeOH-d⁴): δ 13.12 (s, CH₃), 22.32 (s, CH₂), 25.73 (s, CH₂), 26.31 (s, CH₂), 28.92 (s, CH₂), 28.97 (s, CH₂), 29.92 (s, CH₂), 31.57 (s, CH₂), 44.80 (s, 1C, Me₂SO), 44.81 (s, 1C, Me₂SO), 44.90 (s, CH₂S), 49.05 (s, NCH₂), 50.60 (s, NCH₂), 121.26 (s, Imz C5), 121.37 (s, Imz C4), 141.18 (s, Imz C2). MS (ESI-) m/z: Found 644.0769 [(M-Na)⁻ 70%], expected 644.0812.

Na[PtL^{bet}₁₀dmsOCl₂]

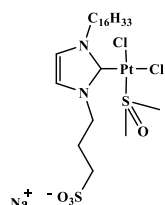
Yield: 71%; ¹H NMR (400 MHz, MeOH-d⁴): δ 0.80 (t, ³J= 8.0 Hz, 3H), 1.15-1.35 (br, 14H), 1.90 (m, 2H), 2.39 (m, 2H), 2.82 (m, 2H, CH₂S), 3.41 (s, 3H, Me₂SO), 3.45 (s, 3H, Me₂SO), 4.20 (m, 1H, NCH₂), 4.36 (m, 1H, NCH₂), 4.36 (m, 1H, NCH₂), 4.58 (m, 1H, NCH₂), 7.16 (d, ³J= 4.0 Hz, 1H, Imz), 7.23 (d, ³J= 4.0 Hz, 1H, Imz). ¹³C{¹H} NMR (100 MHz, MeOH-d⁴): δ 13.04 (s, CH₃), 22.33 (s, CH₂), 25.70 (s, CH₂), 26.29 (s, CH₂), 28.98 (s, CH₂), 29.03 (s, CH₂), 29.22 (s, CH₂), 29.25 (s, CH₂), 29.89 (s, CH₂), 31.66 (s, CH₂), 44.71 (s, 1C, Me₂SO), 44.72 (s, 1C, Me₂SO), 44.74 (s, CH₂S), 49.01 (s, NCH₂), 50.57 (s, NCH₂), 121.11 (s, Imz C5), 121.32 (s, Imz C4), 141.30 (s, Imz C2). MS (ESI-) m/z: Found 672.1055 [(M-Na)⁻ 40%], expected 672.1125.

Na[PtL^{bet}₁₂dmsocCl₂]

Yield: 77%; ¹H NMR (500 MHz, MeOH-d⁴): δ 0.80 (t, ³J= 8.0 Hz, 3H), 1.20-1.40 (br, 18H), 1.91 (m, 2H), 2.39 (m, 2H), 2.82 (m, 2H, CH₂S), 3.41 (s, 3H, Me₂SO), 3.46 (s, 3H, Me₂SO), 4.20 (m, 1H, NCH₂), 4.35 (m, 1H, NCH₂), 4.37 (m, 1H, NCH₂), 4.56 (m, 1H, NCH₂), 7.18 (d, ³J= 4.0 Hz, 1H, Imz), 7.24 (d, ³J= 4.0 Hz, 1H, Imz). ¹³C{¹H} NMR (125 MHz, MeOH-d⁴): δ 13.08 (s, CH₃), 22.35 (s, CH₂), 25.71 (s, CH₂), 26.30 (s, CH₂), 29.00 (s, CH₂), 29.08 (s, CH₂), 29.24 (s, CH₂), 29.31 (s, CH₂), 29.38 (s, CH₂), 29.92 (s, CH₂), 31.68 (s, CH₂), 44.74 (s, 1C, Me₂SO), 44.75 (s, 1C, Me₂SO), 44.82 (s, CH₂S), 49.03 (s, NCH₂), 50.59 (s, NCH₂), 121.21 (s, Imz C5), 121.34 (s, Imz C4), 141.22 (s, Imz C2). MS (ESI-) m/z: Found 700.1391 [(M-Na)⁺ 80%], expected 700.1438.

Na[PtL^{bet}₁₄dmsocCl₂]

Yield: 68%; ¹H NMR (500 MHz, MeOH-d⁴): δ 0.80 (t, ³J= 8.0 Hz, 3H), 1.20-1.35 (br, 22H), 1.90 (m, 2H), 2.40 (m, 2H), 2.82 (m, 2H, CH₂S), 3.41 (s, 3H, Me₂SO), 3.45 (s, 3H, Me₂SO), 4.20 (m, 1H, NCH₂), 4.35 (m, 1H, NCH₂), 4.36 (m, 1H, NCH₂), 4.57 (m, 1H, NCH₂), 7.18 (d, ³J= 4.0 Hz, 1H, Imz), 7.24 (d, ³J= 4.0 Hz, 1H, Imz). ¹³C{¹H} NMR (125 MHz, MeOH-d⁴): δ 13.04 (s, CH₃), 22.34 (s, CH₂), 25.71 (s, CH₂), 26.29 (s, CH₂), 28.99 (s, CH₂), 29.08 (s, CH₂), 29.23 (s, CH₂), 29.31 (s, CH₂), 29.37 (s, CH₂), 29.41 (s, CH₂), 29.90 (s, CH₂), 31.68 (s, CH₂), 44.68 (s, 1C, Me₂SO), 44.69 (s, 1C, Me₂SO), 44.72 (s, CH₂S), 49.01 (s, NCH₂), 50.56 (s, NCH₂), 121.12 (s, Imz C5), 121.31 (s, Imz C4), 141.28 (s, Imz C2). MS (ESI-) m/z: Found 728.1668 [(M-Na)⁺ 70%], expected 728.1751.

Na[PtL^{bet}₁₆dmsocCl₂]

Yield: 69%; ¹H NMR (500 MHz, MeOH-d⁴): δ 0.80 (t, ³J= 8.0 Hz, 3H), 1.20-1.35 (br, 26H), 1.91 (m, 2H), 2.39 (m, 2H), 2.80 (m, 2H, CH₂S), 3.41 (s, 3H, Me₂SO), 3.46 (s, 3H, Me₂SO), 4.20 (m, 1H, NCH₂), 4.35 (m, 1H, NCH₂), 4.36 (m, 1H, NCH₂), 4.56 (m, 1H, NCH₂), 7.18 (d, ³J= 4.0 Hz, 1H, Imz), 7.23 (d,

$^3J = 4.0$ Hz, 1H, Imz). $^{13}\text{C}\{^1\text{H}\}$ NMR (125 MHz, MeOH- d_4): δ 13.08 (s, CH₃), 22.35 (s, CH₂), 22.82 (s, CH₂), 25.72 (s, CH₂), 26.30 (s, CH₂), 29.01 (s, CH₂), 29.09 (s, CH₂), 29.25 (s, CH₂), 29.33 (s, CH₂), 29.38 (s, CH₂), 29.39 (s, CH₂), 29.42 (s, CH₂), 29.92 (s, CH₂), 31.69 (s, CH₂), 44.71 (s, 1C, Me₂SO), 44.72 (s, 1C, Me₂SO), 44.80 (s, CH₂S), 49.03 (s, NCH₂), 50.58 (s, NCH₂), 121.19 (s, Imz C5), 121.34 (s, Imz C4), 141.24 (s, Imz C2). MS (ESI-) m/z: Found 756.1981 [(M-Na)⁻ 70%], expected 756.2064.

General Procedure for the Hydrosilylation of Alkenes/Alkyne in Water

The alkene/alkyne (1.0 mmol) and a slight excess of the appropriate hydrosilane (1.1 mmol) were added to a solution of the corresponding Pt(II)-NHC catalyst (see Tables 5.1–3 for mol % Pt(II)-NHC catalyst) in 2 mL of water previously warmed to 30 °C. The mixture was stirred magnetically until the reaction is completed, then extracted with CDCl₃ and dried over MgSO₄. Conversions and selectivities were obtained by analysis of the deuterated chloroform solutions by (1,3,5-trimethoxybenzene was used as internal standard) ^1H NMR spectroscopy.

5.5. References

1. M. N. Hopkinson, C. Richter, M. Schedler and F. Glorius, *Nature*, 2014, **510**, 485-496.
2. D. Brissy, M. Skander, P. Retailleau and A. Marinetti, *Organometallics*, 2007, **26**, 5782-5785.
3. A. S. K. Hashmi, C. Lothschütz, C. Böhling, T. Hengst, C. Hubbert and F. Rominger, *Adv. Synth. Catal.*, 2010, **352**, 3001-3012.
4. S. Fantasia, J. L. Petersen, H. Jacobsen, L. Cavallo and S. P. Nolan, *Organometallics*, 2007, **26**, 5880-5889.
5. T. Zou, C.-N. Lok, P.-K. Wan, Z.-F. Zhang, S.-K. Fung and C.-M. Che, *Curr. Opin. Chem. Biol.*, 2018, **43**, 30-36.
6. Z. M. Hudson, C. Sun, M. G. Helander, Y.-L. Chang, Z.-H. Lu and S. Wang, *J. Am. Chem. Soc.*, 2012, **134**, 13930-13933.
7. T. K. Meister, K. Riener, P. Gigler, J. Stohrer, W. A. Herrmann and F. E. Kühn, *ACS Catal.*, 2016, **6**, 1274-1284.
8. W. A. Herrmann, M. Elison, J. Fischer, C. Köcher and G. R. J. Artus, *Angew. Chemi. Int. Ed.*, 1995, **34**, 2371-2374.
9. B. Marciniec, H. Maciejewski and P. Pawluć, in *Organosilicon Compounds*, ed. V. Y. Lee, Academ. Press, 2017, pp. 169-217.
10. T. Hayashi and K. Yamasaki, in *Comprehensive Organometallic Chemistry III*, eds. D. M. P. Mingos and R. H. Crabtree, Elsevier, Oxford, 2007, pp. 815-838.
11. I. E. Markó, S. Stérin, O. Buisine, G. Mignani, P. Branlard, B. Tinant and J.-P. Declercq, *Science*, 2002, **298**, 204-206.
12. J. L. Speier, in *Advances in Organometallic Chemistry*, Elsevier, 1979, vol. 17, pp. 407-447.
13. P. B. Hitchcock, M. F. Lappert and N. J. W. Warhurst, *Angew. Chemi. Int. Ed.*, 1991, **30**, 438-440.

14. Y. Nakajima and S. Shimada, *RSC Adv.*, 2015, **5**, 20603-20616.
15. J. J. Dunsford, K. J. Cavell and B. Kariuki, *J. Organomet. Chem.*, 2011, **696**, 188-194.
16. M. A. Taige, S. Ahrens and T. Strassner, *J. Organomet. Chem.*, 2011, **696**, 2918-2927.
17. G. F. Silbestri, J. C. Flores and E. de Jesús, *Organometallics*, 2012, **31**, 3355-3360.
18. T. Lorenzetto, G. Berton, F. Fabris and A. Scarso, *Catal. Sci. Tech.*, 2020, **10**, 4492-4502.
19. B. H. Lipshutz, *J. Org. Chem.*, 2017, **82**, 2806-2816.
20. G. L. Sorella, G. Strukul and A. Scarso, *Green Chem.*, 2015, **17**, 644-683.
21. A. Donner, B. Trepka, S. Theiss, F. Immler, J. Traber and S. Polarz, *Langmuir*, 2019, **35**, 16514-16520.
22. P. Marshall, R. L. Jenkins, W. Clegg, R. W. Harrington, S. K. Callear, S. J. Coles, I. A. Fallis and A. Dervisi, *Dalton Trans.*, 2012, **41**, 12839.
23. C. P. Newman, R. J. Deeth, G. J. Clarkson and J. P. Rourke, *Organometallics*, 2007, **26**, 6225-6233.
24. E. A. Baquero, G. F. Silbestri, P. Gómez-Sal, J. C. Flores and E. de Jesús, *Organometallics*, 2013, **32**, 2814-2826.
25. G. De Bo, G. Berthon-Gelloz, B. Tinant and I. E. Markó, *Organometallics*, 2006, **25**, 1881-1890.
26. P. Žak, M. Bołt, M. Kubicki and C. Pietraszuk, *Dalton Trans.*, 2018, **47**, 1903-1910.
27. W. Caseri and P. S. Pregosin, *Organometallics*, 1988, **7**, 1373-1380.
28. Y. Bai, J. Peng, J. Li and G. Lai, *App. Organomet. Chem.*, 2011, **25**, 400-405.
29. F. Zhang, Y. Bai, X. Yang, J. Li and J. Peng, *Phosphorus, Sulfur, Silicon Relat. Elem.*, 2017, **192**, 1271-1278.
30. G. Hamasaka and Y. Uozumi, *Chem. Lett.*, 2016, **45**, 1244-1246.

31. G. Berthon-Gelloz, J.-M. Schumers, G. De Bo and I. E. Markó, *J. Org. Chem.*, 2008, **73**, 4190-4197.
32. M. Blug, X.-F. Le Goff, N. Mézailles and P. Le Floch, *Organometallics*, 2009, **28**, 2360-2362.
33. J. W. Sprengers, M. J. Agerbeek, C. J. Elsevier, H. Kooijman and A. L. Spek, *Organometallics*, 2004, **23**, 3117-3125.
34. C. Lu, S. Gu, W. Chen and H. Qiu, *Dalton Trans.*, 2010, **39**, 4198.

Chapter



Conclusions and Future Work

| | |
|-----------------------|-----|
| 6.1. Conclusions..... | 179 |
| 6.2. Future Work..... | 180 |

Chapter 6

6.1. Conclusions

This work describes the preparation of amphiphilic cationic, dicationic and zwitterionic imidazolium salts and these amphiphiles have been used as scaffold about which new Ag(I)-NHC and Pt(II)-NHC complexes of the type NHC-Ag-Br, Na⁺[NHC-Ag-Cl]⁻ and Na[PtL^{bet}dmsOCl₂] have been assembled. The amphiphiles which served as proligand and their corresponding metal complexes have been characterised by ¹H and ¹³C NMR and HRMS.

The *in vitro* antimicrobial activity of the synthesized proligands (**HL**₈₋₁₆, **HL**^{mes}₈₋₁₆, **H₂G**₈₋₁₆ and **H₂G**^{mes}₈₋₁₆) and their corresponding silver(I) complexes (**L**_{8-16-Ag-Br}, **L**^{mes}_{8-16-Ag-Br}, **G**_{8-16-Ag₂-Br₂ and **G**^{mes}_{8-16-Ag₂-Br₂) against planktonic and biofilm cells of *Escherichia coli* NCTC 12923, *Staphylococcus aureus* NCTC 6571, *Staphylococcus aureus* NCIMB 9518, *Pseudomonas aeruginosa* ATCC 15692, *Staphylococcus epidermidis* ATCC 14990, *Staphylococcus epidermidis* ATCC RP62A and *Candida albicans* ATCC 90028 have been explored. Furthermore, their antimicrobial activities are compared to triclosan (5-chloro-2-(2,4-dichlorophenoxy)phenol) and AgNO₃.}}

The antimicrobial activity of all the synthesized amphiphilic imidazolium salts and the Ag(I)-NHC complexes tested, show good to moderate activity against the planktonic cells of all the studied strains with MIC value as low as <0.78 μg/mL, except for **HL**₈, **HL**₁₀, **HL**^{mes}₈ and **HL**^{mes}₁₀. Also, the imidazolium salts and the Ag(I)-NHC complexes were found to exhibit moderate to good activity against the biofilm cells of *Candida albicans* ATCC 90028 with MBEC value as low as <50.00 μg/mL. **L**_{12-16-Ag-Br} were found to be active against the biofilm cells of all the gram-positive bacteria strains, while **L**^{mes}_{12-16-Ag-Br} were found to be active against *Staphylococcus aureus* NCTC 6571, *Staphylococcus aureus* NCIMB 9518, *Staphylococcus epidermidis* ATCC 14990 and *Escherichia coli* NCTC 12923, with MBEC value ranging from 200.00-400.00 μg/mL respectively. However, all the proligands were found to be inactive against the biofilm cells of all the strains of bacteria tested. There is a correlation of increasing antimicrobial activity with size of the aliphatic chain and overall, most of the compounds tested have been found to be bactericidal and fungicidal.

Complexes Na[PtL^{bet}₈₋₁₆dmsOCl₂] were assessed as catalysts for hydrosilylation of terminal alkenes and an alkyne with hydrosilanes in water at 30°C to give alkylsilanes and vinylsilanes respectively at a catalyst loading relative to the tertiary silanes. In this study, we employed

three different hydrosilanes (phenyldimethylsilane (PhMe₂SiH), triethylsilane (Et₃SiH), Chlorodimethylsilane (ClMe₂SiH)), two alkenes (1-octene and styrene) and one alkyne (1-octyne). The catalytic system enabled the synthesis of alkylsilanes from different tertiary silanes and alkenes with 70-98% conversions with catalysts loading as low as 10 ppm in some cases. In all cases, the major product is the β -adduct, which is anti-Markonikov in nature.

Similarly, vinylsilanes were prepared in 60-97% conversions as a mixture of α/β isomers (with the β isomers as the major product).

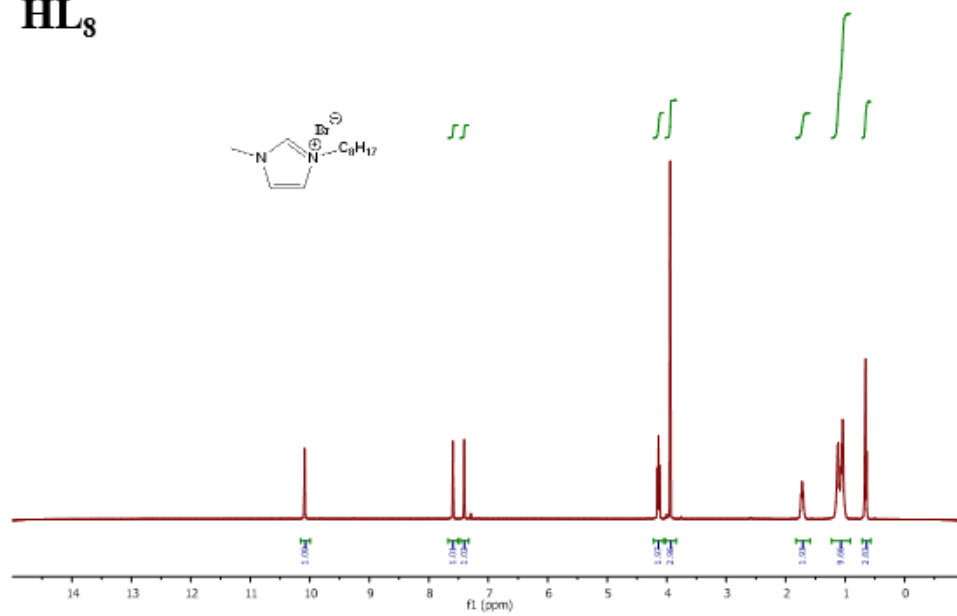
6.2. Future Work

In this work, we have successfully synthesized Ag(I)- and Pd(II)-NHC complexes and applied them as antimicrobial agents and catalysts in hydrosilylation reactions respectively. Further studies on membrane permeation, cellular accumulation, morphology of microorganisms after treatment and cytotoxicity are salient in order to enhance the profile of the synthesised Ag(I)-NHCs used in this study. Additionally, incorporation of the lead Ag(I)-NHC into a urinary catheter in order to generate a catheter surface that will inhibit the growth and swarming of both planktonic and biofilm cells will go a long way in improving the profile of silver-based antimicrobials.

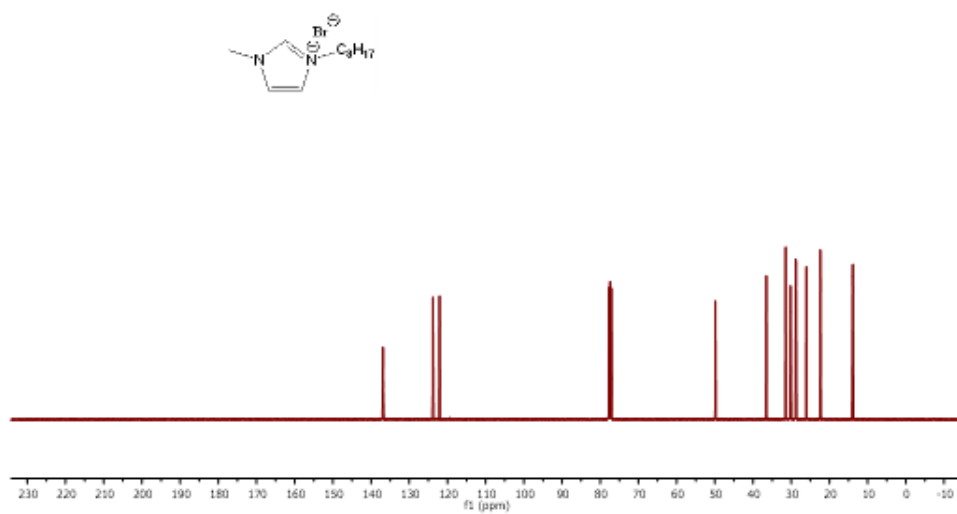
From the results of the hydrosilylation reactions in chapter 5, it is essential to expand the substrate scope of these Pt(II)-NHC metallosurfactants to demonstrate their versatility. Further studies on the morphology of the aggregates formed in water and the mechanistic pathway of these Pt(II)-NHC metallosurfactants with a view to identifying reactive intermediate(s) in hydrosilylation reaction in water are crucial to determine how these catalysts/precatalysts facilitate the hydrosilylation of alkenes and alkyne in water.

Appendix A: ^1H and ^{13}C NMR spectra of **HL₈₋₁₆ and **L₈₋₁₆-Ag-Br****

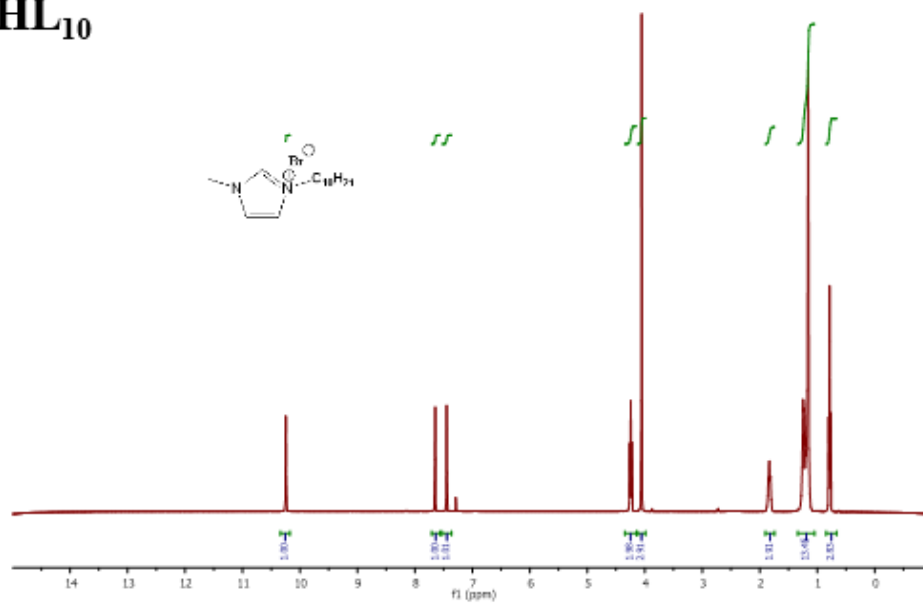
HL₈



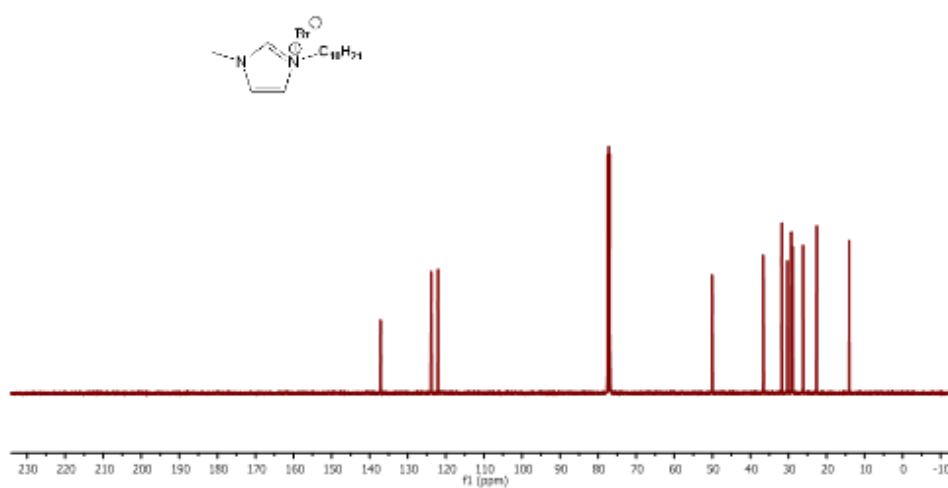
HL₈



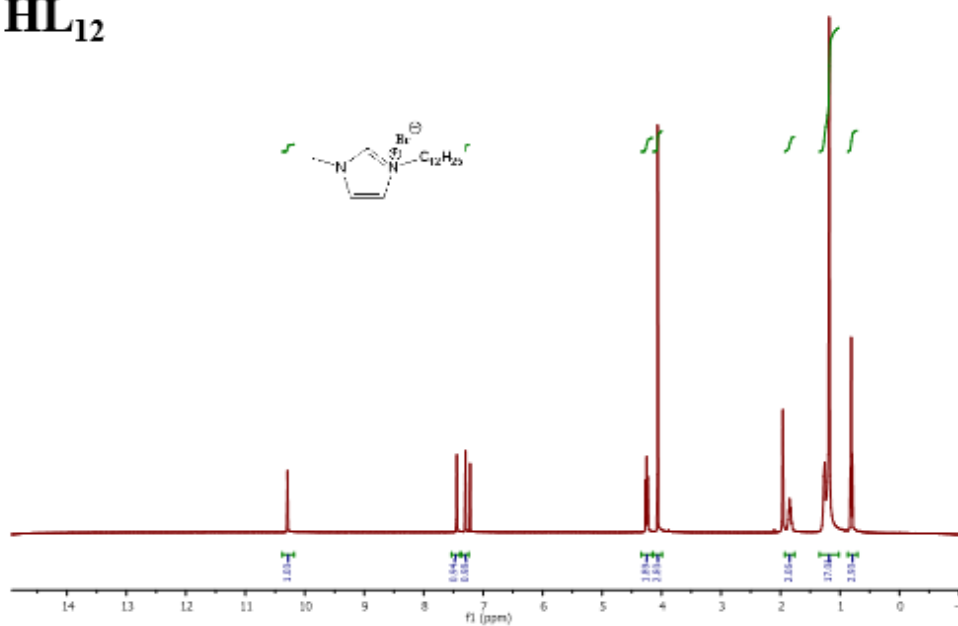
HL₁₀



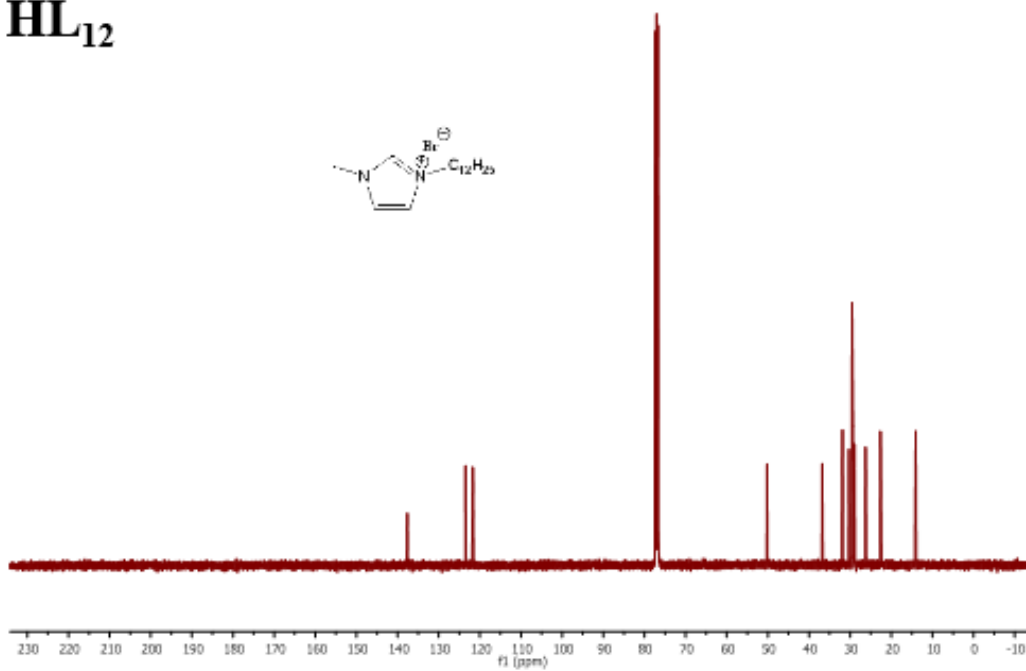
HL₁₀



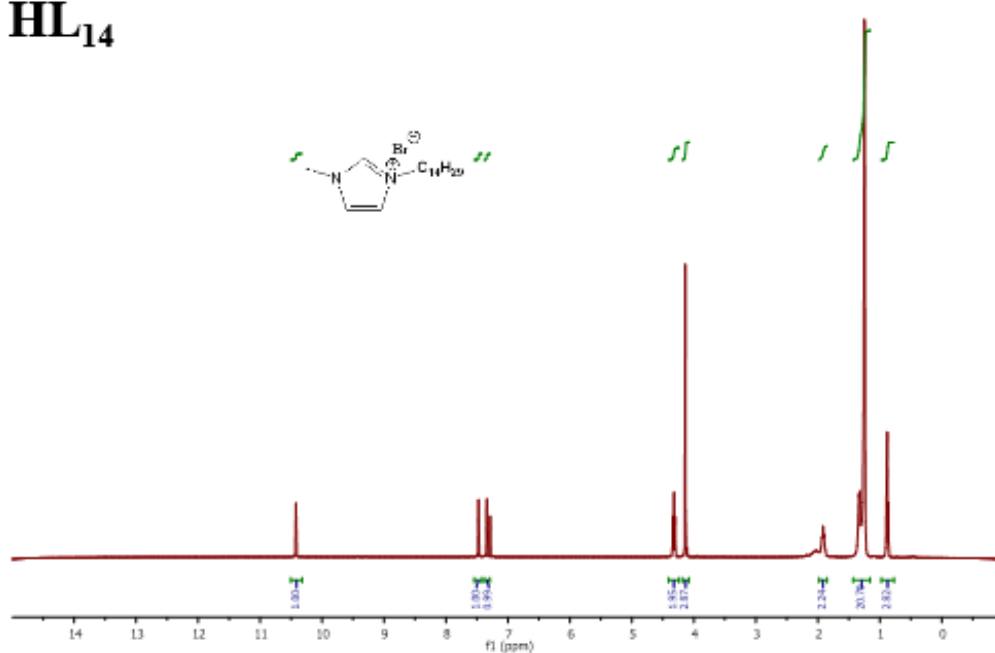
HL₁₂



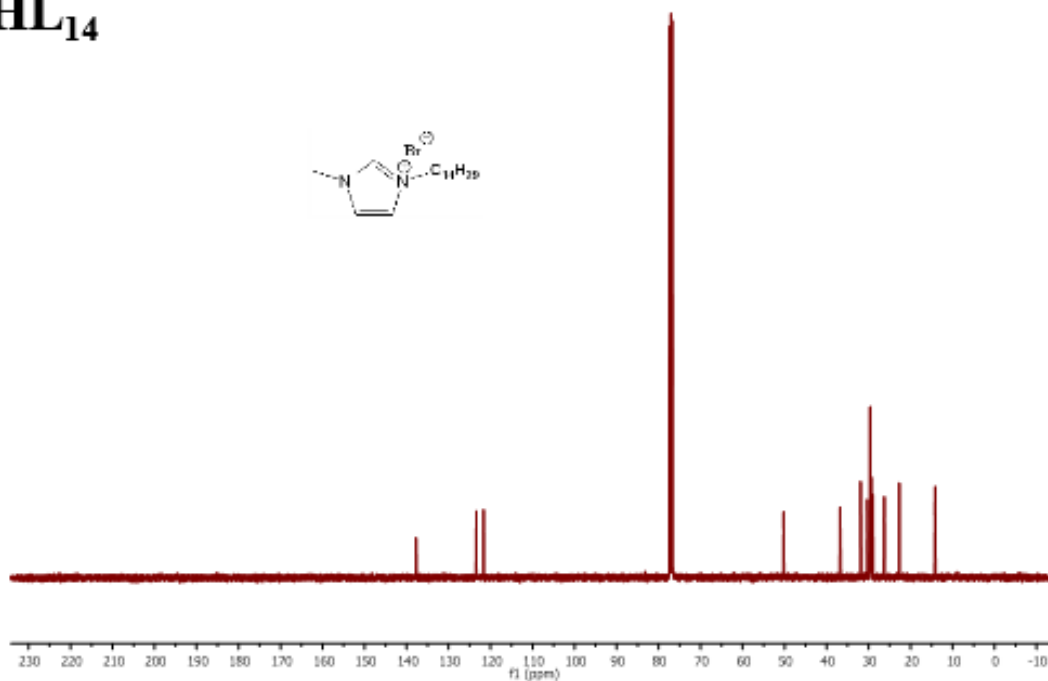
HL₁₂



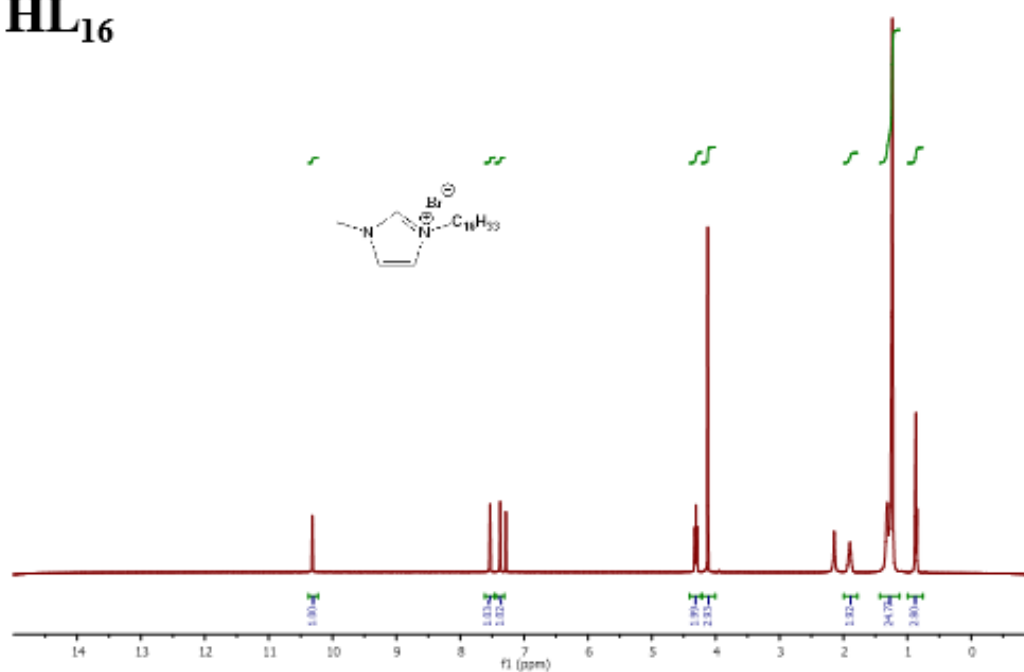
HL₁₄



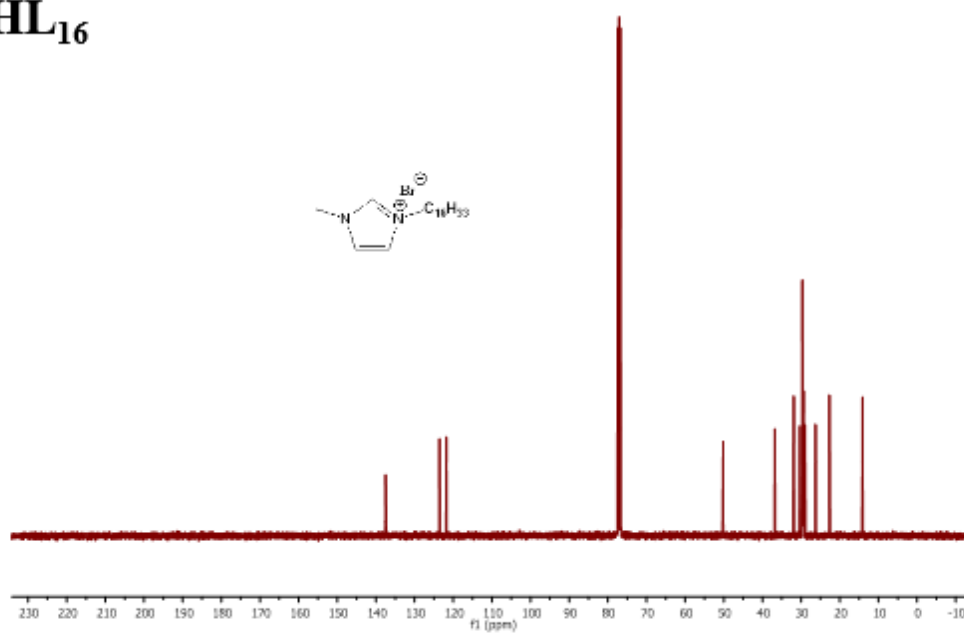
HL₁₄



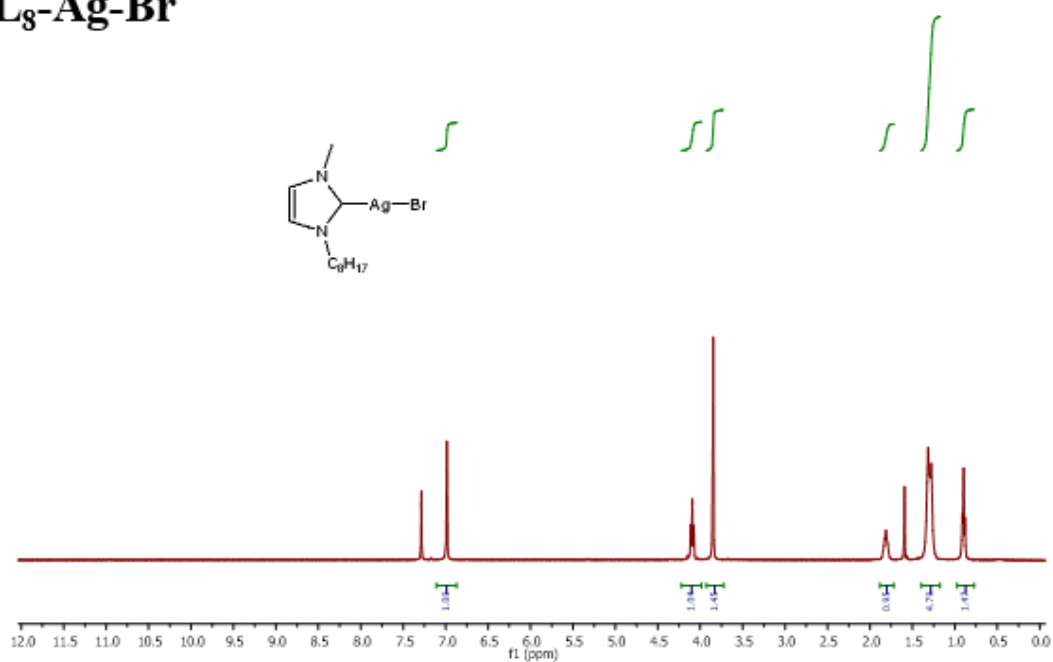
HL₁₆



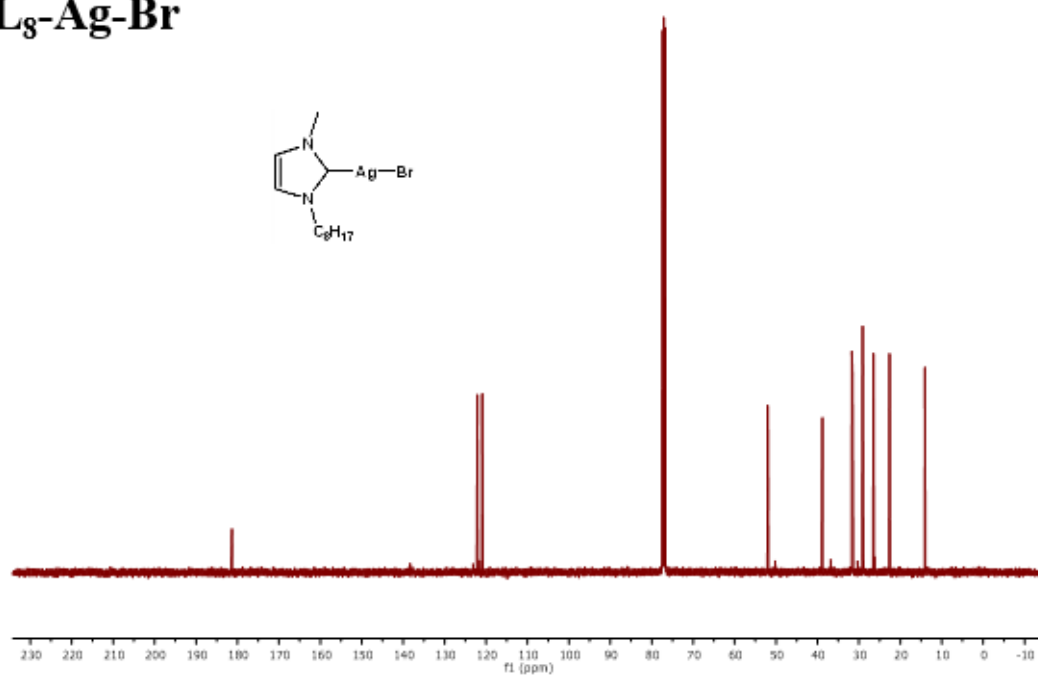
HL₁₆



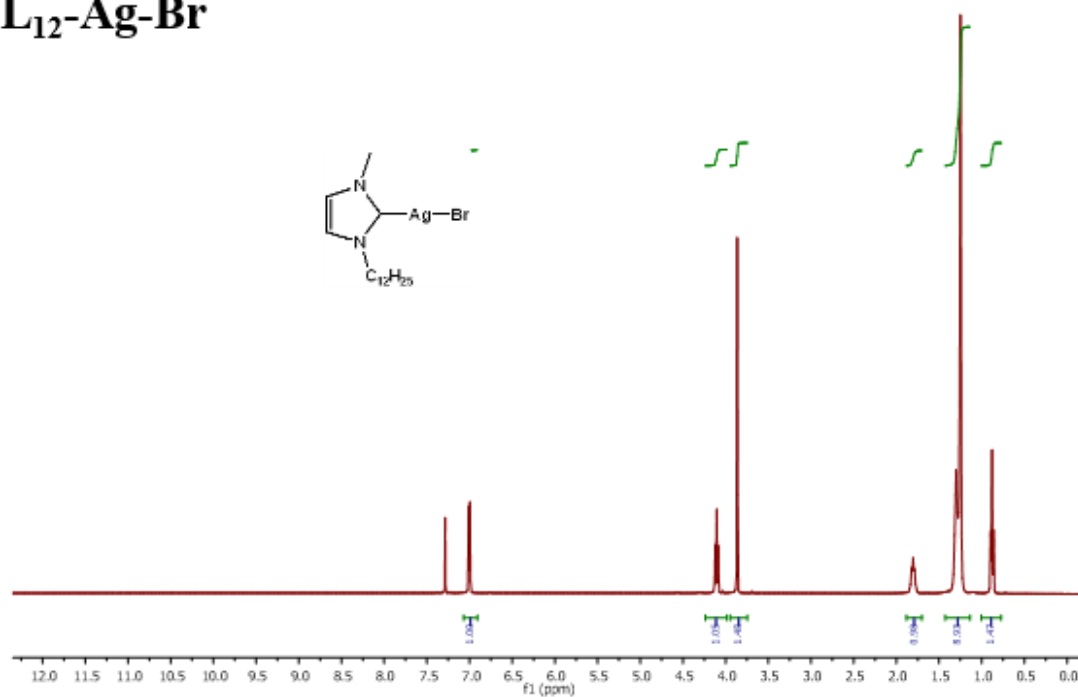
L₈-Ag-Br



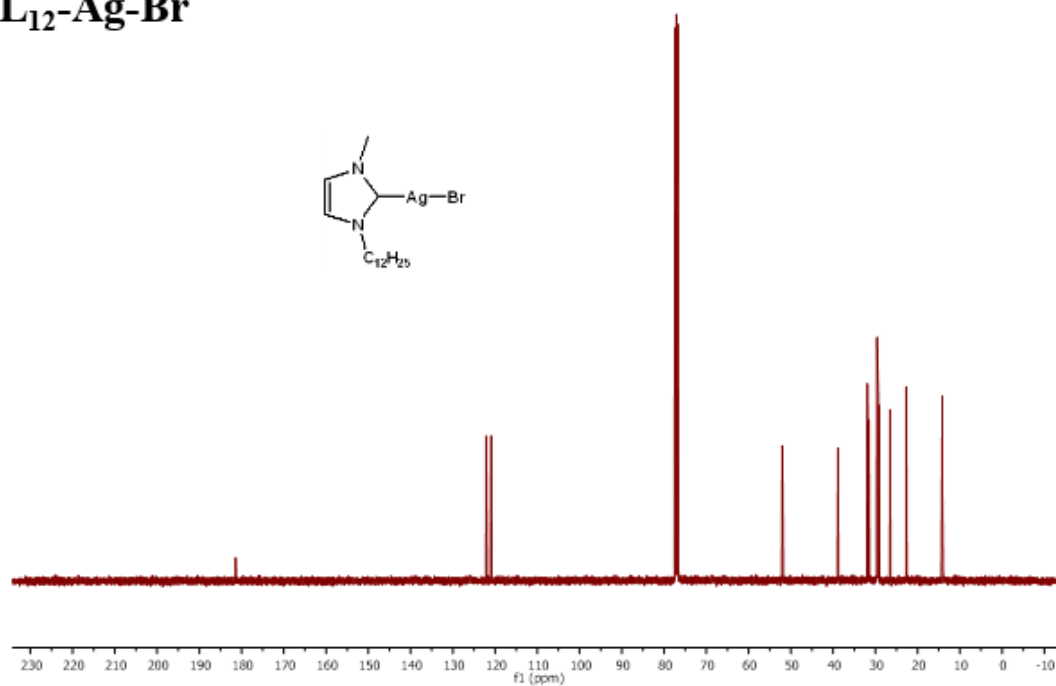
L₈-Ag-Br



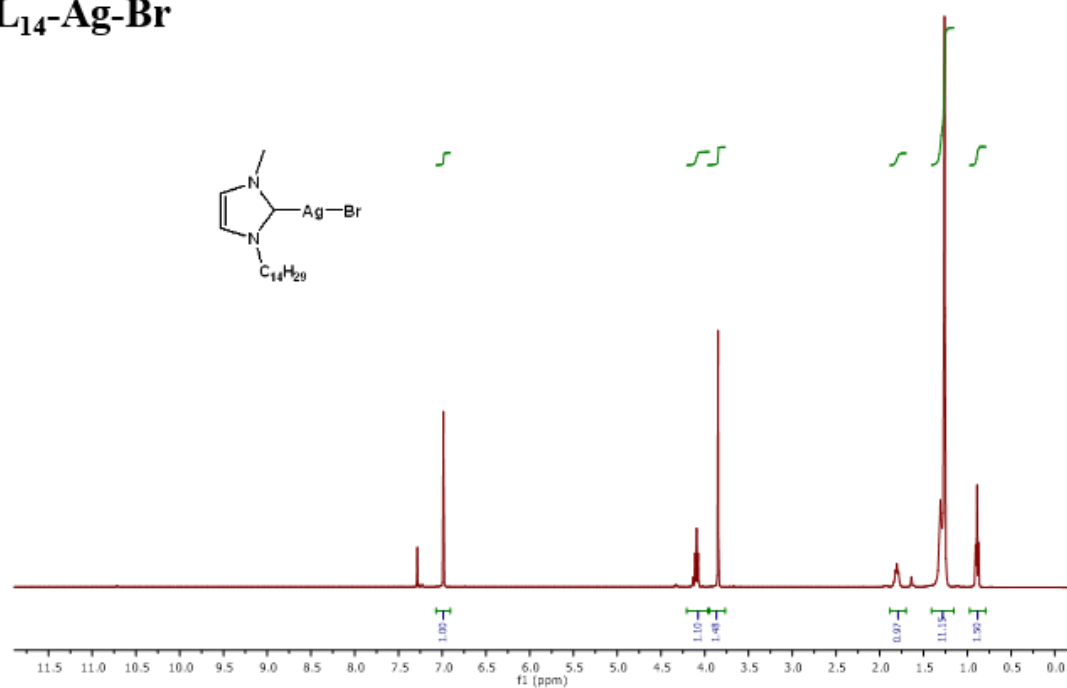
L₁₂-Ag-Br



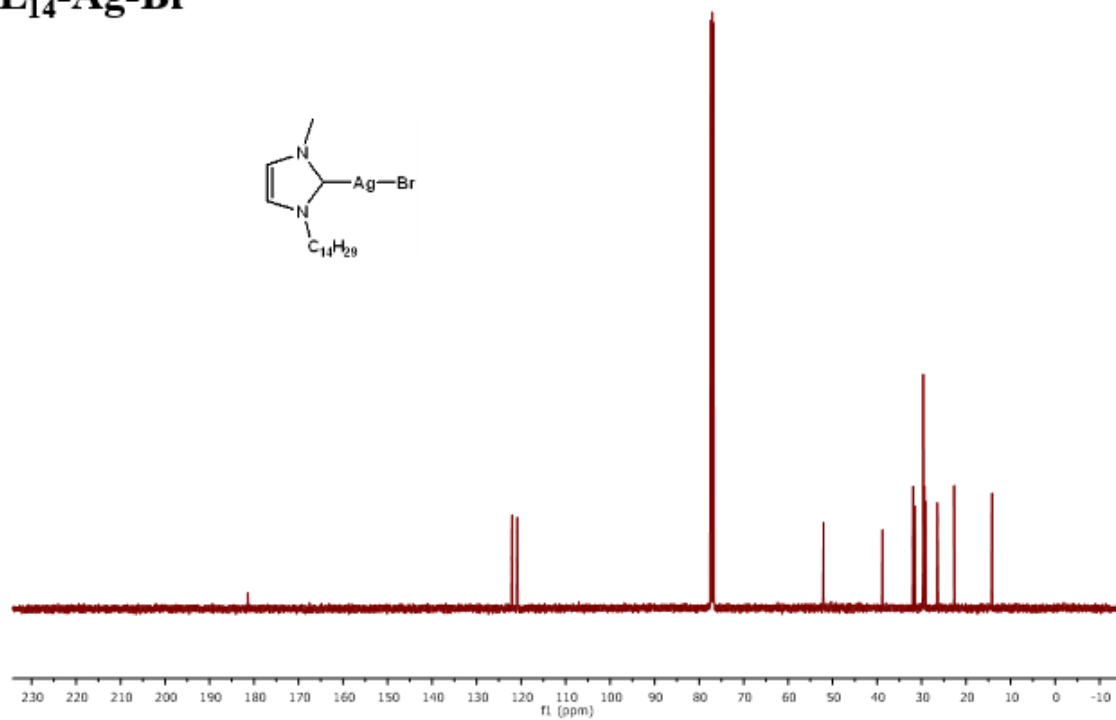
L₁₂-Ag-Br



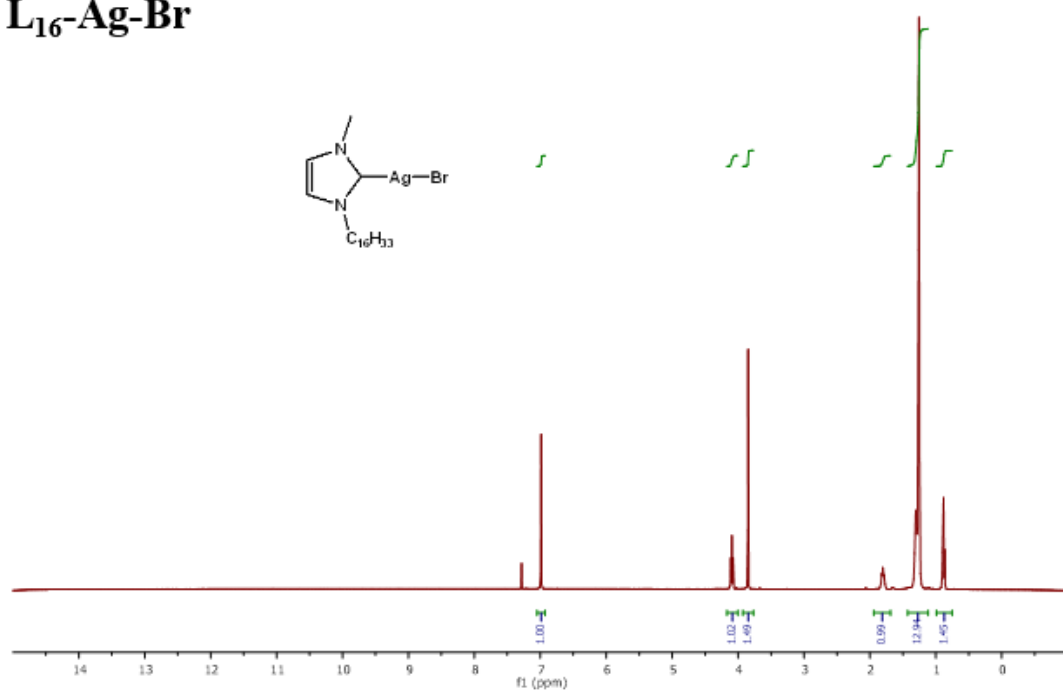
L₁₄-Ag-Br



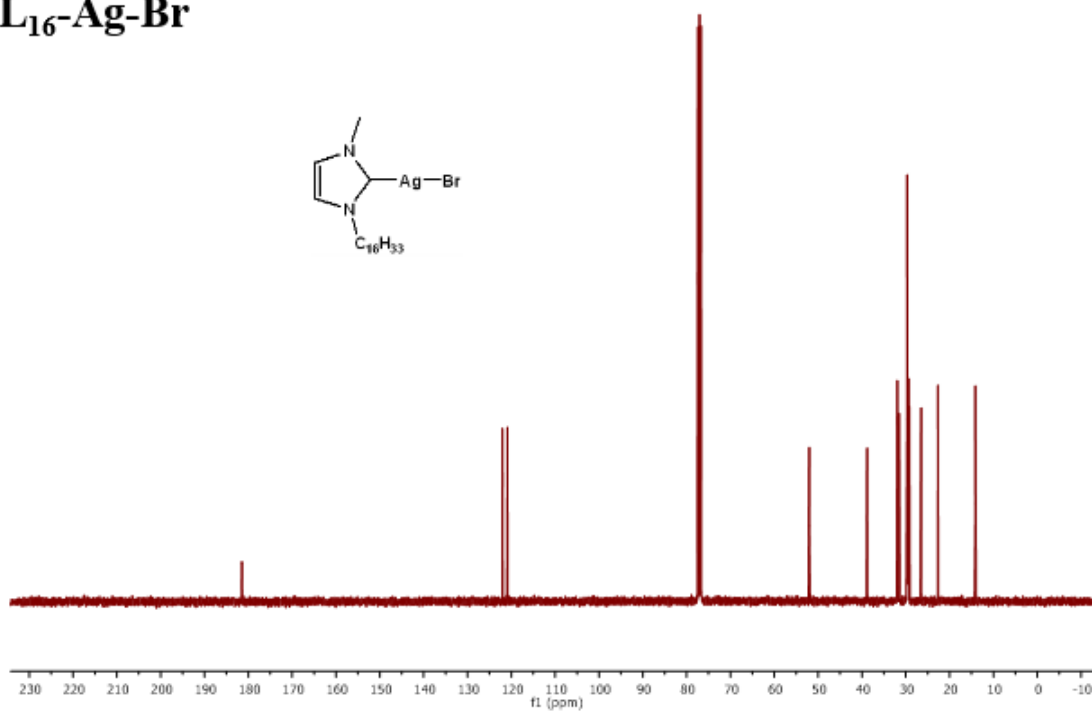
L₁₄-Ag-Br



L₁₆-Ag-Br

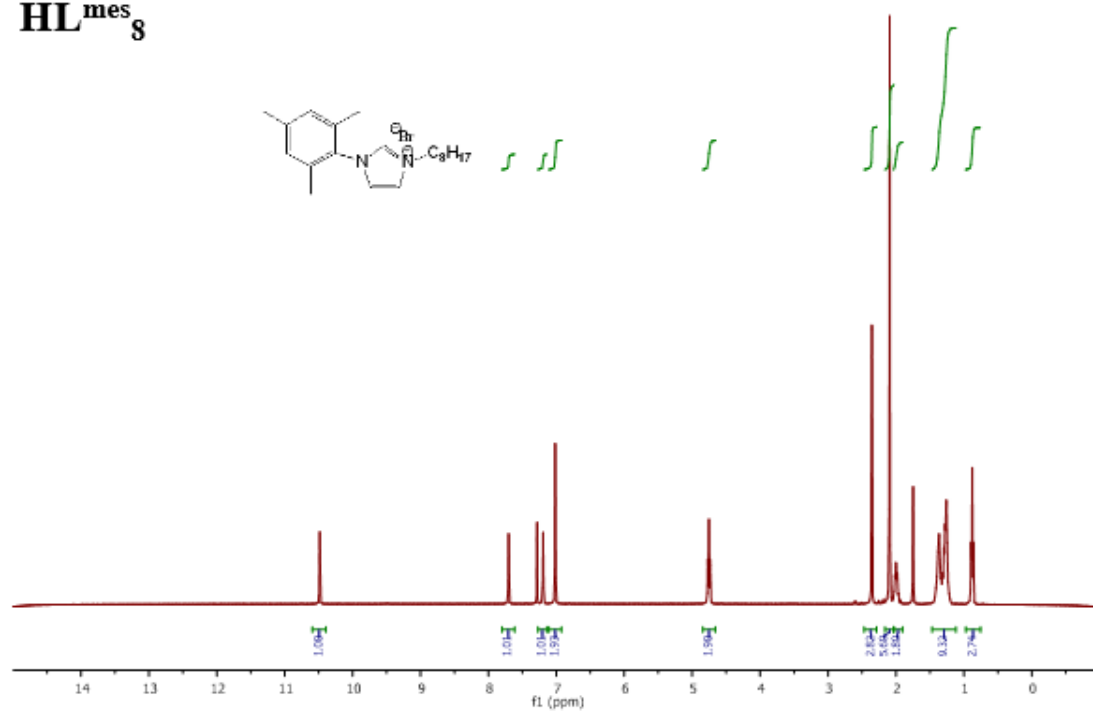


L₁₆-Ag-Br

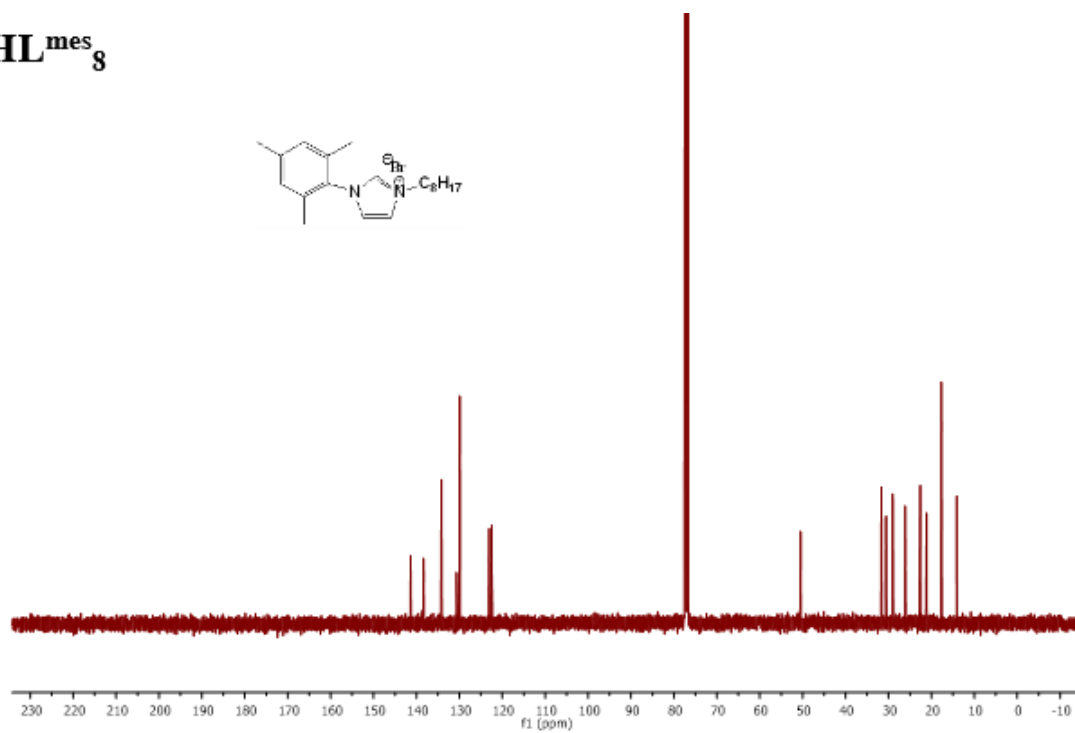


Appendix B: ^1H and ^{13}C NMR spectra of **HL^{mes}₈₋₁₆** and **L^{mes}₈₋₁₆-Ag-Br**

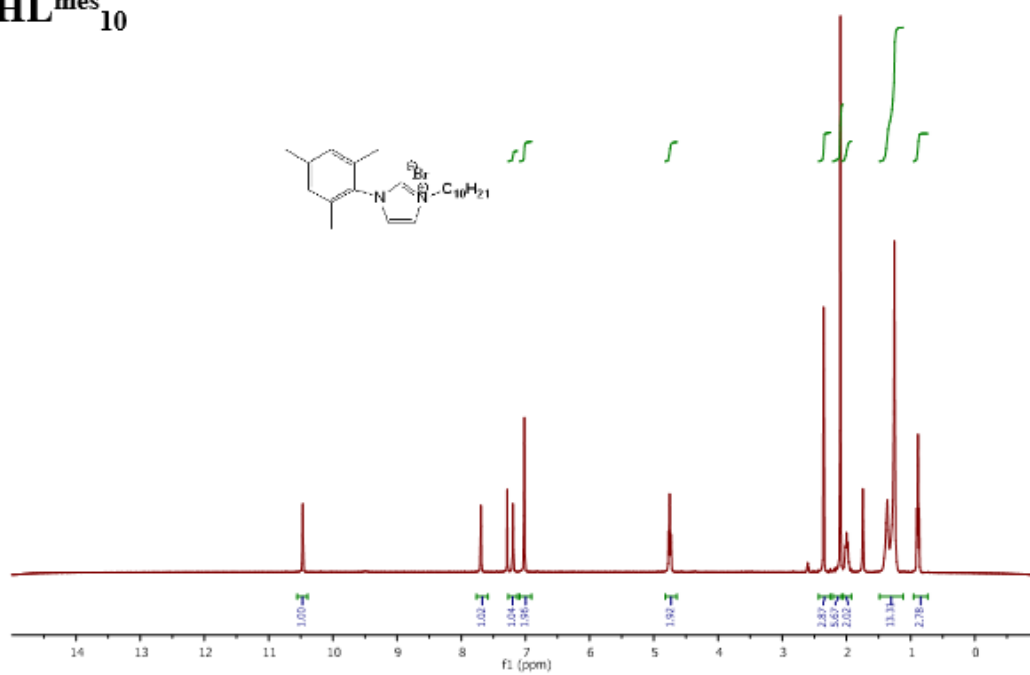
HL^{mes}₈



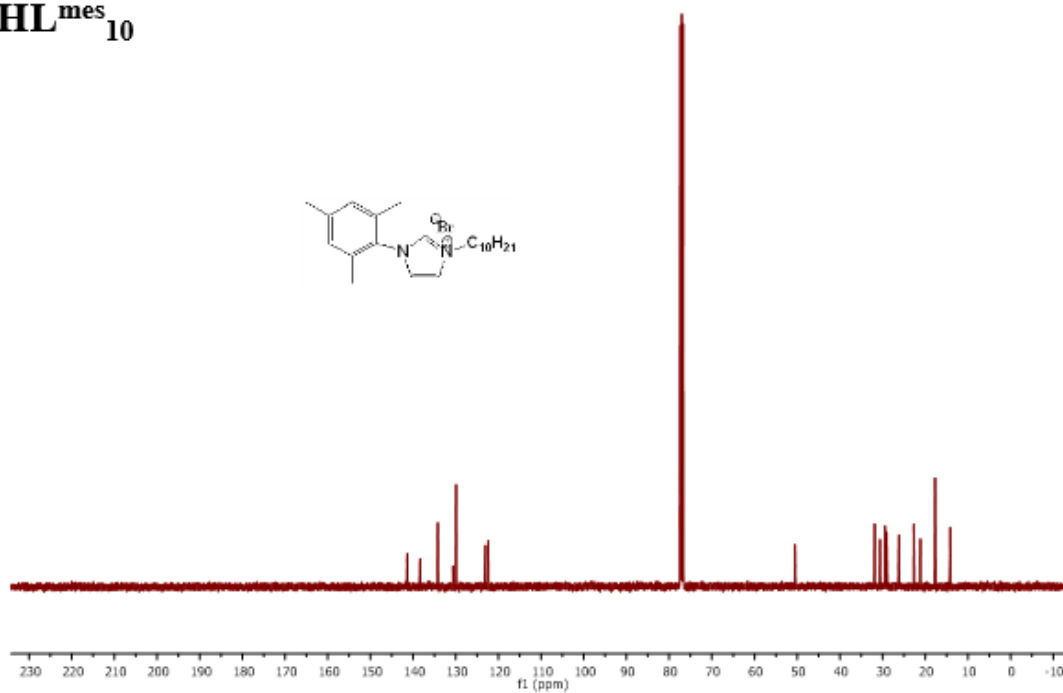
HL^{mes}₈



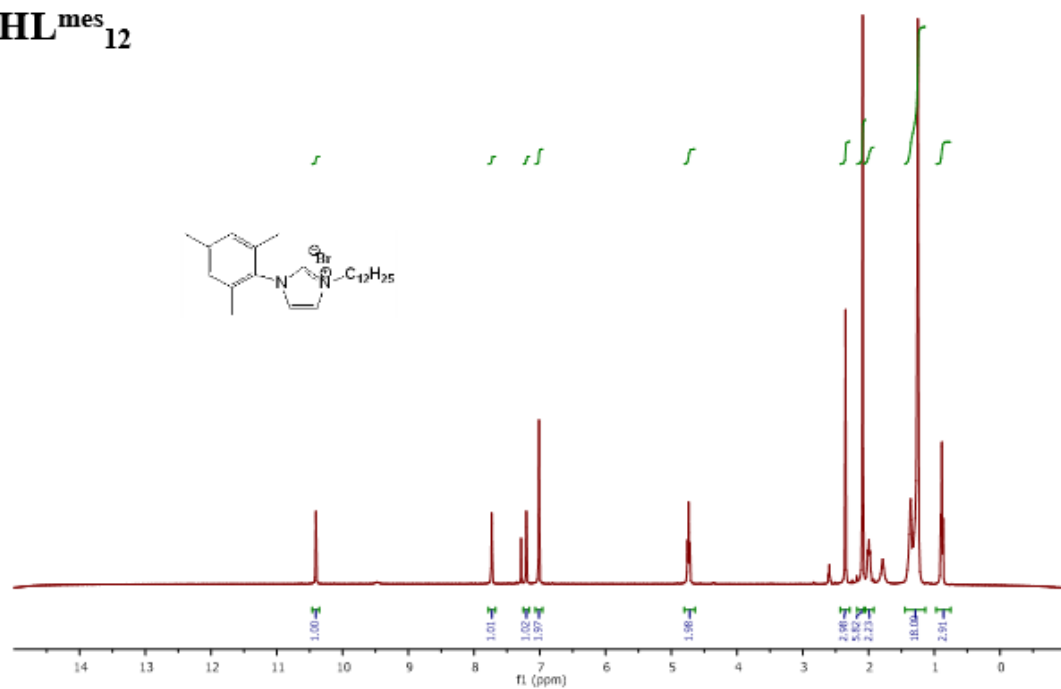
HL^{mes}₁₀



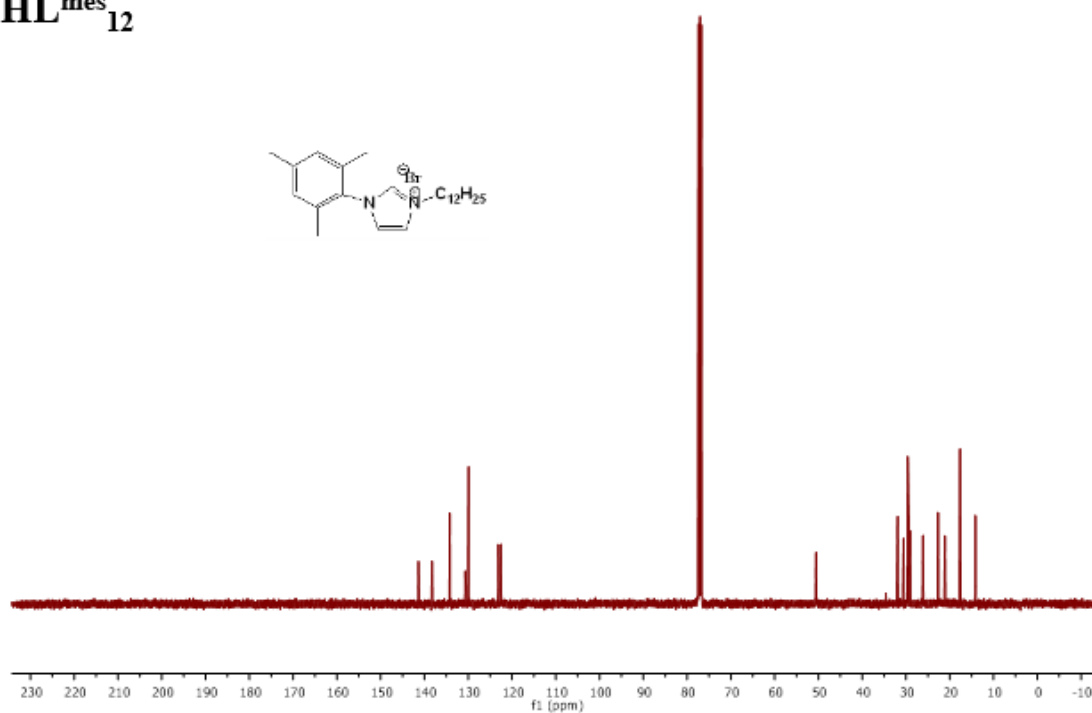
HL^{mes}₁₀



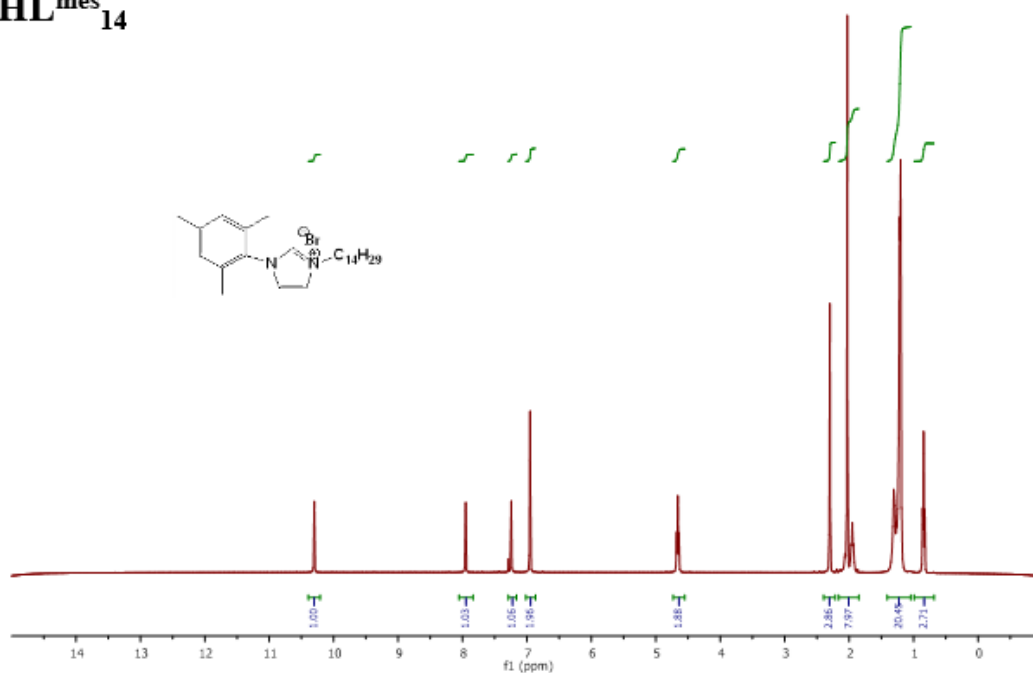
HL^{mes}₁₂



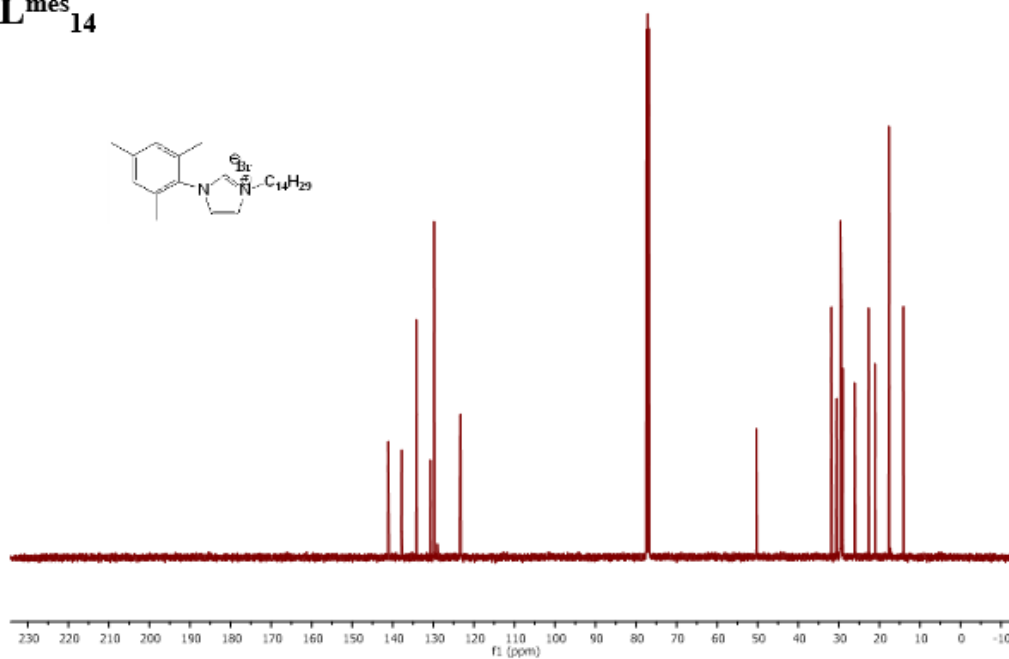
HL^{mes}₁₂



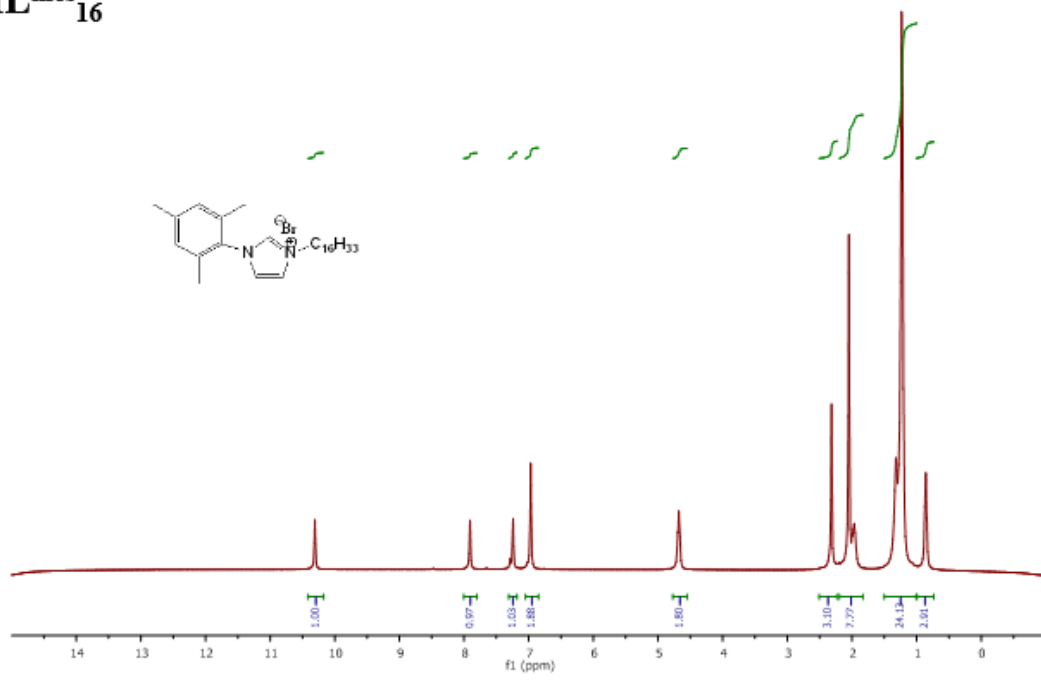
HL^{mes}₁₄



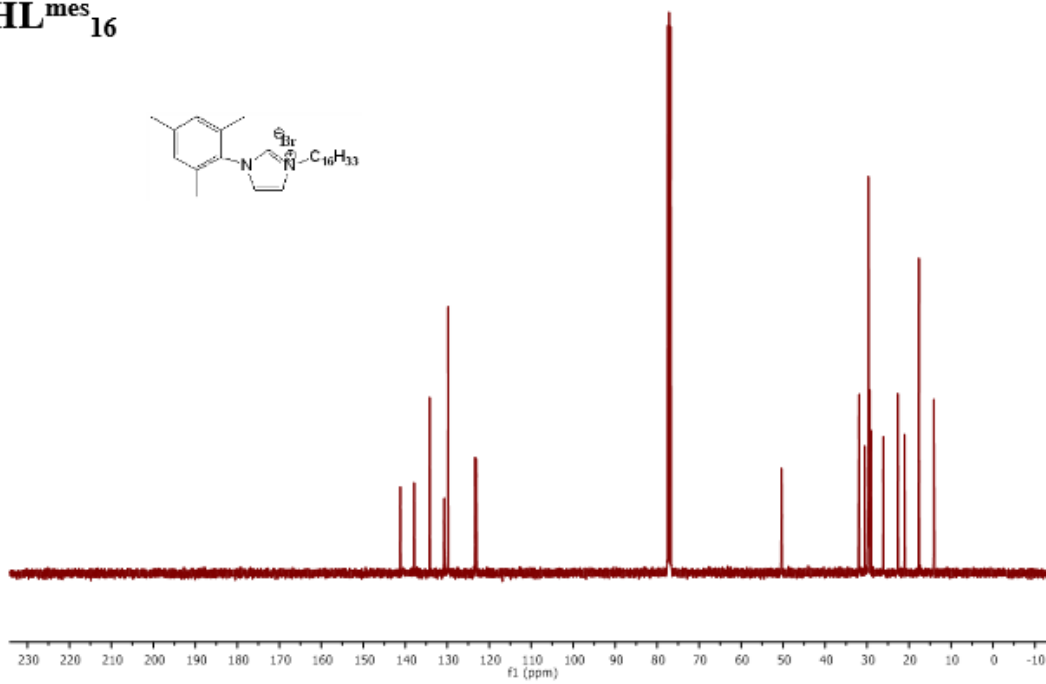
HL^{mes}₁₄



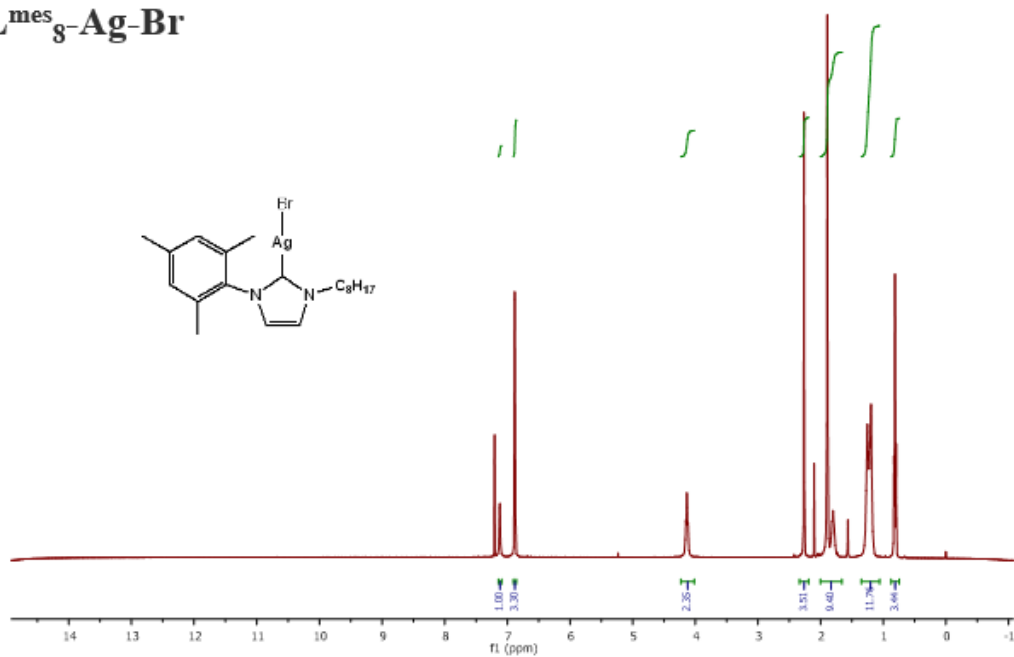
HL^{mes}₁₆



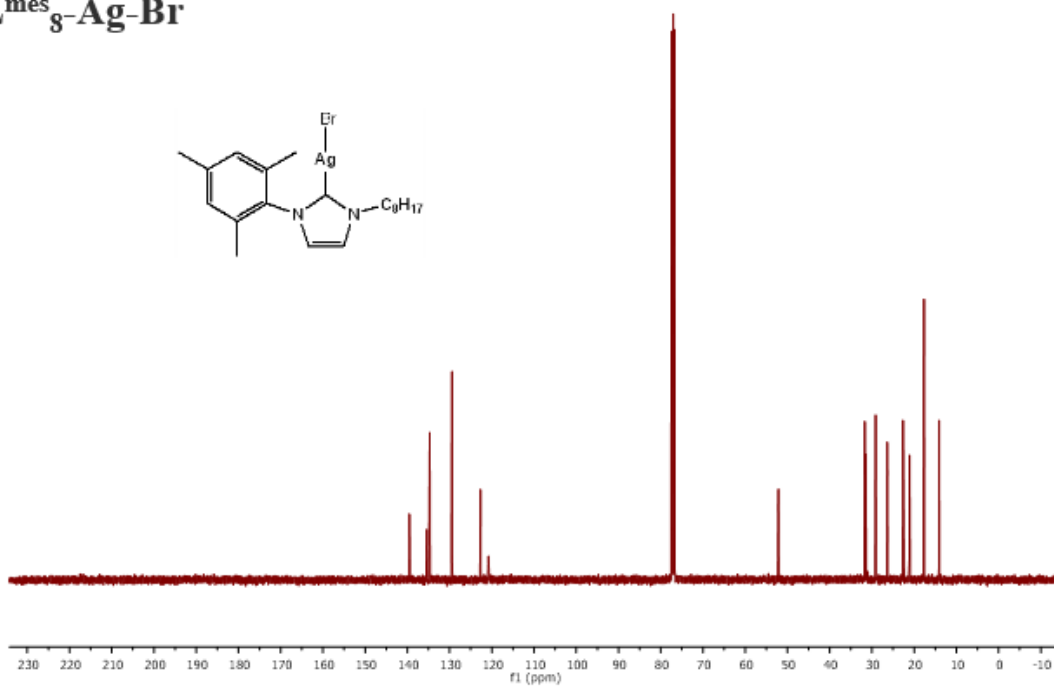
HL^{mes}₁₆



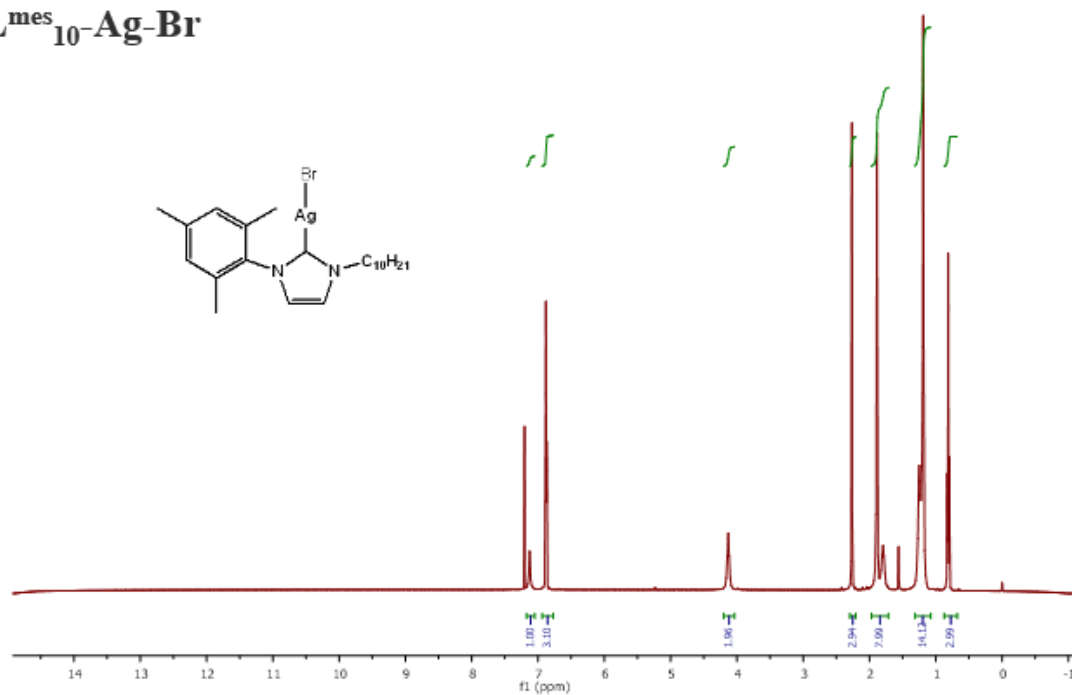
$L^{mes}_8-Ag-Br$



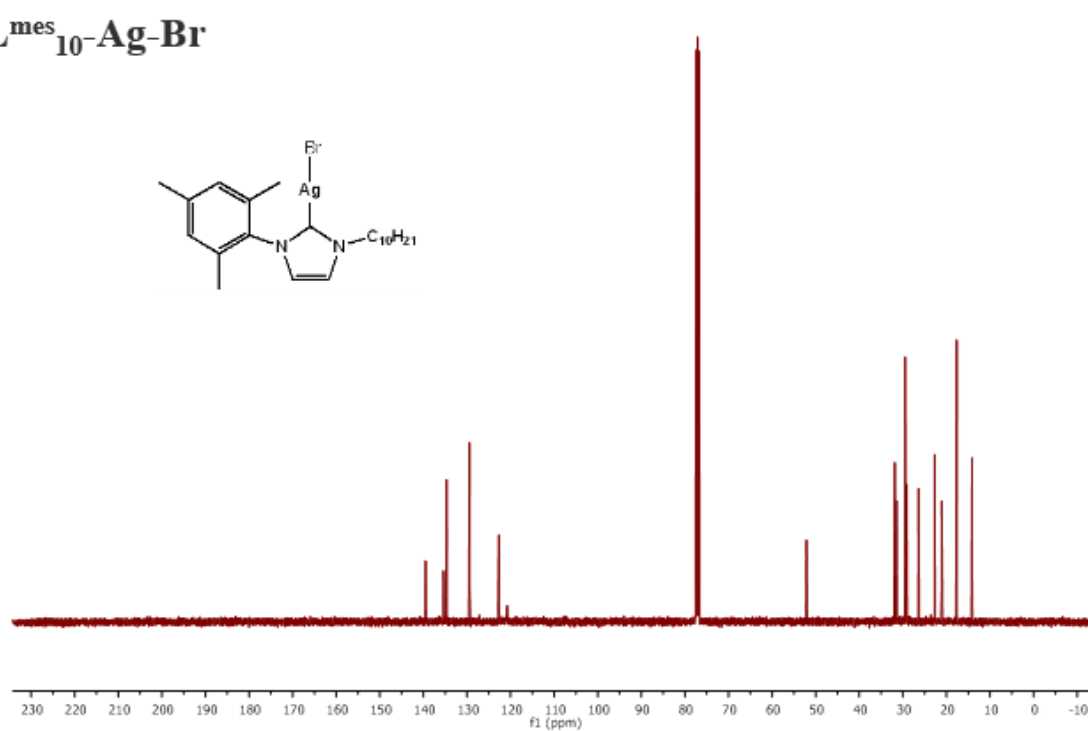
$L^{mes}_8-Ag-Br$



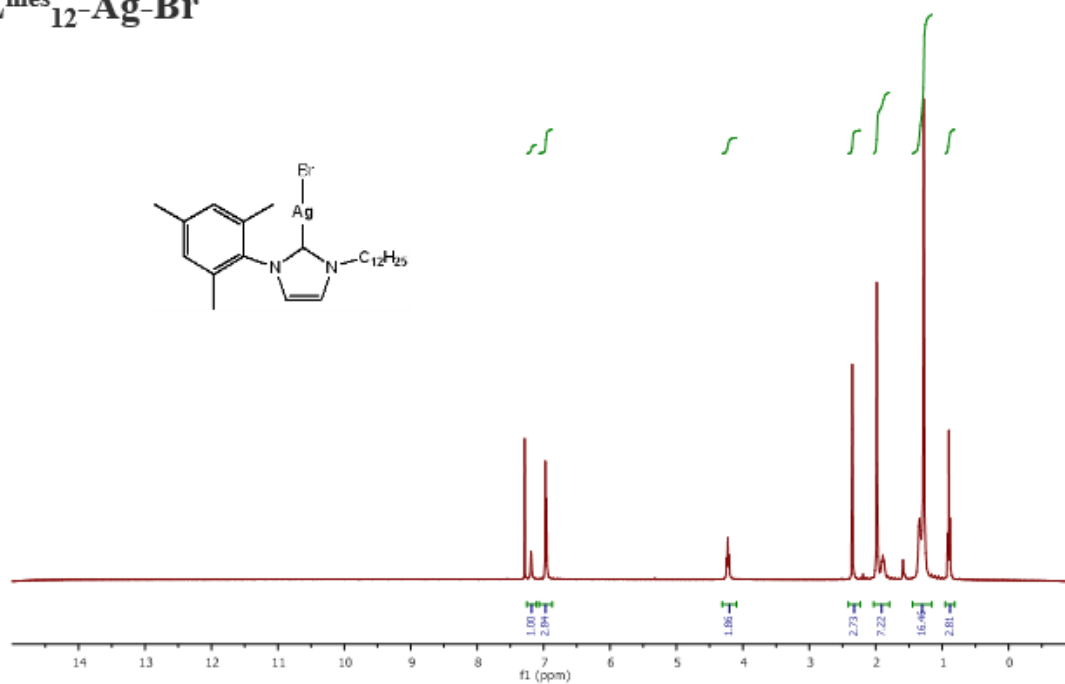
$L^{mes}_{10}\text{-Ag-Br}$



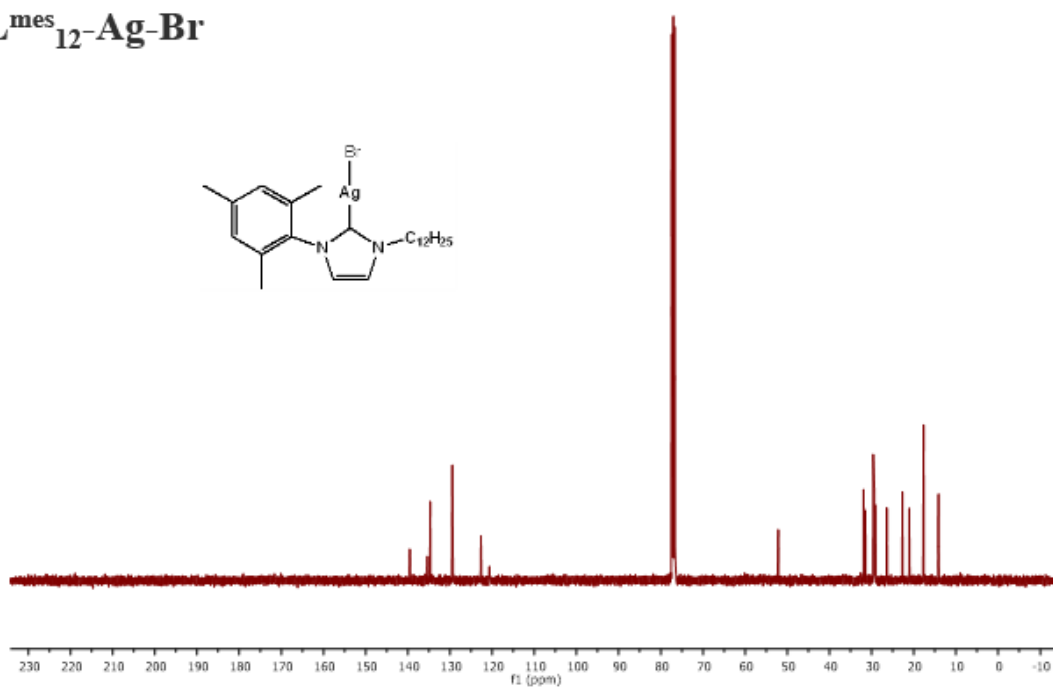
$L^{mes}_{10}\text{-Ag-Br}$



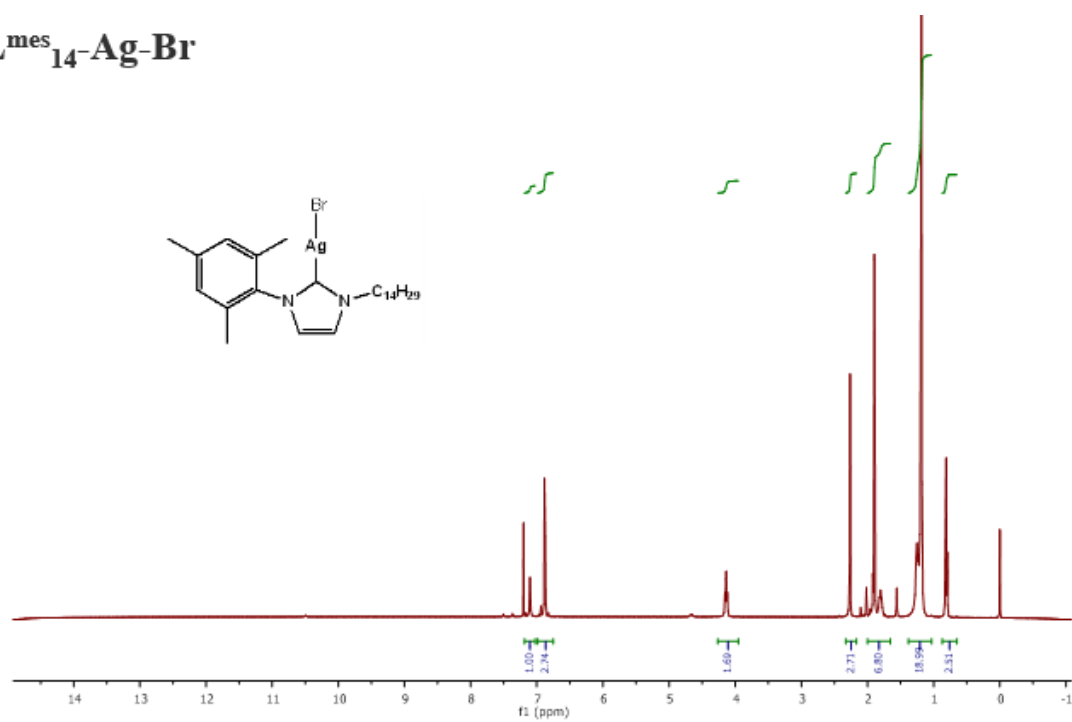
$L^{mes}_{12}\text{-Ag-Br}$



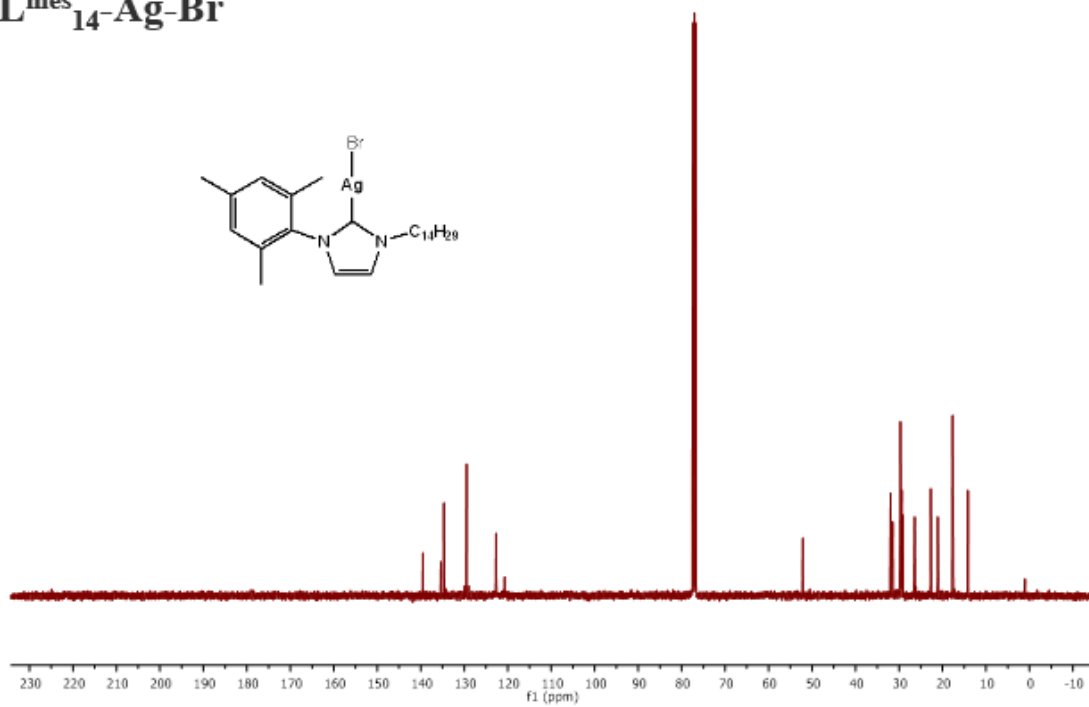
$L^{mes}_{12}\text{-Ag-Br}$



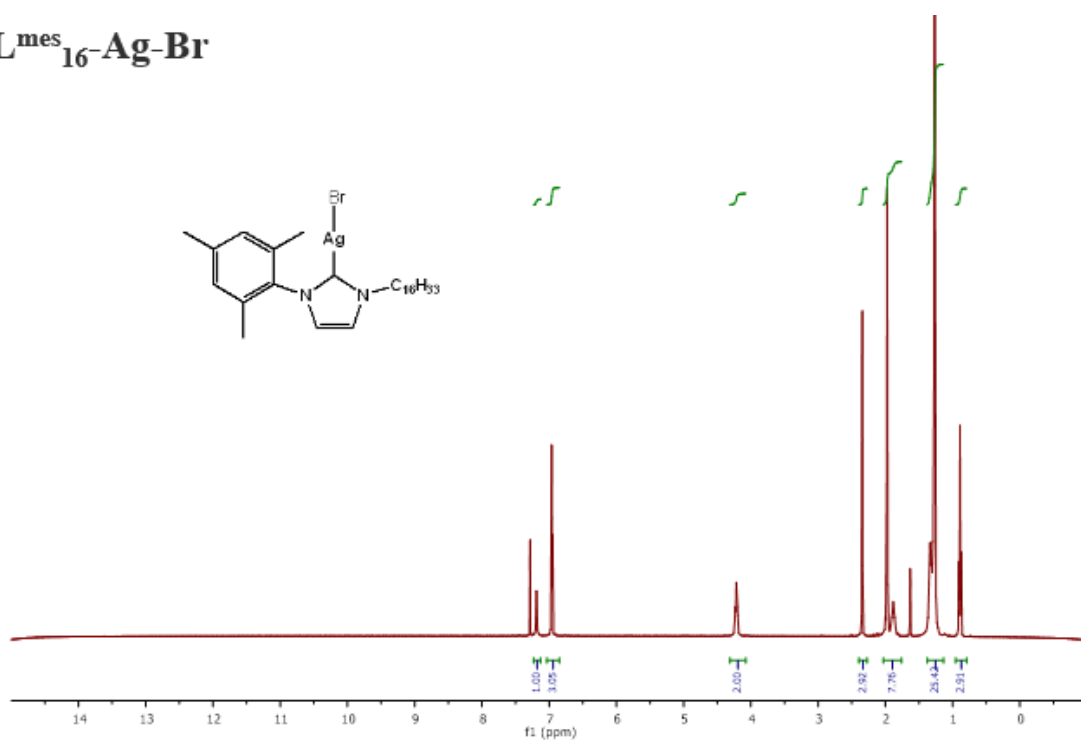
$L^{mes}_{14}\text{-Ag-Br}$



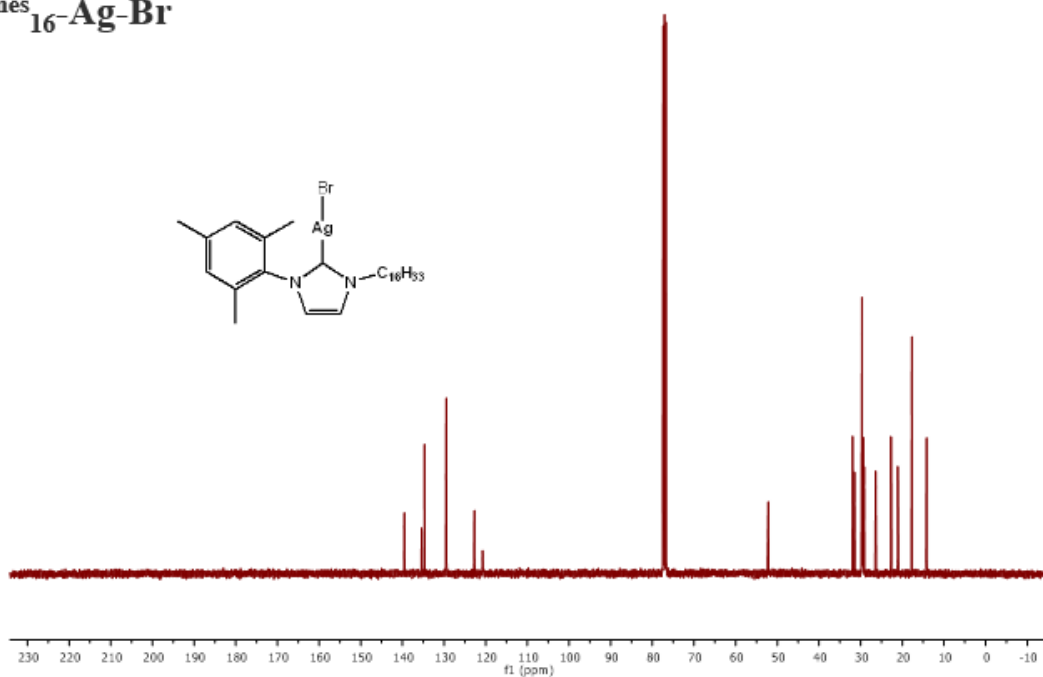
$L^{mes}_{14}\text{-Ag-Br}$



$L^{mes}_{16}\text{-Ag-Br}$

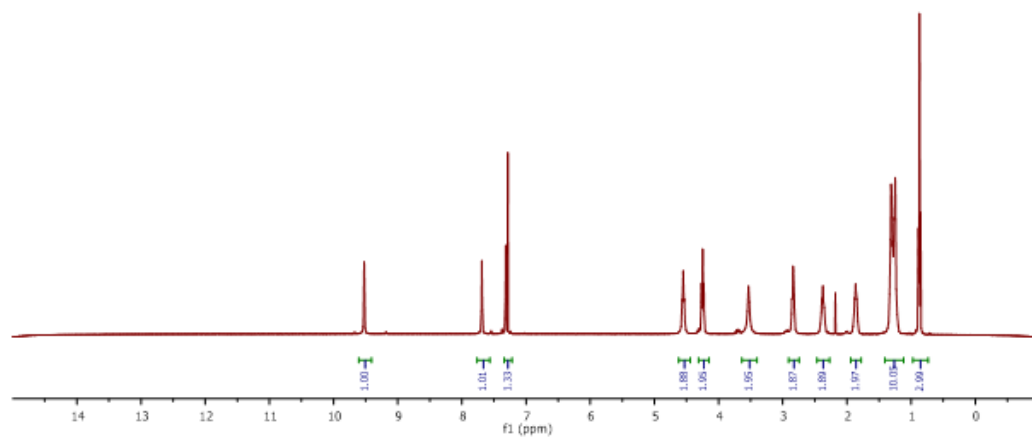
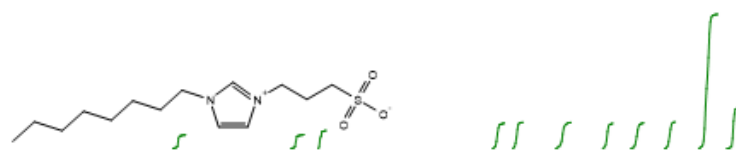


$L^{mes}_{16}\text{-Ag-Br}$

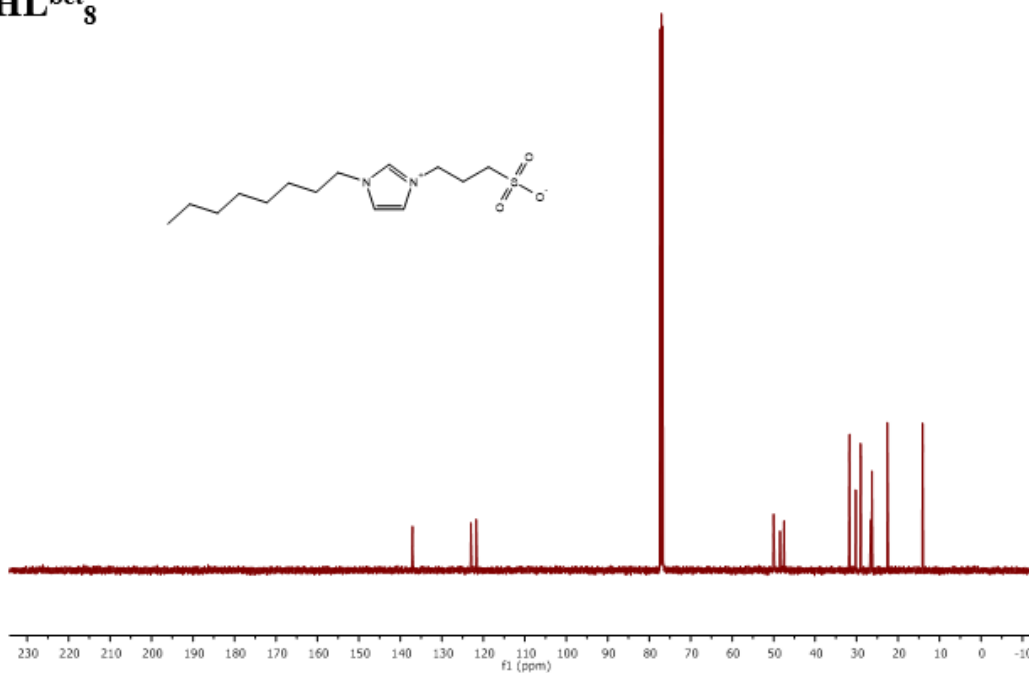
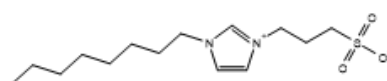


Appendix C: ^1H and ^{13}C NMR spectra of $\text{HL}^{\text{bet}}_{8-16}$, $\text{Na}[\text{L}^{\text{bet}}_{8-16}\text{-Ag-Cl}]$ and $\text{Na}[\text{PtL}^{\text{bet}}_{8-16}\text{dmsOCl}_2]$

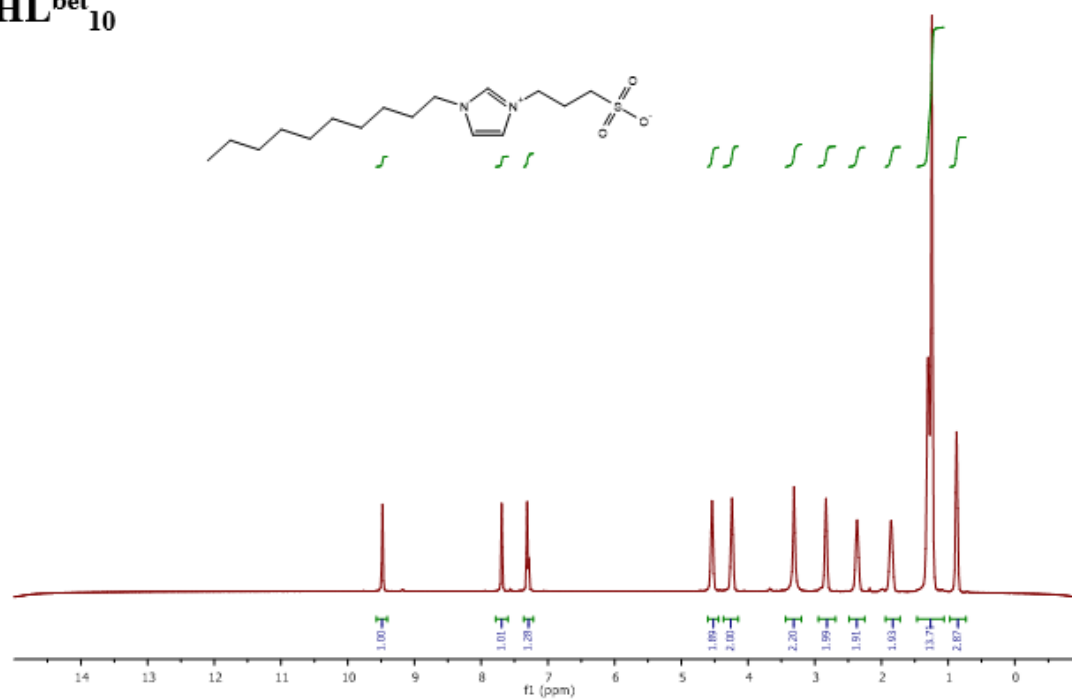
HL^{bet}₈



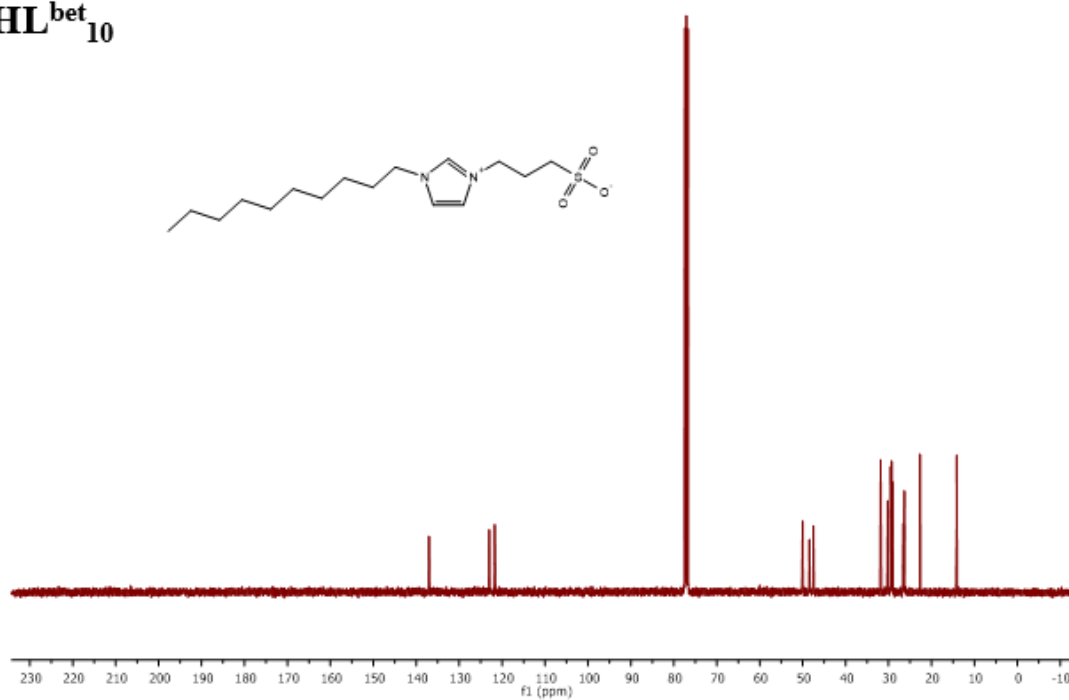
HL^{bet}₈



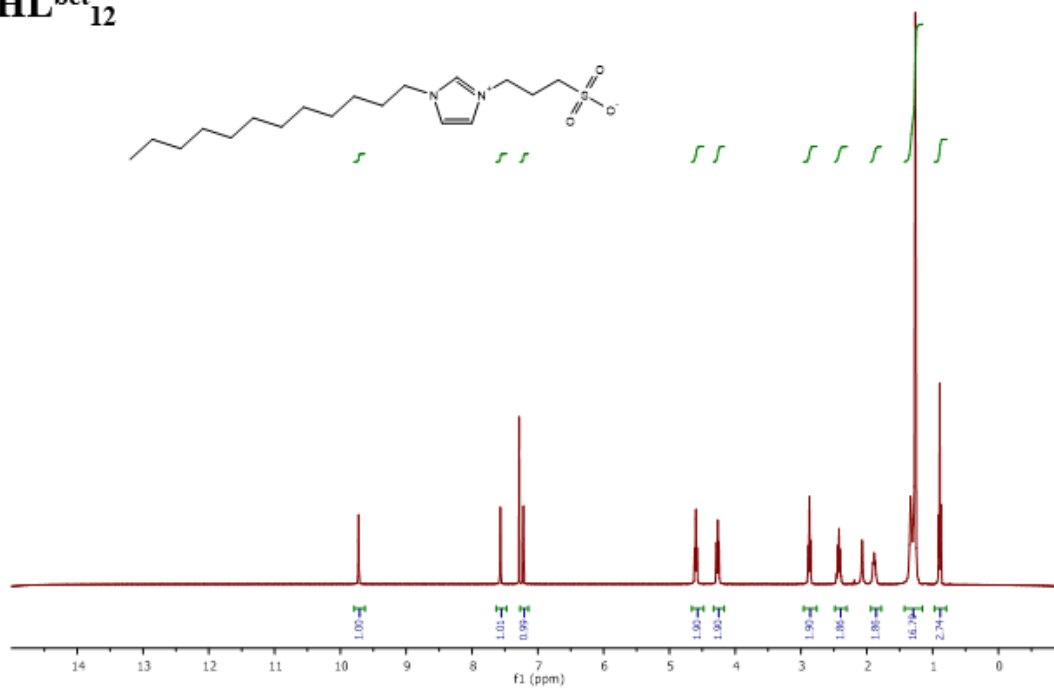
HL^{bet}₁₀



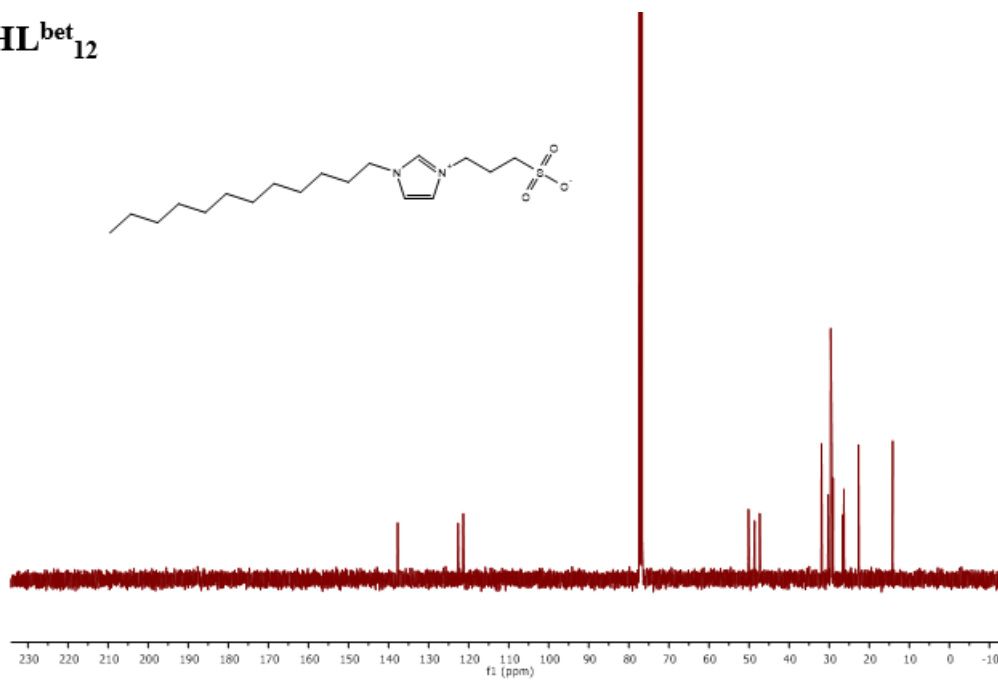
HL^{bet}₁₀



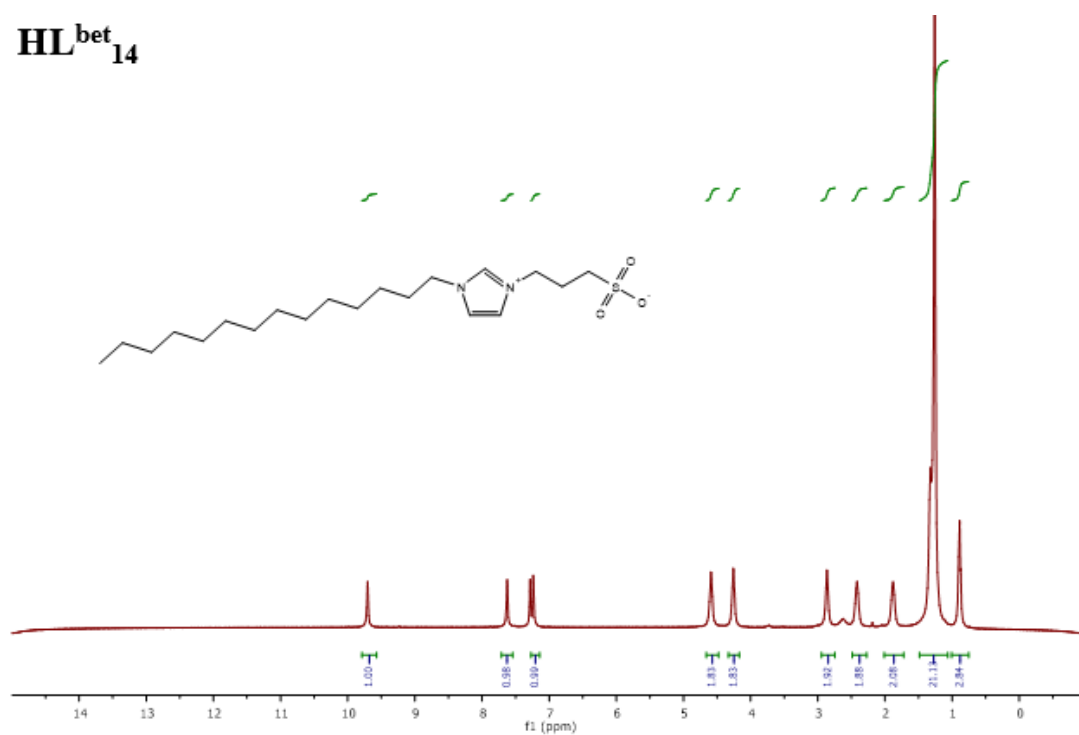
HL^{bet}₁₂



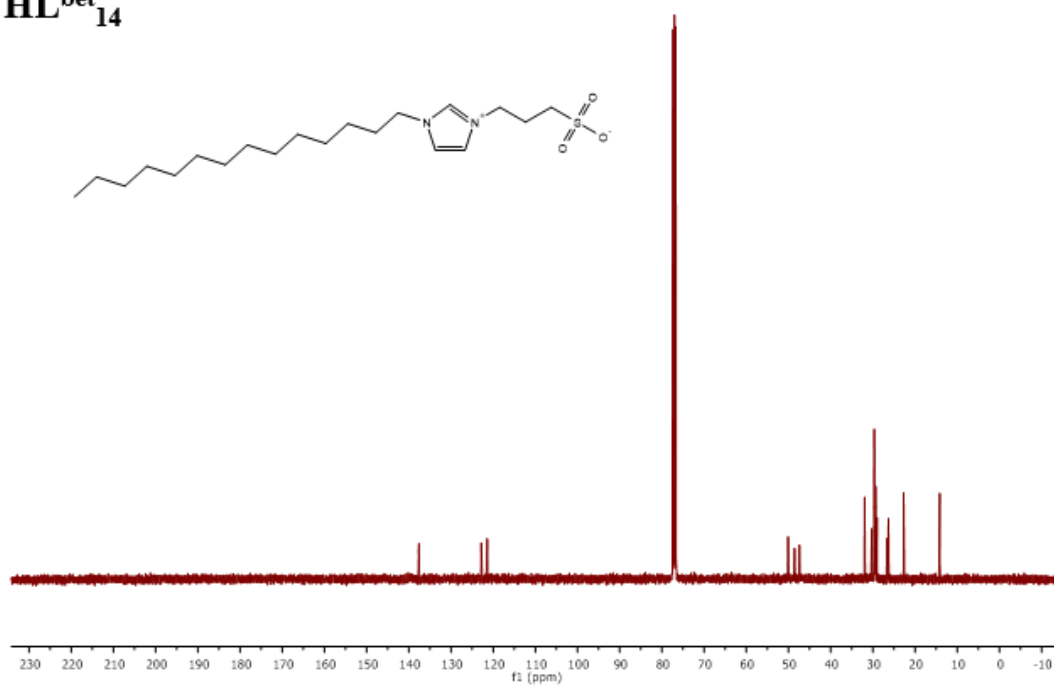
HL^{bet}₁₂



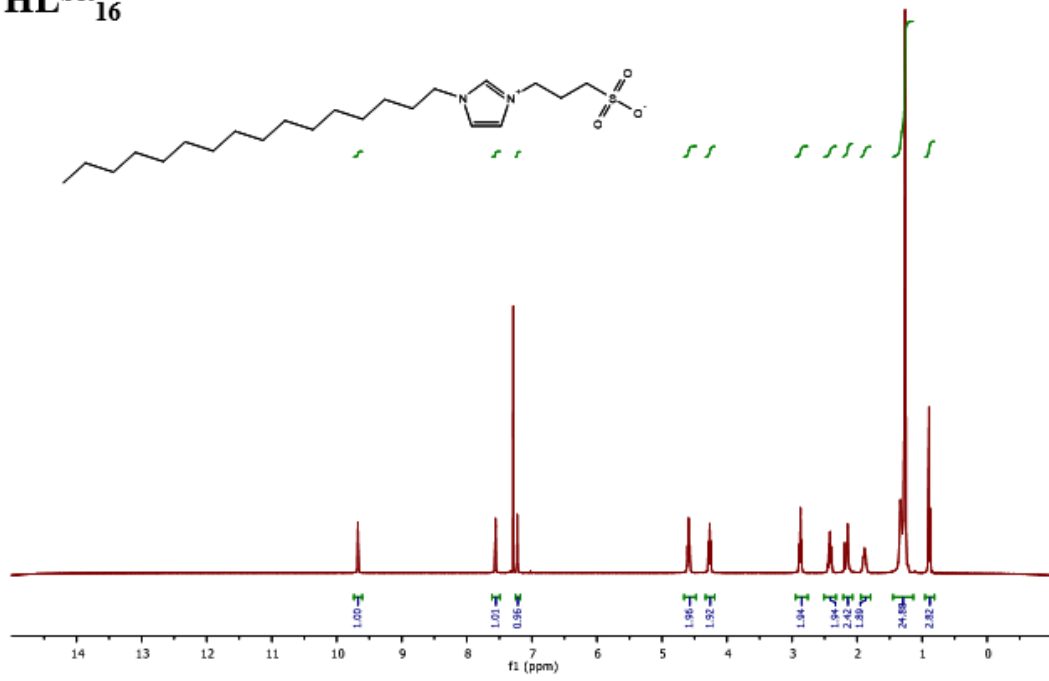
HL^{bet}₁₄



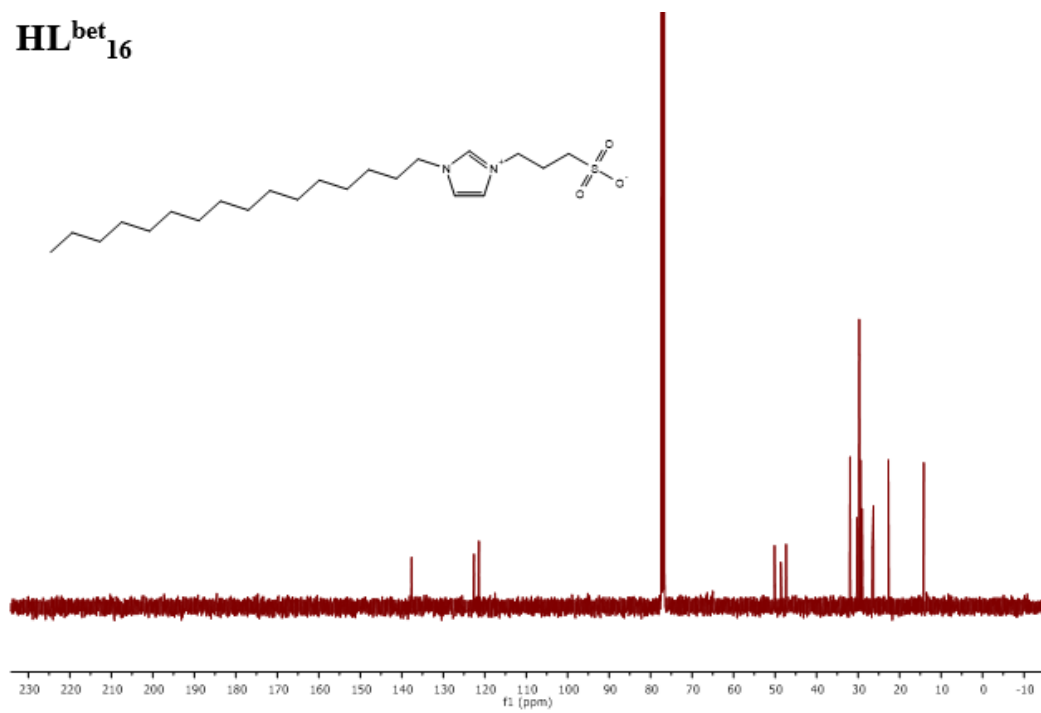
HL^{bet}₁₄



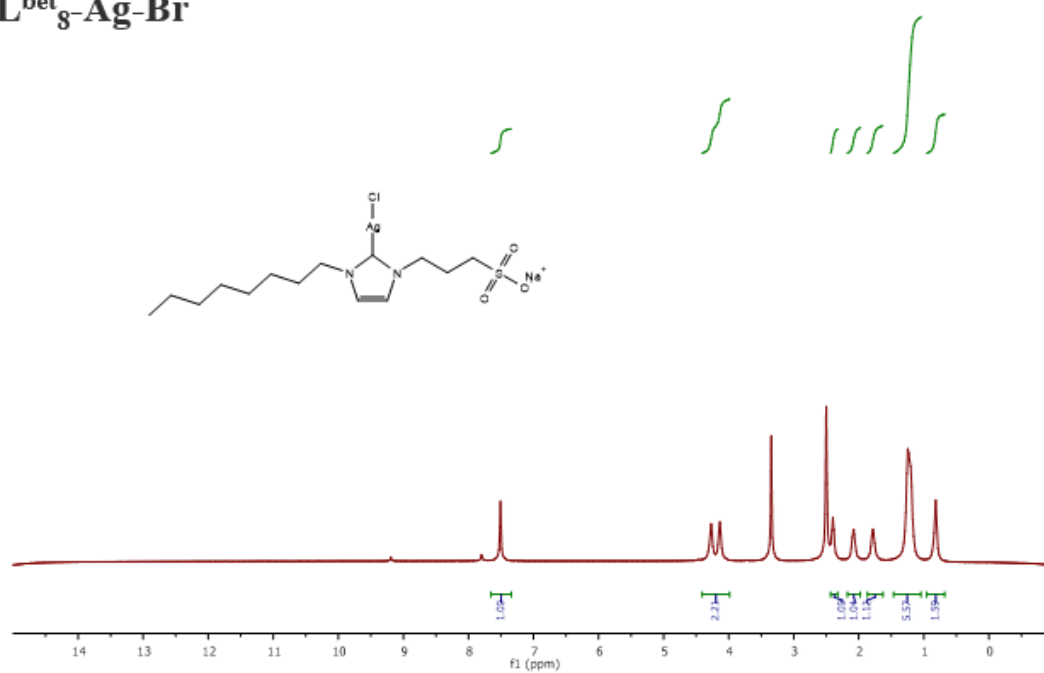
HL^{bet}₁₆



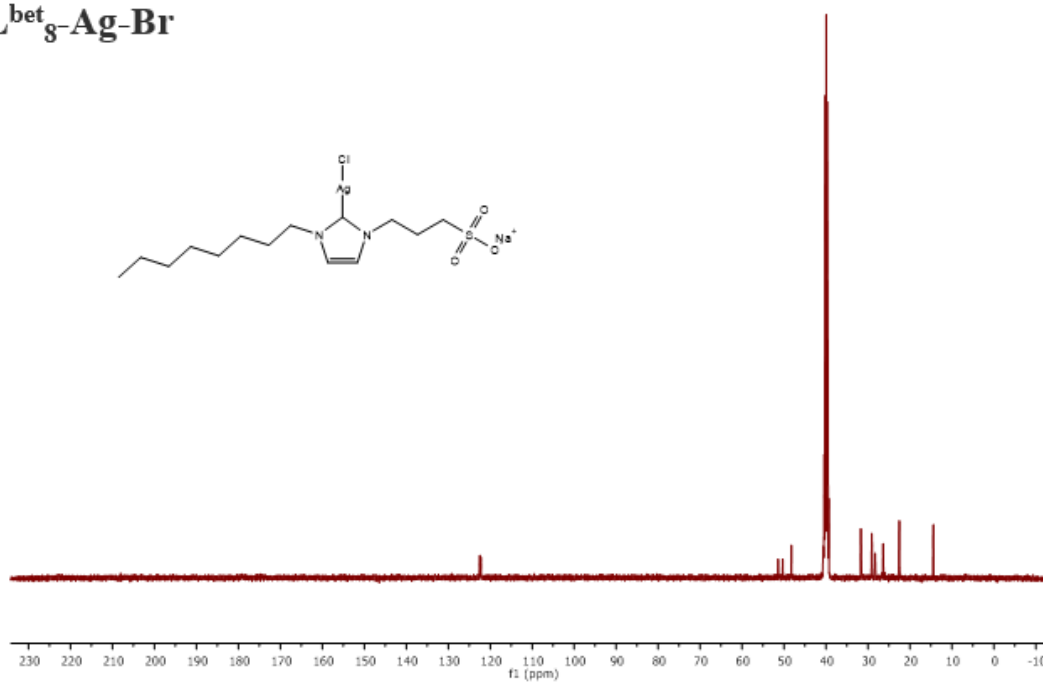
HL^{bet}₁₆



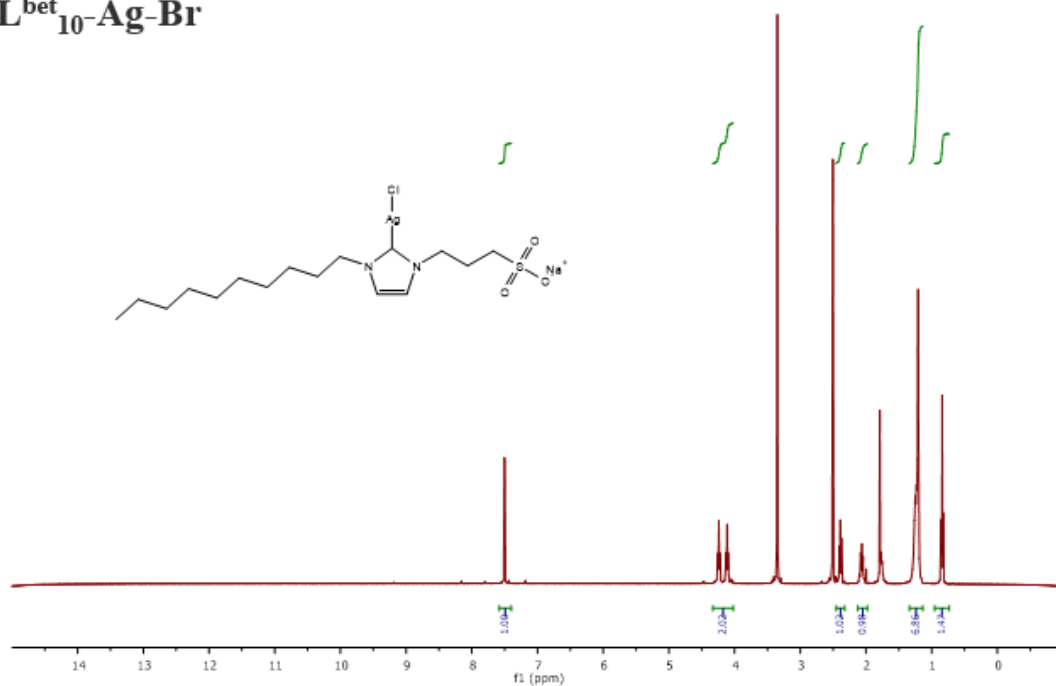
$L^{\text{bet}}_8\text{-Ag-Br}$



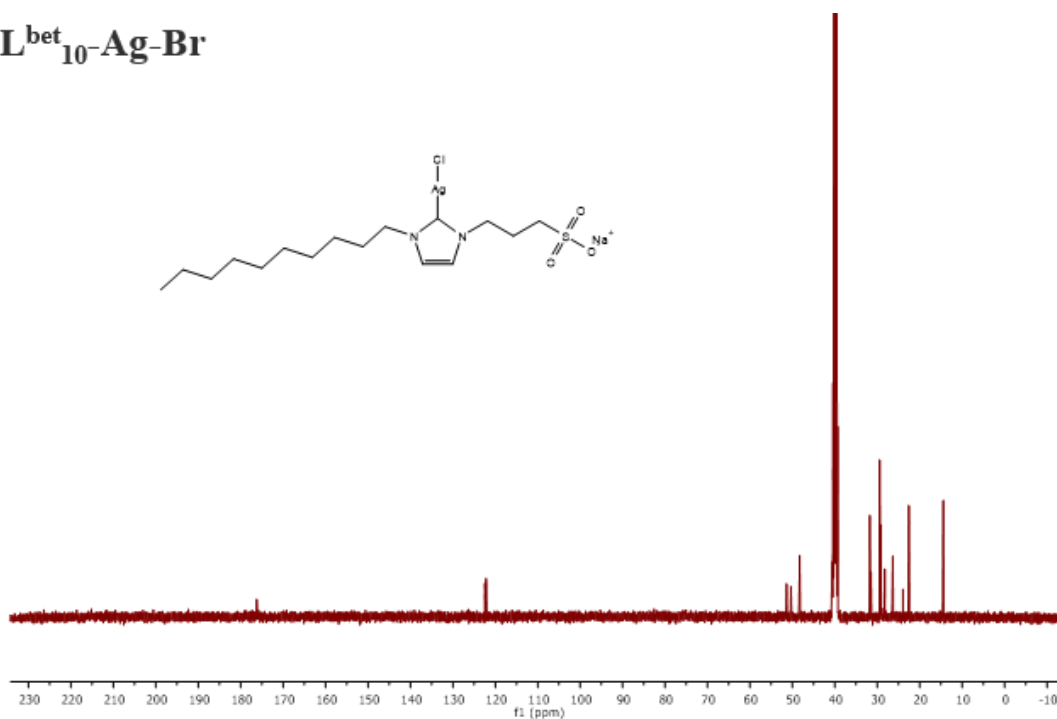
$L^{\text{bet}}_8\text{-Ag-Br}$



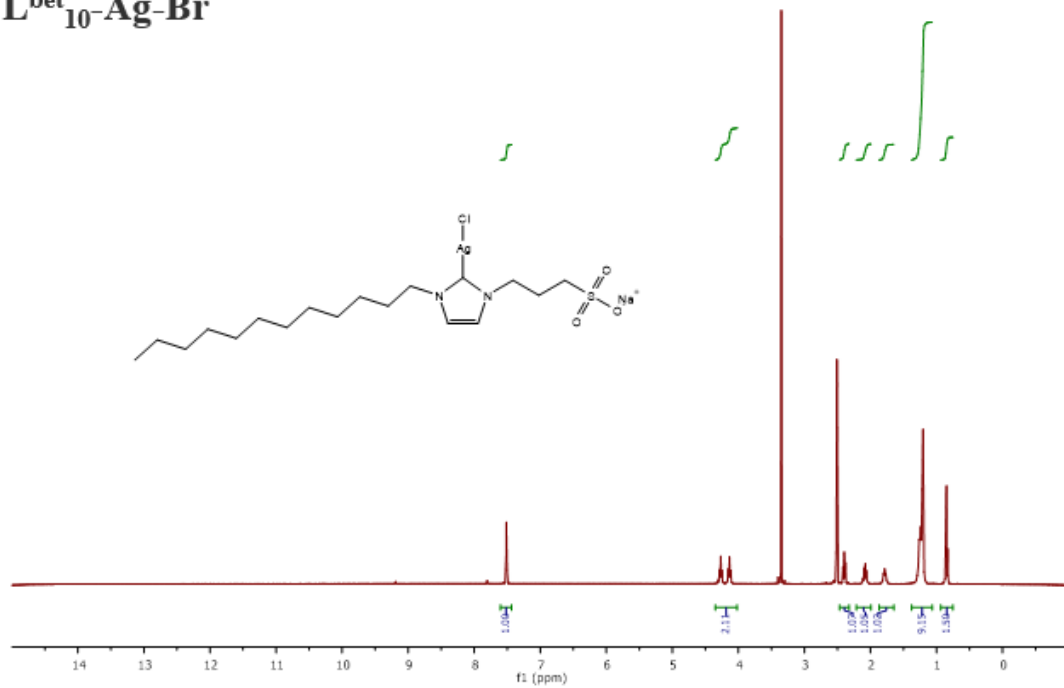
L^{bet}₁₀-Ag-Br



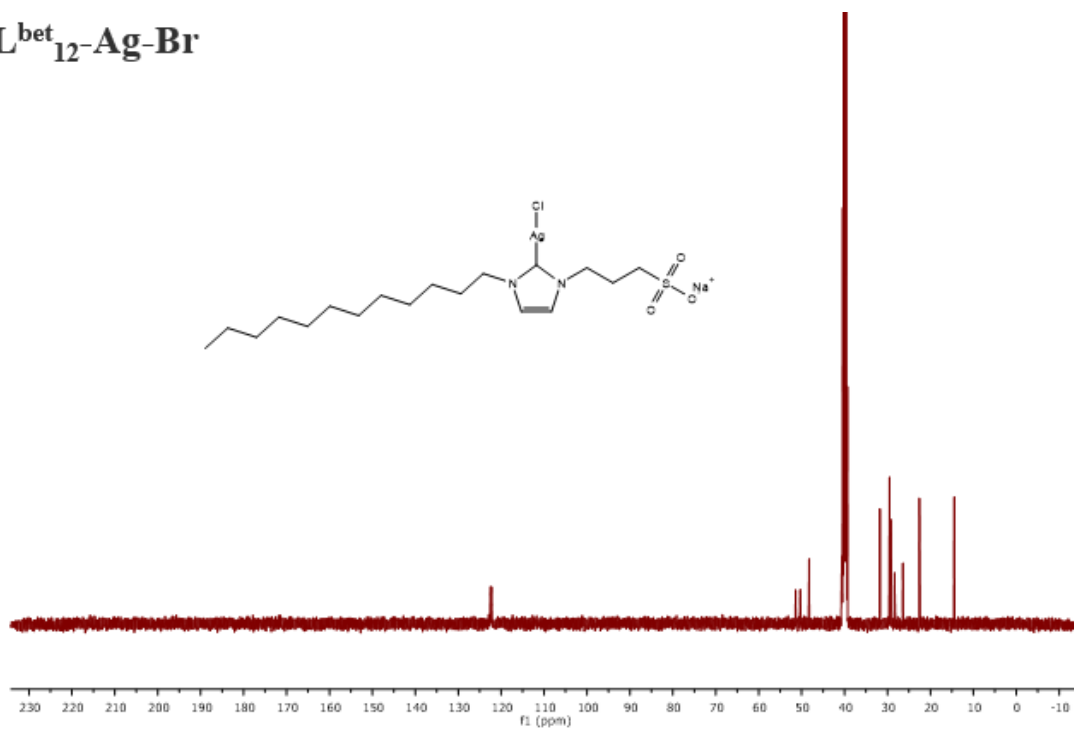
L^{bet}₁₀-Ag-Br



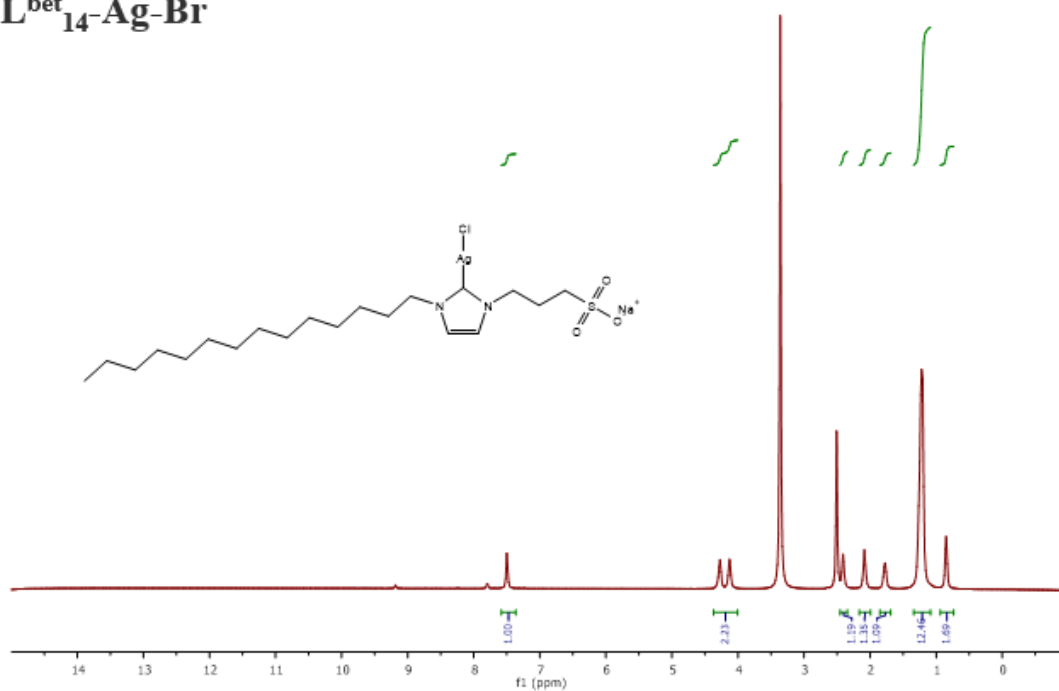
$L^{bet}_{10}\text{-Ag-Br}$



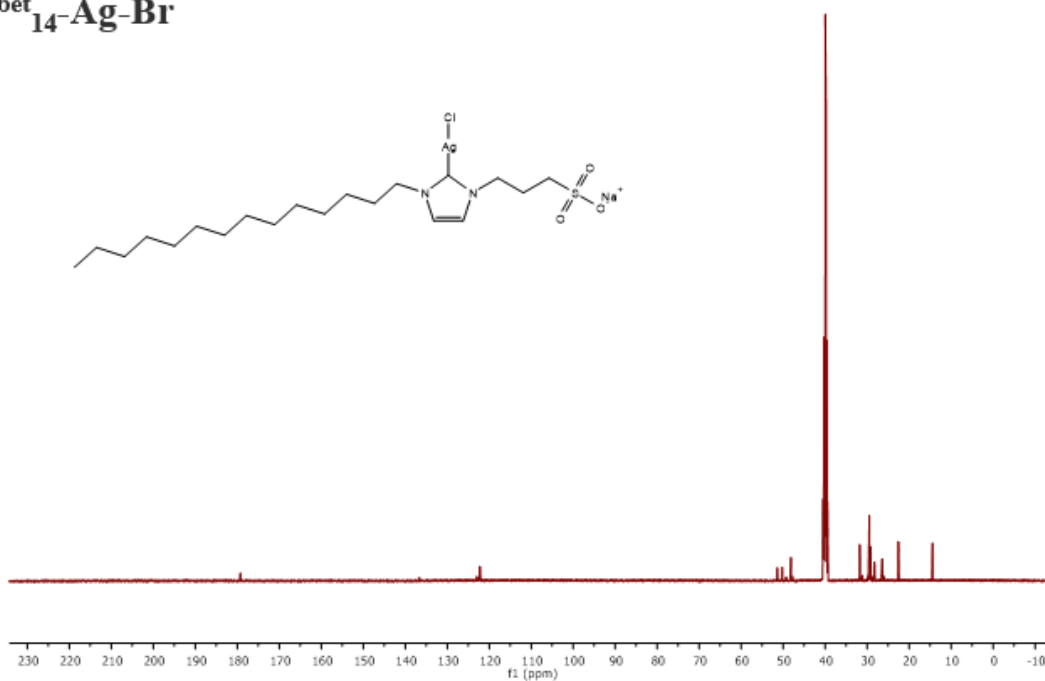
$L^{bet}_{12}\text{-Ag-Br}$



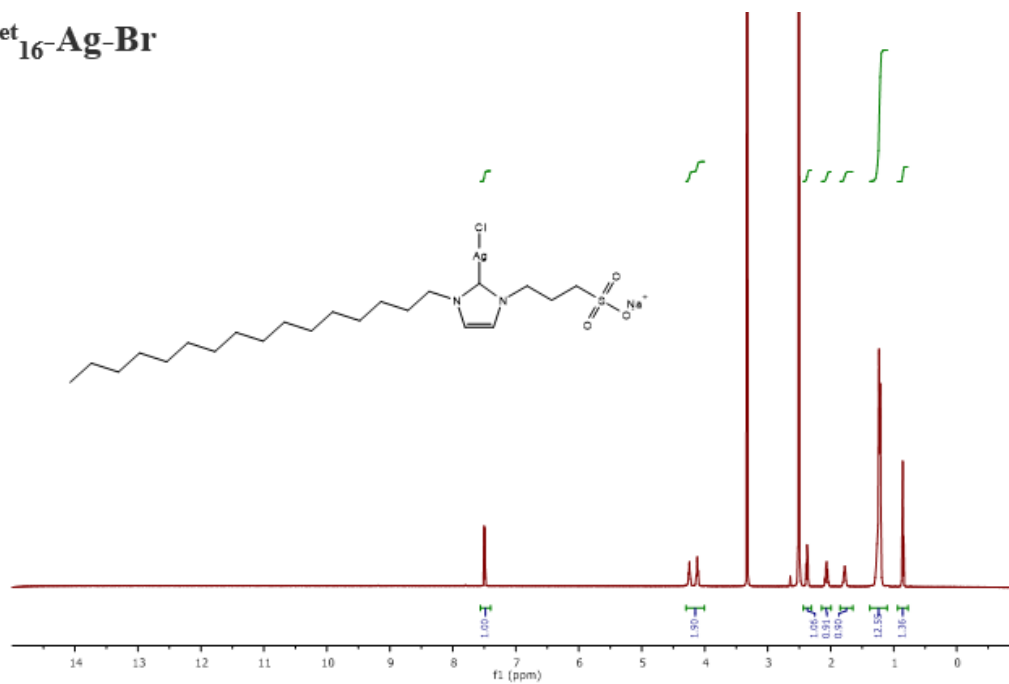
$L^{bet}_{14}\text{-Ag-Br}$



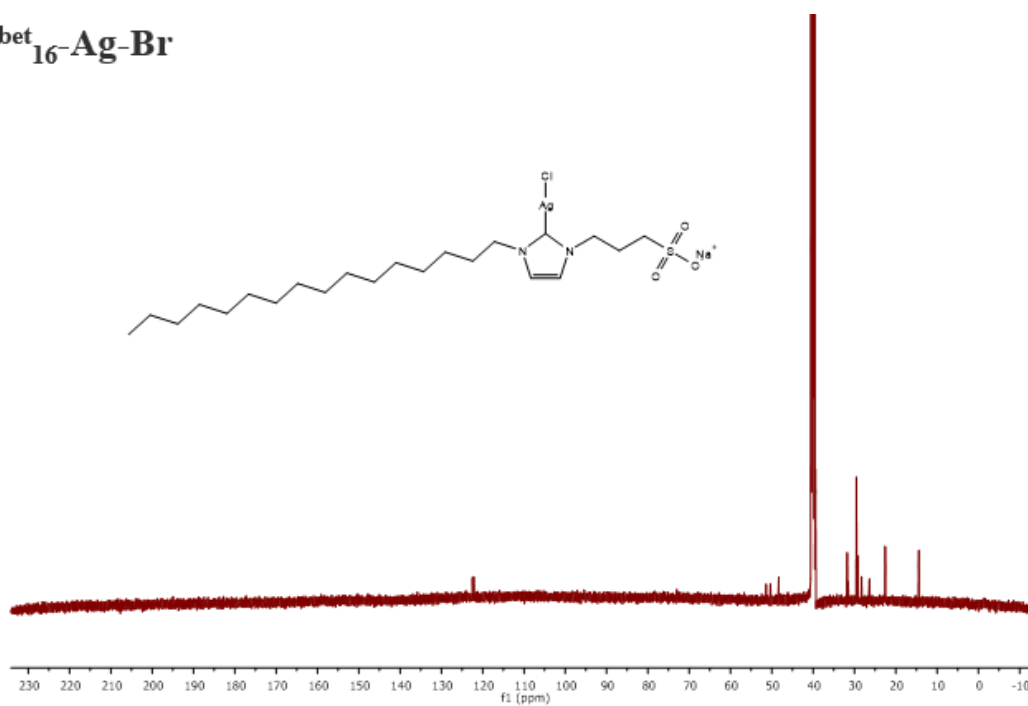
$L^{bet}_{14}\text{-Ag-Br}$



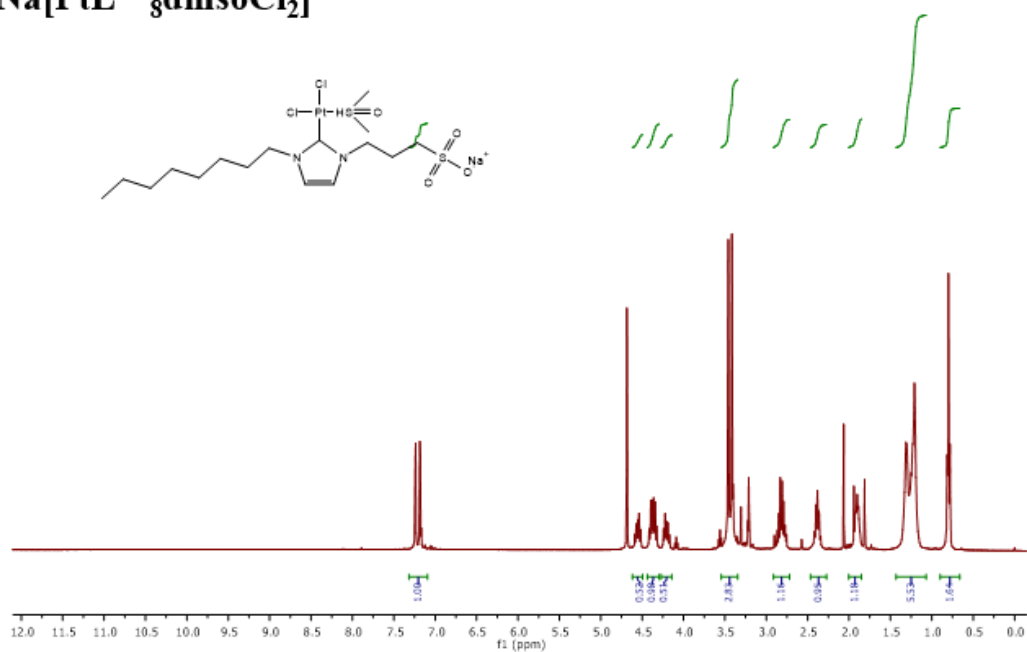
$L_{16}^{bet}\text{-Ag-Br}$



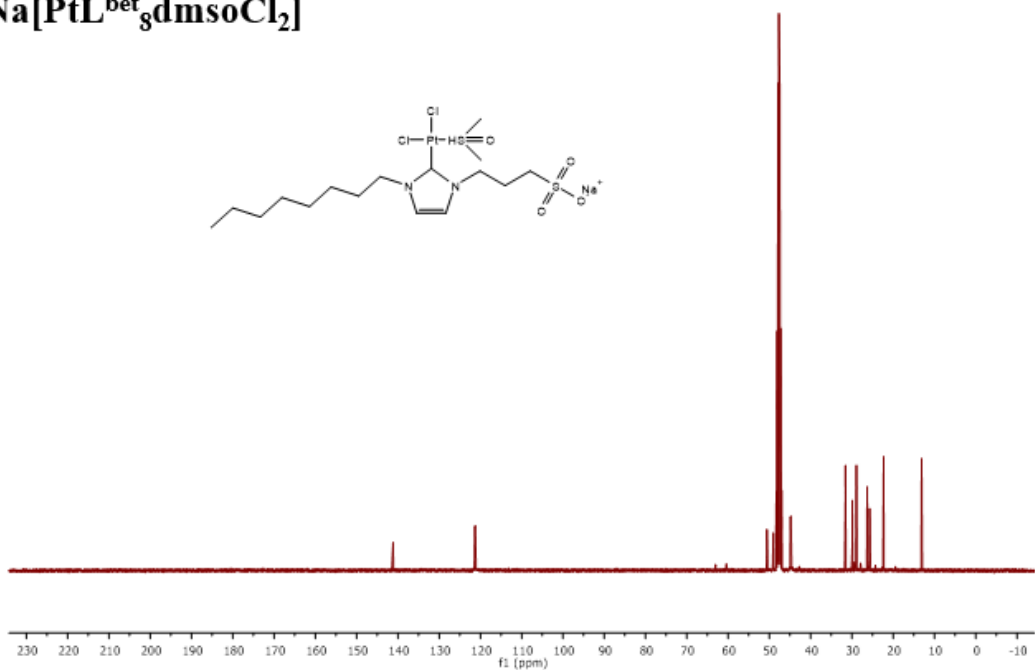
$L_{16}^{bet}\text{-Ag-Br}$



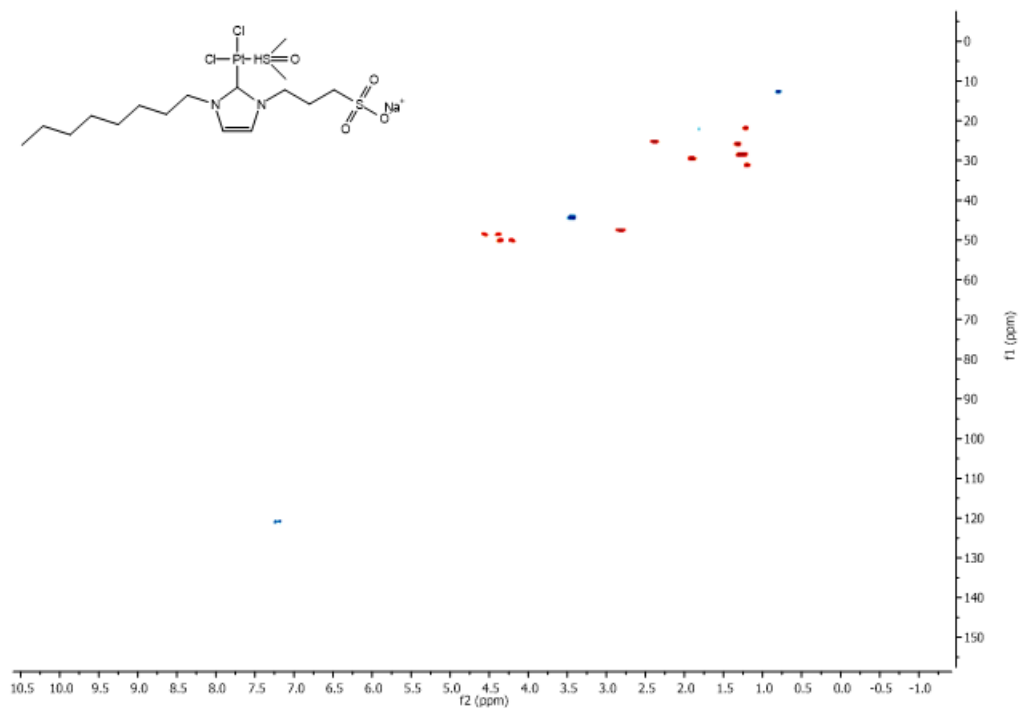
Na[PtL^{bet}₈dmsOCl₂]



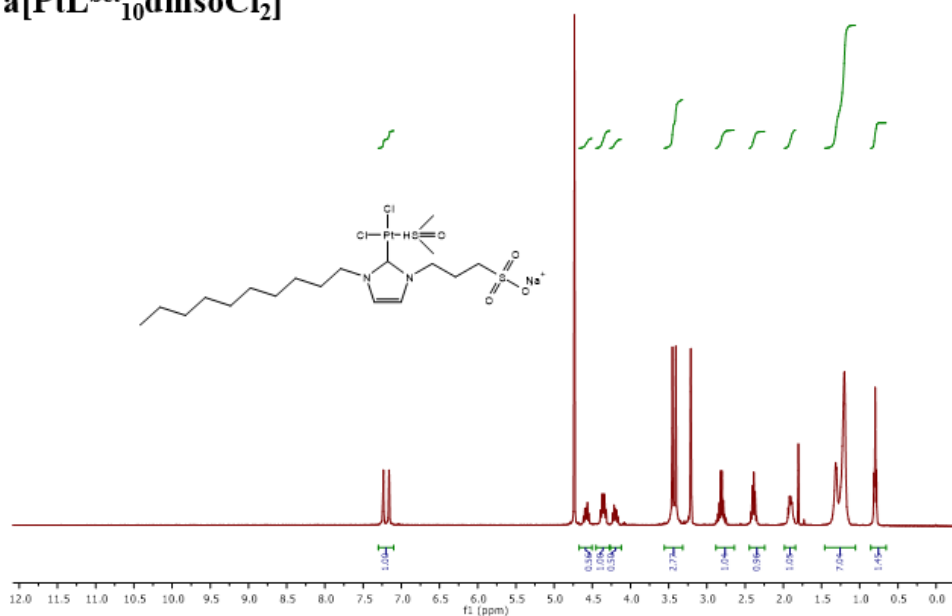
Na[PtL^{bet}₈dmsOCl₂]

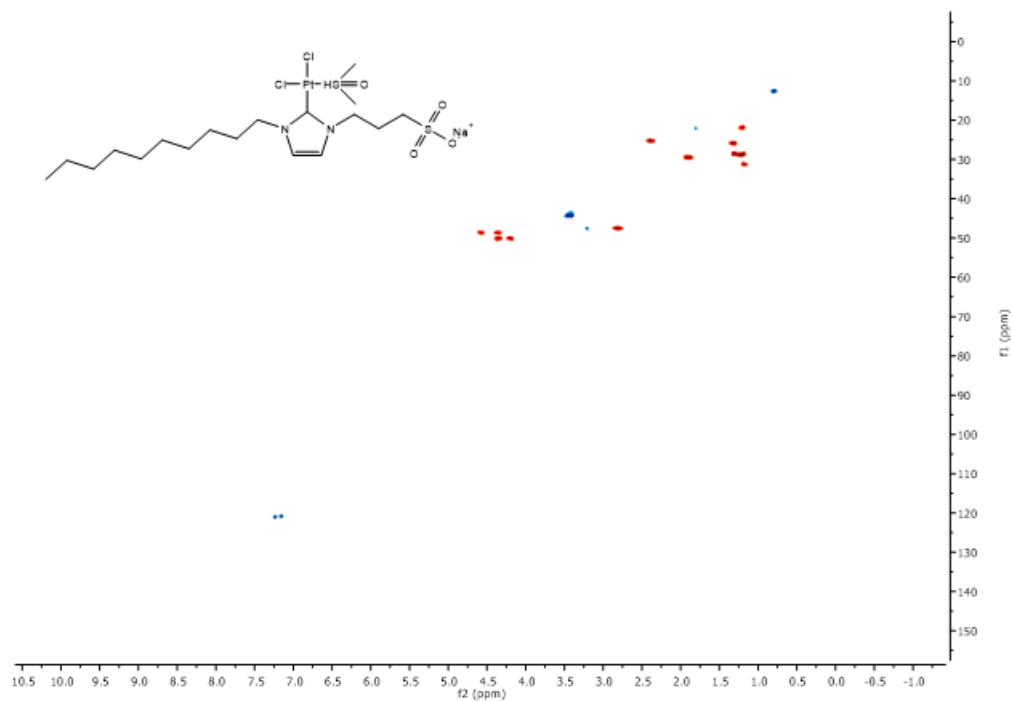
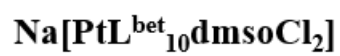
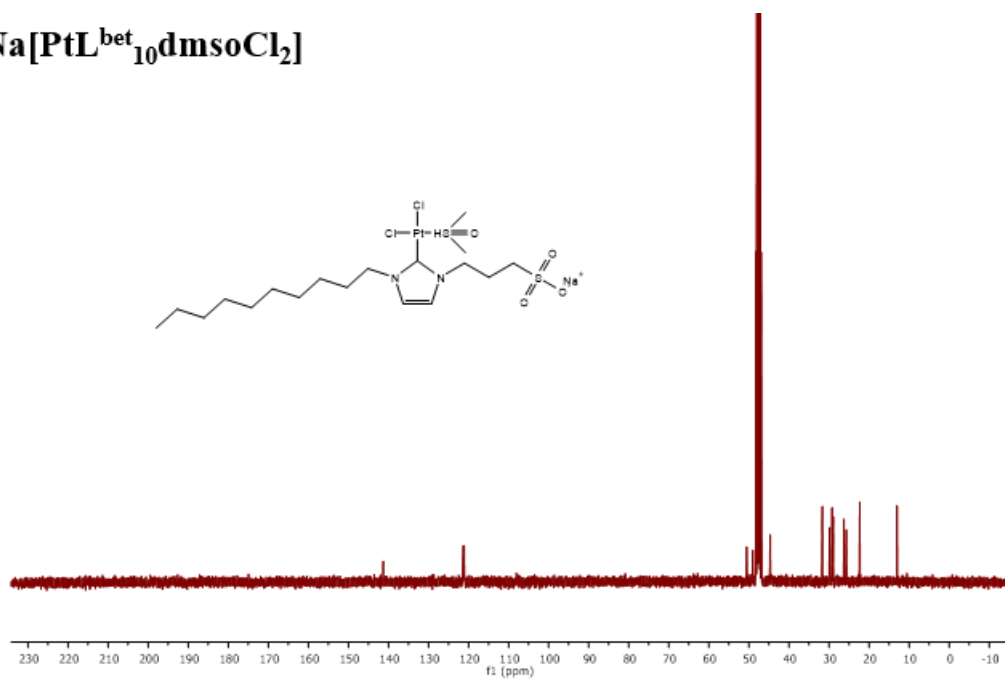
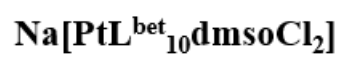


Na[PtL^{bet}₈dmsOCl₂]

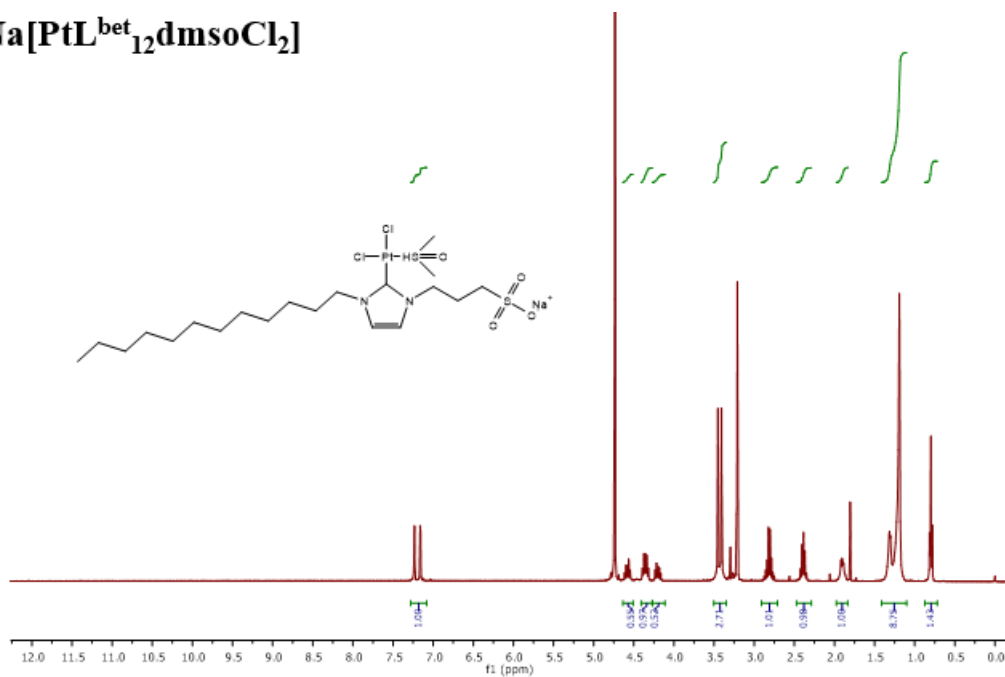


Na[PtL^{bet}₁₀dmsOCl₂]

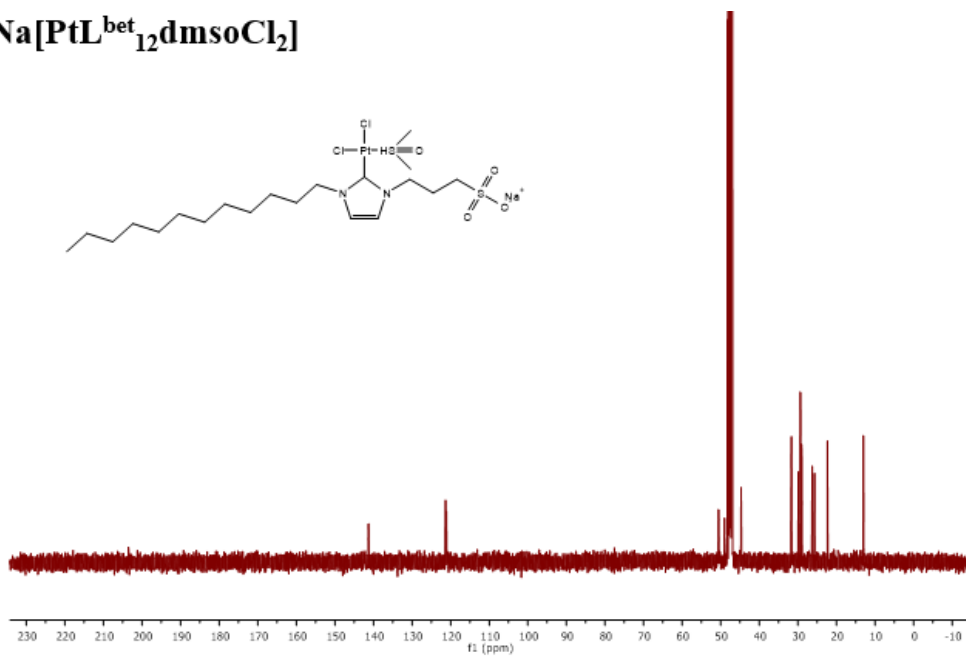




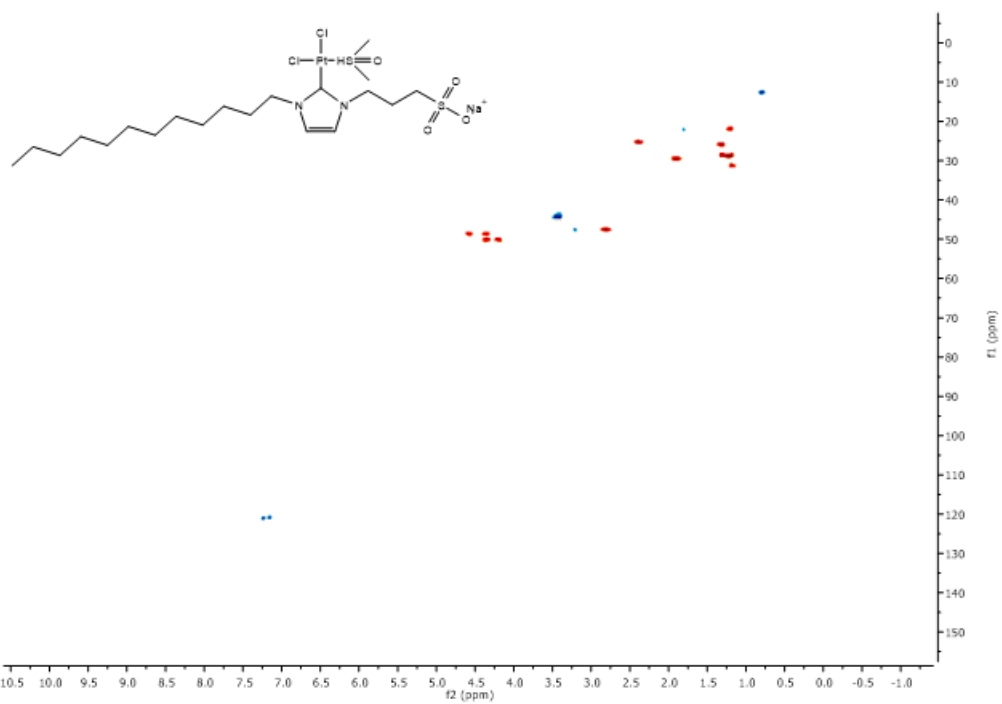
Na[PtL^{bet}₁₂dmsocl₂]



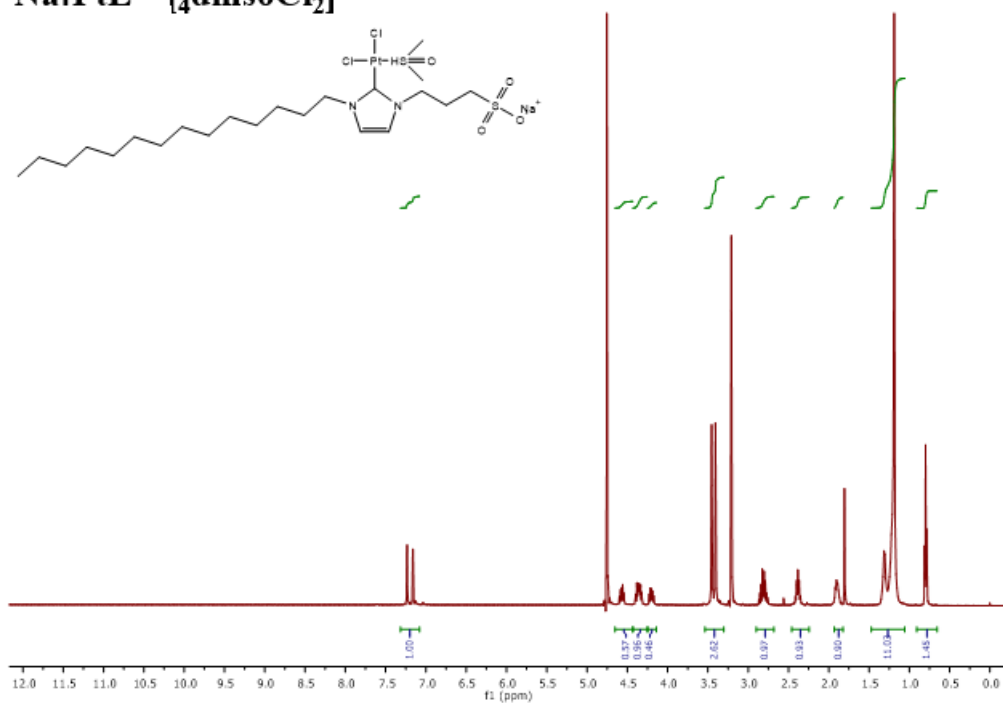
Na[PtL^{bet}₁₂dmsocl₂]



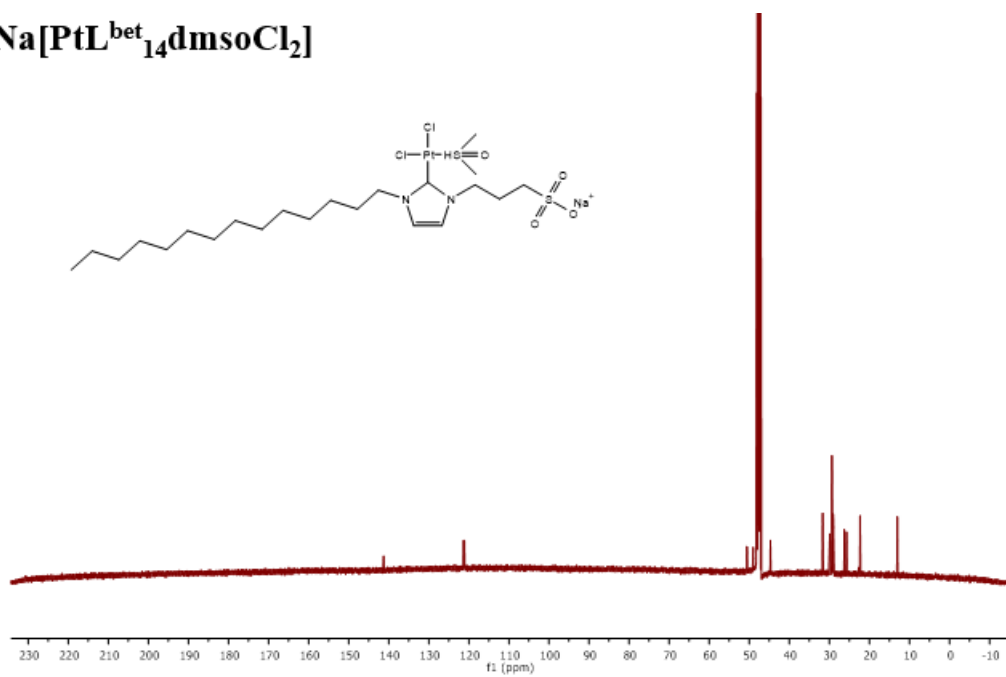
Na[PtL^{bet}₁₂dmsocl₂]



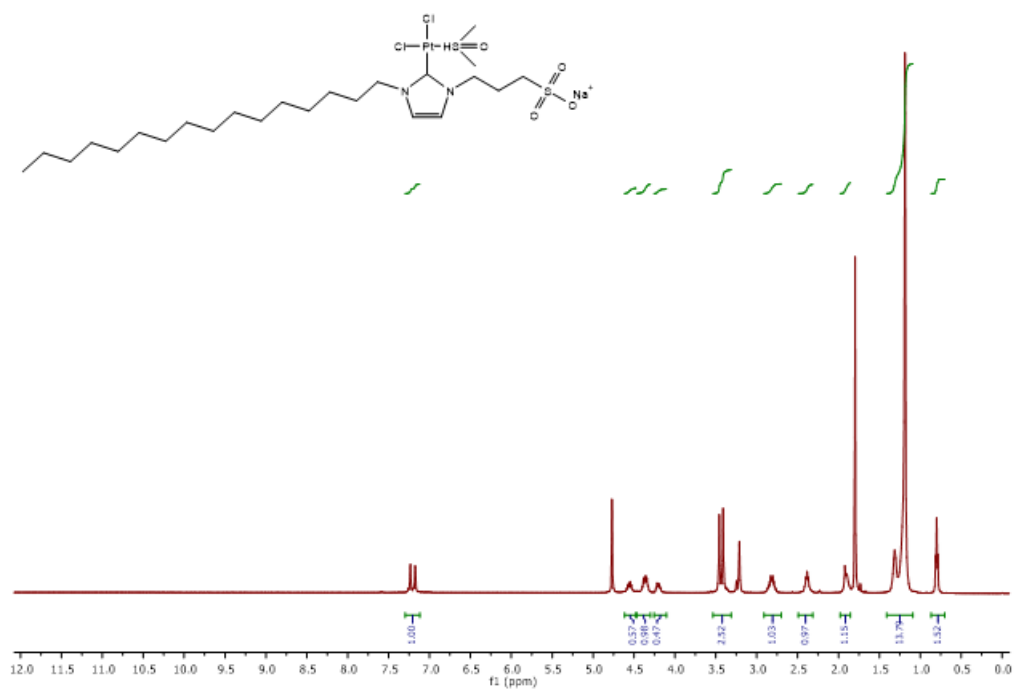
Na[PtL^{bet}₁₄dmsocl₂]



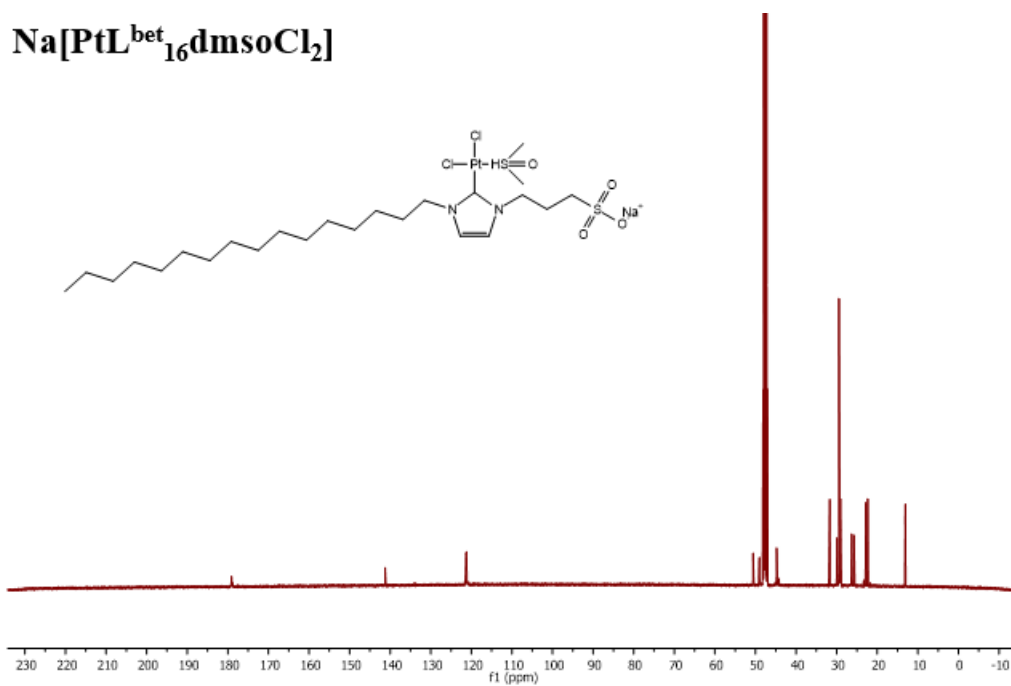
Na[PtL^{bet}₁₄dmsOCl₂]



Na[PtL^{bet}₁₆dmsOCl₂]

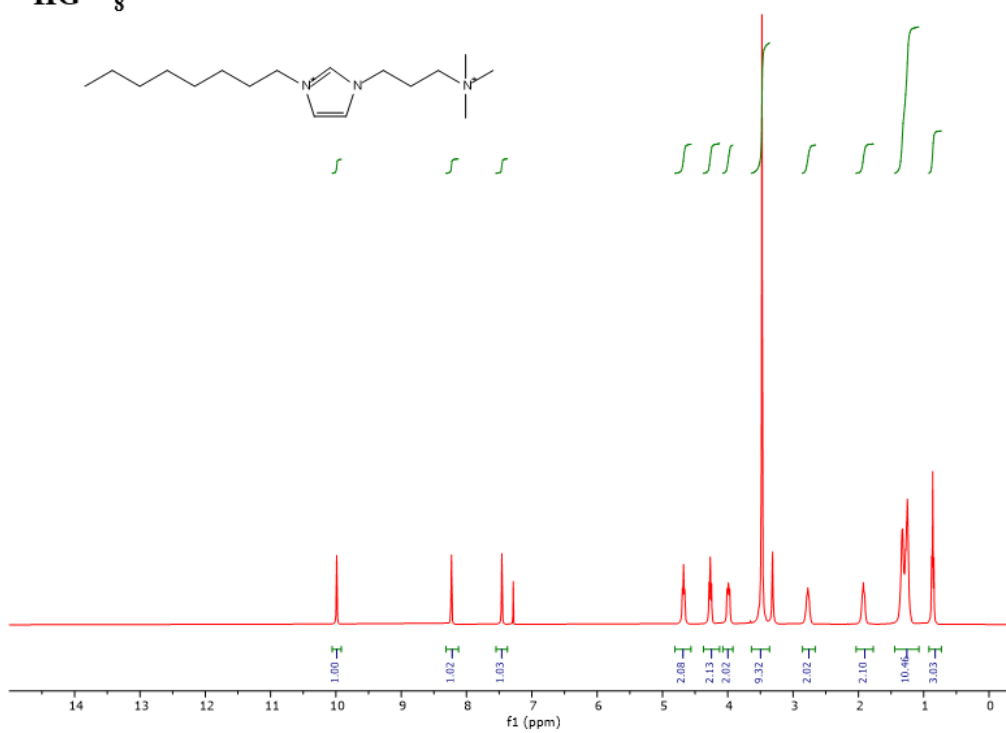


Na[PtL^{bet}₁₆dmsocl₂]

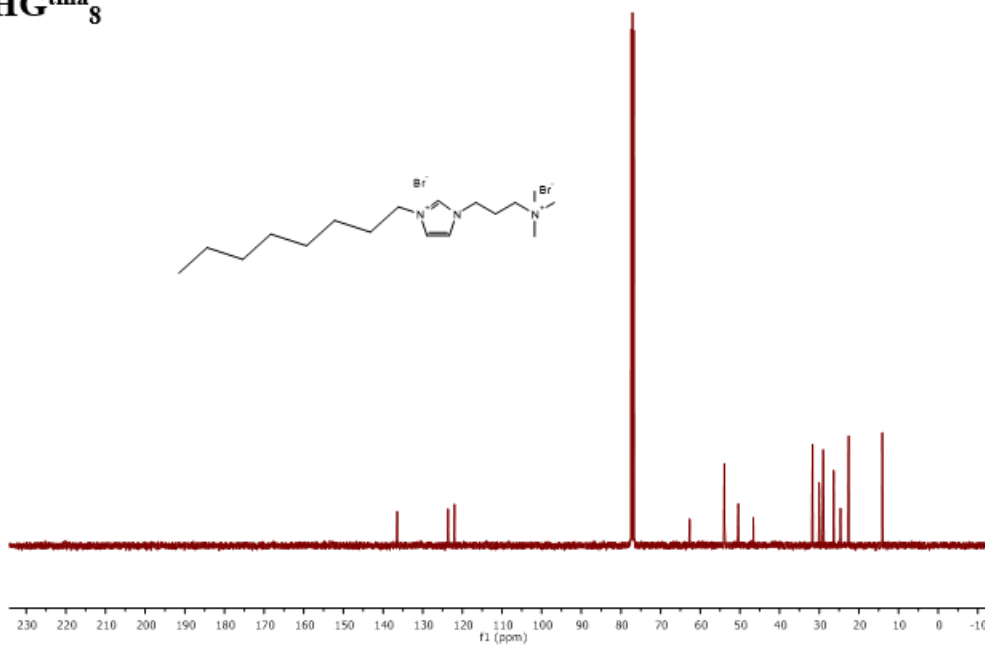


Appendix D: ^1H and ^{13}C NMR spectra of **HG^{tma}₈₋₁₆**

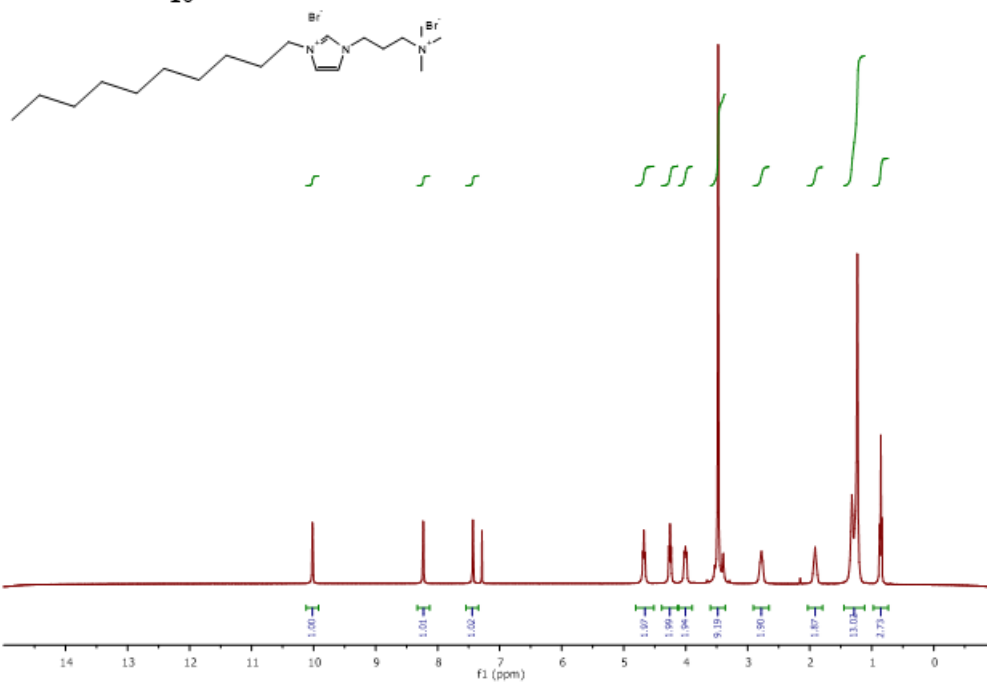
HG^{tma}₈



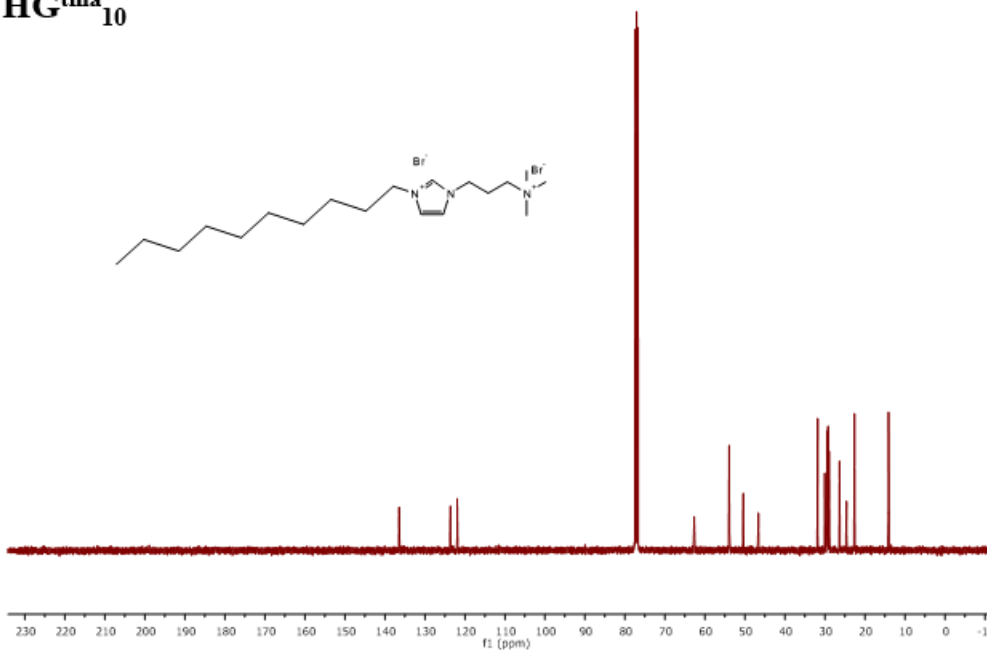
HG^{tma}₈

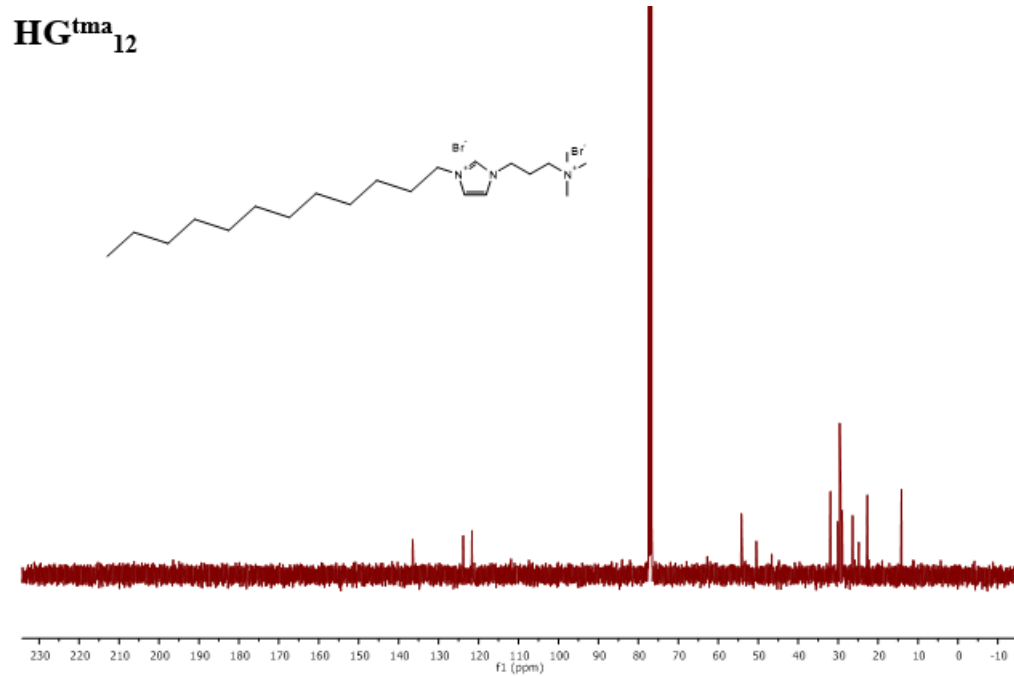
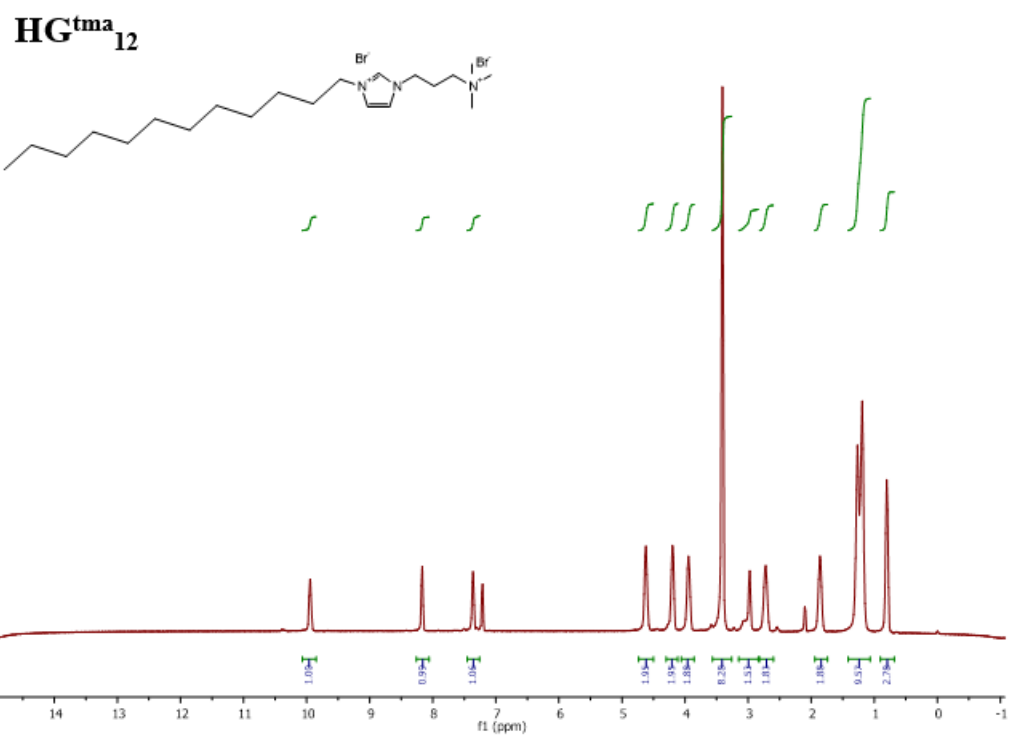


HG^{tma}₁₀

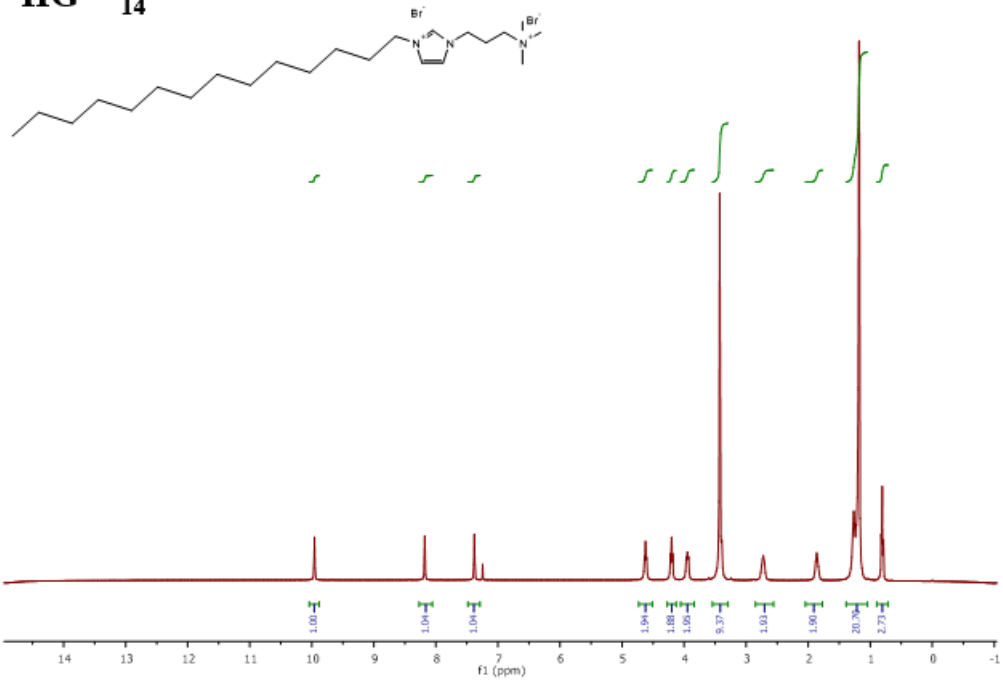


HG^{tma}₁₀

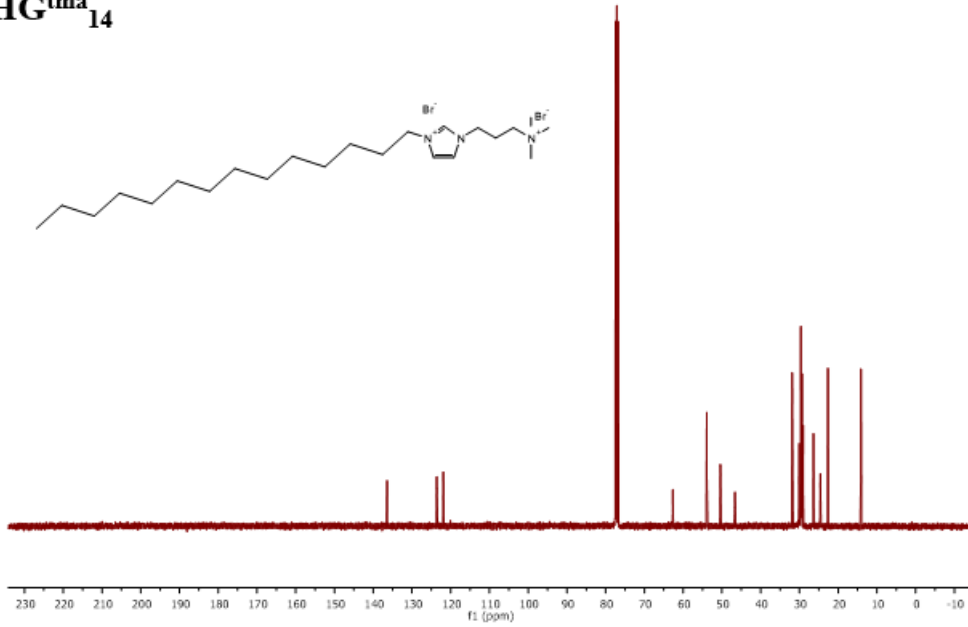




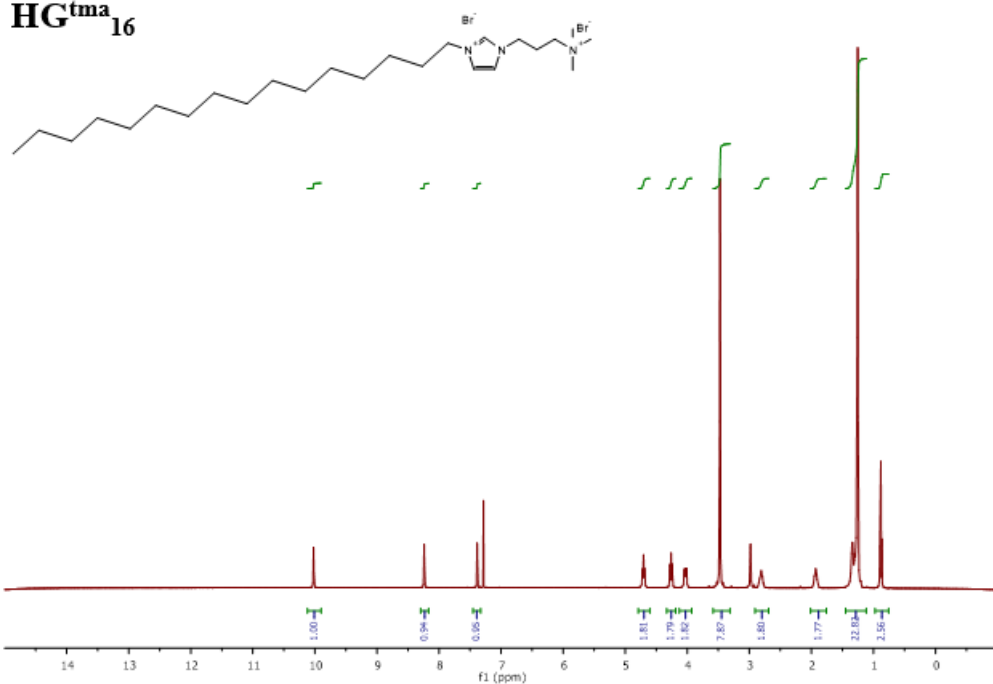
HG^{tma}₁₄



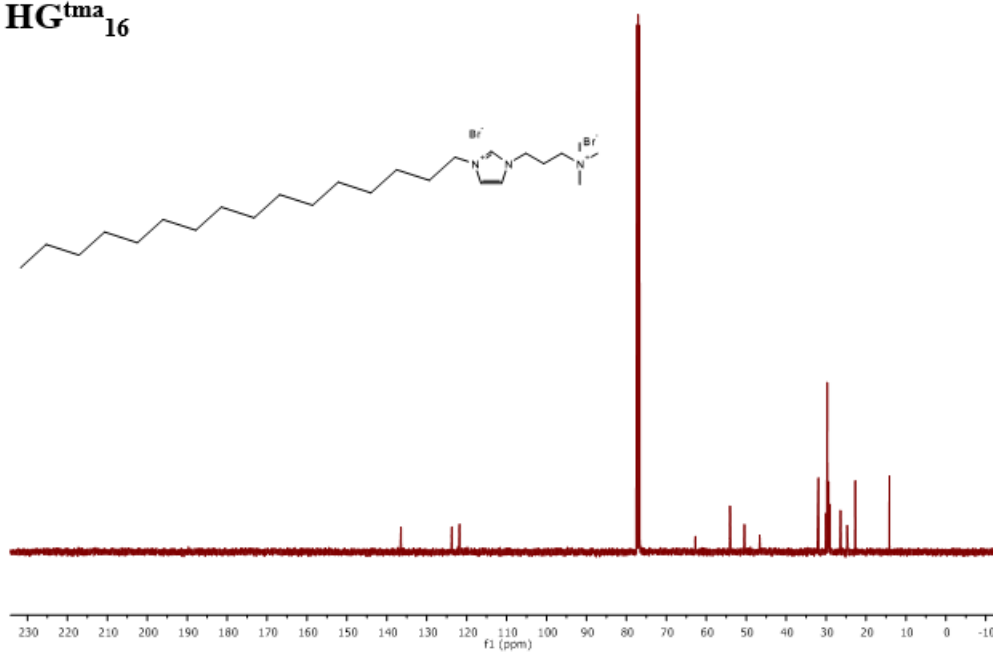
HG^{tma}₁₄



HG^{tma}₁₆

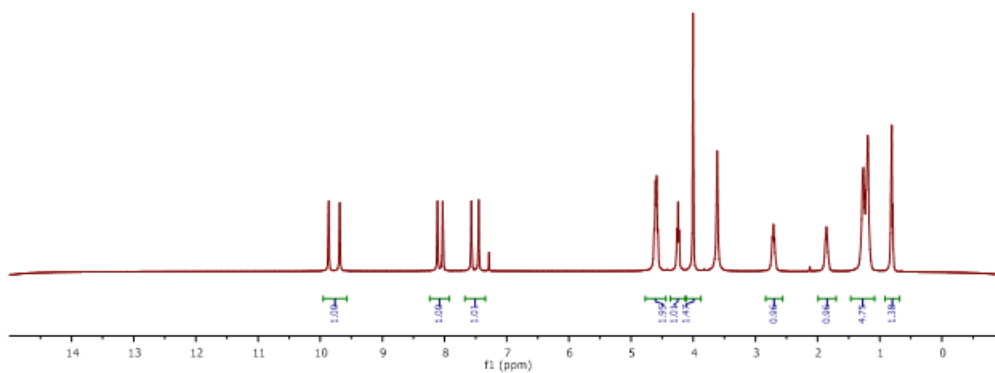
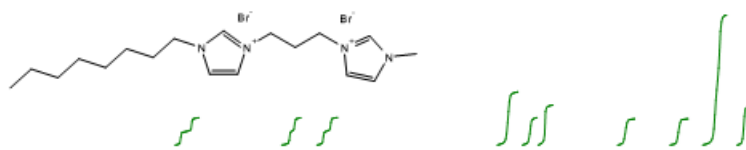


HG^{tma}₁₆

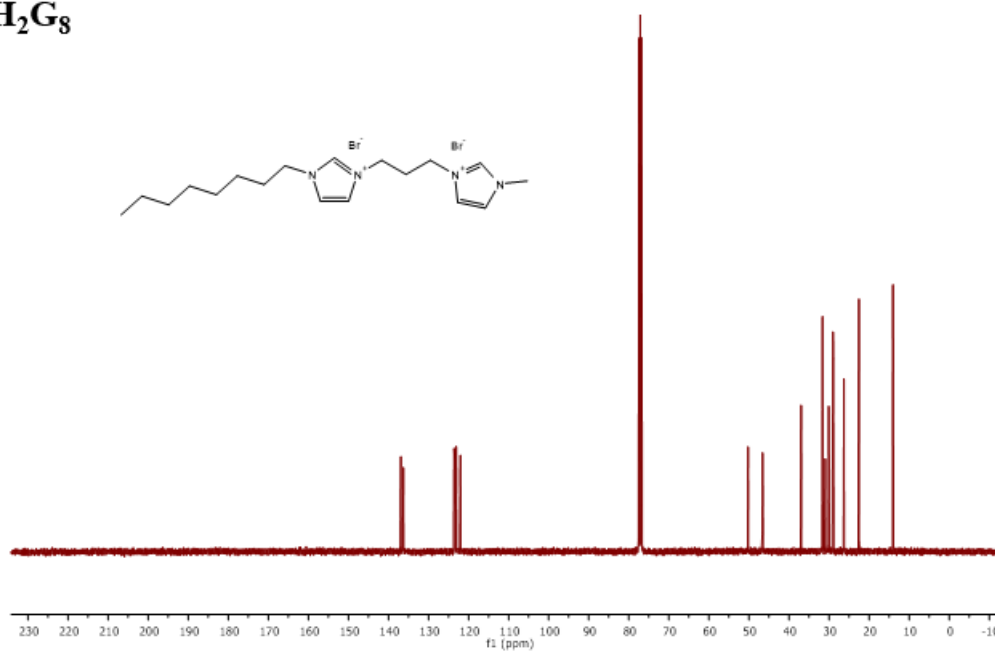
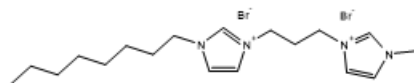


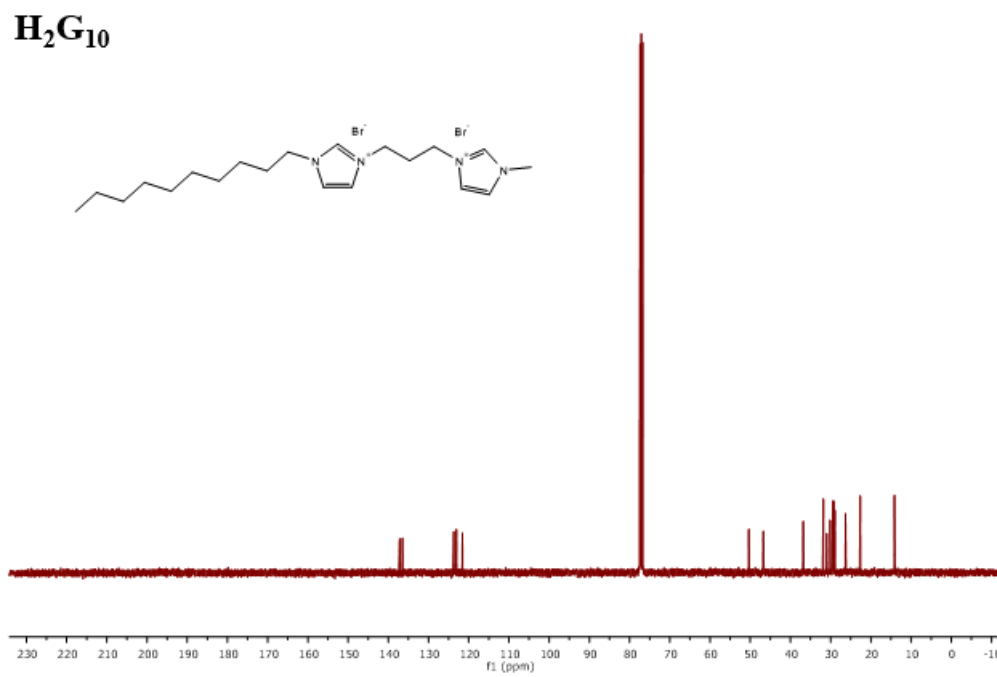
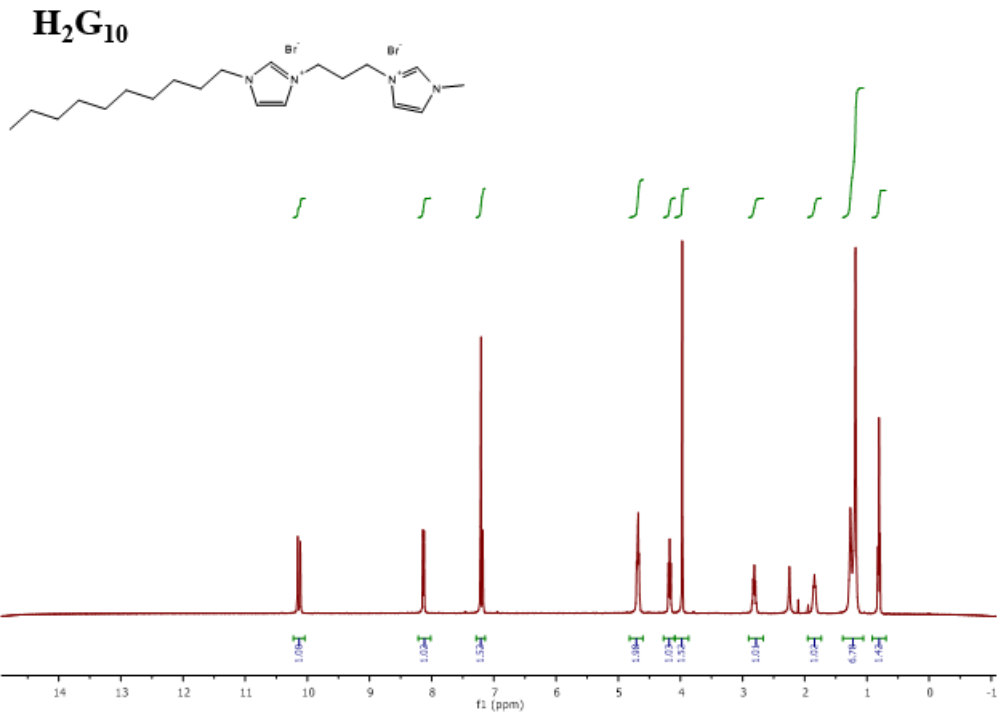
Appendix E: ^1H and ^{13}C NMR spectra of HG_{8-16} and $\text{G}_{8-16}\text{-Ag-Br}$

H₂G₈

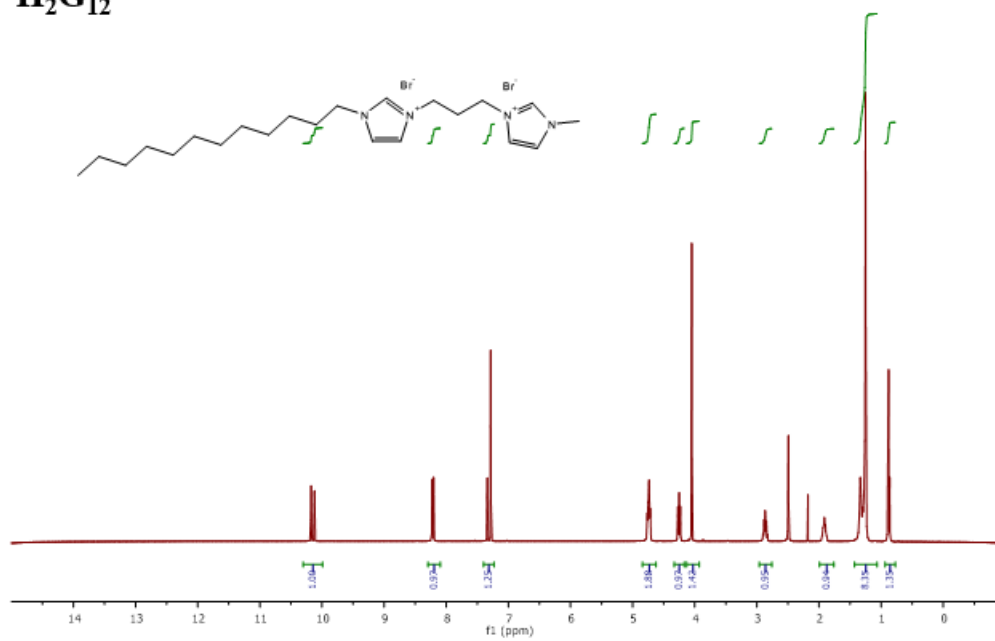


H₂G₈

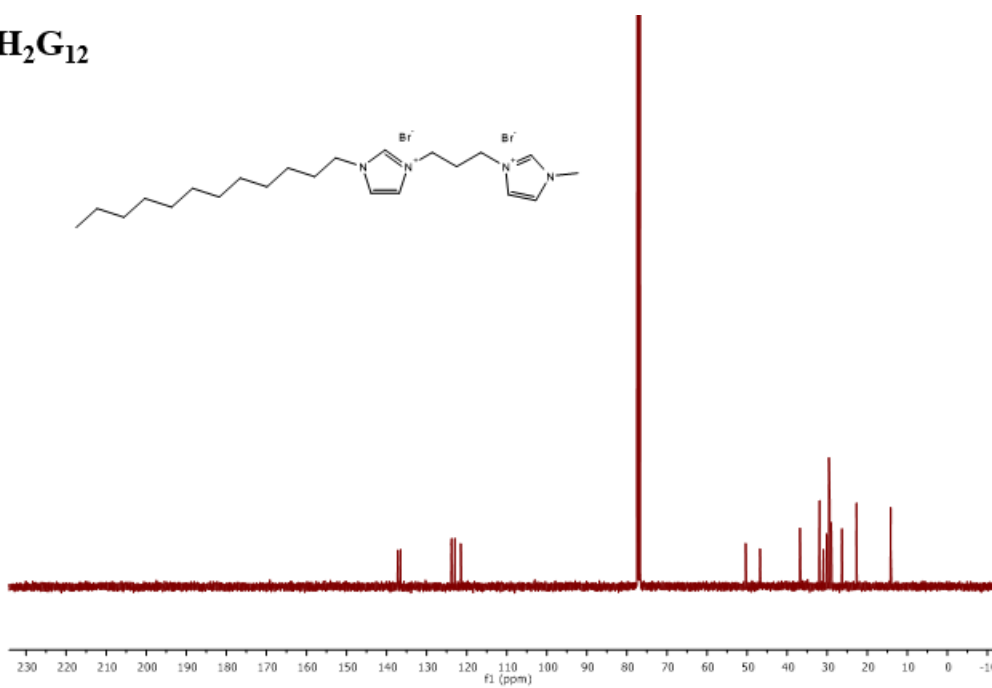




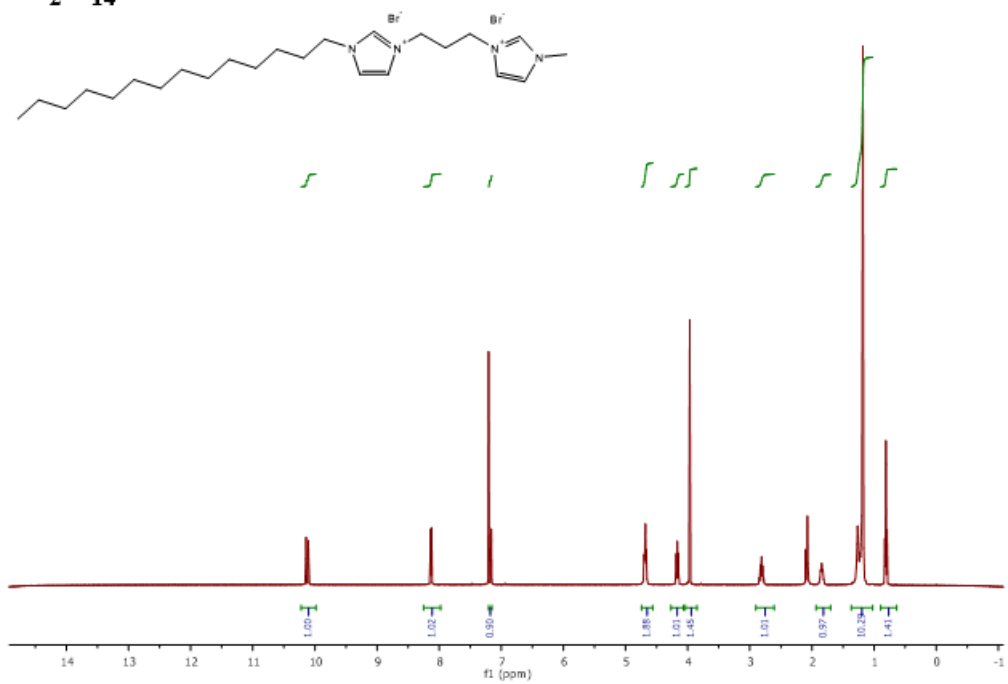
H₂G₁₂



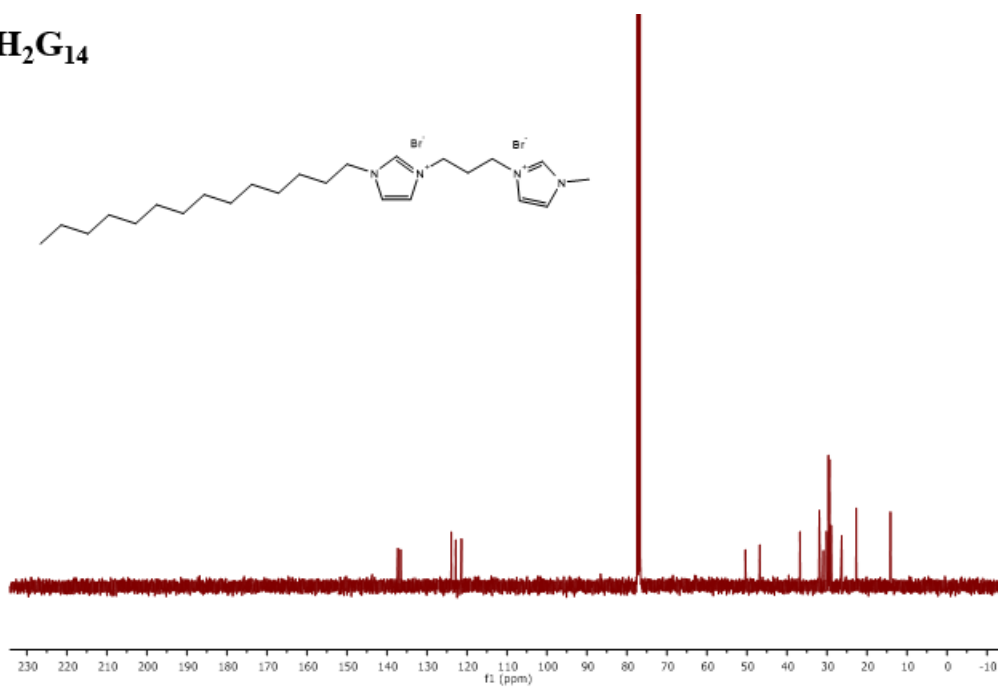
H₂G₁₂



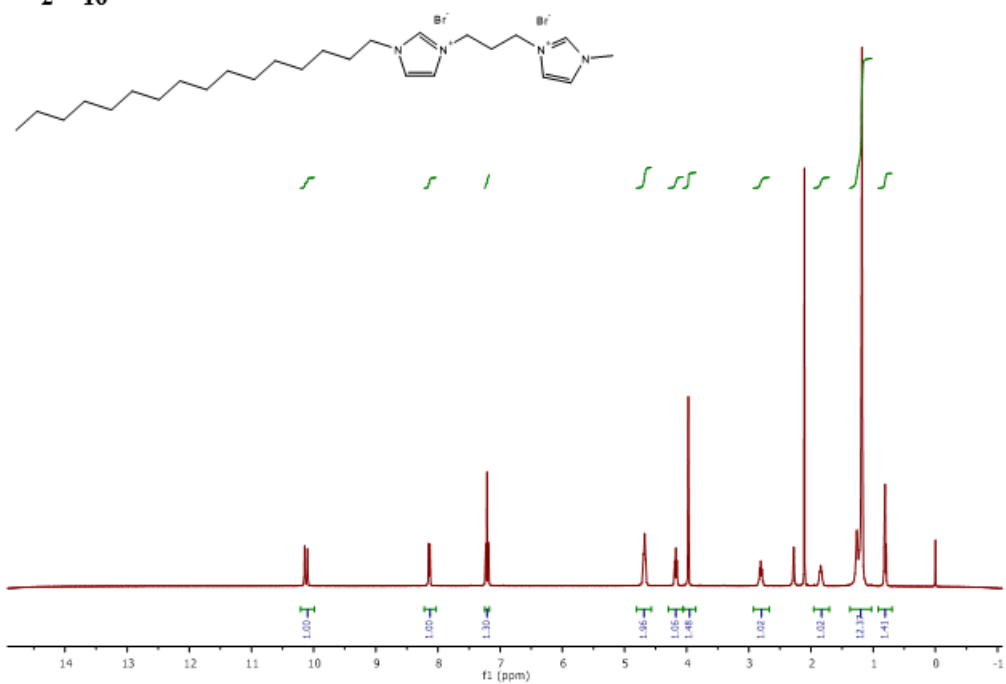
H₂G₁₄



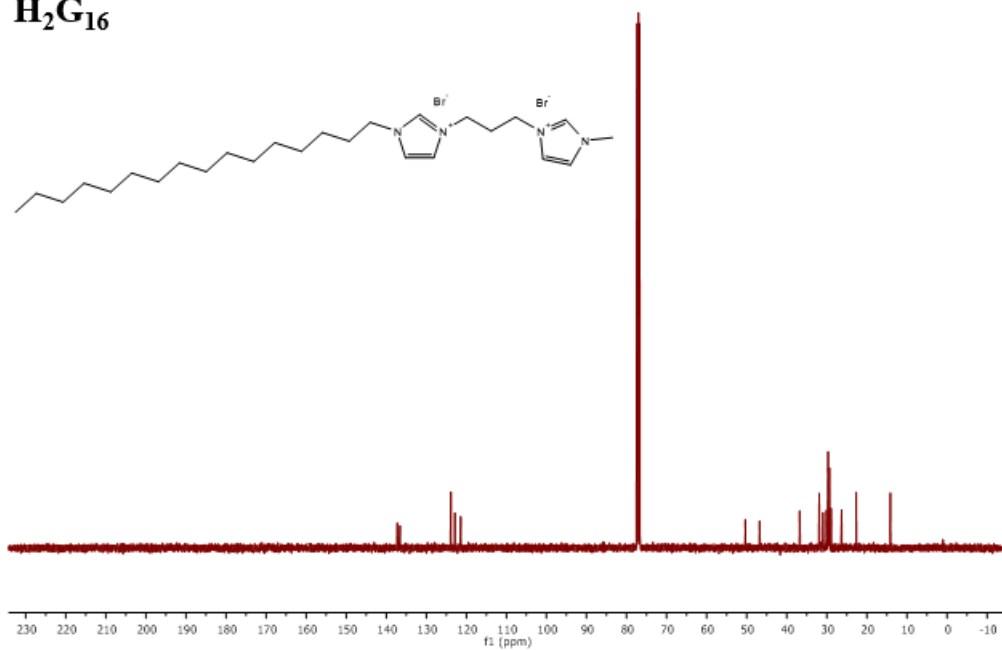
H₂G₁₄



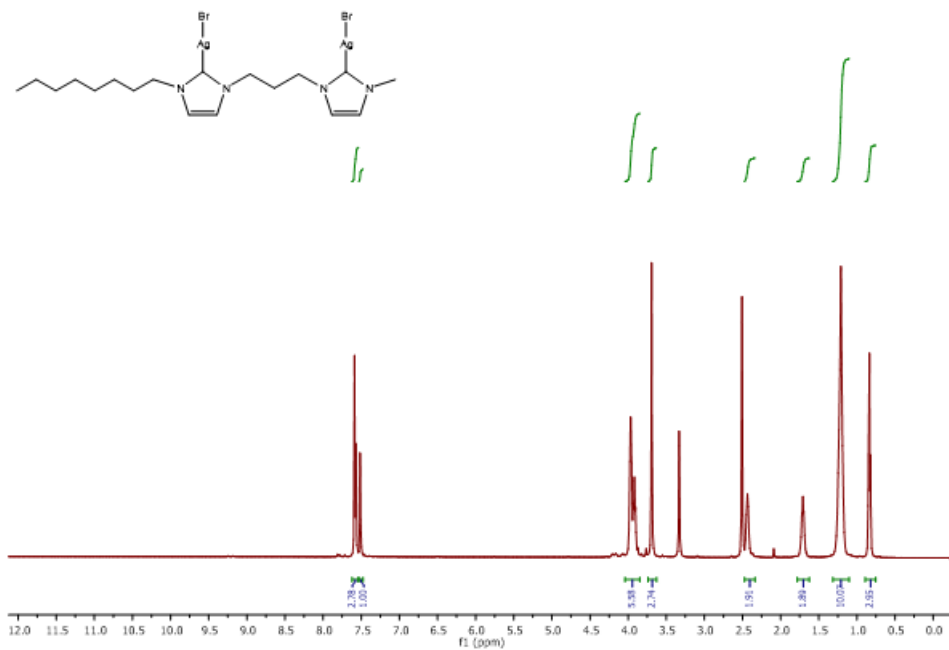
H₂G₁₆



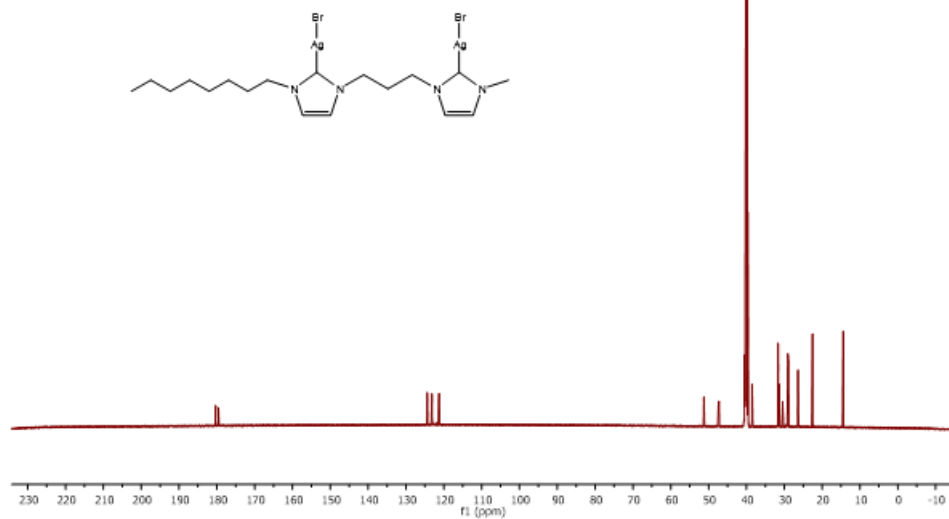
H₂G₁₆



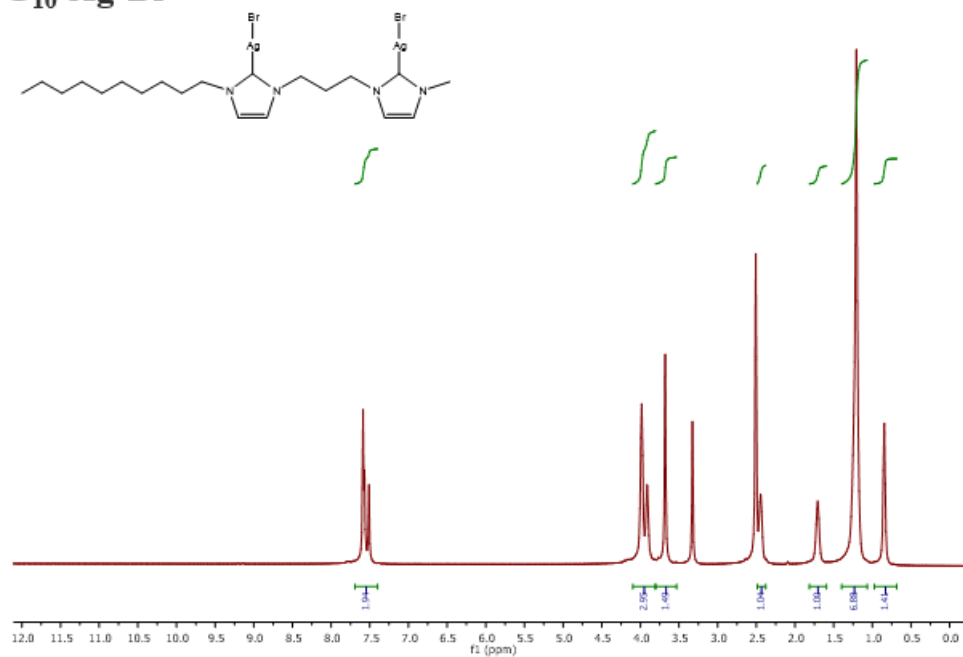
G₈-Ag-Br



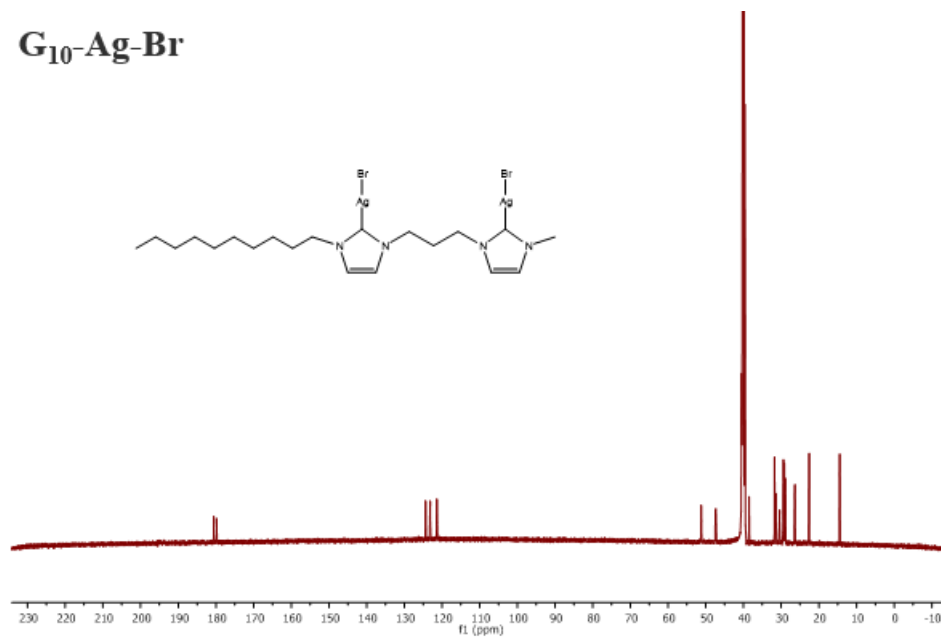
G₈-Ag-Br



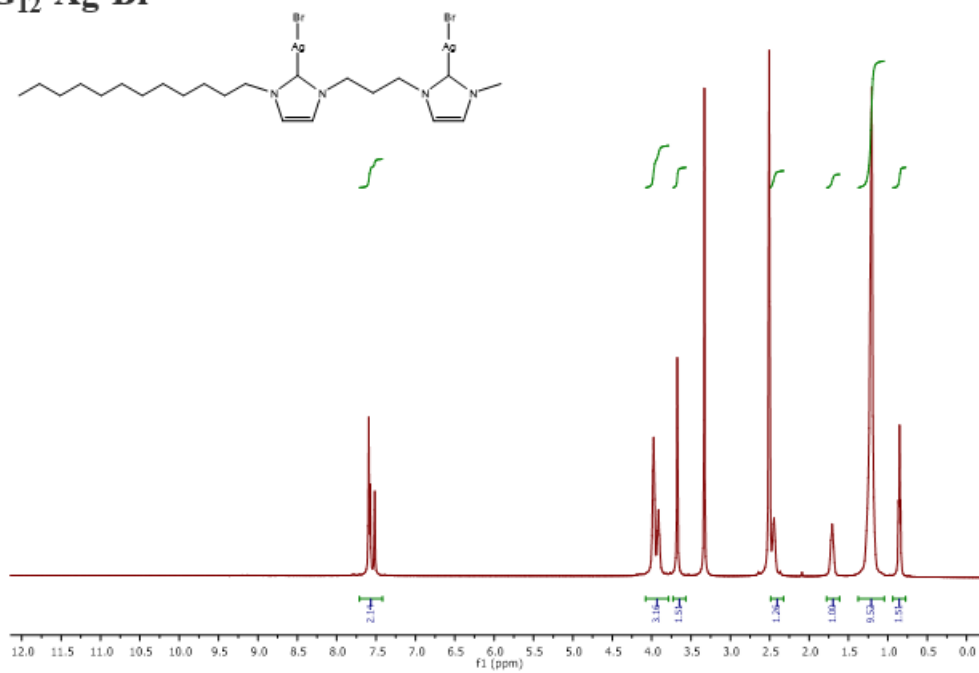
G₁₀-Ag-Br



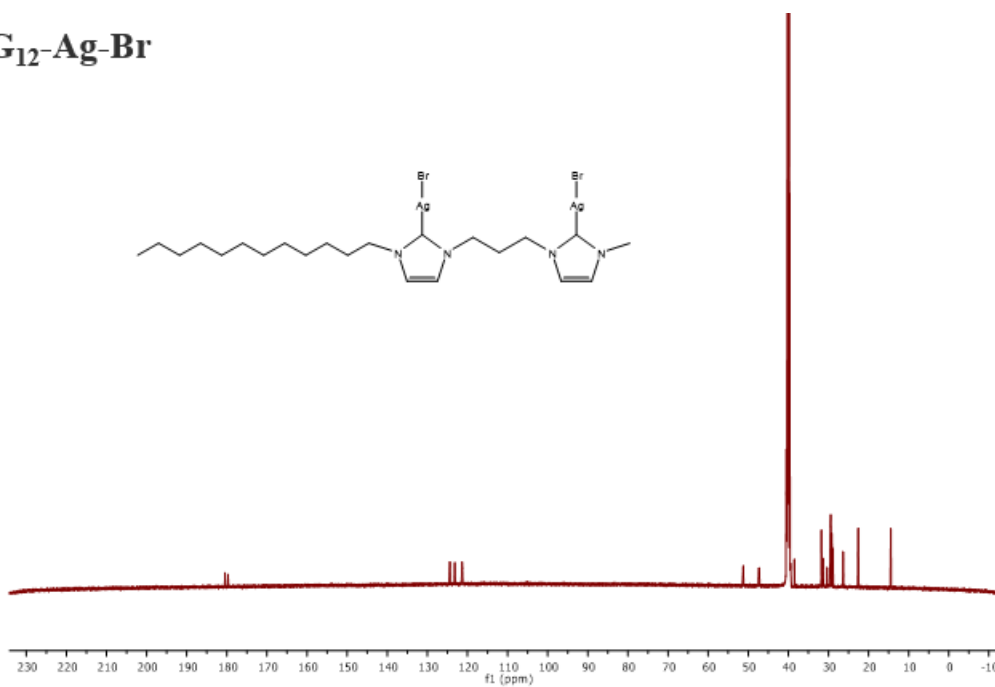
G₁₀-Ag-Br



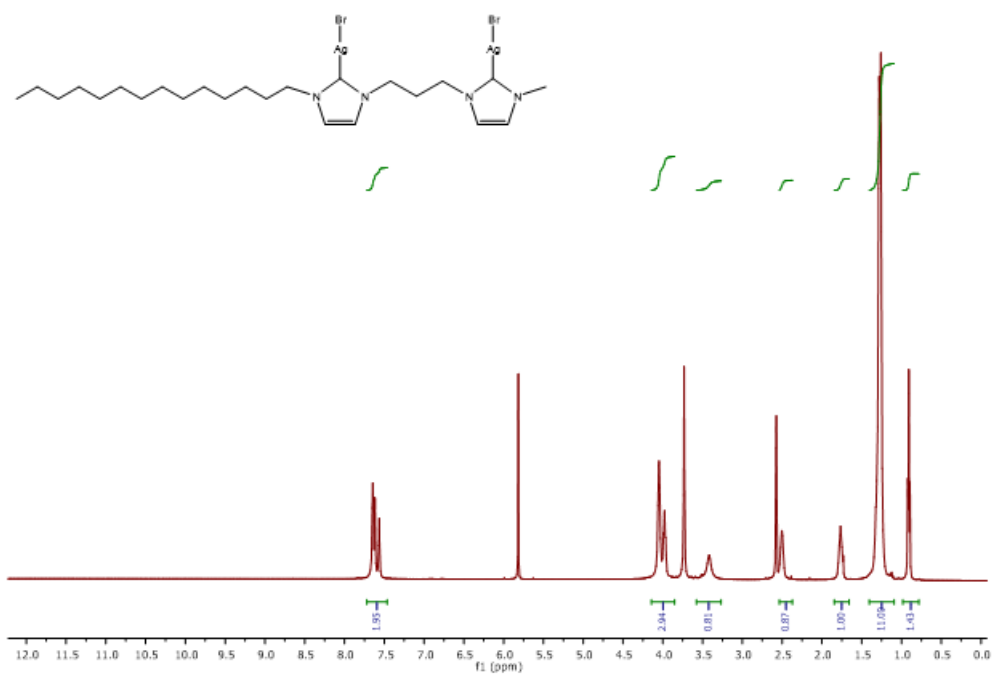
G₁₂-Ag-Br



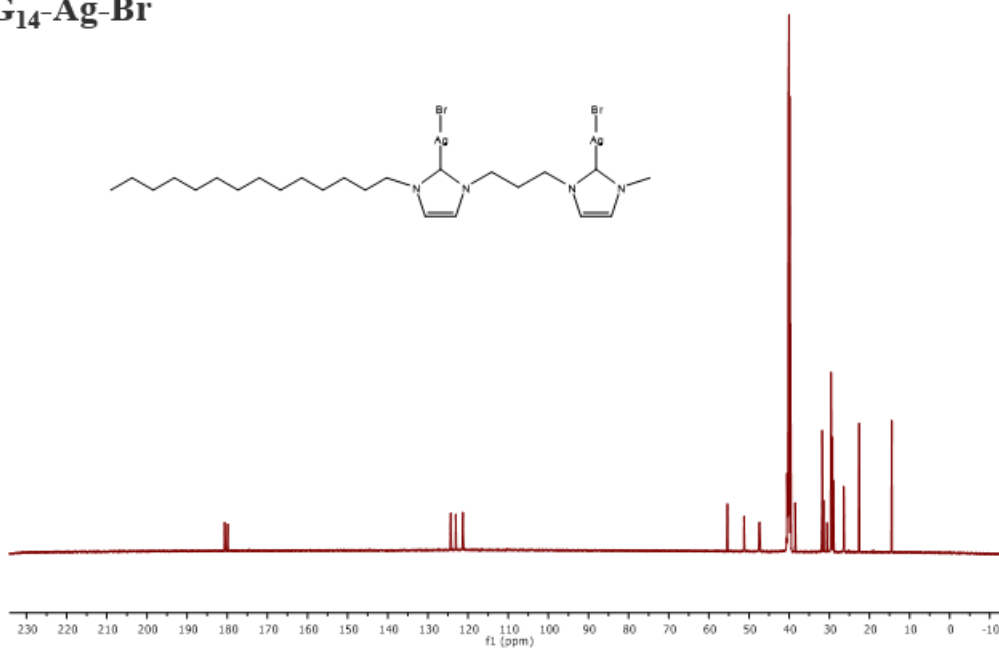
G₁₂-Ag-Br



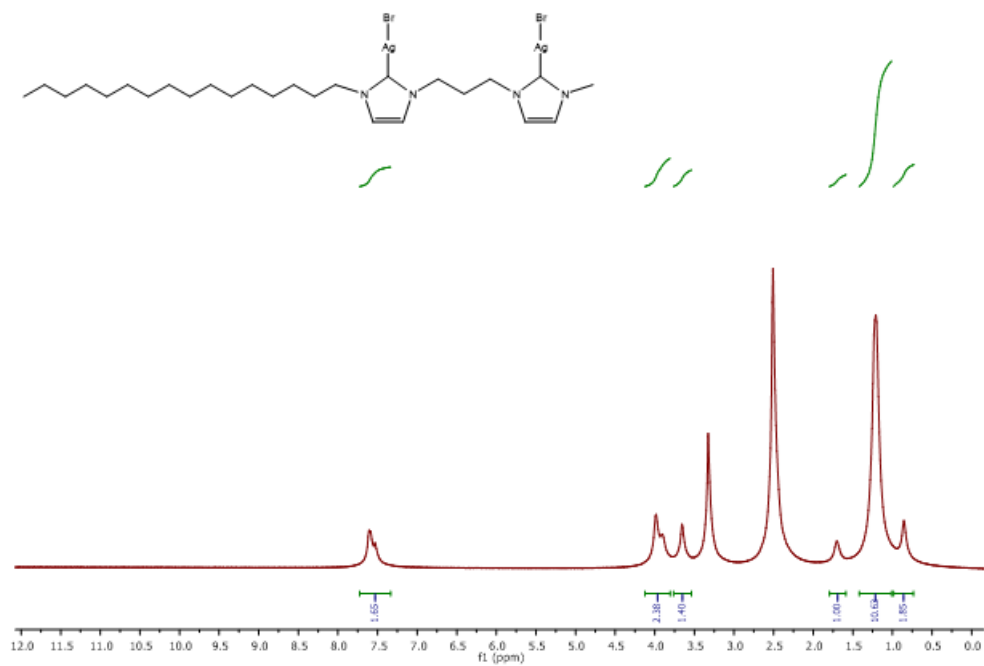
G₁₄-Ag-Br



G₁₄-Ag-Br

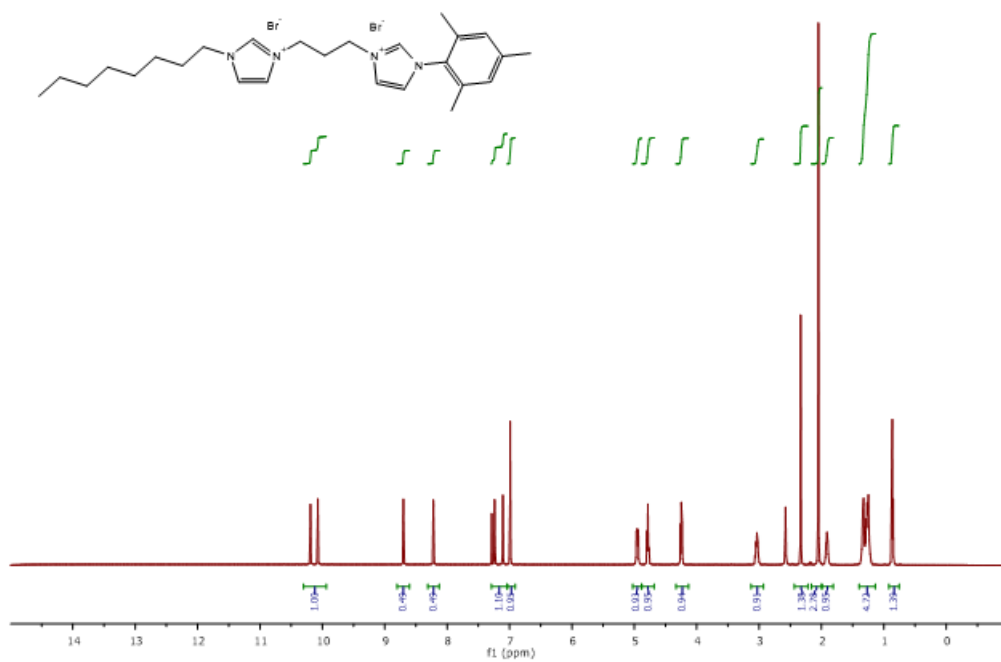


G₁₆-Ag-Br

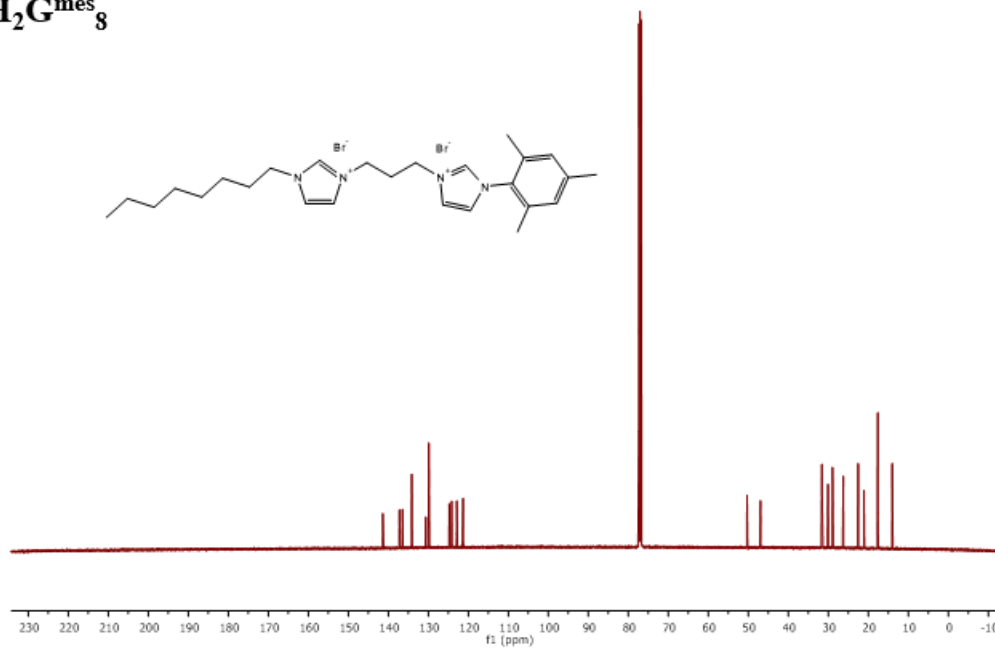


Appendix F: ^1H and ^{13}C NMR spectra of $\text{HG}^{\text{mes}}_{8-16}$ and $\text{G}^{\text{mes}}_{8-16}\text{-Ag-Br}$

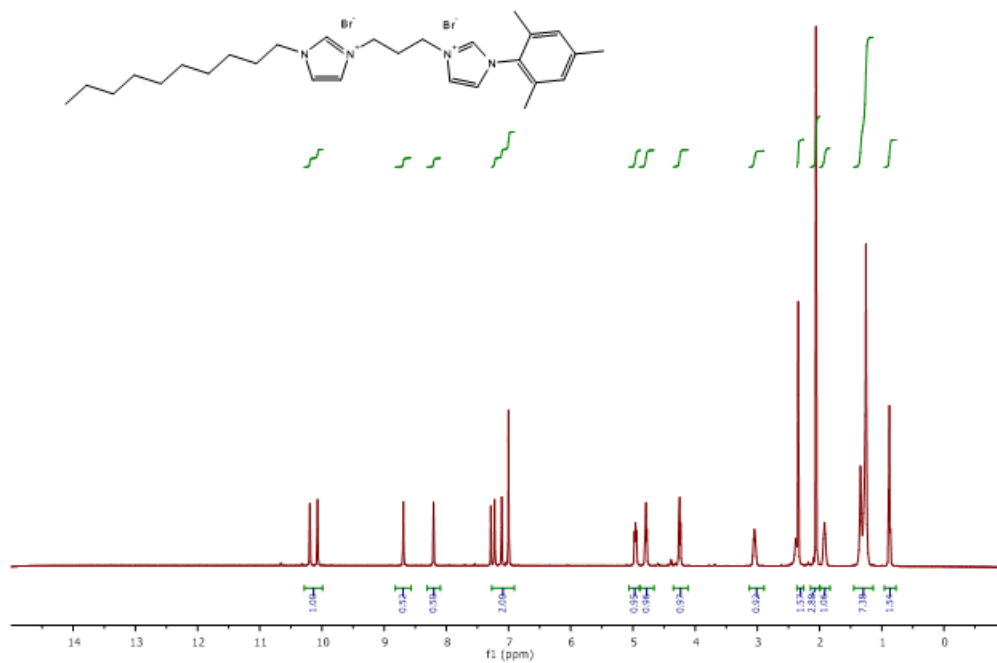
$H_2G^{mes}_8$



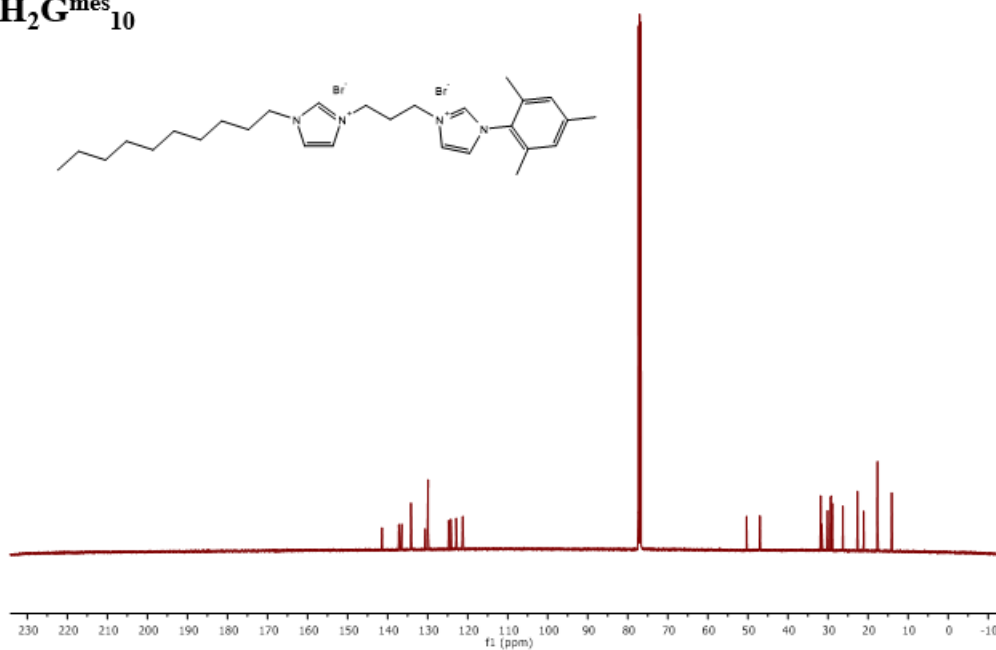
$H_2G^{mes}_8$



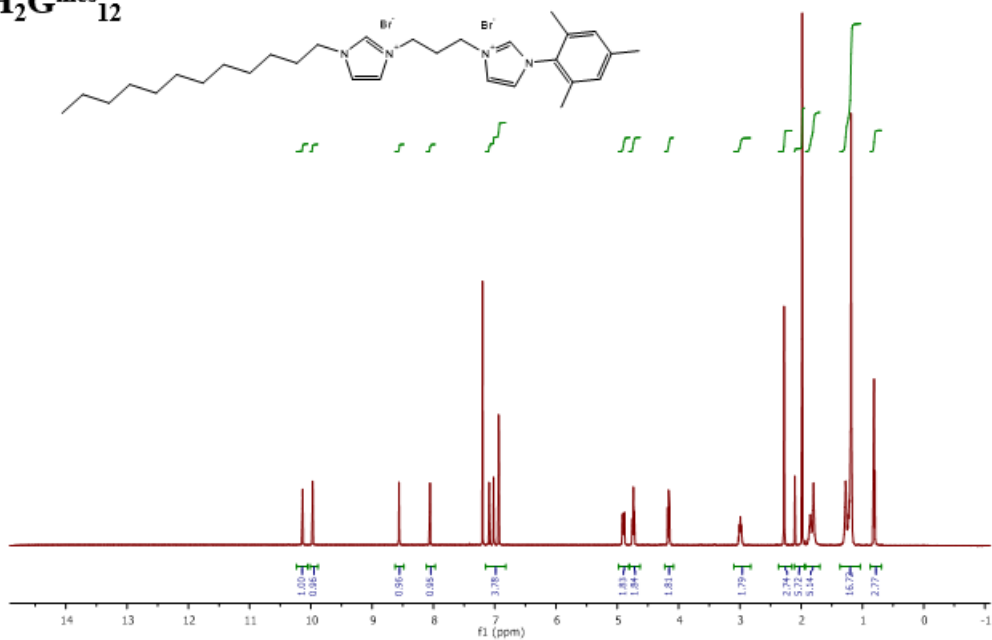
H₂G^{mes}₁₀



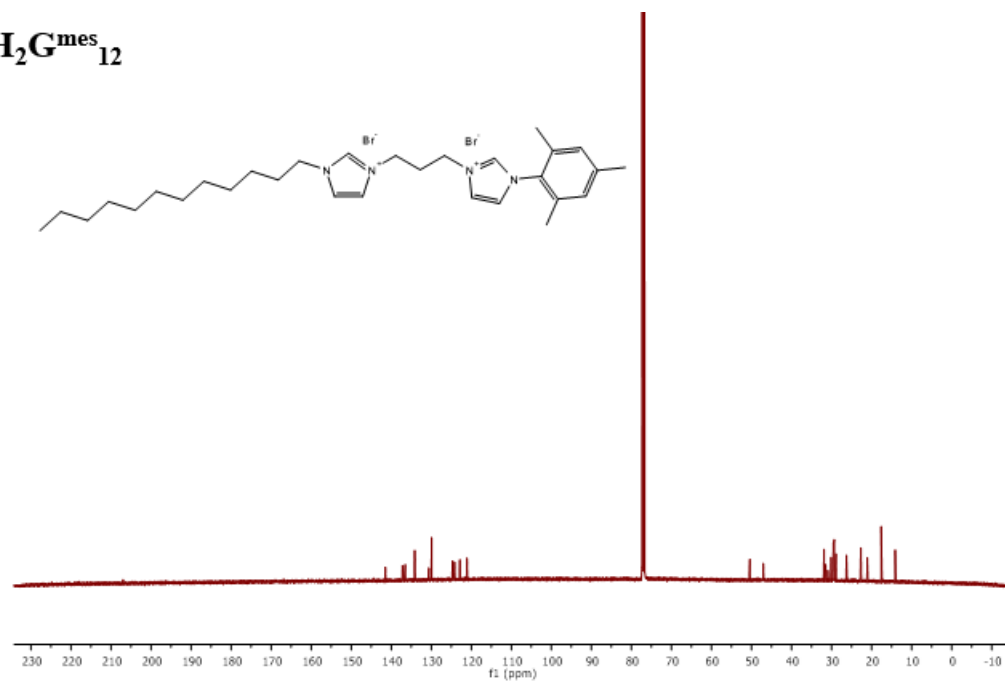
H₂G^{mes}₁₀



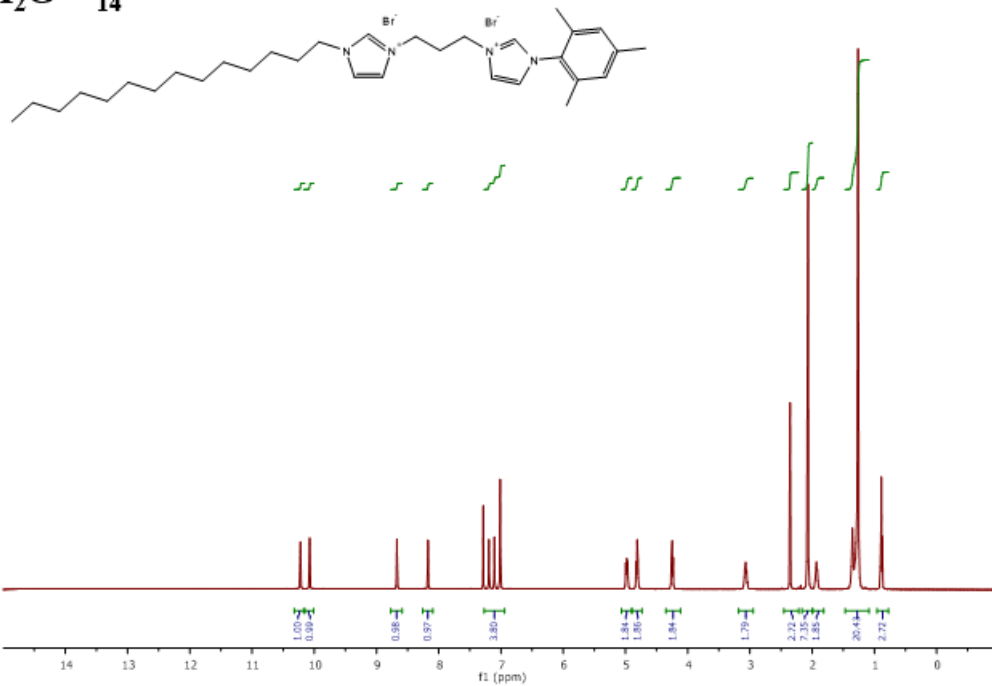
$H_2G^{mes}_{12}$



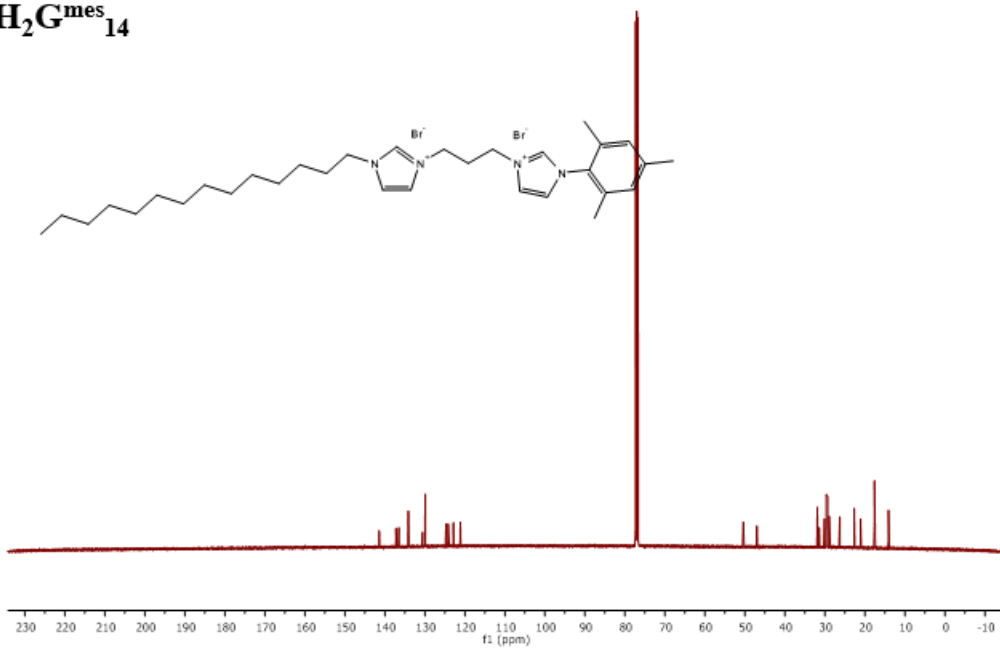
$H_2G^{mes}_{12}$



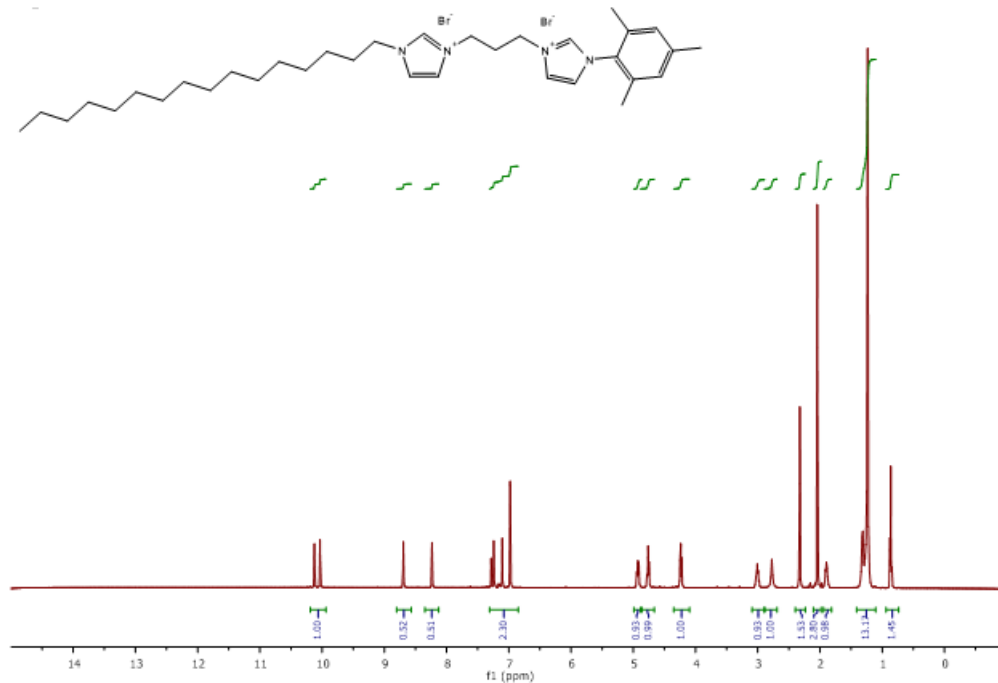
H₂G^{mes}₁₄



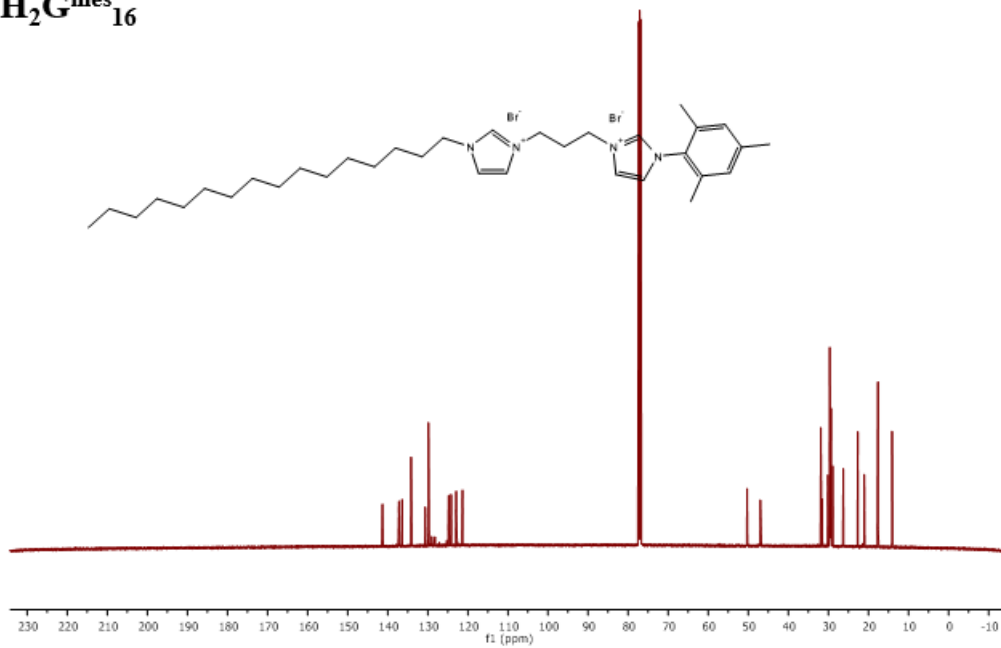
H₂G^{mes}₁₄



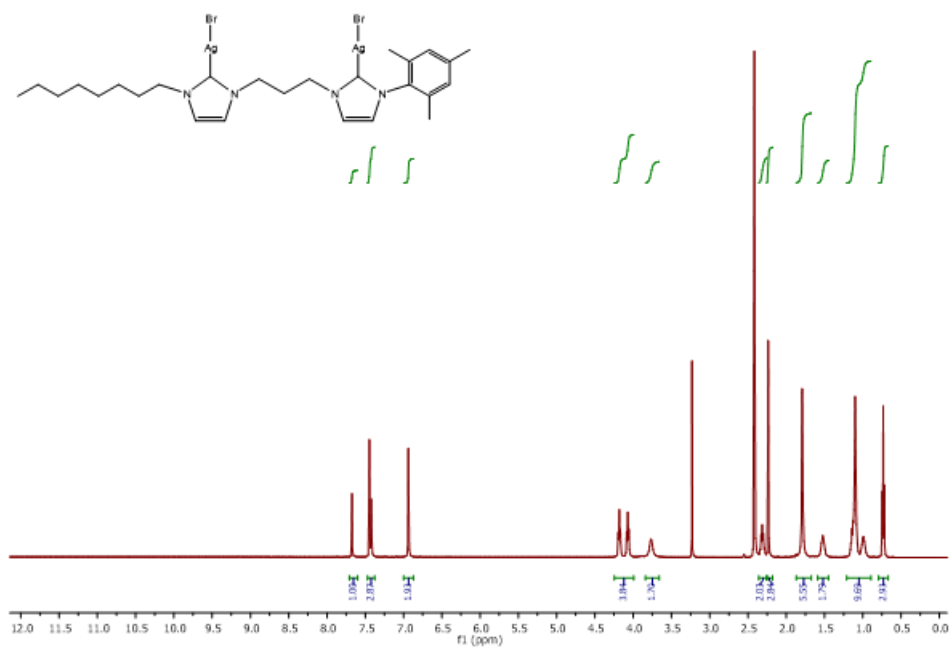
$H_2G^{mes}_{16}$



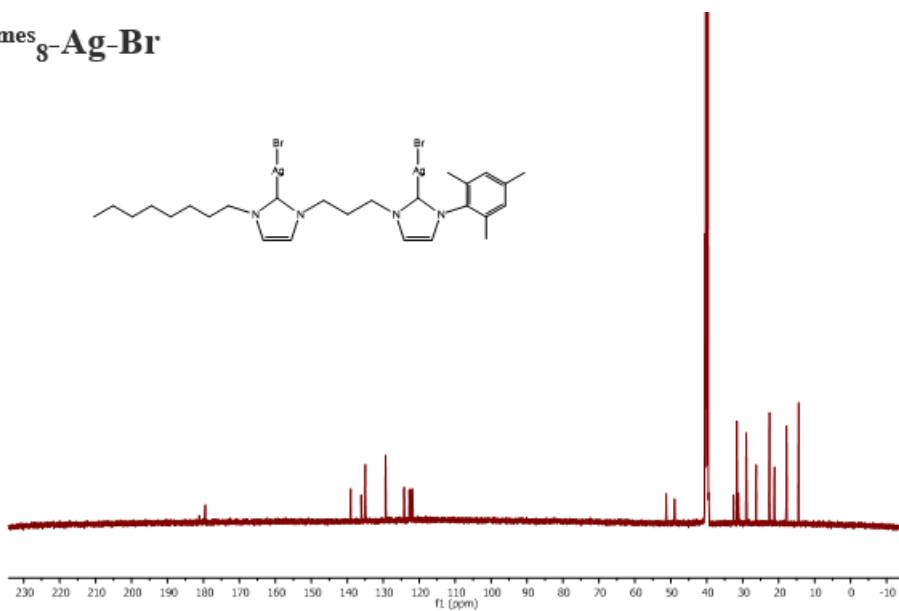
$H_2G^{mes}_{16}$



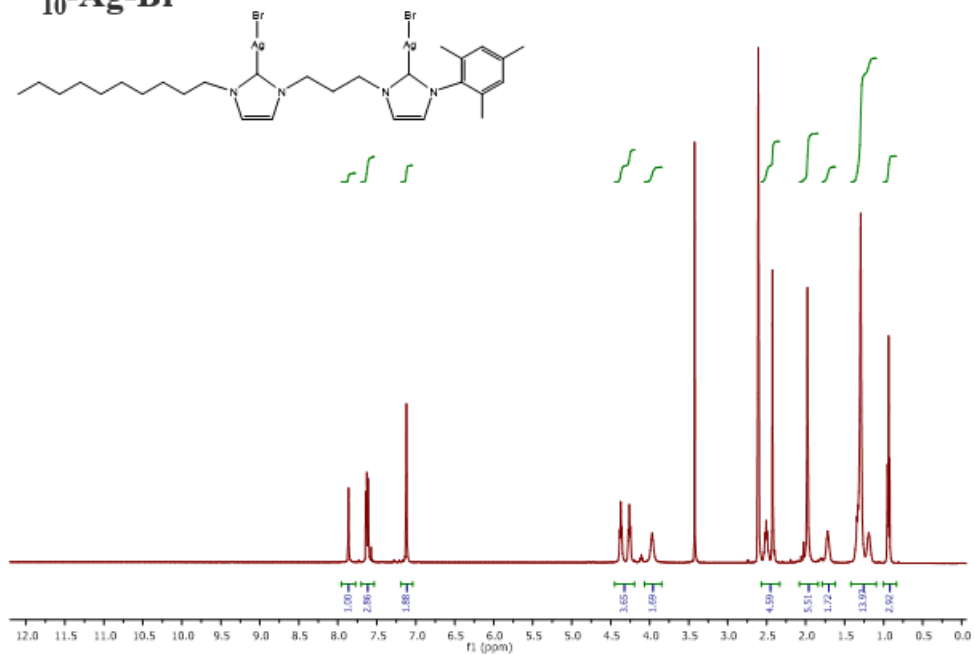
G^{mes}₈-Ag-Br



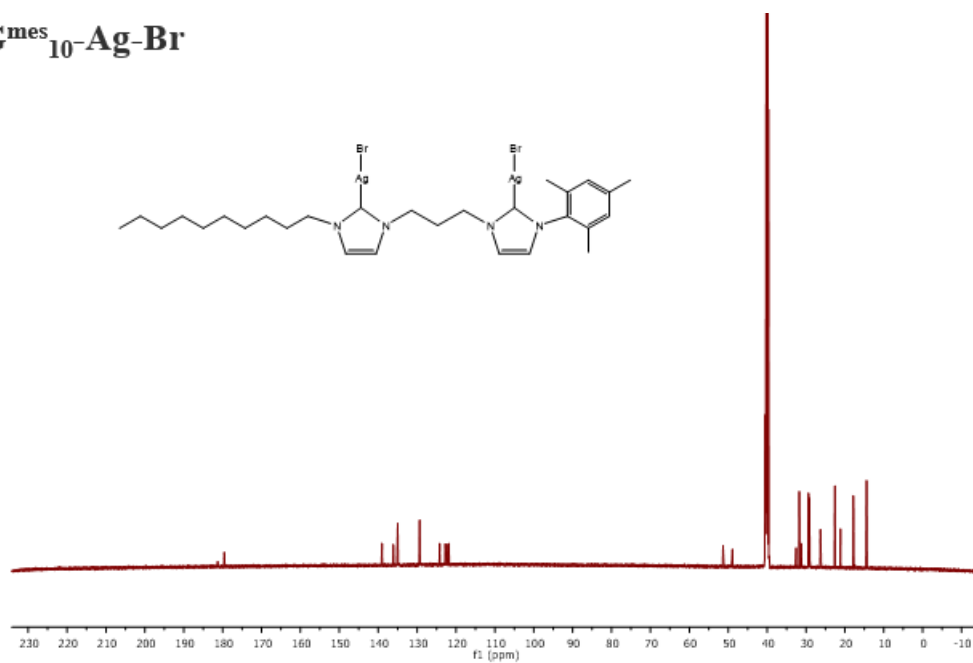
G^{mes}₈-Ag-Br



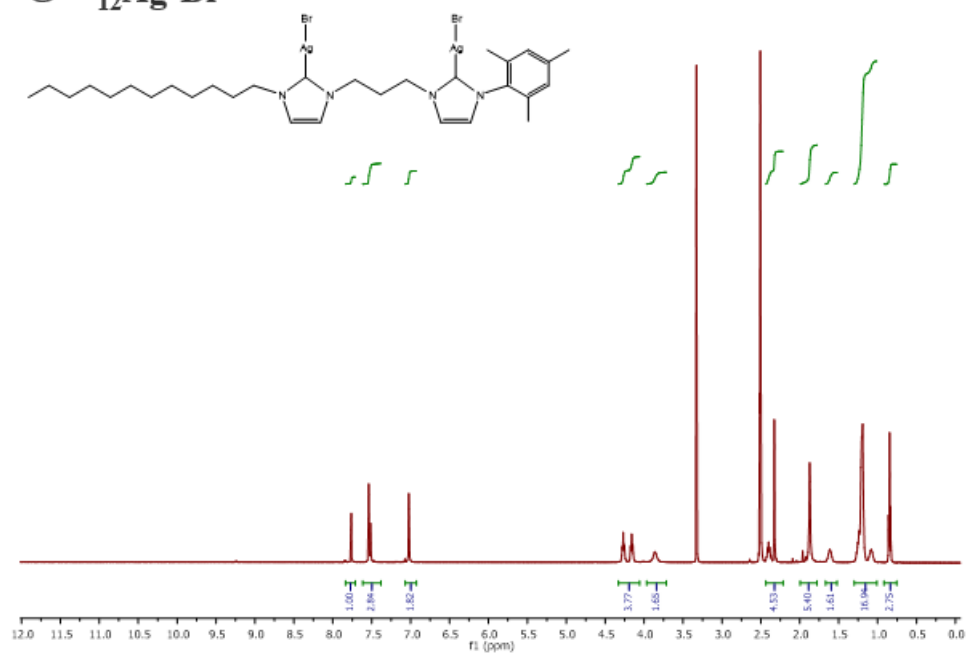
G^{mes}₁₀-Ag-Br



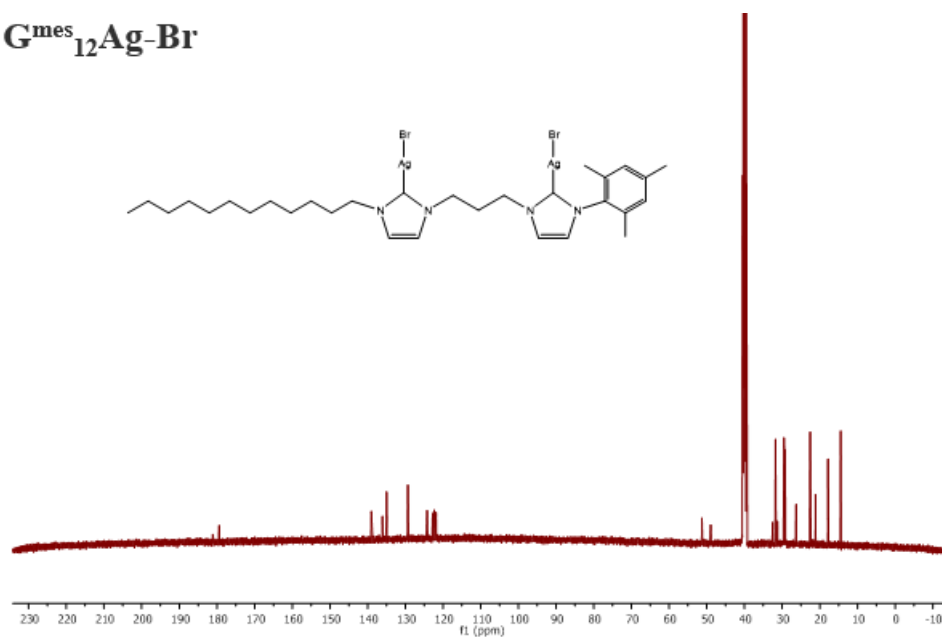
G^{mes}₁₀-Ag-Br



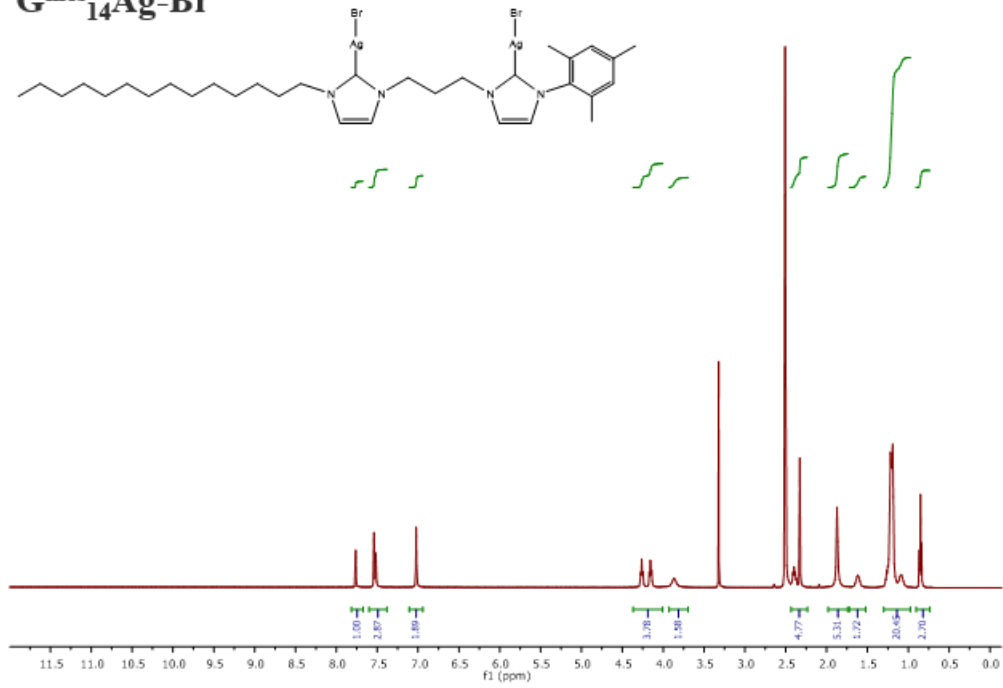
$G^{mes}_{12}Ag-Br$



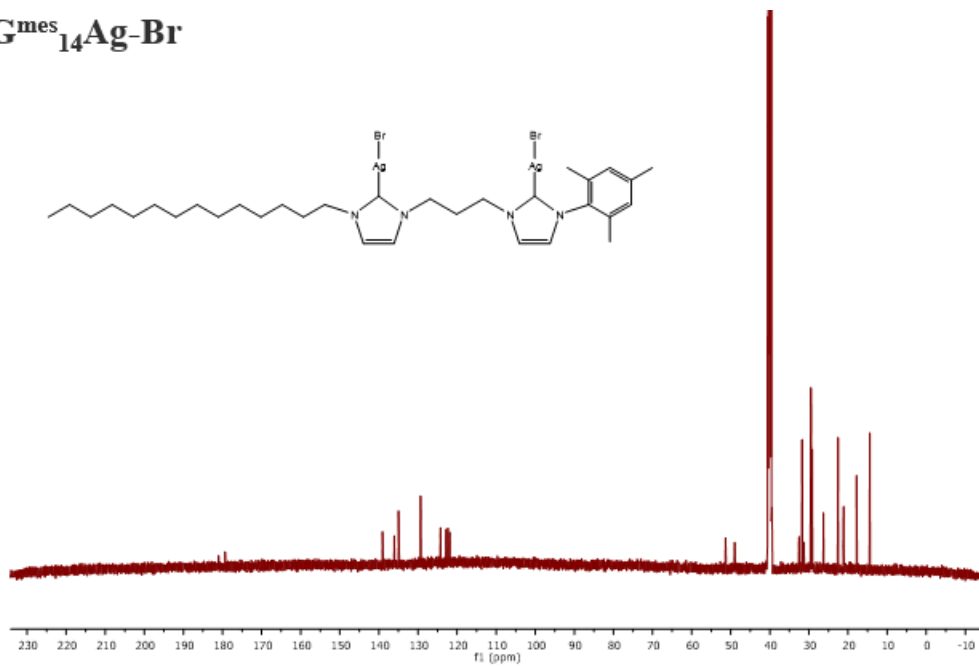
$G^{mes}_{12}Ag-Br$

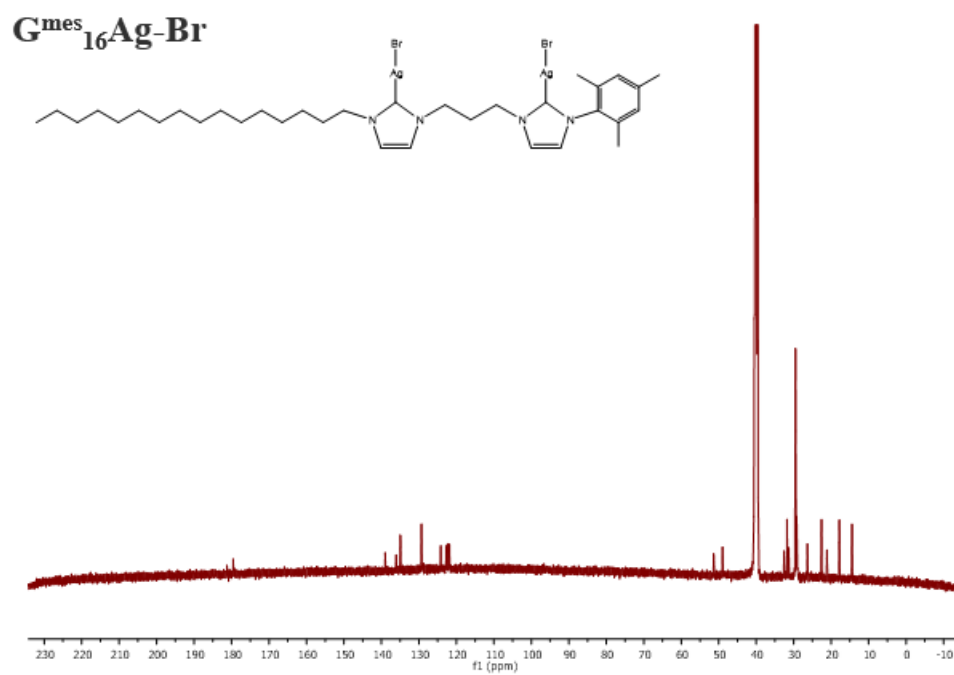
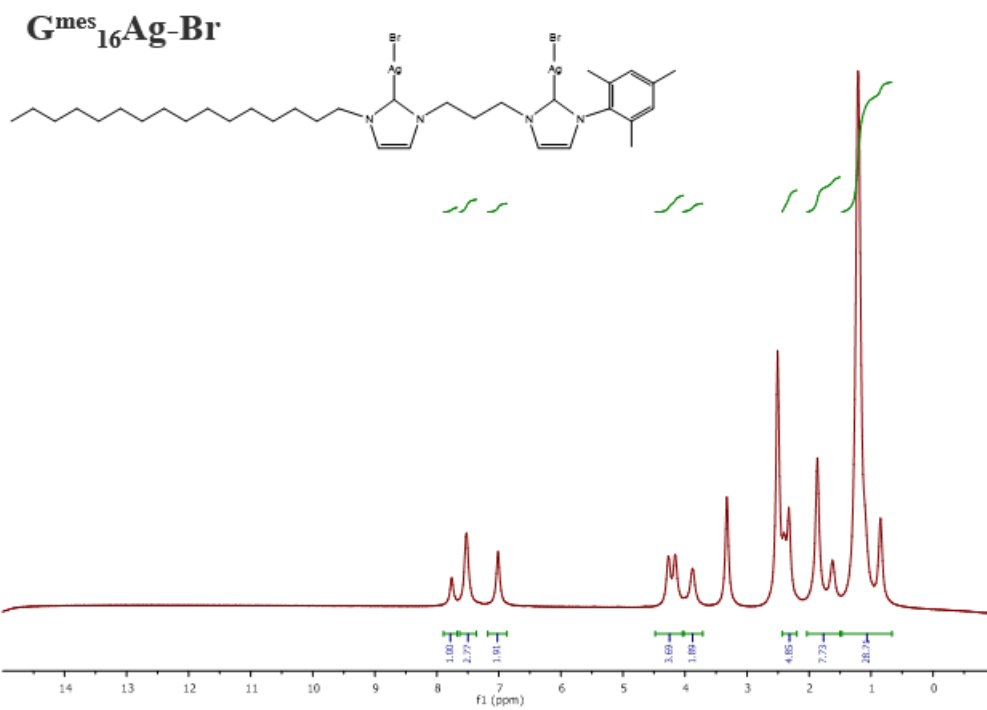


G^{mes}₁₄Ag-Br

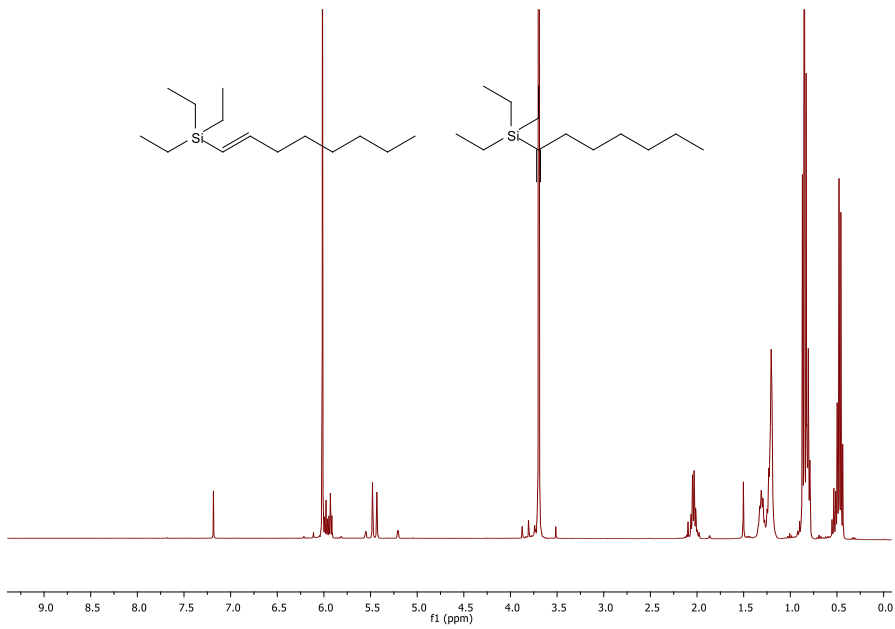
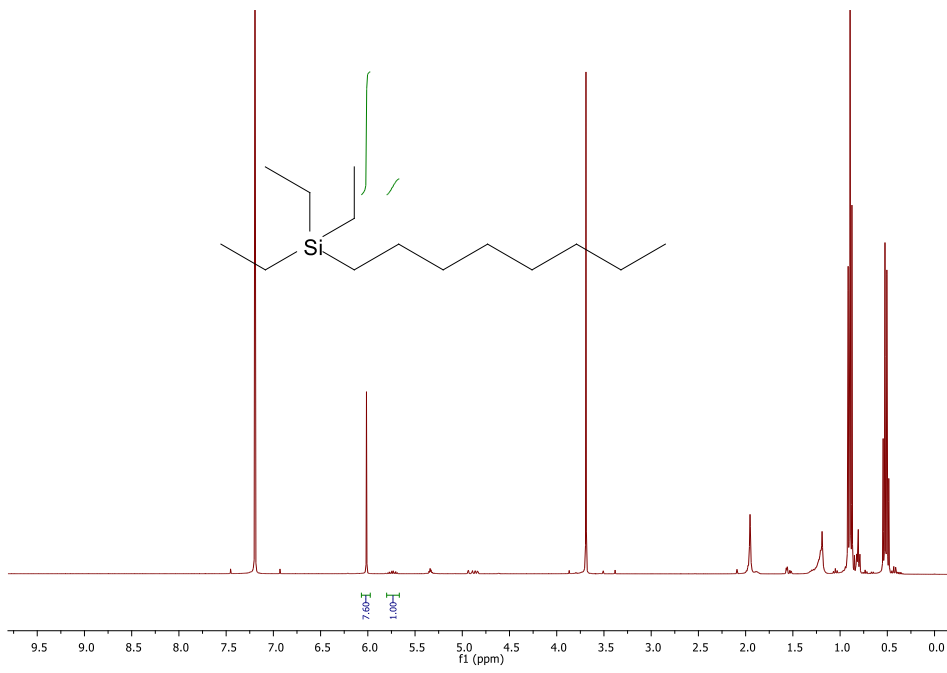


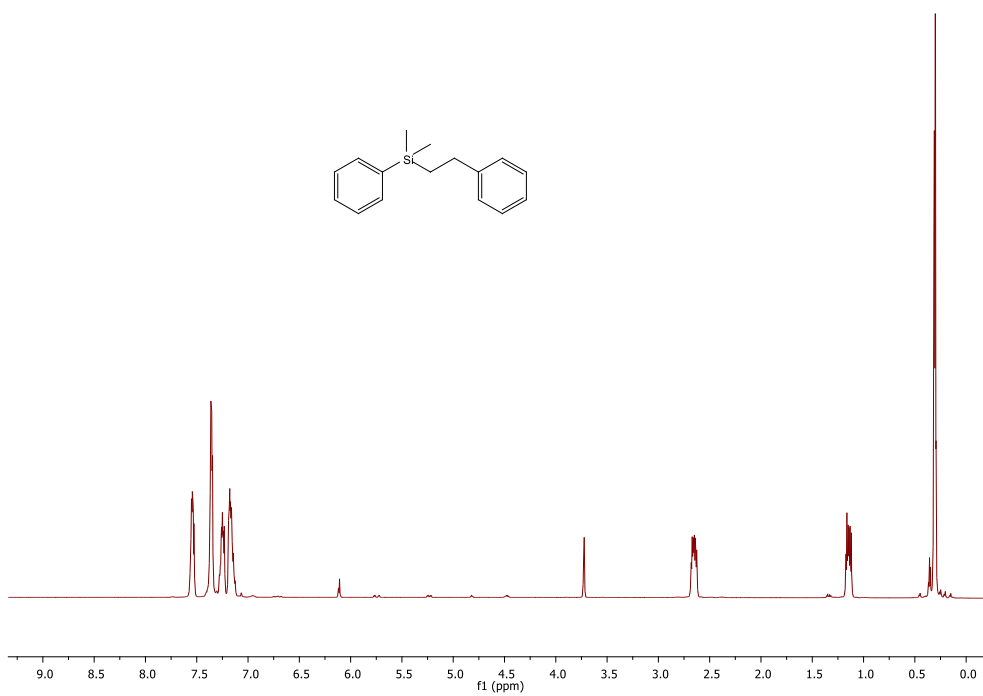
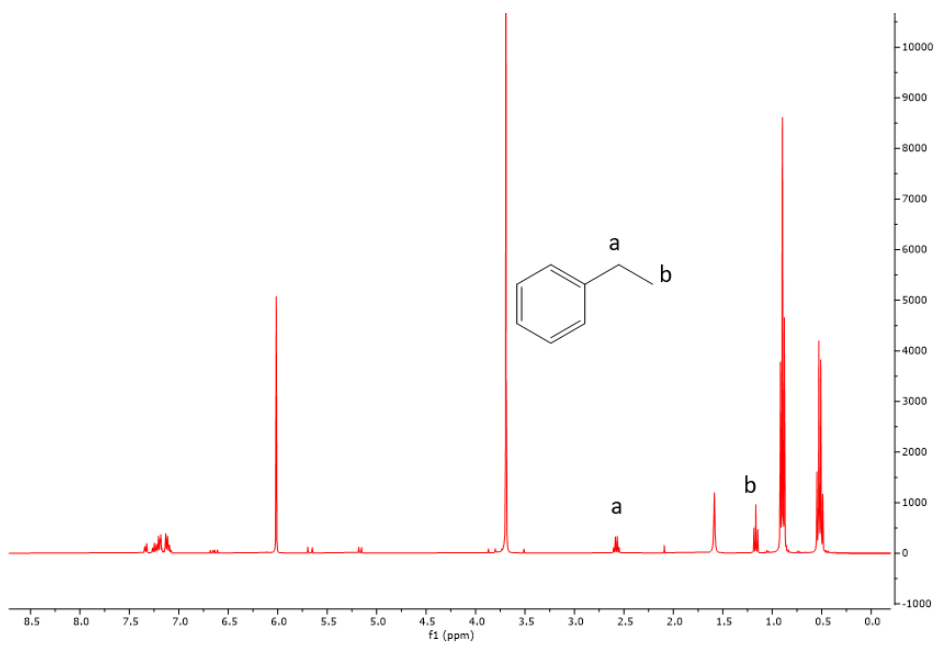
G^{mes}₁₄Ag-Br

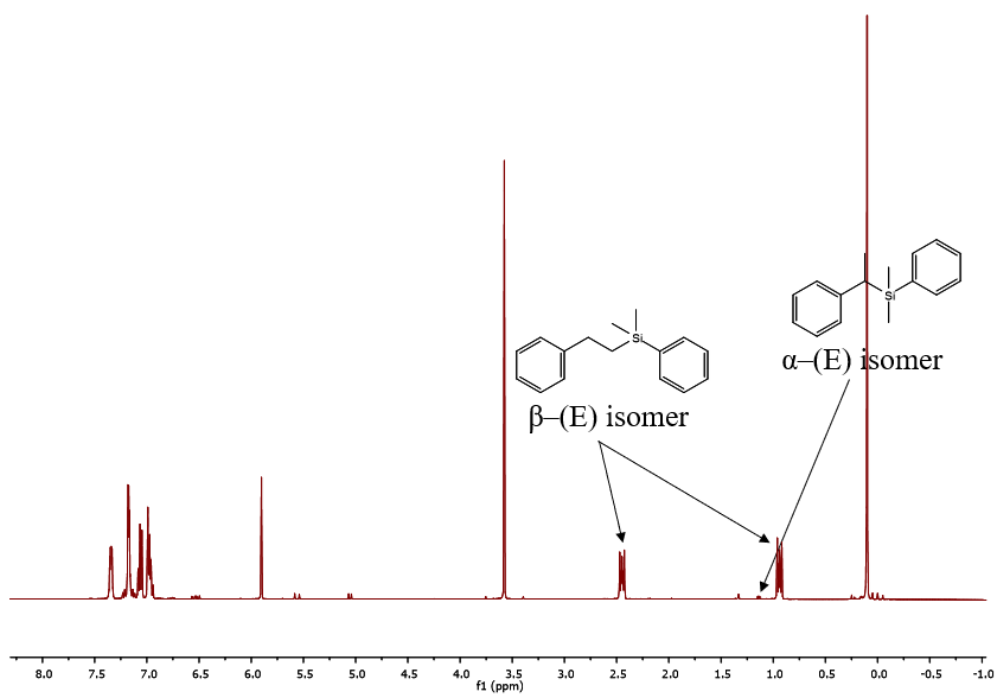
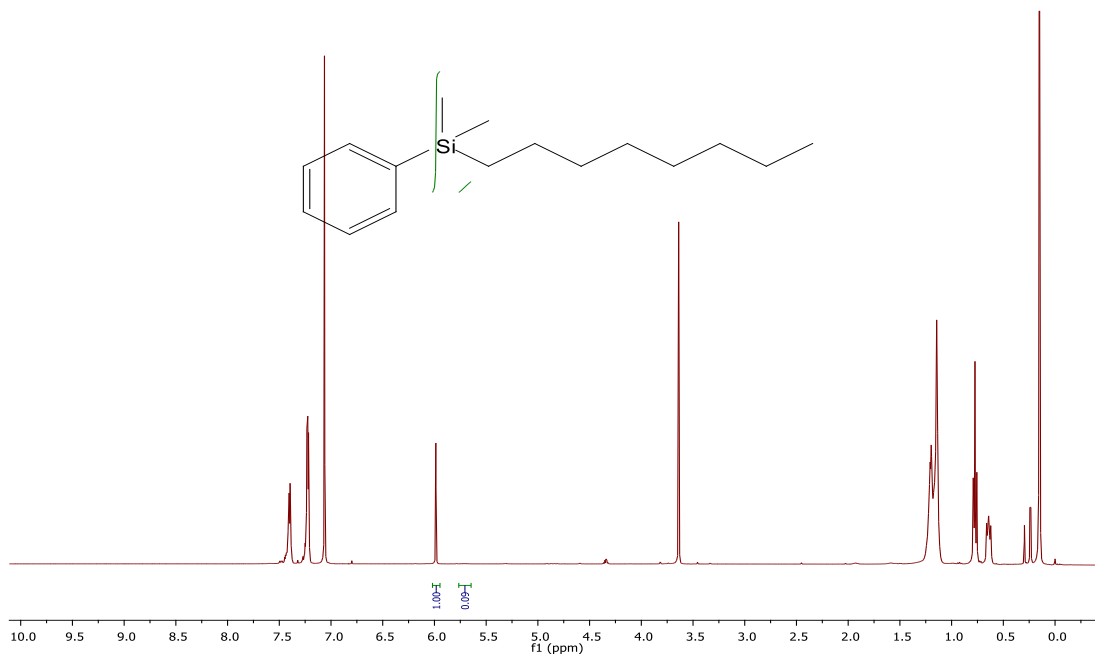


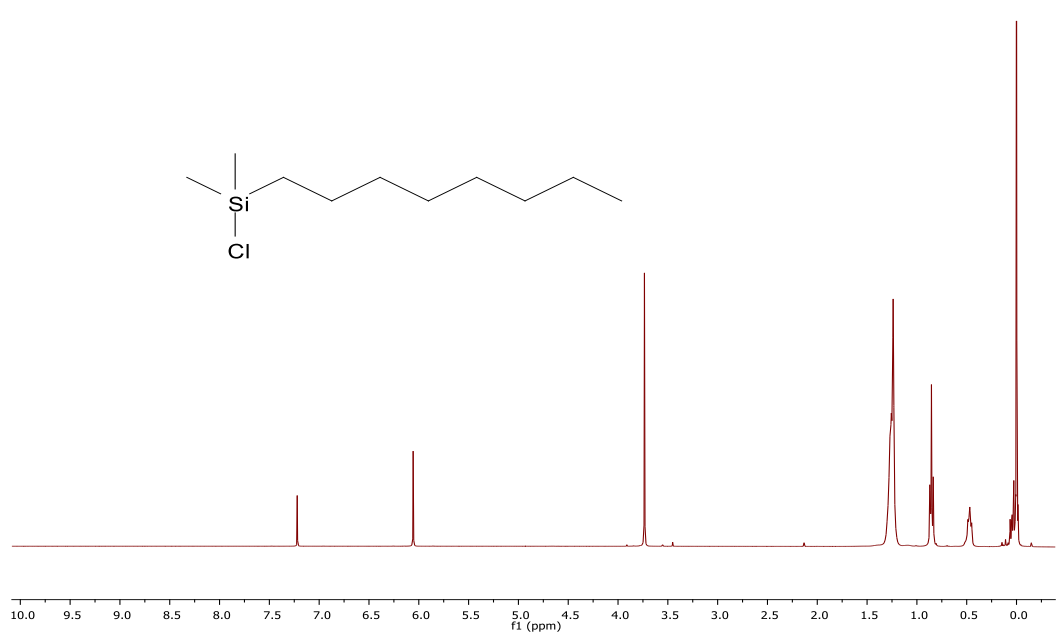
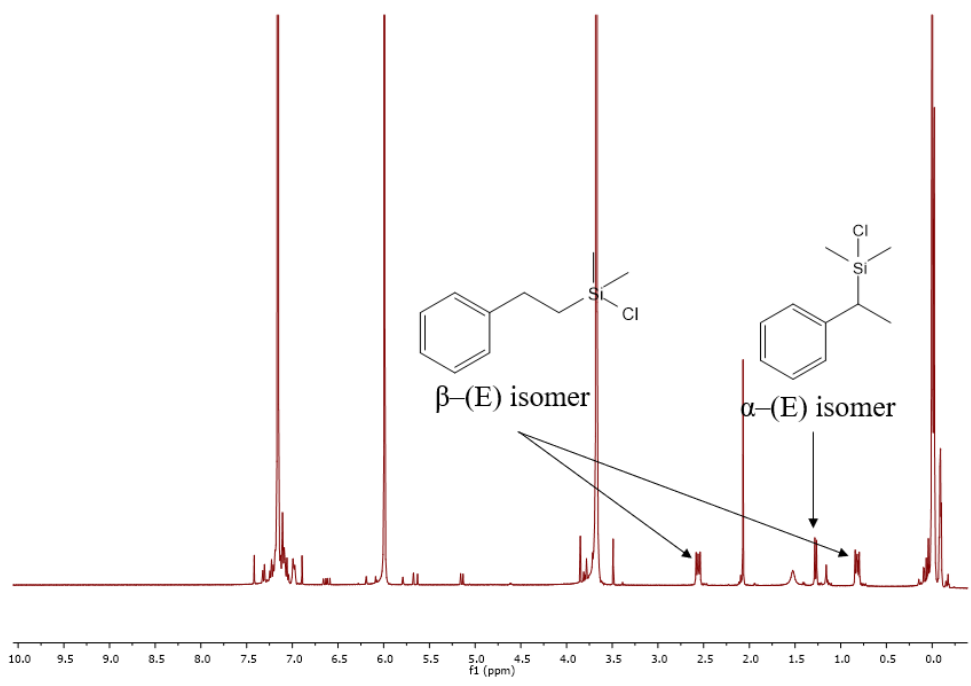


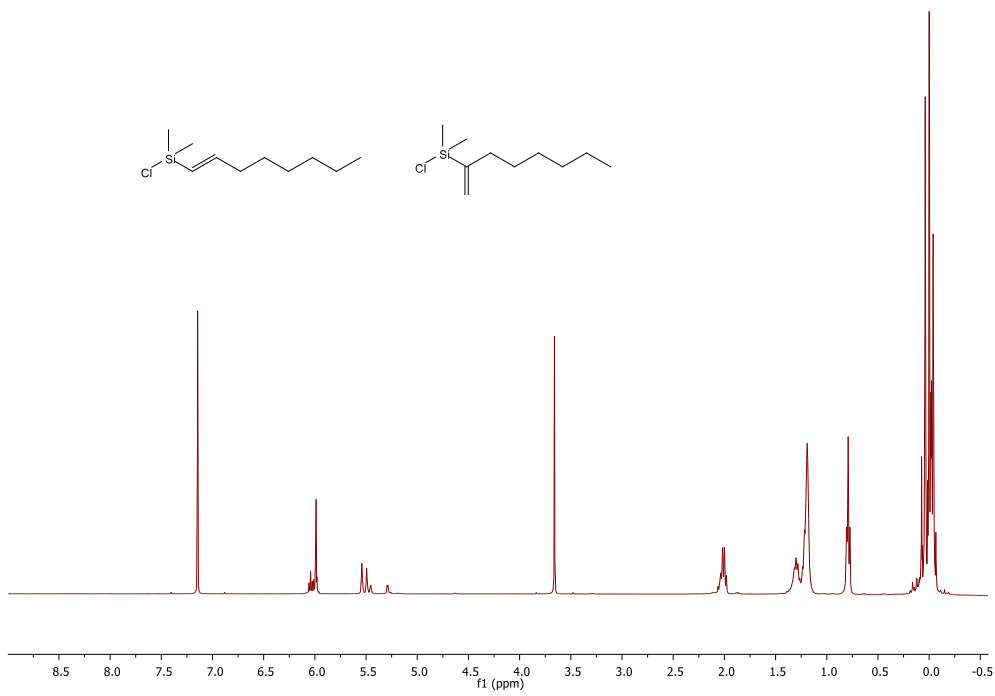
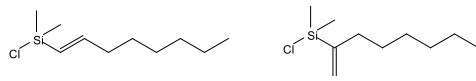
Appendix G: ^1H and ^{13}C NMR spectra of Hydrosilylation Products





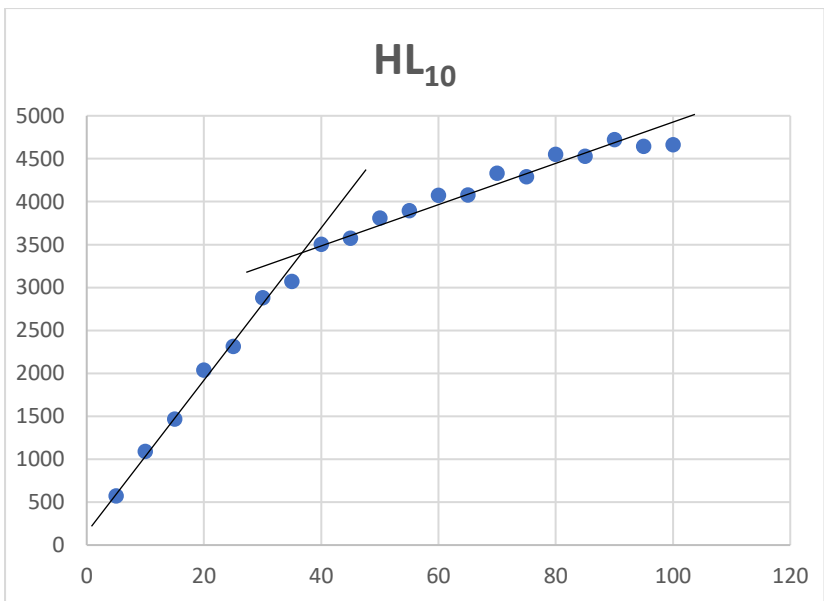
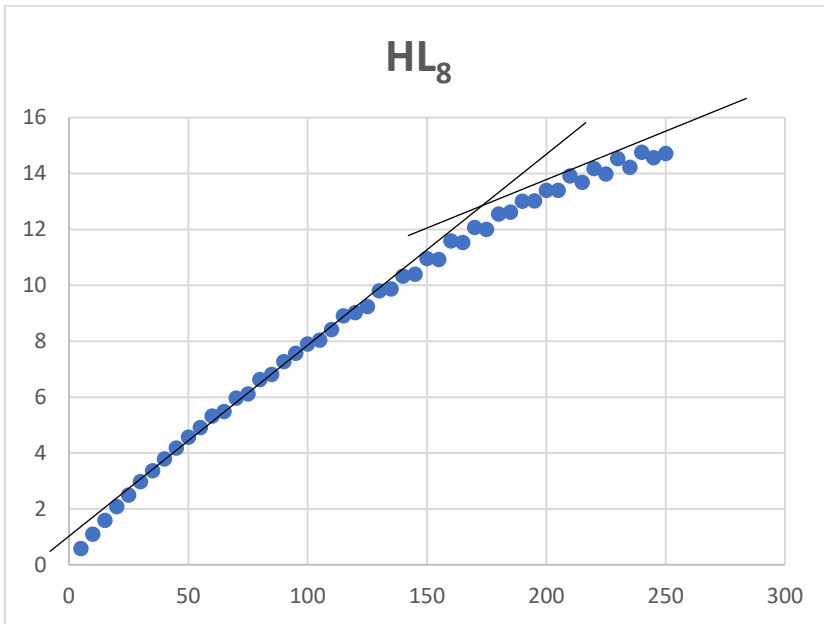


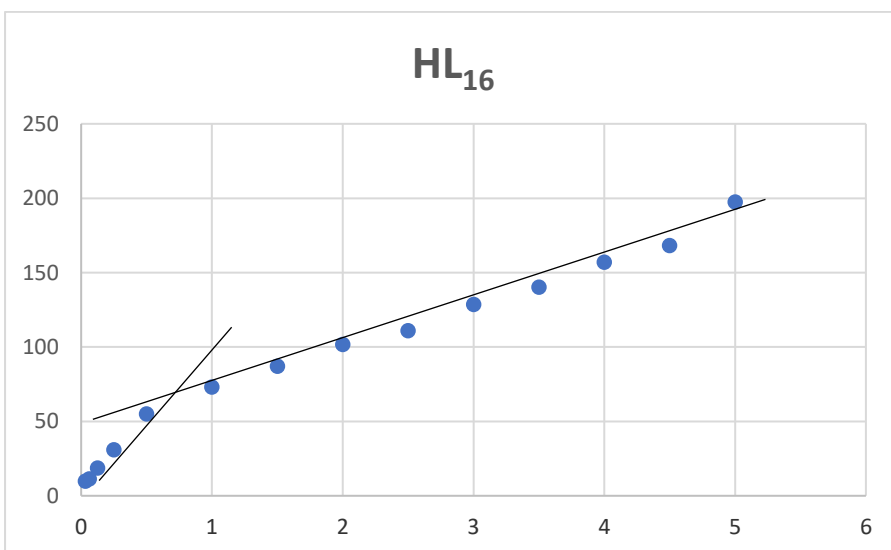
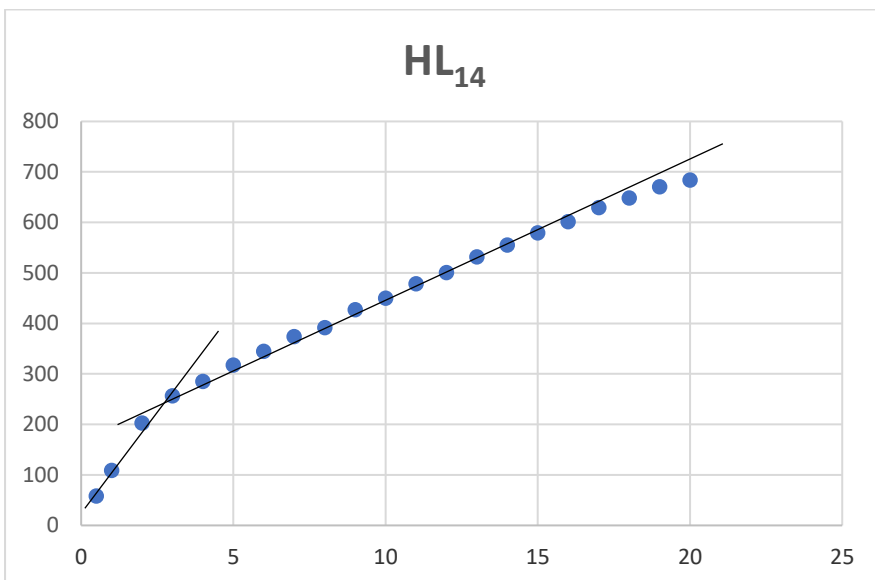
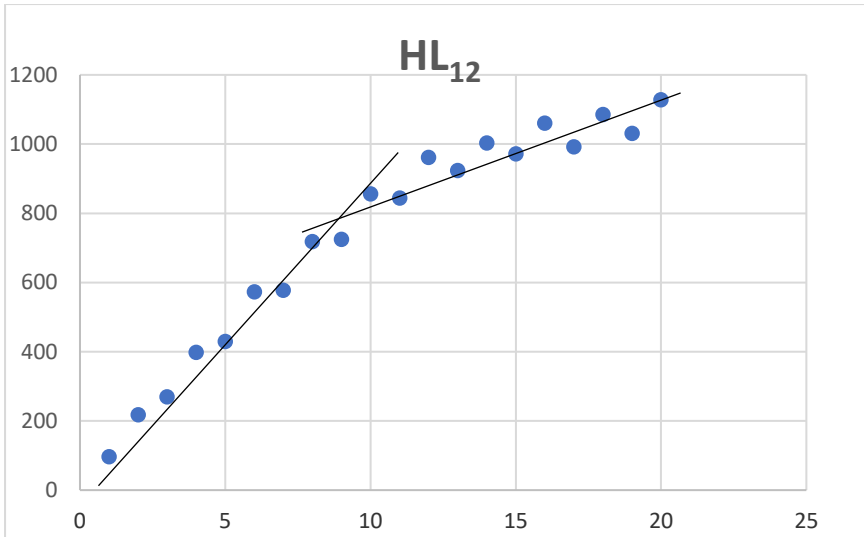




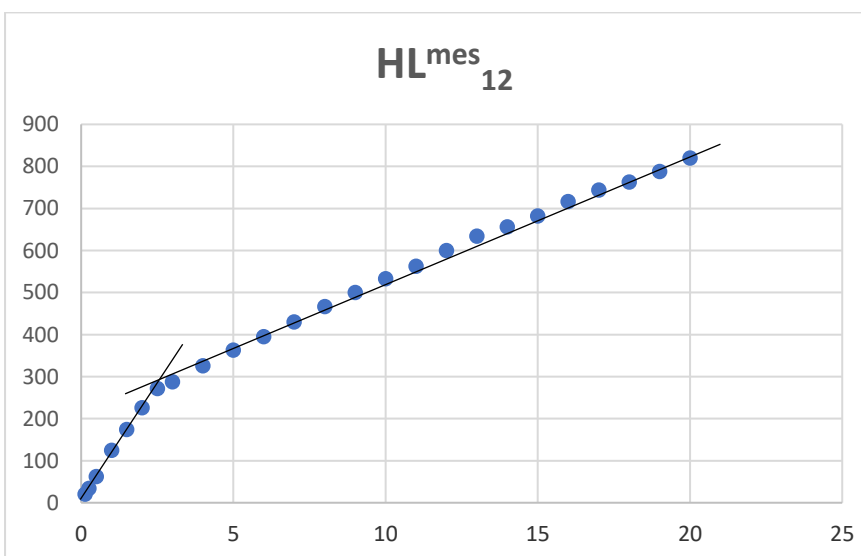
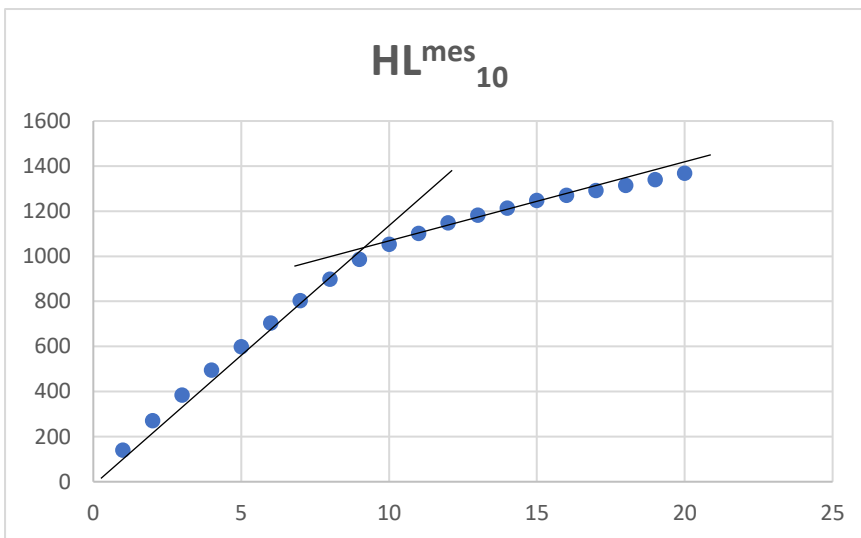
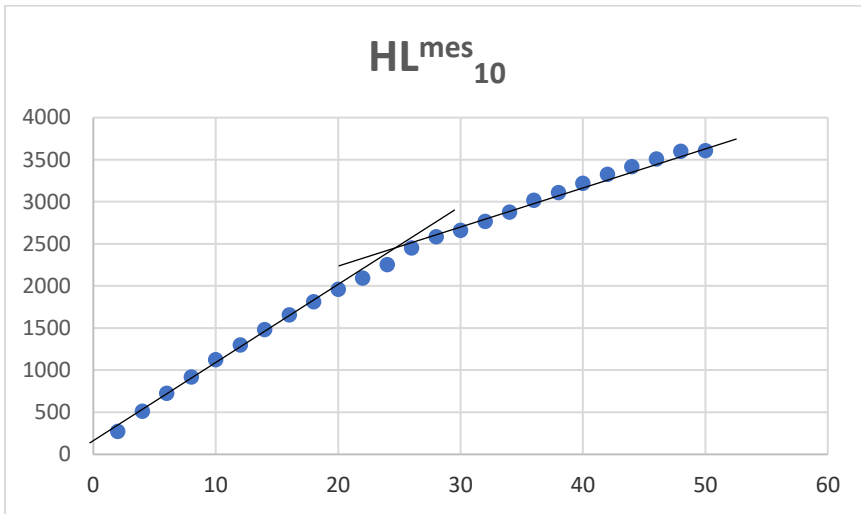
**Appendix H: Graph of Concentration vs Conductivity of \mathbf{HL}_{8-16} ,
 $\mathbf{HL}^{\text{mes}}_{8-16}$, $\mathbf{H}_2\mathbf{G}_{12-16}$ and $\mathbf{H}_2\mathbf{G}^{\text{mes}}_{8-16}$**

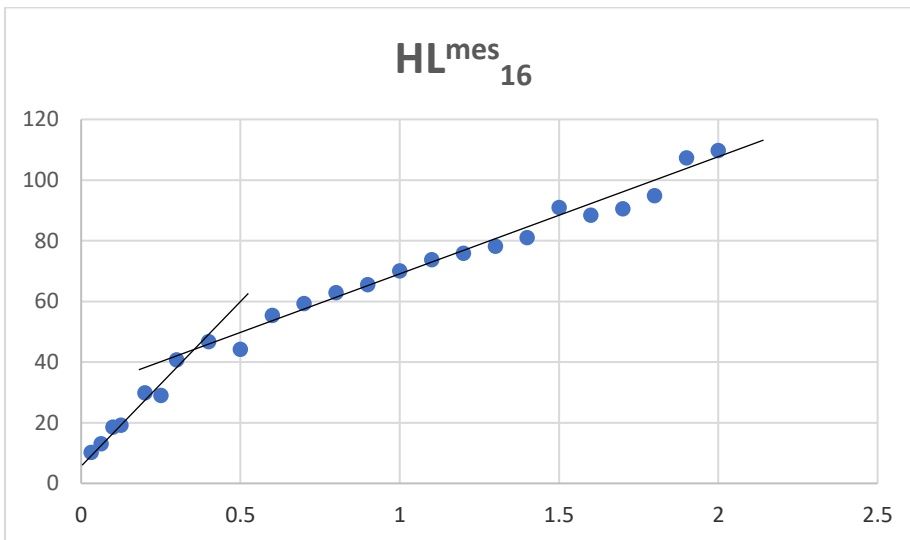
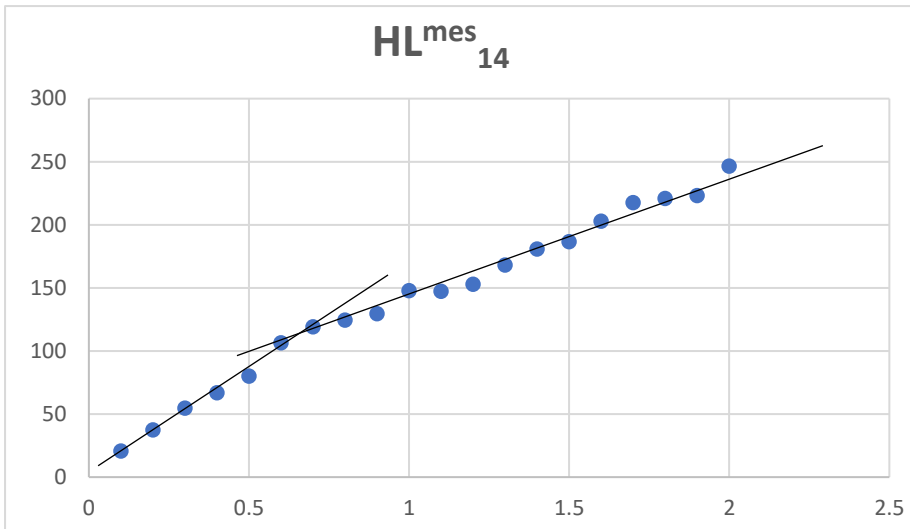
HL8-16



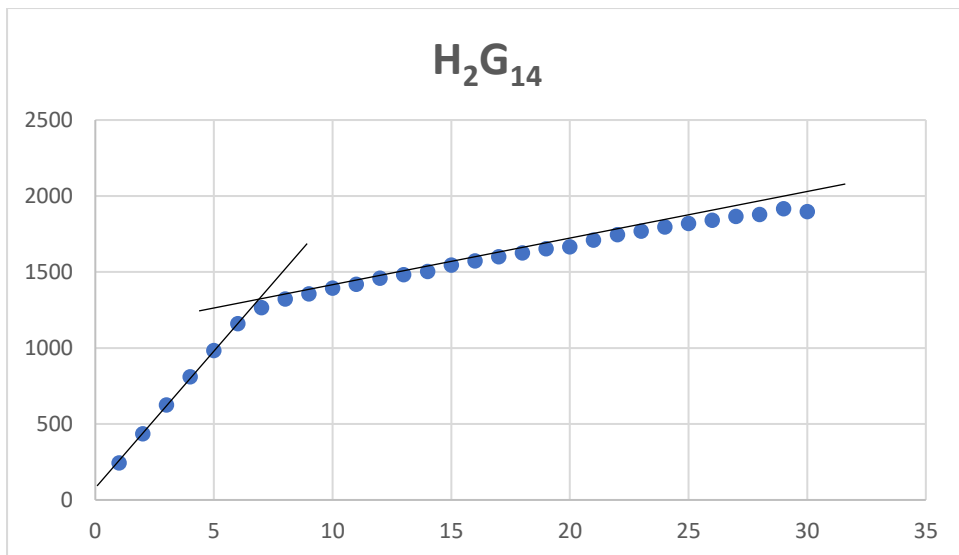
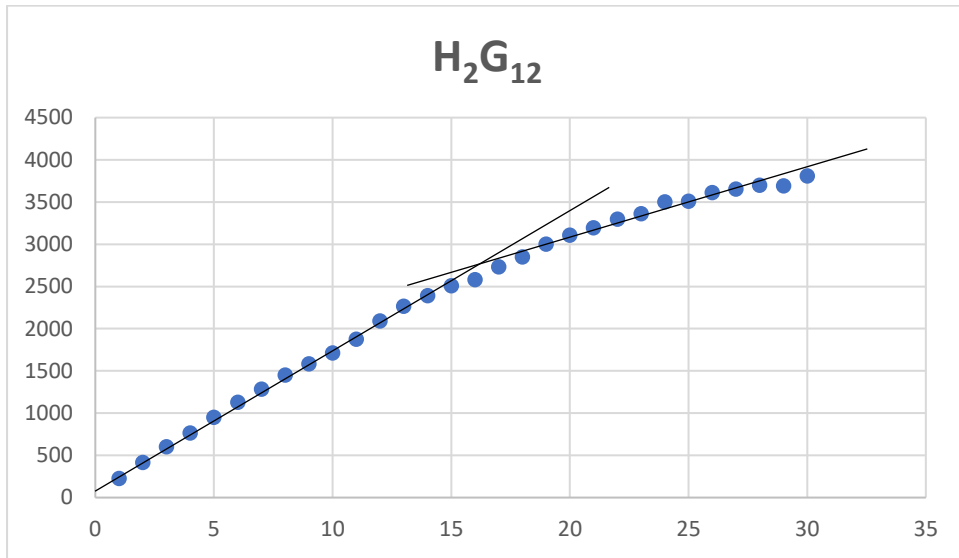


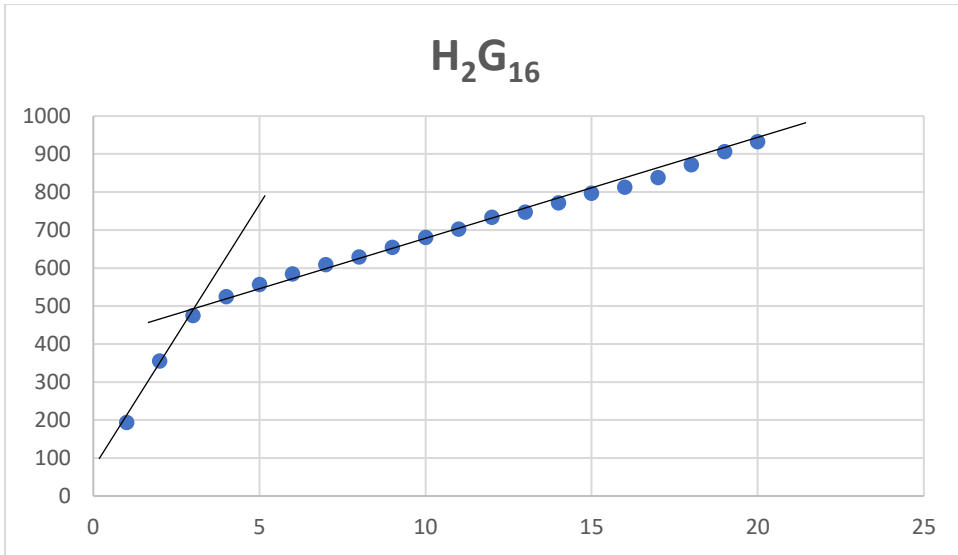
HL^{mes}₈₋₁₆





H₂G₁₂₋₁₆





$H_2G^{mes}_{8-16}$

